



शैक्षणिक प्रतिवेदन
Academic Report
2021-22

होमी भाभा राष्ट्रीय संस्थान
HOMI BHABHA NATIONAL INSTITUTE

परमाणु ऊर्जा विभाग की सहायता प्राप्त संस्था
और यूजीसी अधिनियम 1956 की धारा 3 के तहत विश्वविद्यालय माना जाता है
(A Deemed to be University u/s 3 of UGC Act 1956 and a Grant-in-Aid
Institute of the Department of Atomic Energy, Govt. of India)

Location of HBNI Central Office, Constituent Institutions & Off Campus Centre



Academic Report 2021-22



Homi Bhabha National Institute
(An aided institution of the Department of Atomic Energy and a
Deemed-to-be University under section 3 of the UGC Act 1956)

Contents

From the Vice Chancellor's Desk.....i

Section-1 Overview

Academic Programmes of the Institute.....	01
Composition of the Governing Body of the Institute.....	04
List of Faculty members.....	10
HBNI at a Glance.....	25

Section-II Theses at a Glance

Chemical Sciences.....	29
Engineering Sciences.....	41
Life Sciences.....	77
Mathematical Sciences.....	92
Medical & Health Sciences.....	99
Physical Sciences.....	100

**Section-III List of students who have completed Ph.D. during
August 1, 2021- July 31, 2022.....132**

**Section-IV List of students who have completed M.Tech. and
M.Sc. (Engg.) during August 1, 2021- July 31, 2022.....155**

**Section-V List of students who have completed D.M., M.Ch
and M.D. during August 1, 2021- July 31, 2022.....165**

प्रो. पी. डी. नाईक
कुलपति (कार्यवाहक)
एवं डीन

Prof. P. D. Naik

Vice Chancellor (Officiating)

& Dean



होमी भाभा राष्ट्रीय संस्थान

प्रशिक्षण विद्यालय परिसर, अणुशक्तिनगर, मुंबई-400 094, भारत

Homi Bhabha National Institute

Training School Complex, Anushaktinagar, Mumbai – 400 094, India

Tel. No. 91-22-25595398 ● Mob. : 9221798549

Email : vicechancellor@hbni.ac.in ● deanhbni@hbni.ac.in

● pdnaik@barc.gov.in

From the Vice Chancellor's Desk



It gives me great pleasure to present the academic report of Homi Bhabha National Institute (HBNI) for the year 2021-22. In this academic year we offered 42 academic programmes and have around 3660 students of whom nearly 2000 are doctoral students, spread over eleven campuses across the country. In the present academic year (August 1, 2021-July 31, 2022), HBNI has awarded 252 PhD, 70 MD, 26 MCh, 26 DM and 169 MSc degrees in different disciplines and till July 31, 2022, total degrees awarded include 2133 PhD, 628 MD, and 219 MCh, 194 DM and 1161 M.Sc. degrees.

I am happy to share that in the National Institute Ranking Framework (NIRF), 2022 exercise by the Ministry of Human Resource and Development, HBNI secured 11th rank in Research Institution Category, 17th rank In University Category and 33rd rank in the Overall category. All these recognitions are the testaments of the dedication, commitment and excellence in the academic activities exhibited by HBNI as a whole.

During the academic year 2021-22, HBNI continued to pursue the mission of organizing special webinars and online courses for its faculty and students, exploiting the recent learning from the conduct of online programs, forced upon us by the pandemic. As part of the celebration of Azadi ka Amrit Mahaotsav, several high-value webinars were organized with pioneers such as Dr. Chidambaram, Dr. Kakodkar, Dr. V. S. Ramamurthy, Shri Surendra Sharma and Prof. R. B. Grover. The online courses conducted included, course on Advanced Materials Chemistry, Emerging Trends in Biophysics, Research Methodology and a unique advanced course on Corrosion Degradation in Light Water Reactors organized in association with INSTN France. HBNI also started the Sarabhai Management Program for senior executives of DAE organizations, in which management courses were offered through a Memorandum of Understanding between the Indian Institute of Management, Ahmedabad and HBNI. The syllabus of these courses was carefully designed jointly by IIM and HBNI, to meet the objectives of DAE.

HBNI took several initiatives for the implementation of the National Education Policy 2020. One of the important initiatives taken with respect to the implementation of the Policy 2020 was the establishment of the HBNI-Industry Linkage Centre (HILC), created with the aim to facilitate the skill development of our students through their internship in various industrial establishments.

(i)

To commemorate the International Year of Basic Sciences for Sustainable Development, HBNI brought together, in a discussion meeting, faculty from across all its CIs/OCC to provide an overview of the research programs and research infrastructure available in their respective institutions. The meeting witnessed very enthusiastic participation from the faculty and it is planned to conduct discipline-specific meetings on various topics at different constituent institutions of HBNI. In fact, one such meeting on "Condensed Matter Physics" was held at SINP, Kolkata during June 23-24, 2022. This augurs well for the growth of unique academic programs and active collaborations in the constituent units.

Since its inception in 2005, HBNI has been taking great efforts to promote multidisciplinary as well as interdisciplinary education and research through its CIs/OCC. The output of such efforts is visible through the summary of some of the theses included in this report. I am happy to note that HBNI students and faculties have continued to make a mark nationally and internationally through their high-quality research and publications, which have been recognized by their peers and the Academic Societies in the form of several awards and fellowships conferred on our faculties and students.

I take this opportunity to extend my gratitude to Shri K. N. Vyas, Chairman, Council of Management, HBNI for his valuable support and guidance in all endeavors of HBNI. Thanks are due to Prof. P. R. Vasudeva Rao, for his enormous contributions to taking HBNI activities to newer heights. My sincere thanks to Prof. R. B. Grover, Emeritus Professor, HBNI, who has provided valuable advice and guidance to the HBNI team on several important matters. Thanks, are also due to the members of the Council of Management, Academic Council and the Planning and Monitoring Board of HBNI for their immense contributions. I would also like to place on record my thanks to the members of the Board of Studies, Deans (Academic), Deans (Student Affairs), nodal officers at CIs/OCC of HBNI, and faculties and colleagues of HBNI for their dedicated efforts and contributions in making HBNI an Institute of great repute nationally and internationally.

HBNI has great potential to become one of the favored destinations for the youth of this country who want to engage in challenging research problems in frontier areas of science and technology and I am certain that with the constant efforts and dedication of faculty and using the excellent infrastructure at its various CIs/OCC, this will be fulfilled and HBNI will attain a greater height in its academic and research performance in years to come.


(P. D. Naik)

Section I (OVERVIEW)

Academic Programmes of the Institute

The Homi Bhabha National Institute (HBNI) brings together the academic and research programmes conducted by the following eleven premier institutions of DAE, as its Constituent Institutions (CIs)/ Off Campus Centre (OCC):

1. Bhabha Atomic Research Centre (BARC), Mumbai
2. Indira Gandhi Centre for Atomic Research (IGCAR), Kalpakkam
3. Raja Ramanna Centre for Advanced Technology (RRCAT), Indore
4. Variable Energy Cyclotron Centre (VECC), Kolkata
5. Saha Institute of Nuclear Physics (SINP), Kolkata
6. Institute for Plasma Research (IPR), Gandhinagar
7. Institute of Physics (IoP), Bhubaneswar
8. Harish-Chandra Research Institute (HRI), Allahabad
9. Institute of Mathematical Sciences (IMSc), Chennai
10. Tata Memorial Centre (TMC), Mumbai
11. National Institute of Science Education and Research (NISER), Bhubaneswar

The HBNI offers a range of academic programmes in Chemical Sciences, Engineering Sciences, Medical & Health sciences, Life sciences, Mathematical Sciences and Physical Sciences. It also has a program in Applied Systems Analysis. All institutions, except NISER, conduct programmes at post-graduate level. NISER admits Higher Secondary passed students for its five years Integrated M.Sc. program.

❖ Disciplines in which HBNI Offers Ph.D.

- ✓ Applied System Analysis
- ✓ Chemical Sciences
- ✓ Computer Science
- ✓ Computational Biology
- ✓ Earth & Planetary Science
- ✓ Engineering Sciences
- ✓ Humanities & Social Sciences
- ✓ Life Sciences
- ✓ Mathematical Sciences
- ✓ Medical & Health Sciences
- ✓ Physical Sciences
- ✓ Theoretical Computer Science

Most of the Ph.D. programmes are multi-disciplinary in nature having guides and co-guides from different branches of science and engineering.

❖ **Disciplines in which HBNI Offers Integrated Ph.D.**

- ✓ Applied System Analysis
- ✓ Computational Biology
- ✓ Engineering Sciences

❖ **M.Tech.** in Engineering Sciences consists of one year of course work and one year of project work. The course work is offered at all the campuses of BARC Training School and IPR Training School. Project work is offered at BARC, IGCAR, RRCAT, VECC, IPR and units of DAE. Those who are not able to pursue or are not interested in pursuing a project/research work have the option to get a post graduate diploma in lieu of M.Tech.. BARC training school also offers post graduate diploma in Life Sciences after one year of course work.

❖ **M.Sc. (Engg)** program emphasizes on research project work extending upto one and a half years after one year of course work. This program is offered at BARC, IGCAR, VECC, RRCAT and IPR.

❖ **Integrated M.Sc.** of five-year duration in Physical Sciences, Chemical Sciences, Mathematics and Life Sciences is offered at NISER. M.Sc. in Physical Sciences of two-year duration is offered at HRI. M.Sc. in Medical & Radiological Physics of two-year duration is offered at NISER.

Super Specialty Courses in Medical & Health Sciences offered at TMC are listed below:

- ❖ **Doctor of Medicine (D.M.)** in Medical Oncology, Pediatric Oncology, Gastroenterology, Critical Care, Oncopathology and Interventional Radiology
- ❖ **Master of Chirurgiae (M.Ch)** in Surgical Oncology, Gynecological Oncology, Plastic Surgery & Reconstructive Surgery, Head & Neck Oncology

Two years Certified Fellowship Programmes in Medical & Health Sciences offered at TMC are listed below:

Post-MD fellowship program is offered with specialization in Orthopedic Oncology, Breast Oncology, Thoracic Oncology, Uro Oncology, Interventional Oncology, Surgical Pathology, Haemato Pathology, Dental & Prosthetic Surgery, Preventive Oncology, Infectious Diseases & HIV Medicine, Gastrointestinal Oncology, Pulmonary Oncology, Molecular Haemato Oncology, Oral Oncology with Reconstructive Surger

Post Graduate Courses in Medical & Health Sciences at TMC include:

- ❖ **MD** (Pathology, Anesthesia, Radio-diagnosis, Radiation Oncology, Microbiology, Nuclear Medicine, Palliative Medicine, Immuno-Hematology & Transfusion Medicine and in Nuclear Medicine).
- ❖ **M.Sc. (Nursing), M.Sc. (Clinical research), M.Sc. (Public Health in Epidemiology) and M.Sc. (Occupational Therapy in Oncology)** programmes are offered at TMC.
- ❖ **M.Sc. (Nuclear Medicine and Molecular Imaging Technology)** is offered at TMC & Radiation Medicine Centre of BARC.
- ❖ **M.Sc. (Hospital Radiopharmacy)** is offered at Radiation Medicine Centre of BARC.

Post Graduate Courses in Medical & Health Sciences at RMC-BARC:

- ❖ **M.D. (Nuclear Medicine)**
- ❖ **M.Sc. (Nuclear Medicine and Molecular Imaging Technology)**

PG Diploma at TMC:

- ❖ **Fusion Imaging Technology (PGDFIT)**

PG Diploma Courses at BARC:

- ❖ **Diploma in Radiological Physics (DipRP)**
- ❖ **Diploma in Medical Radio Isotope Techniques (DMRIT)**
- ❖ **Diploma in Nuclear Science and Engineering (DipNSE)**

Management of HBNI

The **Council of Management** chaired by Secretary, DAE is the apex body for the management of HBNI. **Academic Council** chaired by Vice Chancellor, HBNI manages the academic issues and functions on the advice of the **Board of Studies** which has been constituted for each major discipline and has representatives from all CIs and OCC as well as experts from other reputed Indian institutes. To manage the affairs of the HBNI, each CI has one or more **Deans-Academic. Standing Committee of Deans chaired by VC, HBNI** and comprising of Dean, HBNI, Associate Deans at HBNI, Deans (Academic) from all the institutions, ensures harmony in the processes. CIs have also established a robust framework of admission by **Standing Academic Committee**.

The Council of Management is the prime body for the management of the Institute.

Council of Management (CoM)
(As on August 1, 2022)

Shri K. N. Vyas, Secretary DAE & Chairman, AEC	Chairman
Prof. P. R. Vasudeva Rao, Vice Chancellor	Member
Shri Talleen Kumar, Member (Finance), AEC	Member
Prof. A. K. Mohanty, Director, BARC	Member
Prof. B. Venkatraman, Director, IGCAR	Member
Prof. R. A. Badwe, Director, TMC	Member
Prof. Sudhakar Panda, Director, NISER	Member
Prof. Surendra Prasad, Former Chairman NBA & Former Director, IIT Delhi	Member
Prof. Mustansir Barma, Professor Emeritus, TIFR Centre For Inter-Disciplinary Sciences, Hyderabad	Member
Shri S. S. Sandhu, IAS, Additional Secretary, Department of Higher Education, MHRD, New Delhi	Member
Prof. P. D. Naik, Dean, HBNI	Member
Prof. P. C. Selvin, Registrar, HBNI	Secretary

Academic Council**(As on August 1, 2022)**

Prof. P. R. Vasudeva Rao, Vice Chancellor	Chairperson
Prof. A. K. Mohanty, Director, BARC	Member
Prof. B. Venkatraman, Director, IGCAR	Member
Prof. R. A. Badwe, Director, TMC	Member
Prof. Sudhakar Panda, Director, NISER	Member
Prof. S. M. Yusuf, Director, IoP	Member
Shri S. V. Nakhe, Director, RRCAT	Member
Dr. Sumit Som, Director, VECC	Member
Prof. Shashank Chaturvedi, Director, IPR	Member
Prof. Gautam Bhattacharyya, Director, SINP	Member
Prof. Pinaki Majumdar, Director, HRI	Member
Prof. V. Arvind/Prof. V. Ravindran, Director, IMSc	Member
Prof. Indranil Manna, IIT Kharagpur	Member
Prof. Kannan N. Iyer, IIT Bombay	Member
Prof. E. D. Jemmis, IISc, Bangalore	Member
Prof. Shishir Deshpande, Director, ITER-IPR	Member
Prof. P. K. Pujari/Prof. Vivekanand Kain, BARC	Member
Prof. P. D. Naik, Dean, HBNI	Member
Prof. R. B. Grover, Convenor, BoS (Applied Systems Analysis)	Member
Prof. S. M. Yusuf, Convenor, BoS (Physical Sciences)	Member
Prof. A. P. Tiwari, Convenor, BoS (Engineering Sciences)	Member
Prof. Prasanna Venkatraman, Convenor, BoS (Life Sciences)	Member
Prof. Meena Mahajan, Convenor, BoS (Mathematical Sciences)	Member
Prof. S. D. Banavali, Convenor, BoS (Medical & Health Sciences)	Member
Prof. S. Kannan, Convenor, BoS (Chemical Sciences)	Member
Prof. Bedangadas Mohanty, Convenor, BoS (Integrated Masters Programme)	Member
Prof. P. C. Selvin, Registrar, HBNI	Secretary

Advisory Committee

Advisory Committee	
Secretary, DAE and Chairman, AEC	Chairman
Vice Chancellor, HBNI	Member
Director, BARC	Member
Director, IGCAR	Member
Director, RRCAT	Member
Director, VECC	Member
Director, IPR	Member
Director, SINP	Member
Director, TMC	Member
Director, IMSc	Member
Director, TIFR	Member
Director, NISER	Member
Director, HRI	Member
Director, IOP	Member
Dean, HBNI	Member-Secretary

Officers of the Institute

(As on August 1, 2022)

Academic		Administrative	
Prof. P. R. Vasudeva Rao	Vice Chancellor	Dr. P. C. Selvin	Registrar
Prof. B. K. Dutta	Institute Chair Professor	Smt. Bharati Suwarna	Administrative Officer-III
Prof. B. S. Tomar	Institute Chair Professor	Smt. Neeta Rathod	Assistant Registrar
Prof. D. K. Maity	Associate Dean	Shri Shailash Jakhotia	Finance Officer
Prof. A. K. Dureja	Associate Dean		
Prof. B. K. Nayak	Associate Dean		
Prof. H. Pal	Associate Dean		
Prof. Sunil Ghosh	Associate Dean		

Board of Studies of HBNI

(As on August 1, 2022)

❖ BoS (Chemical Sciences)	
1. Prof. S. Kannan, BARC - Convener	
2. Prof. A. K. Tyagi, BARC - Co-Convener	
3. Prof. A. Dutta, IIT, Bombay	
4. Prof. A. Srinivasan, NISER	
5. Prof. D. K. Maity, HBNI	
6. Prof. N. Sivaraman, IGCAR	
7. Prof. P. K. Mohapatra, BARC	
8. Prof. H. S. Biswal, NISER	
9. Prof. Deepa Khushalani, TIFR	
10. Prof. Avinash Kumbhar, SPPU	
Balancing Members:	
1. Prof. K. S. Bindra, RRCAT	
2. Prof. S. Santoshkumar, BARC	
❖ BoS (Engineering Sciences)	
1. Prof. A. P. Tiwari, BARC-Convener	
2. Prof. V. Kain, BARC- Co-Convener	
3. Prof. Archana Sharma, BARC	
4. Prof. V. G. Gaikar, ICT	
6. Prof. J. Chattopadhyay, BARC	
7. Prof. C. P. Paul, RRCAT	
8. Prof. Paramita Mukherjee, VECC	
9. Prof. S. K. Pathak, IPR	
10. Prof. R. Divakar, IGCAR	
Balancing Members:	
1. Prof. Jane Alam, VECC	
2. Prof. A. K. Dureja, HBNI	
3. Prof. A. K. Nayak, BARC	
❖ BoS (Medical & Health Sciences)	
1. Prof. S. D. Banavali, TMC – Convener	
2. Prof. Sandeep Basu, RMC-Co-Convener	
3. Prof. Sudeep Gupta, Director ACTREC, TMC	
4. Dr. Nithya Gogte, KEM Hospital, Mumbai	
5. Dr. Ashutosnath Agarwal, PGIMER, Chandigarh	
6. Dr. Manisha Pawar, TMH	
7. Prof. Siddhartha Laskar, TMC	
8. Dr. Ajay Puri, TMC	
9. Dr. J. P. Agarwal, TMC	
10. Dr. Suyash Kulkarni, TMC	
Balancing Members:	
1. Dr. Rajesh Kinhikar, TMC	
2. Prof. A. K. Dureja, HBNI	
❖ BoS (Life Sciences)	
1. Prof. Prasanna Venataraman, Dy. Director, ACTREC - Convener	
2. Prof. Partha Saha, Sr. Professor, SINP - Co-Convener	
3. Prof. Praful Singru, SBS, NISER	
4. Prof. Rahul Siddharthan, IMSc	
5. Prof. Rajiv Sarin, ACTREC	
6. Prof. Harapriya Mohapatra, NISER	
7. Prof. S. Santoshkumar, BARC	
8. Prof. S. Gautam, BARC	
9. Prof. Hema Rajaram, BARC	
10. Prof. Sharmila Bapat, NCCS, Pune	
Balancing Members:	
1. Prof. D. K. Maity, HBNI	
2. Prof. Sunil Ghosh, HBNI	
❖ BoS (Mathematical Sciences)	
1. Prof. Meena Mahajan, IMSc - Convener	
2. Prof. D. Surya Ramana, HRI Co-Convener	
3. Prof. Anish Ghosh, TIFR, Mumbai	
4. Prof. Mahuya Datta, ISI, Kolkata	
5. Prof. Jugal K. Verma, IIT Bombay	
6. Prof. B. Sury, ISI, Bengaluru	
7. Prof. K. N. Raghavan, IMSc	
8. Prof. K. V. Subrahmanyam, CMI-Chennai	
9. Prof. Brundaban Sahu, NISER	
Balancing Members:	
1. Prof. Sudhir Jain, BARC	
2. Prof. B. K. Nayak, HBNI	
❖ BoS (Physical Sciences)	
1. Prof. S. M. Yusuf, BARC-Convener	
2. Prof. Jane Alam, VECC-Co-Convener	
3. Prof. Anushman Maharana, HRI	

4. Prof. Sandip Kumar Dhara, IGCAR
5. Prof. D. Indumathi, IMSc
6. Prof. Shikha Varma, IoP
7. Prof. Sudip Sengupta, IPR
8. Prof. B. Mohanty, NISER
9. Prof. K. S. Bindra, RRCAT
10. Prof. Kumar Sankar Gupta, SINP
Balancing Members:
1. Prof. Saibal Basu, HBNI
2. Prof. A. K. Tyagi, BARC
❖ BoS (Applied Systems Analysis)
1. Prof. R. B. Grover, HBNI-Convener
2. Prof. Pranay Swain, NISER Co-Convener
3. Prof. Karuna Jain, IIT Bombay
4. Prof. G. Ravikumar, BARC
5. Prof. Surinder Jaswal, TISS
6. Prof. S. Kannan, BARC
7. Prof. B Raja Shekhar, Pro-Vice Chancellor, University of Hyderabad
Balancing Members:
1. Prof. A. K. Dureja, Associate Dean, HBNI

❖ BoS (Integrated Masters Programme)
1. Prof. Bedangadas Mohanty, NISER - Convener
2. Prof. Pranay Swain, NISER – Co- Convener
3. Chair, School of Life Sciences, NISER (Ex-Officio)
4. Chair, School of Chemical Sciences, NISER (Ex-Officio)
5. Chair, School of Mathematics, NISER (Ex-Officio)
6. Chair, School of Physical Sciences, NISER (Ex-Officio)
7. Chair, School of Undergraduate Studies Committee, NISER (Ex-Officio)
8. Prof. Anirban Basu, HRI
9. Prof. B. R. Sekhar, IoP
10. Prof. Sujit Roy, IIT Bhubaneswar
Balancing Members:
1. Prof. B. S. Tomar, HBNI
2. Prof. Meena Mahajan
3. Prof. Partha Saha

Deans Academic at Constituent Institutions (CIs)/Off-Campus Centre (OCC)

(As on August 1, 2022)

S. No.	Name of the CI/Off-campus centre	Discipline	Name of the Dean Academic
1.	Bhabha Atomic Research Centre	Life Sciences	Prof. Hema Rajaram
		Chemical Sciences	Prof. Tapan Kumar Ghanty
		Physical & Mathematical Sciences	Prof. Dinesh Udupa
		Engineering Sciences Stream-I	Prof. Raghavendra Tewari
		Engineering Sciences Stream-II	Prof. S. Mukhopadhyay
		Health Sciences	Prof. Sandip Basu
2.	Indira Gandhi Centre for Atomic Research	Chemical Sciences	Prof. C. V. S. B. Rao
		Physical Sciences	Prof. Awadesh Mani
		Engineering Sciences	Prof. Anish Kumar
3.	Raja Ramanna Centre for Advanced Technology	All Disciplines	Prof. Arup Banerjee
4.	Variable Energy Cyclotron Centre	Physical Sciences	Prof. Parnika Das
		Engineering Sciences	Prof. Sarbajit Pal
5.	Saha Institute of Nuclear Physics	Chemical & Life Sciences	Prof. Partha Saha
		Physical Sciences	Prof. Prakash Mathews
6.	Institute for Plasma Research	All Disciplines	Prof. Sudip Sengupta
7.	Institute of Physics	Physical Sciences	Prof. Pankaj Agrawal
8.	Institute of Mathematical Sciences	Mathematical Sciences	Prof. Vijay Kodyalam
		Physical Sciences	Prof. S. Vemparala
		Life Sciences	Prof. Sitabhra Sinha
9.	Harish-Chandra Research Institute	All Disciplines	Prof. Prasenjit Sen
10.	Tata Memorial Centre	All Disciplines	Prof. Shripad Banavali
11.	National Institute of Science Education and Research	All Disciplines	Prof. Pranay Swain

List of Faculty Members

(As on August 1, 2022)

HBNI	
1.	Prof. P. R. Vasudeva Rao
2.	Prof. Prakash Dattatray Naik
3.	Prof. Ravi Bhushan Grover
4.	Prof. Jyeshtharaj Bhalchandra Joshi
5.	Prof. Bijon Kumar Dutta
6.	Prof. B. S. Tomar
7.	Prof. Haridas Pal
8.	Prof. Sunil Kumar Ghosh
9.	Prof. Dilip K. Maity
10.	Prof. Adarsh Kumar Dureja
11.	Prof. Basanta Kumar Nayak
BARC	
❖ Chemical Sciences	
12.	Prof. A. K. Mohanty
13.	Prof. A. K. Tyagi
14.	Prof. Alok Kumar Ray
15.	Prof. Arya Ashok Kumar
16.	Prof. Awadhesh Kumar
17.	Prof. Chetan Prakash Kaushik
18.	Prof. Lalit Varshney
19.	Prof. Pradeep Kumar Pujari
20.	Prof. Prasanta Kumar Mohapatra
21.	Prof. S. Kannan
22.	Prof. Sharmila Banerjee
23.	Prof. Tapan Kumar Ghanty
24.	Prof. A. K. Tripathi
25.	Prof. A. L. Rufus
26.	Prof. A. C. Bhasikuttan
27.	Prof. A. C. Sahayam
28.	Prof. Ashok Kumar Pandey
29.	Prof. Chiranjib Majumder
30.	Prof. Ghasi Ram Dey
31.	Prof. Hari Prasad Upadhyaya
32.	Prof. P. A. Hassan
33.	Prof. Hirendra Nath Ghosh
34.	Prof. K. Dash
35.	Prof. Niharendu Choudhury
36.	Prof. Patra Chandra Nath
37.	Prof. R. Mishra

38.	Prof. Raghunath Acharya
39.	Prof. Rajesh V. Pai
40.	Prof. Rakesh Kumar Singhal
41.	Prof. S. K. Jha
42.	Prof. S. N. Achary
43.	Prof. Sangita D Kumar
44.	Prof. Sanjiv Kumar
45.	Prof. Soumyakanti Adhikari
46.	Prof. Sreenivas T.
47.	Prof. Subir Kumar Ghosh
48.	Prof. Sudarsan V.
49.	Prof. Sukhendu Nath
50.	Prof. Suresh C. Parida
51.	Prof. Tusar Bandyopadhyay
52.	Prof. Y K Bhardwaj
53.	Dr. A Jahur Mondal
54.	Dr. Adya Prasad Mishra
55.	Dr. Ajay K. Singh
56.	Dr. Anshu Singhal
57.	Dr. Anupkumar B.
58.	Dr. Aparna Banerjee
59.	Dr. Aruna Korde
60.	Dr. Arunasis Bhattacharyya
61.	Dr. Ashis Kumar Satpati
62.	Dr. Asim Kumar Ghosh
63.	Dr. Dayamoy Banerjee
64.	Dr. Dhandeep Dutta
65.	Dr. Dhurva Kumar Singh
66.	Dr. Dimple Dutta
67.	Dr. Drishty Satpati
68.	Dr. Faby Sunny
69.	Dr. Hemant Shivram Sodaye
70.	Dr. Jayshree Ramkumar
71.	Dr. Jyotirmayee Mohanty
72.	Dr. Kallola Kumar Swain
73.	Dr. Kedarnath G.
74.	Dr. Kumar Abhinav Dubey
75.	Dr. M. C. Rath
76.	Dr. M. S. Murali
77.	Dr. Madhava B Mallia

78.	Dr. Madhumita Goswami
79.	Dr. Mainak Roy
80.	Dr. Manidipa Basu
81.	Dr. Manoj Kumbhakar
82.	Dr. Mrinal R. Pai
83.	Dr. Musharaf Ali S. K.
84.	Dr. N. N. Meeravli
85.	Dr. Naina Raje
86.	Dr. Nandita Maiti
87.	Dr. Neetika Rawat
88.	Dr. P. S. Ramanjaneyulu
89.	Dr. P. Mathi
90.	Dr. Pradeep Kumar
91.	Dr. Pramod Sharma
92.	Dr. R. Ganguly
93.	Dr. Rahul Tripathi
94.	Dr. Ritu M Srivastava
95.	Dr. S. Jayakumar
96.	Dr. Salil Varma
97.	Dr. Sandeep Nigam
98.	Dr. Sandip Dey
99.	Dr. Sanjukta A Kumar
100.	Dr. Sharmishtha Dutta Choudhury
101.	Dr. Shilpa N Sawant
102.	Dr. Suchandra Chatterjee
103.	Dr. Suchismita Mishra
104.	Dr. Sudarshan Kathi
105.	Dr. Sumit Kumar
106.	Dr. Suparna Sodaye
107.	Dr. Tapas Das
108.	Dr. Tirumalesh Keesari
109.	Dr. Usha Pandey
110.	Dr. Vandana Pulhani
111.	Dr. Vinita Grover Gupta
112.	Dr. Virendra Kumar
113.	Dr. Aishwarya Soumitra Kar
114.	Dr. Ajish Kumar K. S.
115.	Dr. Amit Kunwar
116.	Dr. Ankita Rao
117.	Dr. Apurav Guleria
118.	Dr. Arijit Sengupta
119.	Dr. Arnab Sarkar
120.	Dr. Arup Kumar Pathak
121.	Dr. Atanu Barik

122.	Dr. Atindra Banerjee
123.	Dr. Balaji Prasad Mandal
124.	Dr. Beena G. Singh
125.	Dr. Brindaban Modak
126.	Dr. Chhavi Agarwal
127.	Dr. Dibakar Goswami
128.	Dr. Gunjan Verma
129.	Dr. J. Selvakumar
130.	Dr. Jayashree Biswal
131.	Dr. Jyoti Prakash
132.	Dr. K. C. Barick
133.	Dr. K. R. S. Chandrakumar
134.	Dr. Kaustava Bhattacharyya
135.	Dr. Mahesh Sundararajan
136.	Dr. Malaya Kumar Nayak
137.	Dr. Manjulata Saha
138.	Dr. Manoj Mohapatra
139.	Dr. Manoj Kumar Sharma
140.	Dr. Mhejabeen Sayed
141.	Dr. Mohini Gurelia
142.	Dr. Nilotoal Barooah
143.	Dr. N. R. Singh
144.	Dr. Pankaj Kumar Patro
145.	Dr. Prabhat Kumar Singh
146.	Dr. Prasad Padmakar Phadnis
147.	Dr. Priya Maheshwari
148.	Dr. Raghunath Chowdhury
149.	Dr. Ritesh Ruhela
150.	Dr. Rubel Chakravarty
151.	Dr. Ruma Gupta
152.	Dr. Sajeev Y.
153.	Dr. Sandeep Kumar Sharma
154.	Dr. Sangita D. Lenka
155.	Dr. Sanhita Chaudhury
156.	Dr. Sanjay Kumar
157.	Dr. Santosh Kumar Gupta
158.	Dr. Saurav Kumar Guin
159.	Dr. Seemita Banerjee
160.	Dr. Seraj Ahmad Ansari
161.	Dr. Sipra Choudhury
162.	Dr. Soumyaditya Mula
163.	Dr. Srinivasu Kancharlapalli
164.	Dr. Sumana Sengupta
165.	Dr. Surajit Panja

❖ Engineering Sciences	
166.	Prof. Akhilanand Pati Tiwari
167.	Prof. Anup Kumar Bhattacharjee
168.	Prof. Archana Sharma
169.	Prof. Arun Kumar Nayak
170.	Prof. Deb Mukhopadhyay
171.	Prof. Gopal Joshi
172.	Prof. Gopalakrishnan Sugilal
173.	Prof. Jayanta Chattaopadhyay
174.	Prof. N. K. Maheshwari
175.	Prof. Prabhakar V. Varde
176.	Prof. Raghvendra Tewari
177.	Prof. Ram Nivas Singh
178.	Prof. Siddaratha Mukhopadhyay
179.	Prof. Soumitra Kar
180.	Prof. Vivekanand Kain
181.	Prof. A. Vinod Kumar
182.	Prof. Alok Awasthi
183.	Prof. Amit Sinha
184.	Prof. Aniruddha Biswas
185.	Prof. Anita Vinay Topkar
186.	Prof. Biswaranjan Dikshit
187.	Prof. D. Mandal
188.	Prof. D. C. Kar
189.	Prof. Deep Prakash
190.	Prof. Dinesh Kumar Chandraker
191.	Prof. Gopika Vinod
192.	Prof. Joydipta Banerjee
193.	Prof. Jung Bahadur Singh
194.	Prof. Kapilesh Bhargava
195.	Prof. Kulwant Singh
196.	Prof. M. K. Samal
197.	Prof. Namita Maiti
198.	Prof. R. K. Bajpai
199.	Prof. Rajeev Kapoor
200.	Prof. S. K. Satpati
201.	Prof. S. R. Shimijith
202.	Prof. Samiran Sengupta
203.	Prof. Sujay Bhattacharya
204.	Prof. Sulekha Mukhopadhyay
205.	Prof. Supratik Roychowdhury
206.	Prof. Tarasankar Mahata
207.	Prof. Tessa Vincent
208.	Prof. V. H. Patankar

209.	Prof. Yogita Parulekar
210.	Dr. Abhijeet Mohan Vaidya
211.	Dr. Anil Kumar Tiwari
212.	Dr. Anindya Chakravarty
213.	Dr. Arijit Laik
214.	Dr. Betty C. A.
215.	Dr. C. B. Basak
216.	Dr. Chiradeep C Gupta
217.	Dr. Debanik Roy
218.	Dr. Gaurav Bhutani
219.	Dr. Imran Ali Khan
220.	Dr. K. K. Singh
221.	Dr. Kamal Sharma
222.	Dr. Kinshuk Dasgupta
223.	Dr. Maha Nand Jha
224.	Dr. Noble Jacob
225.	Dr. Onkar Suresh Gokhale
226.	Dr. Pranesh Sengupta
227.	Dr. Praveen Kumar
228.	Dr. R Karthikeyan
229.	Dr. Ranjan Kumar
230.	Dr. Rishi Verma
231.	Dr. Sangita Pal
232.	Dr. Sanjib Majumdar
233.	Dr. Sudipta Chakraborty
234.	Dr. Suman Neogy
235.	Dr. Suneel Kumar Gupta
236.	Dr. Surender Kumar Sharma
237.	Dr. T. Sree Rama Chandra Murthy
238.	Dr. Vishwanadh Bathula
❖ Life Sciences	
239.	Prof. V. P. Venugopalan
240.	Prof. B. N. Pandey
241.	Prof. Birajalaxmi Das
242.	Prof. Briija Sankar Patro
243.	Prof. Hari S. Misra
244.	Prof. Hema Rajaram
245.	Prof. Prasun Kumar Mukherjee
246.	Prof. Sandur Santosh Kumar
247.	Prof. Sanjay J. Jambhulkar
248.	Prof. Satyendra Gautam
249.	Prof. Savita Kulkarni
250.	Prof. T. R. Ganapathi
251.	Prof. Toleti Subba Rao

252.	Prof. Y. V. Nancharaiah
253.	Dr. Ajay Saini
254.	Dr. Anand D Ballal
255.	Dr. Anand M Badigannavar
256.	Dr. Anu Ghosh
257.	Dr. Archana Mukherjee
258.	Dr. Archana Joshi Saha
259.	Dr. B. K. Das
260.	Dr. Bhakti Basu
261.	Dr. Bhavani S. Shankar
262.	Dr. Deepak Sharma
263.	Dr. Gagan Deep Gupta
264.	Dr. J. Souframanien
265.	Dr. Joy G. Manjaya
266.	Dr. Mahesh Subramanian
267.	Dr. Nagesh Bhat
268.	Dr. R. Shashidhar
269.	Dr. Rajani Kant Chittela
270.	Dr. Rajesh Kumar
271.	Dr. Ramesh Hire
272.	Dr. Rath Devashish
273.	Dr. Ravindra D Makde
274.	Dr. S. N. Jamdar
275.	Dr. S. P. Chawla
276.	Dr. Sheetal Uppal
277.	Dr. Sudhir Singh
278.	Dr. Vishwas M Kulkarni
279.	Dr. Amit Das
280.	Dr. Amit Kumar
281.	Dr. Archana N. Rai
282.	Dr. Aruna Jyothi Kora
283.	Dr. Ashish Kumar Srivastava
284.	Dr. Avik Chakraborty
285.	Dr. Bhaskar Sanyal
286.	Dr. Bibhuti Bhusan Mishra
287.	Dr. Celin Acharya
288.	Dr. Dharmendra Kumar Maurya
289.	Dr. Himanshi N Mishra
290.	Dr. Hiren Joshi
291.	Dr. Jitendra Kumar
292.	Dr. Manisha Banerjee
293.	Dr. Murali M S Balla
294.	Dr. P Sriyutha Murthy
295.	Dr. Rachna Agarwal

296.	Dr. Rahul Checkar
297.	Dr. S. T. Mehetre
298.	Dr. Sachin Nandkumar Hajare
299.	Dr. Shraddha Singh
300.	Dr. Sonia Chadha
301.	Dr. Subhash Chandra Bihani
302.	Dr. Sudhir Kumar Gupta
303.	Dr. Sumit Gupta
304.	Dr. Suwendu Mondal
305.	Dr. Swathi Kota
306.	Dr. Sweetie R Kanatt
307.	Dr. Vandan Nagar
308.	Dr. Yogendra Singh Rajpurohit
❖ Medical & Health Sciences	
309.	Prof. A. J. Khandekar
310.	Prof. Anita Gadgil
311.	Prof. Gaurav Malhotra
312.	Prof. R. V. Jadhav
313.	Dr. Rahul Vithalrao Parghane
314.	Prof. Sandip Basu
315.	Dr. Ashwini Kalshetty
316.	Dr. J. G. Kalbhande
317.	Dr. Priyanka Verma
318.	Dr. Satish C. Mishra
319.	Dr. Sunil Dutta Sharma
320.	Dr. Sunita Nitin Sonavane
321.	Dr. Sushmita Rath
322.	Dr. Yogesh K. Shejul
323.	Dr. Basant L. Malpani
❖ Physical Sciences	
324.	Prof. Dinesh Kumar Aswal
325.	Prof. Kannan Umasankari
326.	Prof. S. M. Yusuf
327.	Prof. Srinivas Krishnagopal
328.	Prof. Vinay Bhaskar Chandratre
329.	Prof. A. K. Debnath
330.	Prof. A. K. Gupta
331.	Prof. Abhas Kumar Mitra
332.	Prof. Aditi Ray
333.	Prof. Alka B. Garg
334.	Prof. Amitabh Das
335.	Prof. Aniruddha Kumar
336.	Prof. Anurag Gupta
337.	Prof. Aradhana Shrivastava

338.	Prof. B. K. Sapra
339.	Prof. B. N. Rajasekhar
340.	Prof. Bency V. John
341.	Prof. D. M. Gaitonde
342.	Prof. Debabrata Biswas
343.	Prof. Debasis Sen
344.	Prof. Dibyendu Bhattacharyya
345.	Prof. Dinesh Venkatesh Udupa
346.	Prof. Dipanwita Dutta
347.	Prof. Divakar K Rao
348.	Prof. J. Padma Nilaya
349.	Prof. K. K. Yadav
350.	Prof. Keshaw D. Joshi
351.	Prof. Lalit Mohan Pant
352.	Prof. Lavanya M. Ramaniah
353.	Prof. M. V. Suryanarayana
354.	Prof. Mala N Rao
355.	Prof. Mukesh Kumar
356.	Prof. Mukund Shrinivas Kulkarni
357.	Prof. N. Padma
358.	Prof. Nandini Garg
359.	Prof. P U Sastry
360.	Prof. Prashant Shukla
361.	Prof. Ranjan Mittal
362.	Prof. Rekha Rao
363.	Prof. S G Nakhate
364.	Prof. Satyaranjan Santra
365.	Prof. Shambhu Nath Jha
366.	Prof. Srikumar Ghorui
367.	Prof. Subhankur Mitra
368.	Prof. Sudhir Ranjan Jain
369.	Prof. T Palani Selvam
370.	Prof. V. K. Aswal
371.	Dr. A. K. Rajarajan
372.	Dr. Ajay Singh
373.	Dr. Ajay Kumar Mishra
374.	Dr. Amitava Roy
375.	Dr. Anil Kumar Chauhan
376.	Dr. Aparna Shastri
377.	Dr. Arup Biswas
378.	Dr. Asavari Santosh Dhavale
379.	Dr. Asawari D Rath
380.	Dr. Ashok Kumar Bakshi
381.	Dr. Ashok Kumar Verma

382.	Dr. Bhushan Dhabekar
383.	Dr. Bidyut Jyoti Roy
384.	Dr. Biplab Ghosh
385.	Dr. Brahmananda Chakraborty
386.	Dr. C. D. Sijoy
387.	Dr. Chitra Murli
388.	Dr. D. R. Mishra
389.	Dr. Debarati Bhattacharya
390.	Dr. G. Sridhar
391.	Dr. Himanshu Kumar Poswal
392.	Dr. Jayanta Mondal
393.	Dr. Keka R. Chakraborty
394.	Dr. Kripamay Mahata
395.	Dr. Manoj Kumar Warriar
396.	Dr. Mayank Shukla
397.	Dr. Munish Kumar
398.	Dr. Paritosh Modak
399.	Dr. Partha Sarathi Sarkar
400.	Dr. Prakash Chandra Rout
401.	Dr. Pratap Baburao Wagh
402.	Dr. Priyamvada M. Dighe
403.	Dr. Raghwendra Kumar
404.	Dr. Rajeev Kumar
405.	Dr. Ramesh Chandra Das
406.	Dr. Renju George Thomas
407.	Dr. Rohit Shukla
408.	Dr. S. Anand
409.	Dr. Sanjay Kumar Sahu
410.	Dr. Sanjay V. Thakare
411.	Dr. Santanu Bera
412.	Dr. Shashwati Sen Yeram
413.	Dr. Soumen Bhattacharyya
414.	Dr. Subir Bhattacharyya
415.	Dr. Sukanta Karmakar
416.	Dr. Surendra Singh
417.	Dr. Swapan Das
418.	Dr. Swarupananda Pradhan
419.	Dr. T. Jayasekharan
420.	Dr. V Jha
421.	Dr. Venkata Ramana Ikkurthi
422.	Dr. Vinod Singh Rawat
423.	Dr. Vir Krishen Dhar
424.	Dr. Yogesh Kashyap
425.	Dr. Amit Kumar

426.	Dr. Amit Verma
427.	Dr. Amit P Srivastava
428.	Dr. Anil Jain
429.	Dr. Anup Kumar Bera
430.	Dr. Apu Sarkar
431.	Dr. B. Sunder Sahayanathan
432.	Dr. Babita Tiwari
433.	Dr. C. L. Prajapat
434.	Dr. Debjani Karmakar
435.	Dr. Goutam Dev Mukherjee
436.	Dr. H. Kumawat
437.	Dr. Himal Bhatt
438.	Dr. Jitendra Bahadur
439.	Dr. Kiran R. M.
440.	Dr. Krishna Kumar Singh
441.	Dr. Manmeet Kaur
442.	Dr. Mayanak Kumar Gupta
443.	Dr. Mohit Tyagi
444.	Dr. Niranjan Suryakant Ramgir
445.	Dr. Nishant Chaudhary
446.	Dr. Pramod Bhatt
447.	Dr. Purushottam Jha
448.	Dr. Rajib Kar
449.	Dr. Ranita Basu
450.	Dr. Rosaline Mishra
451.	Dr. S. P. Tripathy
452.	Dr. Sanjay Kumar Mishra
453.	Dr. Shankar Prasad Koiry
454.	Dr. Shiv Govind Singh
455.	Dr. Shivanand Chaurasia
456.	Dr. Shovit Bhattacharya
457.	Dr. Somsundar Mukhopadhyay
458.	Dr. Sugam Kumar
459.	Dr. Sunit Kedia
460.	Dr. V. V. Parkar
461.	Dr. Veerendra Kumar Sharma
462.	Dr. Vibha Saxena
463.	Dr. Vinayak Mishra
464.	Dr. Yogesh K Gupta
IGCAR	
❖ Chemical Sciences	
465.	Prof. A. Suresh
466.	Prof. K. Ananthasivan

467.	Prof. K. A. Venkatesan
468.	Prof. N. Sivaraman
469.	Prof. R. V. Subbarao
470.	Prof. R. Kumar
471.	Prof. Rajesh Ganesan
472.	Prof. V. Jayaraman
473.	Dr. C. V. S. Brahmmananda Rao
474.	Dr. Durairaj Onraju
475.	Dr. K. Sundararajan
476.	Dr. K. I. Gnanasekar
477.	Dr. Puspallata Rajesh
478.	Dr. Sublime Ningshen
479.	Dr. A. Sree Rama Murthy
480.	Dr. Arindam Das
481.	Dr. Ashish Jain
482.	Dr. B. Anandkumar
483.	Dr. Chowdari Jagadeeswara Rao
484.	Dr. Hrudananda Jena
485.	Dr. N. Ramanathan
486.	Dr. Pavan Kumar Narayanam
487.	Dr. R. Kumaresan
488.	Dr. R Venkata Krishnan
489.	Dr. Satendra Kumar
❖ Engineering Sciences	
490.	Prof. Arun Kumar Bhaduri
491.	Prof. B. P. C. Rao
492.	Prof. A. John Arul
493.	Prof. Aniruddha Moitra
494.	Prof. Anish Kumar
495.	Prof. M. Vasudevan
496.	Prof. V. Karthik
497.	Dr. A. Nagesha
498.	Dr. A. Jasmin Sudha
499.	Dr. C. Sudha
500.	Dr. Chitta Ranjan Das
501.	Dr. Mahadevan S.
502.	Dr. P Mangarjuna Rao
503.	Dr. R. Mythili
504.	Dr. V. S Srinivasan
505.	Dr. Vani Shankar
506.	Dr. A. Ravi Shankar
507.	Dr. David Vijayanand V
508.	Dr. Diptimayee Samantaray
509.	Dr. G. V. Prasad Reddy

❖ Physical Sciences
510. Prof. G. Amarendra
511. Prof. Ramachandran Divakar
512. Prof. Awadhesh Mani
513. Prof. John Philip
514. Prof. K. Devan
515. Prof. N. Subramanian
516. Prof. N. V. Chandra Shekar
517. Prof. R. Govindaraj
518. Prof. R. Rajaraman
519. Prof. Sandip Kumar Dhara
520. Prof. T. R. Ravindran
521. Dr. Arup Dasgupta
522. Dr. B. Sundaravel
523. Dr. C. Venkata Srinivas
524. Dr. G. Mangamma
525. Dr. Nithya Ravindran
526. Dr. Parthasarathi Gangopadhyay
527. Dr. R. Krishnan
528. Dr. R. Ramaseshan
529. Dr. R. Venkatesan
530. Dr. S. Amirthapandian
531. Dr. S. Ganesamoorthy
532. Dr. S. Tripura Sundari
533. Dr. Sharat Chandra
534. Dr. Tom Mathews
535. Dr. V. Sivasubramanian
536. Dr. V. Subramanian
537. Dr. Amit Kumar
538. Dr. Anees P.
539. Dr. Arun K. Prasad
540. Dr. Barid Baran Lahiri
541. Dr. Dipak Kumar Baisnab
542. Dr. Edward Prabu Amaladass
543. Dr. K. Ganesan
544. Dr. K. Prabhakar
545. Dr. N. R. Sanjay Kumar
546. Dr. O. Annalakshmi
547. Dr. Rajendra Ganpat Joshi
548. Dr. Ramanathaswamy Pandian
549. Dr. Ravi Chinnappan
550. Dr. S. Abhaya
551. Dr. S. C. Vanithakumari

552. Dr. Syamalarao Polaki
553. Dr. Vinod K.
RRCAT
❖ Chemical Sciences
554. Dr. Dipankar Nanda
❖ Engineering Sciences
555. Prof. Christ Prakash Paul
556. Dr. Prabhat Kumar Gupta
557. Dr. Rahul Shukla
❖ Life Sciences
558. Prof. Alok Dube
❖ Physical Sciences
559. Prof. Kushvinder Singh Bindra
560. Prof. Alka A Ingale
561. Prof. Anand Moorti
562. Prof. Aparna Chakrabarti
563. Prof. Arup Banerjee
564. Prof. J. A. Chakera
565. Prof. Mohammed Hussein Modi
566. Prof. Mukesh Joshi
567. Prof. Om Prakash
568. Prof. Sanjay Kumar Rai
569. Prof. Satya Ram Mishra
570. Prof. Shovan K Majumder
571. Prof. Sudhir Kumar Dixit
572. Prof. Tapas Ganguli
573. Prof. Tarun Kumar Sharma
574. Prof. Vinit Kumar
575. Dr. Arvind Kumar Srivastava
576. Dr. Avnish K Sharma
577. Dr. Brahma Nand Upadhyaya
578. Dr. Chandrachur Mukherjee
579. Dr. Gurvinderjit Singh
580. Dr. Haranath Ghosh
581. Dr. Indranil Bhaumik
582. Dr. J. Jayabalan
583. Dr. Manoj Kumar Tiwari
584. Dr. Manoranjan Prasad Singh
585. Dr. Maulindu Kumar Chattopadhyay
586. Dr. P K Mukhopadhyay
587. Dr. Pankaj Misra
588. Dr. Rajeev Bhatt
589. Dr. Raktim Dasgupta
590. Dr. Shreyashkar Dev Singh

591. Dr. Srinibas Satapathy
592. Dr. Sunil Verma
593. Dr. Surya Mohan Gupta
594. Dr. Vibhuti Bhushan Tiwari
595. Dr. Vijay Kumar Dixit
596. Dr. Yogesh Verma
597. Dr. Archana Sagdeo
598. Dr. Arun Kumar Rai
599. Dr. C. Kamal
600. Dr. Chandra Pal Singh
601. Dr. Himanshu Singhal
602. Dr. L S Sharath Chandra
603. Dr. Maheswar Nayak
604. Dr. Manoj Kumar Singh
605. Dr. Parasmani Rajput
606. Dr. Pooja Gupta
607. Dr. Salahuddin Khan
608. Dr. Sanyasi Rao Bobbili
609. Dr. Shailesh Kumar Khamari
610. Dr. Shankar Lal
611. Dr. Shilpa Tripathi
612. Dr. Soma Banik
613. Dr. Suparna Pal
614. Dr. T Sathyanarayana Annam
615. Dr. Uday Chakravarty
616. Dr. Vishnu Kumar Sharma
VECC
❖ Engineering Sciences
617. Prof. P. Y. Nabhiraj
618. Prof. Paramita Mukherjee
619. Prof. Sarbajit Pal
620. Dr. Sandip Pal
621. Dr. Tapatee Kundu Roy
❖ Physical Sciences
622. Prof. Jane Alam
623. Prof. Arup Bandyopadhyay
624. Prof. Chandana Bhattacharaya
625. Prof. Parnika Das
626. Prof. Rashid Md. Haroon
627. Prof. Sourav Sarkar
628. Prof. Subhasis Chattopadhyay
629. Dr. Gargi Chaudhri
630. Dr. Gayathri N. Banerjee
631. Dr. Gopal Mukherjee

632. Dr. Kaushik Banerjee
633. Dr. Nisith Kumar Das
634. Dr. Sanyal Dirtha
635. Dr. Sarmishtha Bhattacharyya
636. Dr. Siddhartha Dechoudhury
637. Dr. Tumpa Bhattacharjee
638. Dr. Vaishali Naik
639. Dr. Ajay Kumar Himanshu
640. Dr. Anand Kumar Dubey
641. Dr. Animesh Goswami
642. Dr. Arindam Kumar Sikdar
643. Dr. Ayan Ray
644. Dr. Debasis Bhowmick
645. Dr. Deepak Pandit
646. Dr. Partha Pratim Bhaduri
647. Dr. Prasanta Karmakar
648. Dr. Pratap Roy
649. Dr. Rupa Chatterjee
650. Dr. Sadhukhan Jhilam
651. Dr. Samir Kundu
652. Dr. Shashi C Srivastava
653. Dr. Supriya Mukhopadhyay
654. Dr. Swagata Mallik
655. Dr. Tapan Kumar Rana
656. Dr. Tilak Kumar Ghosh
657. Dr. Zubayer Ahammed
HRI
❖ Mathematical Sciences
658. Prof. Kalyan Chakraborty
659. Prof. Manoj kumar
660. Prof. P. K. Ratnakumar
661. Prof. Punita Batra
662. Prof. R. Thangadurai
663. Prof. Surya D. Ramana
664. Dr. N. Raghavendra
665. Dr. Aprameyo Pal
666. Dr. Gyan Prakash
667. Dr. Hemangi Madhusudan Shah
668. Dr. Umeshkumar V. Dubey
❖ Physical Sciences
669. Prof. Pinaki Majumdar
670. Prof. Aditi Sen De
671. Prof. Arun Kumar Pati
672. Prof. Aresh Krishna Datta

673.	Prof. Dileep Prabhakar Jatkar
674.	Prof. Prasenjit Sen
675.	Prof. Ujiwal Sen
676.	Dr. Anirban Basu
677.	Dr. Anshuman Maharana
678.	Dr. Santosh Kumar Rai
679.	Dr. T. P. Pareek
680.	Dr. Tapas kumar Das
681.	Dr. Tathagata Ghosh
IMSc	
❖ Life Sciences	
682.	Prof. Gautam I. Menon
683.	Dr. Rahul Siddharthan
684.	Dr. Areejit Samal
685.	Dr. Sandeep Choubey
❖ Mathematical Sciences	
686.	Prof. K. N. Raghavan
687.	Prof. Amritanshu Prasad
688.	Prof. C. R. Subramanian
689.	Prof. Jaya N. Iyer
690.	Prof. Meena Bhaskar Mahajan
691.	Prof. Saket Saurabh
692.	Prof. Sankaran Viswanath
693.	Prof. Sanoli Gun
694.	Prof. Srinivas Kotyada
695.	Prof. Venkatesh Raman
696.	Prof. Vijay Kodiyalam
697.	Dr. Anilesh Mohari
698.	Dr. Anirban Mukhopadhyay
699.	Dr. Pralay Chatterjee
700.	Dr. Vikram Sharma
701.	Dr. Anup Biswanath Dixit
702.	Dr. Indrava Roy
703.	Dr. Prakash Saivsan
704.	Dr. S. Sundar
705.	Dr. Sushmita Gupta
706.	Dr. Sushmita Venugopal
❖ Physical Sciences	
707.	Prof. Indumathi D.
708.	Prof. Nita Sinha
709.	Prof. Raghib Hassan Syed

710.	Prof. Rajesh R.
711.	Prof. Satyavani Vemparala
712.	Prof. Sibasish Ghosh
713.	Prof. Sitabhra Sinha
714.	Dr. Gopalakrishna Sharihari
715.	Dr. Manjari Bagchi
716.	Dr. Mukul S. Laad
717.	Dr. Partha Mukhopadhyay
718.	Dr. Pinaki Chaudhuri
719.	Dr. Ronojoy Adhikari
720.	Dr. Sanatan Digal
721.	Dr. Sujay K. Ashok
722.	Dr. V. S. Nemani
723.	Dr. Ajit Coimbatore Balram
724.	Dr. Chandrashekar C. M.
725.	Dr. Dhiraj Kumar Hazra
726.	Dr. Ganesh Ramchadran
727.	Dr. Roji Pius
728.	Dr. Sayantan Sharma
IOP	
❖ Physical Sciences	
729.	Prof. Karuna Kar Nanda
730.	Prof. B K Panigrahi
731.	Prof. Biju Raja Sekhar
732.	Prof. Pankaj Agrawal
733.	Prof. Parlapalli Venkata Satyam
734.	Prof. Pradip Kumar Sahu
735.	Prof. Shikha Varma
736.	Prof. Som Tapobrata
737.	Prof. Sudipta Mukherji
738.	Prof. Suresh Kumar Patra
739.	Dr. Sanjib Kumar Agarwalla
740.	Dr. Arijit Saha
741.	Dr. Aruna Kumar Nayak
742.	Dr. Debasish Chaudhuri
743.	Dr. Debottam Das
744.	Dr. Dinesh Topwal
745.	Dr. Goutam Tripathy

746. Dr. Kirtiman Ghosh
747. Dr. Manimala Mitra
748. Dr. Samal Debakanta
749. Dr. Saptarshi Mandal
750. Dr. Satyaprakash Sahoo
751. Dr. Shamik Banerjee
IPR
❖ Chemical Sciences
752. Prof. Sudhir Kumar Nema
❖ Engineering Sciences
753. Prof. Shashank Chaturvedi
754. Prof. Surya kumar Pathak
755. Prof. Paritosh Chaudhuri
756. Prof. Vipulkumar L. Tanna
757. Dr. Alphonsa Joseph
758. Dr. Nirav I. Jamnapara
759. Dr. Rajesh Kumar
760. Dr. Suryakant B. Gutpa
❖ Physical Sciences
761. Prof. Abhijit Sen
762. Prof. Shishir P. Deshpande
763. Prof. Mahendrajit Singh
764. Prof. Mainak Bandopadhyay
765. Prof. Prabal Kumar Chattapadhyay
766. Prof. Pramod Kumar Sharma
767. Prof. Subrata Pradhan
768. Prof. Subroto Mukherjee
769. Prof. Sudip Sengupta
770. Prof. Vinay Kumar
771. Dr. Anitha V. P.
772. Dr. Asim Kumar Chattopadhyay
773. Dr. Debasis Chandra
774. Dr. Ganesh Rajaraman
775. Dr. Hem Chandra Joshi
776. Dr. Hiteshkumar B Pandya
777. Dr. Indranil Bandyopadhyay
778. Dr. Jana Mukti Ranjan
779. Dr. Joydeep Ghosh

780. Dr. Lalit Mohan Awasthi
781. Dr. Mrityunjay Kundu
782. Dr. Mukesh Ranjan
783. Dr. Nirmal Kumar Bisai
784. Dr. Rajendra Kumar Bhattacharyaya
785. Dr. Raju Daniel
786. Dr. Saikia Bipul
787. Dr. Samir Khirwadkar
788. Dr. Sanjeev Kumar Sharma
789. Dr. Sanjeev Kumar Varshney
790. Dr. Shantanu Kumar Karkari
791. Dr. Ziauddh Khan
792. Dr. C. Balasubramanian
793. Dr. Devendra Sharma
794. Dr. Gourab Bansal
795. Dr. Jinto Thomas
796. Dr. Kishore Kanti Mishra
797. Dr. N Ramasubramanian
798. Dr. Pintu Bandyopadhyay
799. Dr. Ramkrishna Rane
800. Dr. Ravi G.
801. Dr. Sarveshwar Sharma
802. Dr. Sejal Shah
803. Dr. Shishir Purohit
804. Dr. Smruti R. Mohanty
805. Dr. Subhash P. V.
NISER
❖ Applied Systems Analysis
806. Dr. Amarendra Das
807. Dr. Amarjeet Nayak
808. Dr. Debashis Pattanaik
809. Dr. Joe Varghese Yeldho
810. Dr. Pranaya Kumar Swain
811. Dr. Rooplekha Khuntia
❖ Chemical Sciences
812. Prof. Alagar Srinivasan
813. Dr. Bhargava B. L.
814. Dr. Chandra Shekhar Purohit

815. Dr. Chidambaram Gunanathan
816. Dr. Himansu Sekhar Biswal
817. Dr. Jogendra Nath Behera
818. Dr. Moloy Sarkar
819. Dr. Nagendra Kumar Sharma
820. Dr. Nembenna Sharanappa
821. Dr. P. C. Ravikumar
822. Dr. Prasenjit Mal
823. Dr. Sanjib Kar
824. Dr. Saravanan Peruncheralathan
825. Dr. Subhadip Ghosh
826. Dr. Sudip Barman
827. Dr. Upakarasamy Lourderaj
828. Dr. Venkatasubbaiah Krishnan
829. Dr. Arindam Ghosh
830. Dr. Bidraha Bagh
831. Dr. Bishnu Prasad Biswal
832. Dr. Dipak Samanta
❖ Engineering Sciences
833. Dr. Anup Kumar Bhattacharya
834. Dr. Sabyasachi Karati
❖ Life Sciences
835. Dr. Chandan Goswami
836. Dr. Debasmita Pankaj Alone
837. Dr. Harapriya Mohapatra
838. Dr. K. Chandrasekhar Panigrahi
839. Dr. Manjusha Dixit
840. Dr. Palok Aich
841. Dr. Pankaj Vidyadhar Alone
842. Dr. Praful S. Singru
843. Dr. Subhasis Chattopadhyay
844. Dr. Anirudhha Datta Roy
845. Dr. K. Venkatsai Badireenath
846. Dr. Mohammed Saleem
847. Dr. Renjith Mathew
848. Dr. Rudresh Acharya
849. Dr. Srinivasan Ramanujam
850. Dr. Tirumala Kumar Chowdary

❖ Mathematical Sciences
851. Dr. Anil Kumar Karn
852. Dr. Binod kumar Sahoo
853. Dr. Brundaban Sahu
854. Dr. Anisur Rahaman Molla
855. Dr. Anupam Pal Chowdhary
856. Dr. Arita Banik
857. Dr. Deepak Kumar Dalai
858. Dr. Chitrabhanu Chaudhury
859. Dr. Dinesh Kumar Keshari
860. Dr. Kamal Lochan Patra
861. Dr. Kaushik Majumder
862. Dr. Krishanu Dan
863. Dr. Manas Ranjan Sahoo
864. Dr. Manoj Mishra
865. Dr. Meher Jaban
866. Dr. Nabin Kumar Jana
867. Dr. Panchugopal Bikram
868. Dr. Ramesh Manna
869. Dr. Rishiraj Bhattacharyya
870. Dr. Ritwik Mukherjee
871. Dr. Roy Sutanu
872. Dr. Sanjay Parui
873. Dr. Senthil Kumar K.
874. Dr. Subhankar Mishra
❖ Physical Sciences
875. Prof. Sudhakar Panda
876. Prof. Bedangadas Mohanty
877. Dr. Ashok Kumar Mohapatra
878. Dr. Colin Benjamin
879. Dr. Prasanjit Samal
880. Dr. Pratap Kumar Sahoo
881. Dr. Ritwik Das
882. Dr. Sanjay Kumar Swain
883. Dr. Subhankar Bedanta
884. Dr. A.V. Anil Kumar
885. Dr. Abdur Rahman
886. Dr. Ajaya Kumar Nayak

887.	Dr. Amaresh Kumar Jaiswal
888.	Dr. Anamitra Mukherjee
889.	Dr. Ashis Kumar Nady
890.	Dr. Chethan N. Gowdigere
891.	Dr. Guneshwar Thangjam
892.	Dr. Jaya Khanna
893.	Dr. Jayesh M Goyal
894.	Dr. Joydeep Bhattacharjee
895.	Dr. Kartikeswar Senapati
896.	Dr. Kush Saha
897.	Dr. Liton Majumdar
898.	Dr. Najmal Haque
899.	Dr. Nishikanta Khandai
900.	Dr. Prathikrit Bhattacharya
901.	Dr. Prolay Kumar Mal
902.	Dr. Sayantani Bhattacharyya
903.	Dr. Subhasish Basak
904.	Dr. Sumedha
905.	Dr. Tuhin Ghosh
906.	Dr. V. Ravi Chandra
907.	Dr. Victor Roy
908.	Dr. Yogesh Kumar Srivastava
SINP	
❖ Chemical Sciences	
909.	Dr. Dulal Senapati
910.	Dr. Montu K. Hazra
911.	Dr. Padmaja Prasad Mishra
❖ Life Sciences	
912.	Dr. Debashis Mukhopadhyay
913.	Dr. Gautam Garai
914.	Dr. Partha Saha
915.	Dr. Rahul Banerjee
916.	Dr. Sampa Biswas
917.	Dr. Udayaditya Sen
918.	Dr. Chandrima Das
919.	Dr. H. Raghuraman
920.	Dr. Kaushik Sengupta
921.	Dr. Oishee Chakrabarti
922.	Dr. Sangram Bagh
923.	Dr. Soumen Kanti Manna
924.	Dr. Subhabrata Majumder

925.	Dr. Subhendu Roy
❖ Physical Sciences	
926.	Prof. Satyajit Saha
927.	Prof. Abhik Basu
928.	Prof. Ambar Ghosal
929.	Prof. Bijay Kumar Agrawal
930.	Prof. Bireswar Basu Mallick
931.	Prof. Chandan Mazumder
932.	Prof. Debasish Majumdar
933.	Prof. Harvendra Singh
934.	Prof. Indranil Das
935.	Prof. Kumar Sankar Gupta
936.	Prof. Mustafa Munshi Golam
937.	Prof. Mylavarapu Sita Janki
938.	Prof. Nikhil Chakrabarti
939.	Prof. P. M. G. Namissan
940.	Prof. Pradip Kumar Roy
941.	Prof. Prakash Mathews
942.	Prof. Satyajit Hazra
943.	Prof. Sukalyan Chattaopadhyay
944.	Prof. Supratik Mukhopadhyay
945.	Prof. Tapas Kuamr Chini
946.	Prof. Ushasi Datta
947.	Dr. Amit Ghosh
948.	Dr. Anjali Mukherjee
949.	Dr. Arunava Mukherjee
950.	Dr. Chandi Charan Dey
951.	Dr. Chinmay Basu
952.	Dr. Krishnakumar S. R. Menon
953.	Dr. Maitreyee Nandy
954.	Dr. Manoj K. Sharan
955.	Dr. Nayana Majumdar
956.	Dr. Satyaban Bhunia
957.	Dr. Satyaki Bhattacharya
958.	Dr. Subir Sarkar
959.	Dr. Suchandra Dutta
960.	Dr. Supratic Chakraborty
961.	Dr. Arnab Kundu
962.	Dr. Arti Garg
963.	Dr. Biswajit Karmakar
964.	Dr. Biswarup Satpati
965.	Dr. Debasish Banerjee
966.	Dr. Debasish Das
967.	Dr. Kalpataru Pradhan

968. Dr. Mala Das
969. Dr. M. K. Mukhopadhyay
970. Dr. Pratik Majumdar
971. Dr. Sankar De
972. Dr. Tinku Sinha Sarkar
973. Dr. Sayantani Bhattacharyya
974. Dr. Subhasish Basak
975. Dr. Sumedha
976. Dr. Tuhin Ghosh
977. Dr. V. Ravi Chandra
978. Dr. Victor Roy
979. Dr. Yogesh Kumar Srivastava
TMC
❖ Life Sciences
980. Prof. Arvind D Ingle
981. Prof. Sorab Nariman Dalal
982. Dr. Abhijit De
983. Dr. Amit Dutta
984. Dr. Ashok Varma
985. Dr. Chilakapati Murali Krishna
986. Dr. Joyti Anand Kode
987. Dr. Kakoli Bose
988. Dr. Manoj Balkrishna Mahimkar
989. Dr. Pritha Ray
990. Dr. Rukmini Balkrishna Govekar
991. Dr. Sanjay Gupta
992. Dr. Tanuja Rajendra Teni
993. Dr. Venkatraman Prasanna
994. Dr. Vikram Suryaprakash Gota
995. Dr. Dibyendu Bhattacharyya
996. Dr. Khizer Hasan Syed
997. Dr. Nandini Verma
998. Dr. Rohan Jayant Khadilkar
999. Dr. Sanjeev Waghmare
1000. Dr. Sejal Patwardhan
1001. Dr. Sharath Chandra Arandkar
1002. Dr. Shilpee Dutt
1003. Dr. Sonam Mehrotra
❖ Medical & Health Sciences
1004. Prof. Rajendra Achyut Badwe
1005. Prof. Ajay Puri
1006. Prof. Aliasgar V Moiyadi
1007. Prof. Asmita Maheswari
1008. Prof. Amol Trymbakrao Kothekar

1009. Prof. Anant Gokarn
1010. Prof. Anant Ramaswamy
1011. Prof. Anuja Dhananjay Deshmukh
1012. Prof. Aparna Sanjay Chatterjee
1013. Prof. Archi Ramesh Agrawal
1014. Prof. Ashwin Luis Desouza
1015. Prof. Ashwini Narsingrao Budrukhar
1016. Prof. Atul Prabhakar Kulkarni
1017. Prof. Avanish Parmesh Saklani
1018. Prof. Bharat Rekhi
1019. Prof. Bhausaheb Pandurang Bagal
1020. Prof. Conjeevaram S. Parmesh
1021. Prof. Deepa Ravindranathan Nair
1022. Prof. Devendra Arvind Chaukar
1023. Prof. Dushyant Jaiswal
1024. Prof. Gagan Prakash
1025. Prof. Gaurav Narula
1026. Prof. Gauravi Ashish Mishra
1027. Prof. George Karimundackal
1028. Prof. Girish Chinnaswamy
1029. Prof. Goda Jayant Sastri
1030. Prof. Gouri Himalaya Pantvaidya
1031. Prof. Gulia Ashish
1032. Prof. Gulia Seema
1033. Prof. Hasmukh Kantilal Jain
1034. Prof. Jai Prakash Agarwal
1035. Dr. Jaya Ghosh
1036. Dr. Jayita Kedar Deodhar
1037. Dr. Jeson Rajan Doctor
1038. Prof. Jigeeshu Vasishtha Divatia
1039. Prof. Jyoti Bajpai
1040. Prof. Kedar Kamalakar Deodhar
1041. Prof. Madhavi Gopalkrishna Shetmahajan
1042. Prof. Mahendra Pal
1043. Prof. Mahesh Goel
1044. Prof. Malini Premkumar Joshi
1045. Prof. Manish Suresh Bhandare
1046. Prof. Manisha Nandkumar Pawar
1047. Prof. Manju Sengar
1048. Prof. Maya Prasad
1049. Prof. Mukta Ravindra Ramdwar
1050. Prof. Munita Meenu Bal
1051. Prof. Murthy Vedang

1052. Prof. Navin Khattry
1053. Prof. Nayana Shekar Amin
1054. Prof. Neha Mittal
1055. Prof. Nehal Rishi Khanna
1056. Prof. Nikhil Vijay Patkar
1057. Prof. Nilendu C. Purandare
1058. Prof. Nilesh Pandurang Sable
1059. Prof. Nita Sukumar Nair
1060. Prof. Nitin Sudhakar Shetty
1061. Prof. Pankaj Chaturvedi
1062. Prof. Papagudi G. Subramanian
1063. Prof. Poonam K. Panjwani
1064. Prof. Prabhash Kumar
1065. Prof. Prachi Sunil Patil
1066. Prof. Prakash Shetty
1067. Prof. Prashant Ramesh Tembhare
1068. Prof. Prashant Ramesh Tembhare
1069. Prof. Prathamesh Pai Srinivas
1070. Prof. Priti Dhansukhbhai Desai
1071. Prof. Priya Ranganathan
1072. Prof. Raghu Sudarshan Thota
1073. Prof. Rajesh Ashok Kinhikar
1074. Prof. Rajesh Prabhakar Dikshit
1075. Prof. Rajiv Kumar
1076. Prof. Reena Zarir Engineer
1077. Prof. Reshma Ambulkar
1078. Prof. Sabita Shambhulal Jiwnani
1079. Prof. Sachin Punatar
1080. Prof. Sajid Shafique Quresh
1081. Prof. Sandeep Vivek Gurav
1082. Prof. Sangeeta Bhikaji Desai
1083. Prof. Sanjay Biswas
1084. Prof. Santosh Menon
1085. Prof. Sarbani Ghosh Laskar
1086. Prof. Sarin Rajiv
1087. Prof. Shaesta Abdulaziz Mehta
1088. Prof. Shailesh Vinayak Shrikhande
1089. Prof. Shalaka Prakash Joshi
1090. Prof. Sharmila Anil Pimple
1091. Prof. Shashank Ojha
1092. Prof. Sheela Prashant Sawant
1093. Prof. Sheila Nainan Myatra
1094. Prof. Shilpushp Jagannath Bhosale
1095. Prof. Shraddha Patkar

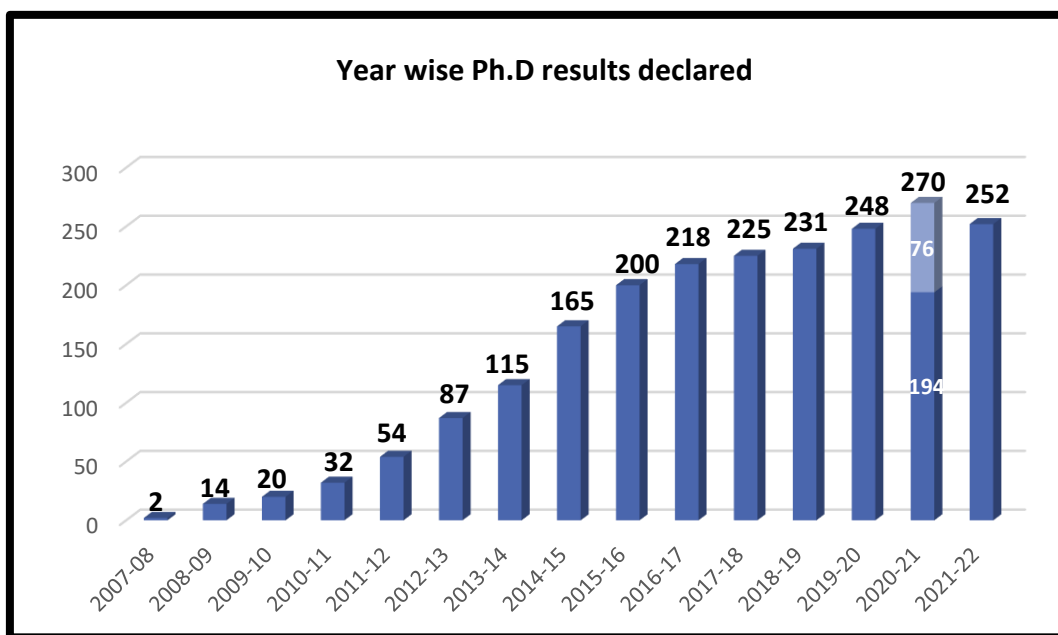
1096. Prof. Shripad Dinanath Banavali
1097. Prof. Siddhartha Sankar Laskar
1098. Prof. Sneha Shah
1099. Prof. Sohan Lal Solanki
1100. Prof. Sridhar Epari
1101. Prof. Subhash Chotelal Yadav
1102. Prof. Sudeep Gupta
1103. Prof. Sudhir Vasudevan Nair R.
1104. Prof. Sumeet Gujral
1105. Prof. Sumitra Ganesh Bakshi
1106. Prof. Sunil Bhagwant Rajadhyaksha
1107. Prof. Supriya Jayant Sastri
1108. Prof. Suyash Sureshchandra Kulkarni
1109. Prof. Swapnil Yeshwant Parab
1110. Prof. Tabassum Abdulwahid Wadasadawala
1111. Prof. Tanuja Manjanath Shet
1112. Prof. Tejpal Gupta
1113. Prof. Vandana Agarwal
1114. Prof. Vani Parmar
1115. Prof. Vanita Maria Noronha
1116. Prof. Venkatesh Rangarajan
1117. Prof. Vijay Maruti Patil
1118. Prof. Vijaya Prakash Patil
1119. Prof. Vikas Sureshchand Ostwal
1120. Prof. Vikram Anil Chaudhari
1121. Prof. Vinay Kant Shankhdhar
1122. Prof. Vivek Gajanan Bhat
1123. Prof. Anita D'Souza
1124. Dr. Abhishek Chatterjee
1125. Dr. Aekta Shah
1126. Dr. Amrita Guha
1127. Dr. Anjana S Wajekar
1128. Dr. Anuprita Dilip Daddi
1129. Dr. Asawari Jingonda Patil
1130. Dr. Badira Cheriyaalinkal Parambil
1131. Dr. Bhakti Dushyant Trivedi
1132. Dr. Bindiya Gaurav Salunke
1133. Dr. Chetan Anil Dhamne
1134. Dr. Janu Amit Kumar
1135. Dr. Kinjalka Ghosh
1136. Dr. Kunal B Gala
1137. Dr. Lingaraj Nayak

1138. Dr. Madhavi Dattatraya Desai
1139. Dr. Naveen Mummudi
1140. Dr. Palak Bhavesh Popat
1141. Dr. Poonam Joshi
1142. Dr. Prabhat Bhargava
1143. Dr. Rahul Krishnatry
1144. Dr. Richa Vaish
1145. Dr. Shiva Kumar Thiagarajan
1146. Dr. Sudivya Prashast Sharma
1147. Dr. Sumathi S Hiregoudar
1148. Dr. Swapnil Rane
1149. Dr. Vasundhara Patil
1150. Dr. Vikas Kumar Singh
1151. Dr. Akanksha Chichra
1152. Dr. Amit Kumar Jayant Choudhari
1153. Dr. Anisha A Navkudkar
1154. Dr. Aparna Katdare
1155. Dr. Ashwini D Rane

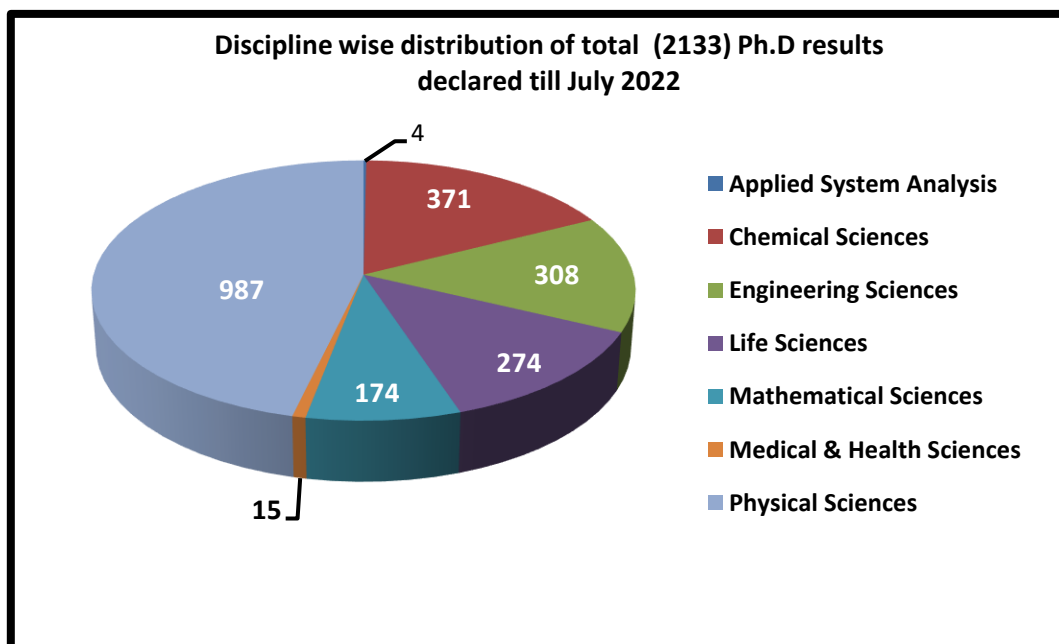
1156. Dr. Atanu Bhattacharjee
1157. Dr. Avinash Ramesh Rao Pagdhune
1158. Dr. Dhanlaxmi L. Shetty
1159. Dr. Gaurav Vijay Salunke
1160. Dr. Gauri Raman Gangakhedkar
1161. Dr. Gauri Rohan Deshpande
1162. Dr. Jifmi Jose Manjali
1163. Dr. Katha Nikhil Rabade
1164. Dr. Nivedita Chakrabarty
1165. Dr. Omshree Shetty
1166. Dr. Parthiban K Velayutham
1167. Dr. Pratik Chandrani
1168. Dr. Ritu Raj Upreti
1169. Dr. Sangeeta Kakoti
1170. Dr. Shrikant C Raut
1171. Dr. Shwetabh Sinha
1172. Dr. Sujata Lall

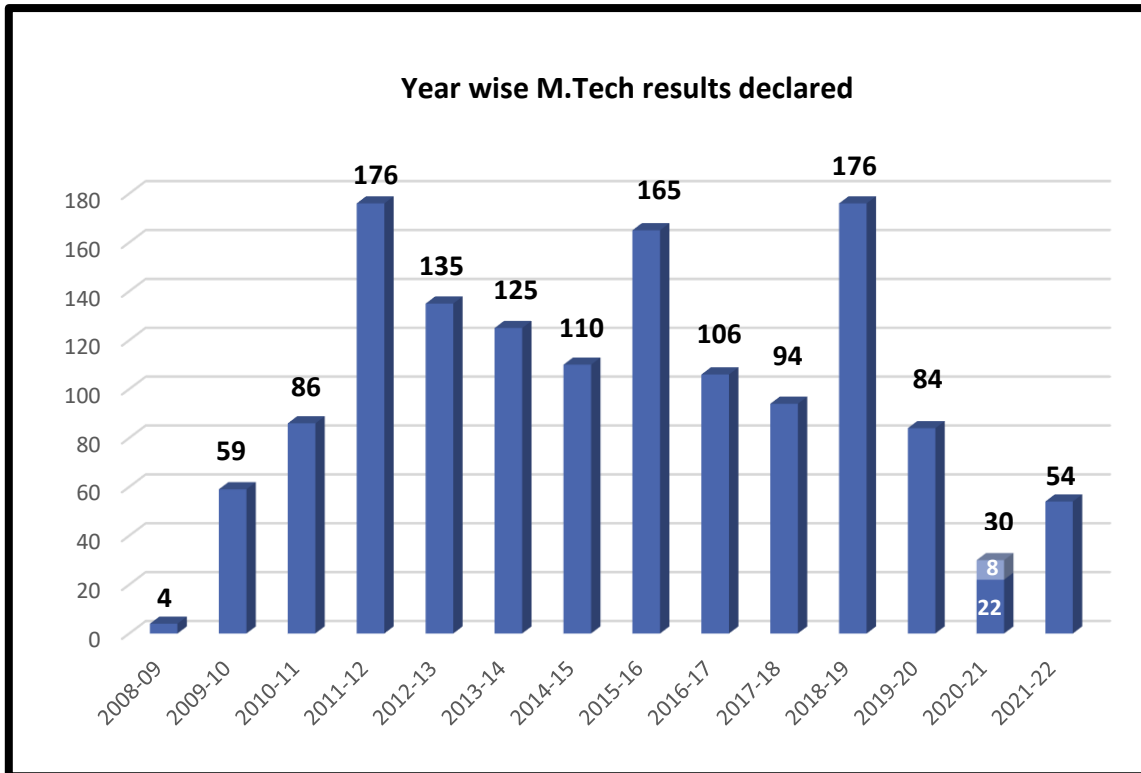
HBNI at a Glance

During the last academic year (August 1, 2021-July 31, 2022), HBNI has awarded 252 Ph.D. degrees. The total number of Ph.D. degrees awarded by HBNI till July 31, 2022 stands at 2133. HBNI also awarded 54 M. Tech., 156 M.Sc./Integrated M.Sc. in various science disciplines, 122 post graduate & super specialty medical degrees with specializations in Oncology, and 10 post graduate diplomas in Fusion Imaging Technology (PGDFIT) during this period. 838 students have been admitted to different academic programmes during 2021-22, out of which 354 students are for Ph.D. program.

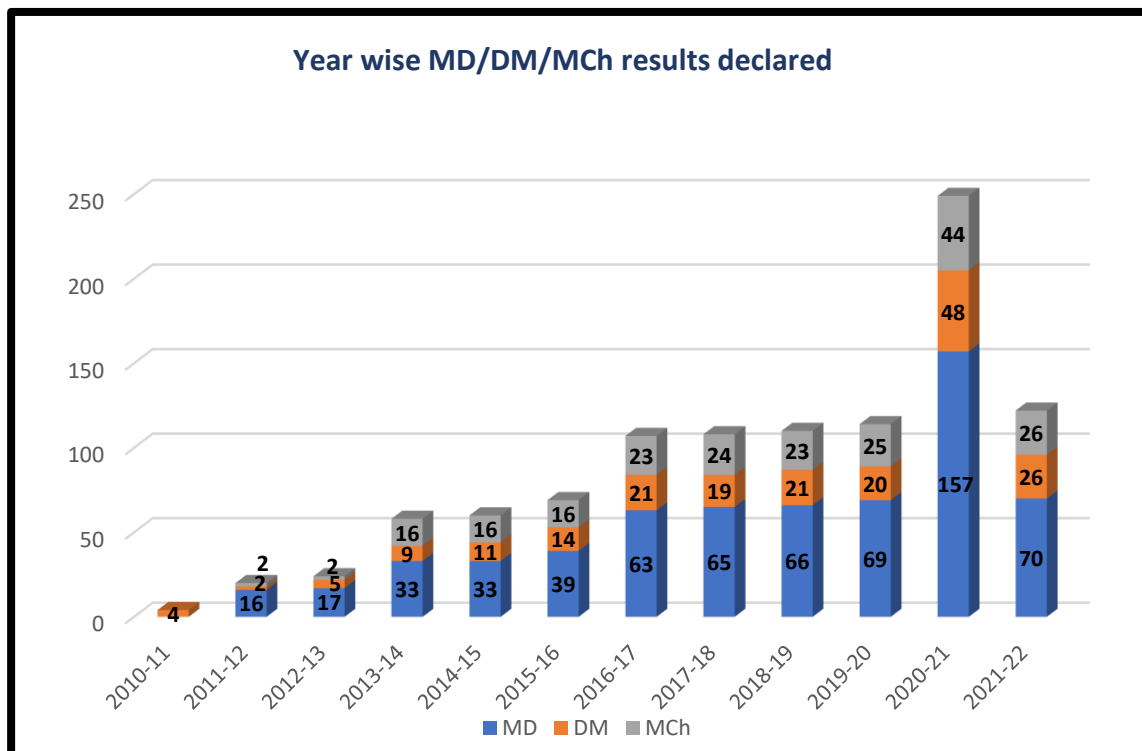


*The data from 2007-08 to 2019-20 is for the period April 1 of preceding year to March 31 of the ending year. The data for 2020-21 is for the period April 1, 2020 to July 31, 2021. Dark blue area (194) gives the data from April 1, 2020 to March 31, 2021, light blue area (76) gives the data from April 1, 2021 to July 31, 2021. The data for 2021-22 is for the period August 1, 2021 to July 31, 2022.

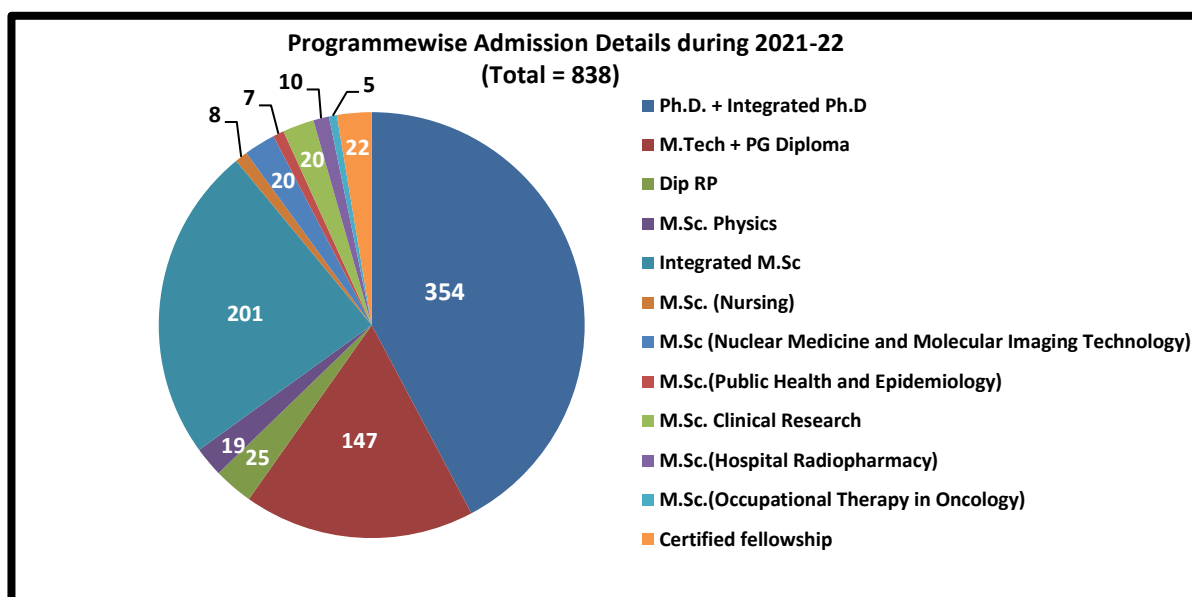




*The data from 2008-09 to 2019-20 is for the period April 1 of the preceding year to March 31 of the ending year. The data for 2020-21 is for the period April 1, 2020 to July 31, 2021. Dark blue area (22) gives the data from April 1, 2020 to March 31, 2021, light blue area (8) gives the data from April 1, 2021 to July 31, 2021. The data for 2021-22 is for the period August 1, 2021 to July 31, 2022.



*The data from 2010-11 to 2019-20 is for the period April 1 of preceding year to March 31 of the ending year. The data for 2020-21 is for the period April 1, 2020 to July 31, 2021. The data for 2021-22 is for the period August 1, 2021 to July 31, 2022.



Number of students admitted to the different academic programmes of CIs/OCC during August 1, 2021 –July 31, 2022

Academic Programme	BARC	IGCAR	RRCAT	VECC	SINP	IPR	TMC	IoP	IMSc	HRI	NISER	Total
Ph.D. + Integrated Ph.D	118	4	18	15	19	15	21	12	31	17	84	354
M.Tech + PG Diploma	119	20	8	147
MD	0
Dip RP	25	25
DM/MCh	0
M.Sc. Physics	19	19
Integrated M.Sc	201	201
M.Sc. (Nursing)	8	8
M.Sc (Nuclear Medicine and Molecular Imaging Technology)	10	10	20
M.Sc. (Public Health and Epidemiology)	7	7
M.Sc. Clinical Research	20	20
M.Sc. (Hospital Radiopharmacy)	10	10
M.Sc. (Occupational Therapy in Oncology)	5	5
Certified fellowship	22	22
Total	282	24	18	15	19	23	93	12	31	36	285	838

Section II (Theses at a Glance)

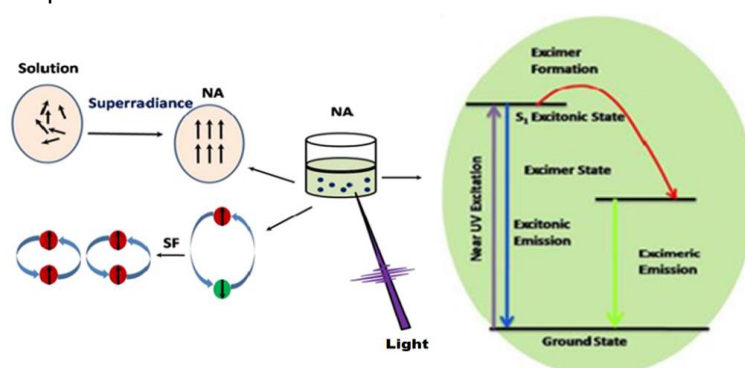
1. Chemical Sciences

During the period of report, HBNI awarded 39 Ph.D. degrees in Chemical Sciences in variety of research areas including exotic organic synthesis, materials chemistry, nanoscience, environmental chemistry, theoretical chemistry, actinide separation & speciation, molecular modelling for elective extraction, radiopharmaceuticals, and so on. Highlights of some of the selected these are given below.

1.1 Bhabha Atomic Research Centre, Mumbai

1.1.1 Ultrafast dynamics of excitons and charge carriers in thin films and nanoaggregates of polyaromatic molecules

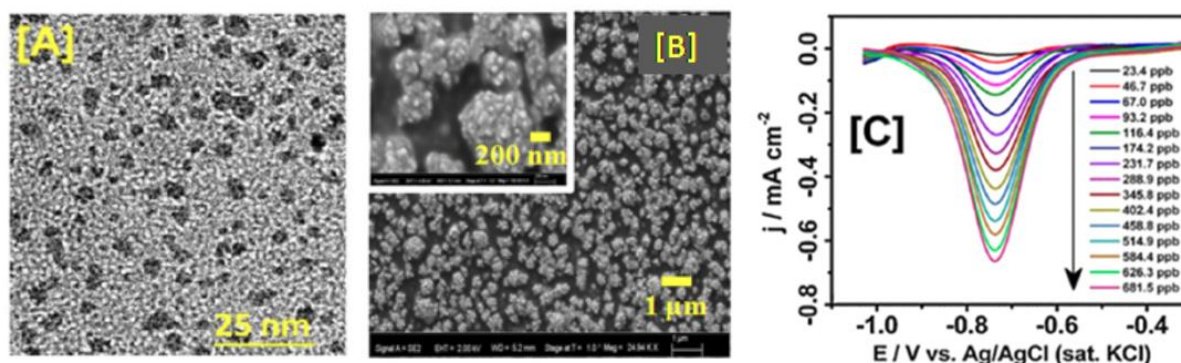
Due to their low cost, less toxicity and ease of fabrication, organic semiconductor materials are the alternatives to inorganic semiconductors for different opto-electronic applications. A thorough understanding of the photophysics and exciton dynamics of these organic semiconductors is important for effective utilization of these materials in optoelectronics. In the present work, exciton dynamics of a series of polyarenes in nanoaggregate (NA) and thin film (TF) has been investigated along with their morphological and photophysical characterizations. Singlet fission (SF) in organic semiconductors, which generates two triplet excitons from one singlet exciton, has attracted extensive interest in recent past, as it can lead to the multiplication of charge carriers and hence a much higher photovoltaic efficiency. In the present thesis efficient ultrafast SF process in several polyaromatic systems has been investigated in details, to understand the relation between the SF efficiency and the structure of the polyaromatic molecules. Observed results indicate that phenylethynyl substitution in anthracene and tetracene molecules leads to the SF process. Role of intermolecular interaction in the solid state of these molecules on their SF process has also been explored in the present thesis. It is revealed that exciton-exciton annihilation in the organic semiconductor materials is controlled largely by the molecular packing and intermolecular coupling in their NAs and TFs. Compared to molecules with non-planar structures, the ones with planar structures show much faster exciton mobility, suggesting their better prospects for photovoltaic applications. It is seen that the radiative rate of the nonlinear polyacenes can be improved significantly in the NA state in comparison to their monomeric forms, attributed to the correlated alignment of the molecular dipoles at a particular direction.



Polyacene group of molecules shows different types of properties like singlet fission (SF), superradiance and excimeric emission depending upon molecular structure and electronic coupling in aggregate or thin film.

1.1.2 Electrochemistry of uranium (VI) and plutonium (IV) on carbon- and platinum-nanostructures

Towards the development of precise and accurate electroanalytical methods for U, present thesis investigates the electrocatalysis of U electron transfer reactions on carbon nanostructures like graphene quantum dot (GQD), oxygenated single walled carbon nanohorn (o-SWCNH), multiwalled carbon nanotube (MWCNT), and NH₂-functionalised MWCNT materials as potential alternatives to noble metal electrodes. With GQDs, U(VI) determinations have been investigated using both photophysical and electrochemical methods, and in both the cases the estimated LOD values are found to be in the ppb range, suggesting the usefulness of these materials in the environmental analysis of U(VI). With o-SWCNHs, meaningful insights have also been obtained on the role of oxygen functionalities in the redox characteristics [Ru(NH₃)₆]³⁺/[Ru(NH₃)₆]²⁺, Fe(CN)₆³⁻/[Fe(CN)₆]⁴⁻ and [UO₂(CO₃)₃]⁴⁻/[UO₂(CO₃)₃]⁵⁻ redox couples. The electrocatalytic sensitivity for o-SWCNHs in the U(VI) determination is found to be about 0.75 $\mu\text{A cm}^{-2} (\mu\text{g L}^{-1})^{-1}$. The electrocatalysis of U (VI) by carbon nanostructures like MWCNTs and NH₂-functionalised MWCNTs have also been investigated and compared with glassy carbon (GC) electrode. Both of these carbon materials provide better electrocatalysis than the bare glassy carbon (GC) electrode. Present thesis also investigates the electrocatalytic properties of platinum nano-cauliflower (PtNCF) materials, as deposited on ITO electrodes through template-free electrosynthesis. The PtNCFs exhibit narrow size distribution with uniform coverage on ITO electrode and show better electrocatalytic behaviour as compared to bare ITO electrode, for the electrocatalysis of Pu(IV)/Pu(III) redox couple in 1 M H₂SO₄ solution.

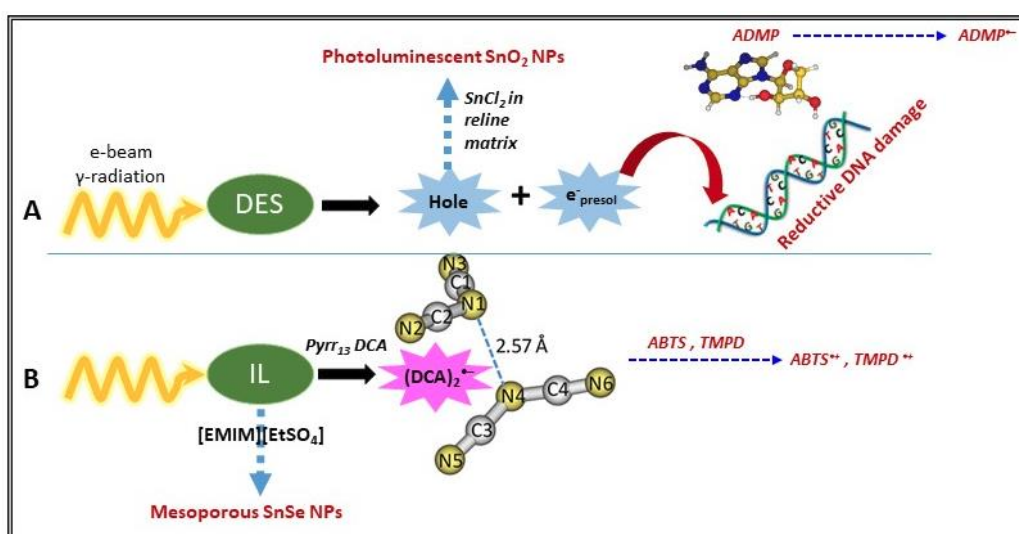


[A] TEM image of GQDs. [B] SEM image of PtNCFs on ITO; Inset shows a magnified image image. [C] Square wave voltammogram (SWV) on ERGQDs with different concentration of U(VI) in saturated Na₂CO₃.

1.1.3 Radiation chemical studies of ionic liquids and deep eutectic solvents for their application in the synthesis of IV-VI semiconductor nanomaterials

The room temperature ionic liquids (RTILs) and deep eutectic solvents (DESs) are the exotic solvents and potential alternatives to conventional volatile organic solvents, essentially due to their exceptional physico-chemical properties like negligible vapor pressure, non-flammability, wide electrochemical windows, thermal stability, high conductivity, and ability to solubilize a wide variety of compounds. In the present work, radiation chemical studies of these solvents have been carried out using nanosecond pulse radiolysis technique to investigate the yield, lifetime, decay kinetics,

bimolecular rate of reaction, and redox characteristics of the transient species generated through irradiation. Experimental results are also supplemented by first principle based computational studies. Existence of presolvated electrons is observed in DESs in nanosecond timescale which are efficiently scavenged by DNA base adenosine, having relevant to the research on reductive DNA damage. Following computational and experimental techniques, a redox and radiation stable DES consisting of 1:2 molar ratio of choline acetate and malonic acid has been realized. In the context of semiconductor nanomaterial synthesis with defined morphology and properties, both IL and DES have been successfully utilized in the present study. Radiation chemical method for nanomaterial synthesis is found to be superior over other contemporary methods. Photoluminescent tin oxide nanoparticles (NPs) were synthesized via radiation chemical technique in the standard DES reline. These NPs are found to be non-toxic and are suitable in cell imaging applications. Mesoporous SnSe nanopaterials having high porosity was also prepared successfully in the RTIL, [EMIM][EtSO₄], using electron beam irradiation method.

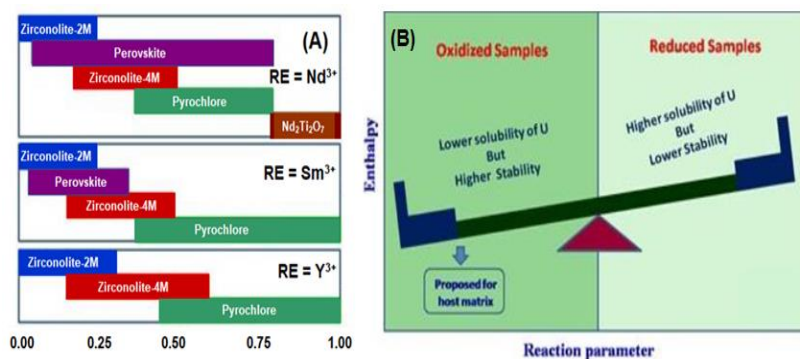


Schematics of (A) Pre-solvated electron scavenging of in DES by DNA nucleobase ADP leading to radiation mediated synthesis of SnO₂ NP in reline medium and (B) Identification and characterization of (DCA)₂•⁻ radical generated by pulse radiolysis of Pyr₁₃ DCA and radiation induced synthesis of SnSe NPs in [EMIM][EtSO₄] RTIL.

1.1.4 Preparation and structural investigations on zirconolite and pyrochlore based ceramics: Potential materials for nuclear back end application

Management of nuclear high-level waste (HLW) is a major challenge in nuclear industry. To address this, research is going on wide varieties of ceramic, glass and glass ceramics materials. Present thesis presents a systematic investigation on different ceramic matrices based on zirconolite and pyrochlore structures, prominent members of synthetic rock (SYNROC) formulations. In the zirconolite-pyrochlore based multiphasic systems (CaZrTi₂O₇-RE₂Ti₂O₇, where RE= Nd³⁺, Sm³⁺ and Y³⁺) the major phase fields observed are part of the components of SYNROC formulation. Structural characterization and stability studies on Gd_{2-2x}Ca_xZr_xTi₂O₇ (0.0 ≤ x ≤ 0.4) based pyrochlore systems revealed that about 40 mol% of aliovalent cations can be accommodated without any major alteration in structure. Thermodynamic stability studies also revealed that only a small (3.5%) decrease in the relative stability occurs even after incorporation of 40 mol % of heteroatoms. Quick processing condition has been

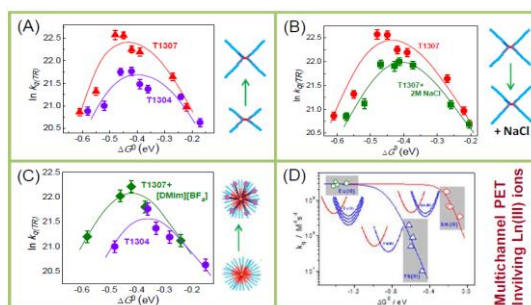
developed in the present study, which is supported by the structural characterizations and thermodynamic measurements of the materials. Structural and thermodynamic investigations on urania and urania-ceria (surrogate for plutonia) incorporated $Gd_2Zr_2O_7$ systems indicated that the stabilities are higher with U^{6+} and Ce^{4+} as compared to their reduced forms, namely, U^{4+} and Ce^{3+} . A novel formulation of borosilicate glass matrix has also been developed where solubility of gadolinia is found to increase by almost 2.5 times, from 8 wt% to ~ 20 wt%, suggesting a great prospect of this ceramic material.



(A) Representative phase fields in $CaZrTi_2O_7-RE_2Ti_2O_7$ matrices, where RE = Nd^{3+} , Sm^{3+} and Y^{3+} . (B) Stability of the uranium incorporated matrix.

1.1.5 Photoinduced electron transfer processes in homogeneous and microheterogeneous media involving organic and inorganic donor-acceptor systems

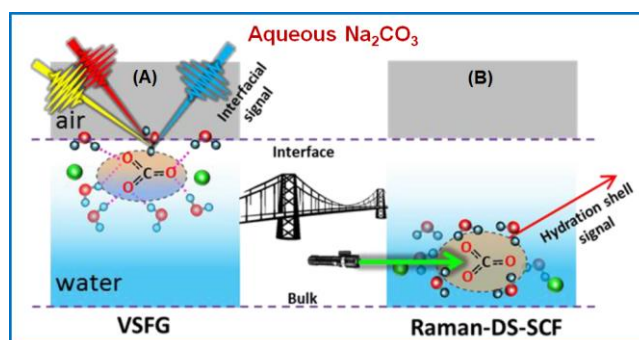
Electron transfer (ET) is fundamental redox process occurring ubiquitously in chemistry and biology. Understanding intricate details of ET reactions using model systems has been the topic of intense research for long. In this respect photoinduced electron transfer (PET) reactions have been investigated quite extensively, as the process is having direct relevance to solar energy conversion. In bimolecular ET or PET kinetics, theoretically predicted Marcus Inversion (MI) behavior is a long-lasting controversy. Present thesis demonstrates how such evasive MI can be observed convincingly for bimolecular PET processes carried out in constrained media, investigating the reactions in Tetronic and Pluronic block copolymer micelles, involving coumarin dyes as acceptors and aromatic amines as donors. In all the cases, MI behavior is observed very convincingly, which is attributed to the non-diffusional nature of the bimolecular reactions in constrained media and slow solvent relaxation that enforces two-dimensional ET (2DET) mechanism to be applicable in these systems. Interestingly, both the PET kinetics and the onset of MI along the exergonicity scale ($-DG^0$) can be modulated very significantly either by using different copolymer micelles or by using additives like salt or co-surfactant, having implications in the practical applications of the PET reactions. Another interesting aspect investigated in present work is the involvement of multichannel ET on using Ln(III) ions as electron acceptors along with suitable coumarin dyes as electron donors. Since most Ln(III) ions have many low lying electronic states that can be accessed easily by the exergonicity of the PET reactions, these systems can support multichannel PET, which is otherwise very unusual for organic donor-acceptor systems. Since the landscapes of the low lying electronic states vary largely with different Ln(III) ions, they lead to largely different correlations for the k_q versus $-DG^0$ plots involving different Ln(III) ions as the electron acceptors.



Modulation of the PET kinetics and energetics following different approaches. In micellar media: (A) Using different Tetronic systems, (B) With the addition of a salt, and (C) On using a co-surfactant. In homogeneous aqueous medium: (D) On using Ln(III) ions to support multichannel PET processes.

1.1.6 Studies of metabolites and ions at aqueous interfaces by surface-sensitive spectroscopic technique

Aqueous interfaces play pivotal role in diverse chemical, biological and atmospheric phenomena. Present thesis investigates on the molecular-level understanding of the non-covalent interactions that operate at the air/water interfaces in the presence of different metabolites, electrolytes, and pollutants. State-of-the-art heterodyne-detected vibrational sum frequency generation (HD-VSFG) technique and Raman based “difference spectroscopy and simultaneous curve fitting (Raman-DS-SCF) technique have been used in the present study to understand the aforementioned non-covalent interactions. In a study, perturbing effects of the metabolites of different hydrophobicity on the water structure at the air/water interface have been investigated. In another study, orientation-specific interaction of a zwitterionic metabolite, trimethylamine N-oxide (TMAO), with the charged and uncharged molecular hydrophobes has been investigated. Unique interactions of fluoroalcohols (organic pollutant) with both interfacial and bulk water have been investigated in a study, having relevance to atmospheric chemistry. The issue on the formation of electric double layer (EDL) at the air/water interface involving kosmotropic electrolytes has also been explored in this study and it is revealed that the ionic perturbation of interfacial water happens due to hydration shell of the kosmotropic anions (e.g., CO_3^{2-} and F^-) at the interface, and not due to the formation a well-defined EDL. Using Raman-DS-SCF technique, the “counter ion-free” spectrum of water in the hydration shell of different multivalent metal ions (Mn^+ , $n=2$ or 3) has been successfully retrieved in this study. Formation of water-shared ion pairs in aqueous MgCl_2 and LaCl_3 solutions have also been demonstrated convincingly in the present thesis.

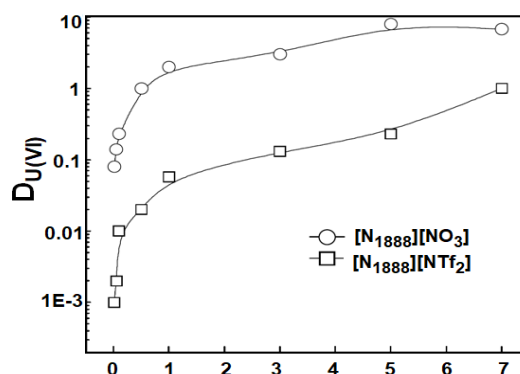


Strongly hydrated CO_3^{2-} anion acting as the structure-maker; (A) for interfacial water and (B) for bulk water. Average H-bonding for CO_3^{2-} increases due to interfacial hydration shell.

1.2 Indira Gandhi Centre for Atomic Research, Kalpakkam

1.2.1 Investigations on the extraction behavior of actinides in ionic liquid medium and the physicochemical and aggregation properties of the ionic liquid phase

Reprocessing of spent nuclear fuel is essential for sustained growth of nuclear power programme. Owing to their fascinating properties, room temperature ionic liquids (RTILs) are receiving importance in nuclear fuel reprocessing and waste management applications. In actinide and lanthanide extractions from aqueous solution, 1-alkyl-3-methylimidazolium ([Cnmim]⁺) based RTILs have some limitations due to their cation and anion exchange reactions. Thus, development of RTILs that are devoid of the the above limitations is of utmost necessity. It is also desirable to select RTILs made up of CHON-atoms exclusively so that these ILs can be completely incinerated for easy disposal of used ILs. In these contexts, present thesis has developed and investigated some ammonium based RTILs for solvent extraction of actinides and lanthanide fission products from nitric acid solutions. The study has also been focused on the understanding of the insights of solvent extraction by probing the coordination chemistry of metal-ligand complexes present in the extracted ionic liquid phase. Polarity index of the extracted phase and radiolytic stability of the used RTILs have also been evaluated using various spectroscopic studies.

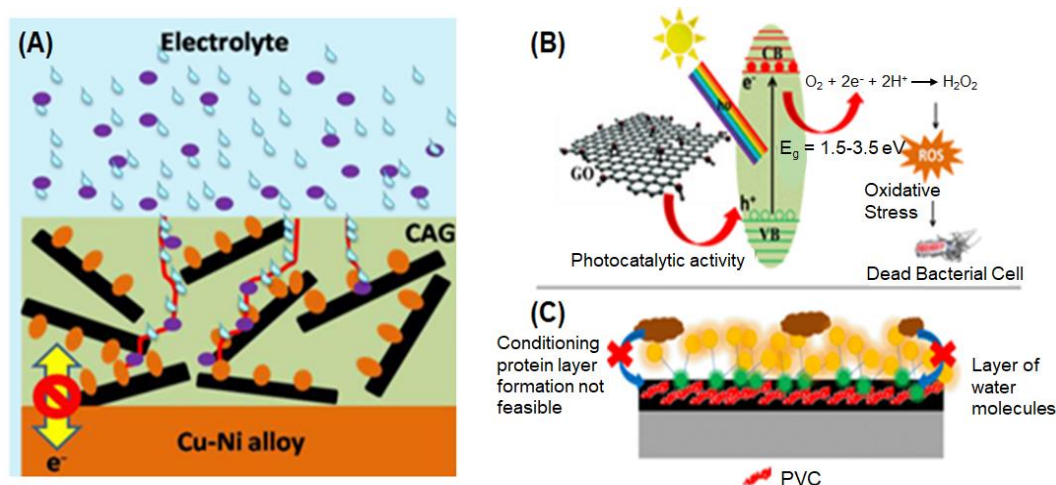


Distribution ratio of U(VI) in two different phases as a function of nitric acid concentration; RTIL phase: methyl-tri-n-octylammonium nitrate or ([N1888][NO₃]) or ([N1888][NTf₂]) & Aqueous phase: (0.01-7 M) nitric acid containing 4×10^{-4} M U(VI); Equilibration time = 1 hour; Temperature = 298K; Phase volume ratio = 1.

1.2.2 Development of graphene oxide based composite coating with improved corrosion resistance and antibacterial properties

The objective of the thesis work has been to develop robust graphene oxide (GO) based corrosion resistant and antibacterial coatings for structural materials like Cu-Ni alloy, carbon steel, and 316L SS, etc. using a simple, cheap, and scalable approach. GO based composite coating over Cu-Ni specimen has been fabricated successfully by EPD technique followed by dip coating of poly(methyl methacrylate) (PMMA) polymer which shows four orders increase in corrosion resistance, attributed to the inhibition of galvanic contact between GO and alloy surface by PMMA. A novel ternary composite coating consisting of chitosan-silver-GO as fabricated on Cu-Ni alloy using the EPD

technique show as two orders better corrosion protection along with excellent antibacterial activity, due to reactive oxygen species mediated oxidative stress induced by silver nanoparticles and damage of cell membranes by the sharp edges of GO sheet. A facile electro-codeposition approach combined with dip coating has been developed to fabricate superhydrophobic (SHP) coating on carbon steel surface where presence of air cushion between the micro/nano protrusions on the coating provided approximately three orders better corrosion resistance under chloride environment. A polydimethylsiloxane coating with an interlayer of GO-nano-SiO₂ (GSP) was fabricated on carbon steel has also been developed that shows six orders higher charge transfer resistance due to the lower permeation of chloride through the GSP layer. A composite coating consists of (3-glycidyloxypropyl)trimethoxysilane (GPTMS) and GO, as fabricated on 316L SS exhibit three orders higher corrosion resistance, attributed to synergetic effects of barrier property of GO and the insulating property of silane matrix. This coating also shows an excellent pitting corrosion resistance along with five orders of magnitude improved antibacterial activity. In addition, a GO-polyvinylpyrrolidone (PVP) composite coating on 316L SS is also developed, which showed nearly four orders better antibacterial activity due to reactive oxygen species mediated oxidative stress and reduced bio-adhesion of biofilm due to GO and PVP, respectively. The findings of the work carried out in the thesis are very useful for the design of robust corrosion resistant, antibacterial and antibiofouling coatings for marine applications.

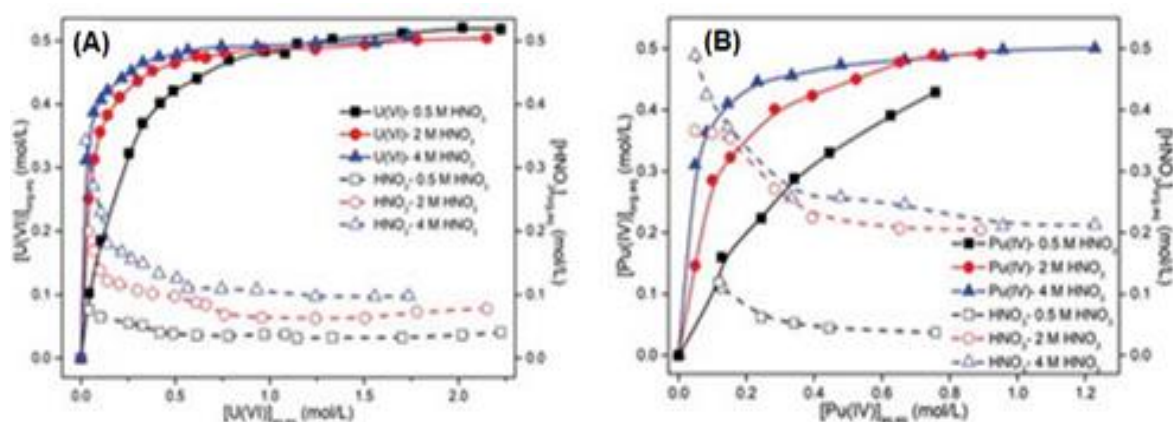


Schematics of the (A) corrosion resistance provided by chitosan-silver-GO based composite coating, (B) antibacterial efficacy, and (C) antifouling property provided by GO/PVP based composite coating.

1.2.3 Evaluation of tris(2-methylbutyl) phosphate as an extractant for nuclear materials processing applications: A comparison with tri-n-alkyl phosphates

The distribution ratio (D) for the troublesome fission products such as trivalent lanthanides, heptavalent Tc and tetravalent Zr were found to be marginally lower for 1.1 M solution of tris(2-methylbutyl) phosphate (T2MBP) in n-dodecane (n-DD) as compared to the corresponding tri-n-butyl phosphate (TBP) based solvent, suggesting a better decontamination factor for the spent nuclear fuel reprocessing using T2MBP based extractant. Thus, maximum extraction of ~122 g/L Pu(IV) could be achieved with 1.1 M T2MBP/n-DD from Pu(NO₃)₄ in 4 M HNO₃ solution at 303 K, revealing it to be

a better system in contrast to 1.1 M TBP/n-DD, which forms a third phase at ~ 55 g/L under similar condition. Density, viscosity and interfacial tension of T2MBP were measured to be higher than the corresponding TBP based solution. The thermal and radiation behavior of T2MBP were observed to be at par with TBP. Lower third phase formation and lower aggregation behavior of T2MBP were seen during the extraction of mineral acids and tetravalent metal ions, as compared to TBP based systems. The study shows the potential of T2MBP as the extractant in various stages of nuclear fuel cycle, especially in the reprocessing of fast nuclear spent fuel and for the separation processes involving the extraction of tetravalent metal ions. A non-aqueous route has been developed to determine the phase splitting and aggregation behaviour of the extractant systems that are sparingly soluble in aqueous phase. Matrix isolation infrared spectroscopy and DFT studies confirmed that the gauche conformer of T2MBP is energetically preferred over the trans ones due to the overwhelmed stabilization hyperconjugative delocalization over destabilization steric interactions.



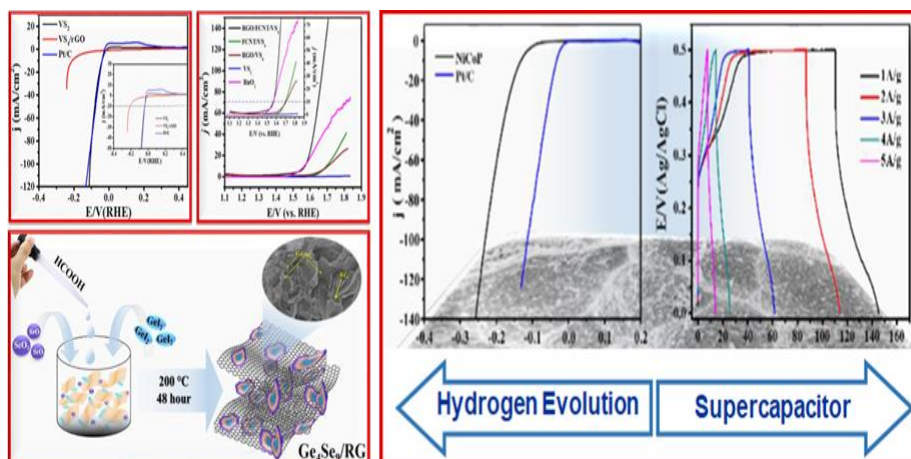
Variation of the concentration of solutes in the organic phase during (A) U(VI) and (B) Pu(IV) extraction by 1.1 M T2MBP/n-DD from nitric acid media as a function of $[metal]_{aq,eq}$ at 303 K.

1.3 NISER, Bhubaneswar

1.3.1 Metal chalcogenides and phosphides based electrode materials: an efficient catalyst for energy conversion and storage applications

Electrochemical water splitting is the most cost-effective and efficient method for producing hydrogen (H₂) and oxygen (O₂). State-of-the-art water splitting techniques use catalysts made from precious elements like Pt and Ir to reduce the overpotential required to overcome the kinetic barrier associated with the hydrogen bond in a water molecule. However, improving the production scale of hydrogen and oxygen through the aforementioned catalysts is not cost-effective. Therefore, cheaper, and better alternatives should be developed to achieve better catalytic efficacy and improved durability for the water-splitting process. Striking examples are transition metal chalcogenides (TMCs), and metal phosphides (TMPs), as they display peculiar electrocatalytic properties, enabling them to impart substantial progress in the field of energy storage and energy conversion. With this perspective, present thesis deals with the successful synthesis of vanadium-based metal chalcogenides and their hybrids with reduced graphene oxide (RGO) and functionalized carbon nanotubes (FCNTs) and investigate the prospects of these materials in the oxygen evolution reaction (OER). A tetra

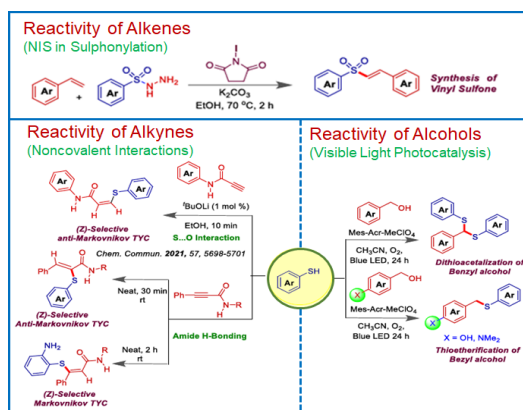
germanium nonaselenide (Ge_4Se_9) and reduced graphene oxide (RGO) hybrid has also been developed in this study for supercapacitor applications. Hydrothermal synthesis of a three-dimensional nickel-cobalt phosphide hollow sphere useful for energy conversion and storage applications has also been reported in the present work. Synthesis methods and possible applications of the studied materials are schematically presented in the below.



Schematic diagram of nucleation growth and applications of TMCs and TMPs.

1.3.2 Reactivity control of alkenes, alkynes, and alcohols for C-S bond formation reactions

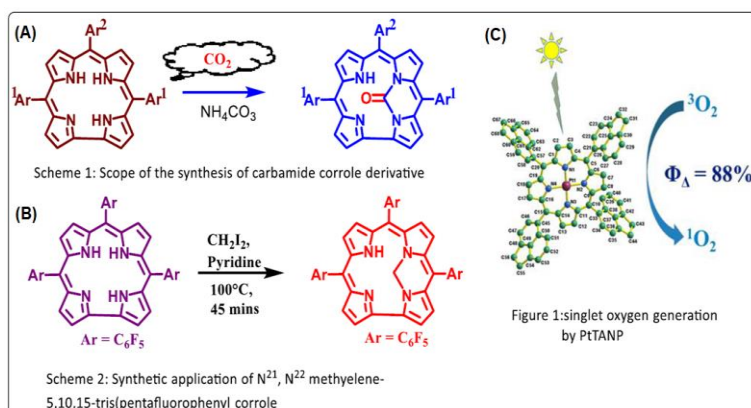
Sulfur-containing compounds are well existing in natural products and in many commercial drugs. Further, organosulfur compounds are universally used in agrochemical and material sciences. Therefore, research on sulfur-based molecules is always appealing and challenging. Chemists are making assiduous efforts in mimicking and modifying synthetic methods for building exotic molecular architectures utilizing mild reaction conditions, new synthons, improving atom-economic and step-economic processes. With this perspective, the focus of the present thesis has been to control reactivity of alkenes, alkynes, and alcohols in the C-S bond formation reactions. Many sustainable tactics like the use of N-iodosuccinimide (NIS) as cheap and eco-friendly iodine reagents, exploitation of noncovalent interactions like N-H...S hydrogen bonding, S...O interaction, and visible light photocatalysis have been utilized in the present thesis to form various C-S bonds. As the alkene source, styrene was functionalized with sulfonyl hydrazine in the presence of NIS (2.5 equiv) and K_2CO_3 (1.5 equiv) to provide (E)-selective vinyl sulfones. Similarly, addition of various thiophenols to N,3-diphenylpropionamide as the internal alkyne showed exclusive switching of selectivity from (Z)-anti-Markovnikov to (Z)-Markovnikov vinyl sulfide on (Z)-anti-Markovnikov vinyl sulfides via N-H...S H-bonding and N-H...N type H-bonding interactions. In continuation, reactivity of terminal alkynamide was also controlled by newly identified S...O interaction to attain the (Z)-selectivity of vinyl sulfides in the presence of *t*BuOLi. The use of 9-mesityl-10-methylacridinium perchlorate organophotocatalyst for the direct formation of dithioacetals or thioethers reaction from benzyl alcohol via C-O bond functionalization has also been discussed. Thus, the reactivity of benzyl alcohol was also controlled by using an appropriate photocatalyst. In conclusion, the work carried out in the thesis offers an excellent guideline in the research area of organosulfur chemistry by merging the novel concept of weak interactions and catalysis.



Various strategies for controlling reactivity of alkenes, alkynes, and alcohols for C-S bond formation.

1.3.3 N-substituted and N-unsubstituted porphyrinoids: Synthesis, structure, spectroscopic characterization, and applications

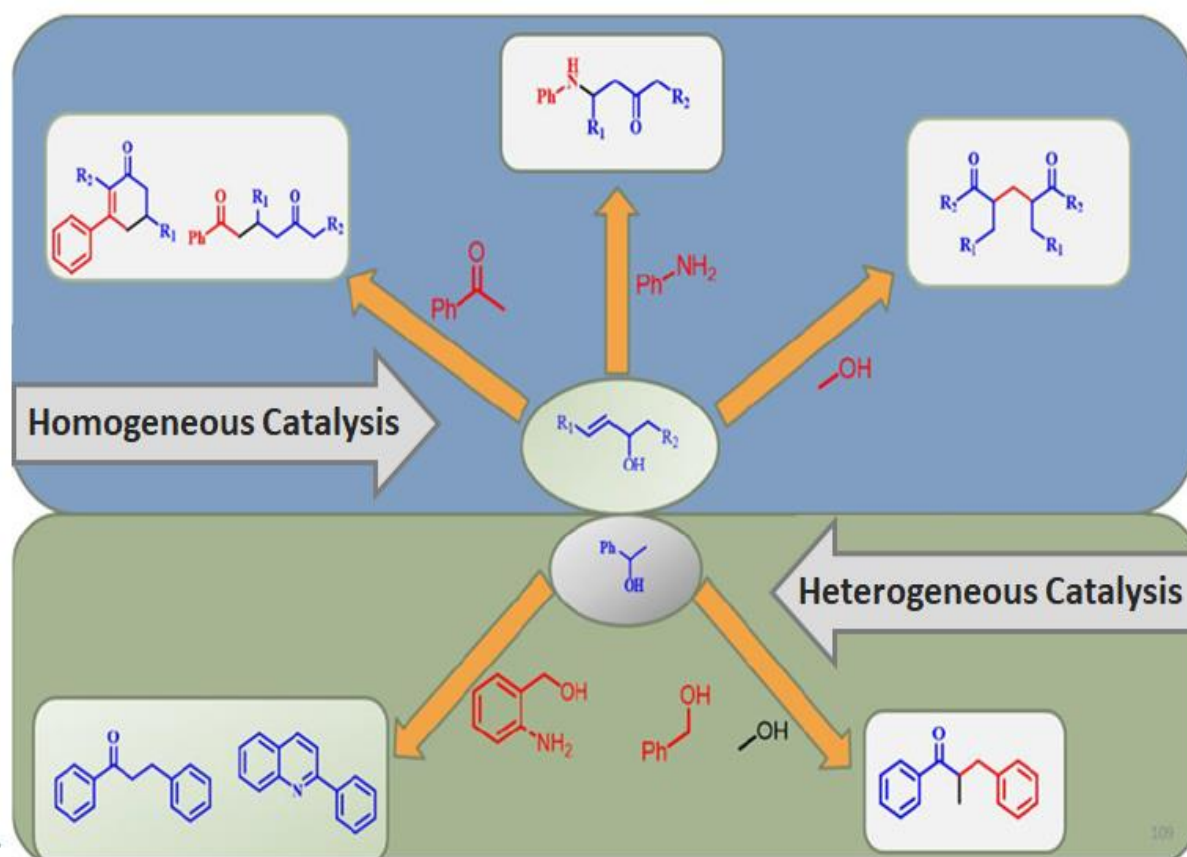
Studies on N-substituted corroles are rarely reported in the literature. Present thesis reports an efficient, high yielding, single step and relatively greener methodology for facile synthesis of inner core modification of corroles like N^{21}, N^{22} -carbamide corrole derivatives. Further complete characterizations of these carbamide corrole derivatives and generalization of the newly designed synthetic protocols have been achieved. The first report on the methylene bridge of 5,10,15-tris(pentafluorophenyl)corrole has also been reported and highlighted in the present thesis. The superiority of the newly designed synthetic protocol over the previously reported N, N' -one carbon bridged porphyrin synthesis method has also been discussed. Optimization of the developed methodology and comprehensive characterization of the new macrocyclic molecules prepared in the present work have been carried out using different physicochemical techniques. Synthesis of a new platinum(II)-porphyrin complex, [5,10,15,20-tetra(5-acenaphthyl)-porphinato]platinum(II); PtTANP) and its characterization have also been accomplished. The so prepared PtTANP complex behaves as a light harvesting antenna and helps in the singlet oxygen production with a quantum efficient of $\sim 88\%$, indicating the potential applications of this material in the field of photodynamic therapy as well as in the development of an oxygen sensor.



Synthesis of (A) carbamide corrole derivatives, and (B) N^{21}, N^{22} methylene-5,10,15-tris(pentafluorophenyl) corrole. (C) Singlet oxygen generation by PtTANP complex.

1.34 Pyrazole and BINOL phosphoric acid based palladium catalysts and their application in organic transformations

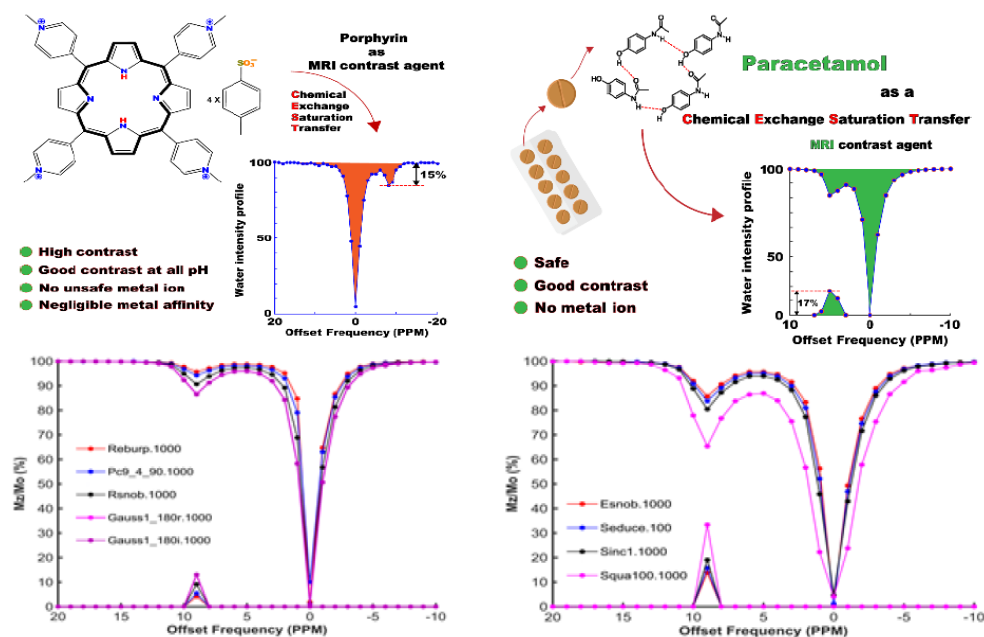
Palladium based catalysts have gained immense importance to the synthetic organic chemists to carry out C-C and C-N bond formation reactions in the synthesis of natural products and medicinal compounds following cross-coupling reactions. Being abundant feedstocks, alcohols have been used recently for their transformation under borrowing hydrogen and/or interrupted borrowing hydrogen methodology, replacing more toxic substrates in the C-C and C-N bond forming reactions. In the present thesis, development and use of pyrazole and BINOL phosphoric acid (BPA) based palladium catalysts have been presented for the functionalization of alcohols under homogeneous and heterogeneous catalysis conditions. In relation to the homogeneous catalysis, the tandem isomerization and functionalization of allyl alcohols have been used for the synthesis of important precursor compounds for natural products. Accordingly, synthesis of 3-arylcyclohexenone, 1,5-diketones, and β -aminoketone have been developed using Pd-BPA system under homogeneous catalysis. Using polystyrene anchor, three heterogeneous palladium-based catalysts have also been developed in the present work. Use of these catalysts have been studied in the activation of secondary alcohols for the synthesis of α -alkylated ketones, quinolines, and one pot three component synthesis of α -branched ketones. The cross-linked anchored catalyst has been reused suitably for seven times for alkylation and quinoline reaction and for five times for one pot reaction.



Allyl alcohol functionalization by Pd-BPA system under homogeneous condition (top) and secondary alcohol functionalization under heterogeneous condition.

1.3.5 Enhancement of diamagnetic CEST MRI contrast efficiency: An electronic and NMR experimental parameter optimization approach

Widespread popularity of Magnetic Resonance Imaging (MRI) as a non-invasive imaging technique is attributed largely to the invention of MRI contrast agents that bring out clarity in the images by creating a difference in brightness (intensity) between the region of interest and the surroundings. Traditional contrast agents act to shorten either the longitudinal or the transverse relaxation time constants of water to infuse the intensity variation in the image. As these contrast agents contain metal (gadolinium) they are somewhat unsafe. Search for an alternate has led to the introduction of Chemical Exchange Saturation Transfer (CEST) based contrast agents in the year 2000, which are broadly of two categories, some having the presence of metal center (paraCEST) and the others having the absence of a metal center (diaCEST). Though paraCEST agents are more efficient in creating contrast, considering safety aspects the diaCEST agents are considered to be the preferred ones. Present thesis investigates on the methods for enhancement of CEST efficiency either by altering the electronic structure of the chemical system or by suitably modifying the experimental NMR parameters. It is shown that a simple chemical modification makes a porphyrin derivative to act as a potential diaCEST contrast agent having high CEST contrast efficiency for a large pH range as compared to the first reported porphyrin-based contrast agent for which CEST efficiency drops drastically at physiologically relevant pH and temperature. The thesis also demonstrates how hydrogen bonding in acetanilide derivatives enhances the CEST efficiency and can work as a diaCEST agent at physiological condition. The study also proposes that paracetamol, a well-known analgesic, can also act as a potential diaCEST contrast agent for MRI. Studies dealing with modifying experimental NMR parameters show that efficiency of an already high efficiency diaCEST contrast agent (e.g. salicylic acid) can be enhanced further through suitable parameter optimizations.



Enhancement of diaCEST contrast efficiency for MRI by altering the electronic structure and NMR experimental parameters.

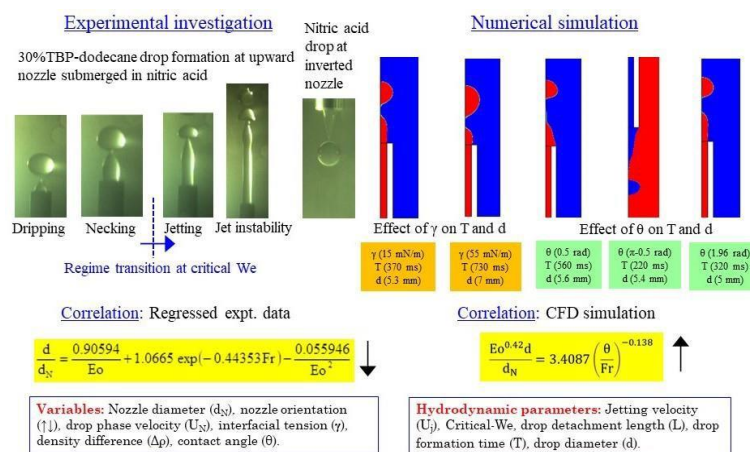
2. Engineering Sciences

During the period of report, HBNI awarded 39 Ph.D. degrees in Engineering Sciences. The summary of some of the theses is given below.

2.1 Bhabha Atomic Research Centre, Mumbai

2.1.1 Hydrodynamics of drop formation in liquid - liquid systems: experimental and simulations

The research work carried out in the thesis is aimed at experimental and numerical investigation of hydrodynamics of drop formation at upward and inverted nozzles submerged in an immiscible quiescent liquid phase. The liquid-liquid systems used in the experimental study are 30%TBP-dodecane and varying concentrations of nitric acid (0.01, 1, 3N). The experiments using high speed imaging enabled capturing of drop growth, necking, onset of jetting and drop pinch-off. Regime transition is identified at critical Weber number and depicted in a state diagram between Eötvös and Weber number. A case study on comparison of drop formation in coflowing liquids in microcapillary device and at nozzles submerged in quiescent liquid phase revealed resemblance in regime transition from dripping to jetting - an interesting observation. Outcome of the experimental study are the quantification of jetting velocity, drop detachment length, drop formation time and drop diameter for various combinations of independent variables. Effects of nozzle orientation on hydrodynamics of drop formation is explicitly studied. Correlations are proposed for jetting velocity and drop diameter based on regressed experimental data.



Experimentally captured images and snapshots of transient CFD simulation of hydrodynamics of drop formation. Typical correlations based on regressed experimental data and simulation are indicated.

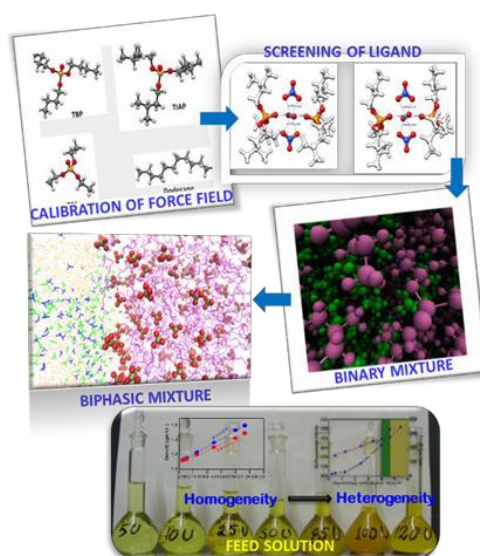
A CFD model is developed based on phase-field method for simulation of drop formation and validated using the experimental data of this work. CFD model based parametric analysis is carried out to study the effects of selective variation of physical properties on drop diameter and drop formation time. Simulation-based correlations with contact angle as a variable are proposed for drop diameter. Outcome of the research has first-of-its-kind deliverables with relevance to design and operation of reprocessing plants.

2.1.2 Structure and dynamics of radionuclide-ligand solvent system in the fuel reprocessing: MD simulation studies

Separation of metal ions from spent nuclear fuel is of immense importance in the development of fresh fuel for 2nd generation nuclear reactor. The selection of ligand and its characterization in binary and biphasic mixture along with the characterization of feed solution through computational chemistry to mimic the PUREX process are some of the best ways to develop a liquid-liquid extraction process.

In view of inherent limitations of TBP in reprocessing applications, novel ligands are in demand. TiAP, a homologous of TBP may be an alternative. Starting from the calibration of OPLS-AA force field and then screening of ligands exhibited that Mulliken embedded force field is the best choice and TiAP is the potential ligand. The superiority of TiAP over TBP for the extraction of UO₂ ion has been demonstrated by free energy of extraction using DFT. The studies were extended on the evaluation of various molecular properties of TiAP and TiAP/dodecane mixture with different mole fraction of TiAP. The composition of the binary mixture was decided based on the dynamical properties and it was 20- 30%. The work was further extended on the various structural and dynamical properties of simple and complex biphasic system. The interfacial properties were investigated in the presence of TiAP and nitric acid employing molecular dynamics (MD) simulations.

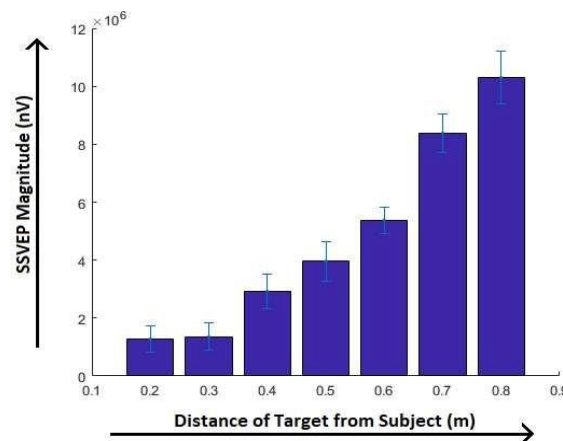
The inverse relation between interface thickness and interfacial tension was established. Furthermore, a simple equation was obtained by fitting the MD results of total interface thickness for a wide range of composition of third component. Additionally, the versatility of single force field was observed. The super-saturation effects were captured by inflection in the plot of surface tension and shear viscosity against concentration due to solution heterogeneity and was correlated by an inflection in the scattering intensity by performing dynamic light scattering (DLS) experiment. The limiting concentration of uranyl nitrate in feed solution was decided.



Calibration of force field, screening of ligand and characterization in binary and biphasic mixture and finally evaluation of limiting concentration of uranyl nitrate in feed

2.1.3 Continuous and intuitive control of a robot manipulator using brain-computer interface

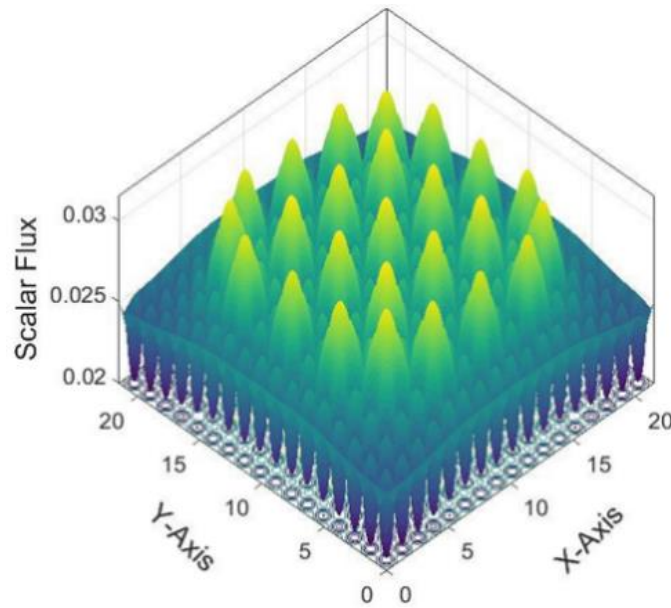
The Brain-Computer Interfaces (BCIs) decode the human brain signals in order to control some external device like a robotic arm. The electrical activity of the brain can be non-invasively acquired using Electroencephalography (EEG). Literature provides several BCI paradigms, to achieve voluntary variation in the EEG activity, generally offering discrete output commands that cannot continuously and spontaneously control a motion parameter of a robotic arm e.g., the speed of the robotic arm. One such BCI paradigm is Steady-State Visually Evoked Potential (SSVEP). The SSVEP based BCIs are based on the fact that, when multiple flickering stimuli (flickering at different frequencies) are shown to a person on a computer screen, the frequency of that stimulus on which the person is gazing becomes higher in his/her occipital EEG. Hence, multiple discrete commands are offered by the traditional SSVEP paradigm in which a person has to gaze at a particular stimulus to output the command corresponding that stimulus. If a passive fixation target is placed between a stimulus and the person, focusing on the target causes blurring of the stimulus, thereby reducing the SSVEP magnitude corresponding to the stimulus. The thesis presents a novel setup that utilizes the SSVEP magnitude modulation due to eye-accommodation or focusing away from the stimulus. A person could vary his SSVEP magnitude by focusing at fixation targets placed at different distances (on a metallic strip) between the stimulus screen and the person. The SSVEP magnitude continuously reduces as the person focuses away from the stimulus as can be seen in schematic below. A mathematical relationship was established between the SSVEP magnitude and the focusing distance using which the focusing distance could be predicted from the SSVEP magnitude. This prediction was then mapped to continuously control the speed of a robotic arm. This BCI provided an intuitive slider-like control of the robotic arm's speed. The SSVEP magnitude modulation could also be used to extract multiple discrete commands from a single stimulus unlike the traditional SSVEP setup where multiple stimuli are required to generate multiple commands. Electrooculography (EOG) and Electromyography (EMG) based interfaces are also developed in the present work for robotic arm control. The EOG based interface offers discrete control of a robotic arm using eye blinks and eye closing/opening activities while the EMG based interface provides continuous speed control of a robotic arm using teeth clenching activity.



Mean and standard deviation plot of the SSVEP magnitude vs. Focused Target's distance for one of the subject

2.1.5 Study of neutron transport in heterogeneous assemblies using method of characteristics coupled with Delaunay triangulation

Neutron transport modeling is the most essential part of physics simulations of reactor cores. Accuracy of high-fidelity nuclear reactor simulations relies on the comprehensive modeling of all heterogeneity with minimum simplifications and/or assumptions as well as the use of detailed nuclear cross-sections. The method of characteristics (MOC) is particularly well-suited for such exhaustive whole core simulations due to its accuracy and geometric flexibility. Neutron transport in 2D heterogeneous systems has been studied in the present work using MOC and triangular unstructured meshes. As a part of this work, a new high fidelity neutronic analysis code DIAMOND has been developed which has been used to perform a systematic comparison between conventional and triangular unstructured meshes. The Modified Bowyer-Watson algorithm has been proposed as an improved technique to enable Delaunay triangulation in the presence of only degenerate vertices and eliminate the requirement of a bounding box in the conventional Bowyer-Watson algorithm. A fast and efficient linear search based ray tracing scheme has also been developed by transforming the ray tracing process into an array based search. Further, the optimally diffusive coarse mesh finite difference (odCMFD) method has been used to accelerate the MOC transport calculations, odCMFD has shown unconditional stability w.r.t. coarse mesh (CM) thickness with significant performance gains of 25-35x on the average and a peak speed up of 195x. The convergence performance of CMFD based acceleration schemes has been studied with an alternate perspective by varying the CM size rather than total cross-section. It has been shown that for best acceleration, the optimum CM size should be chosen to not only minimize the number of high-order transport iterations but also ensure the low-order odCMFD linear system is not prohibitively large to dominate the overall computation time. It has been found that convergence criteria for low-order odCMFD system ϵ_{LO} should not be chosen arbitrarily and must be finer than the high-order convergence criteria ϵ_{HO} . Optimum performance is obtained with $\epsilon_{LO} = 10^{-1} \times \epsilon_{HO}$ and the results should be applicable to other non-linear acceleration schemes for steady state transport calculations. For the first time, the asymptotic convergence properties of CMFD based methods for acceleration of neutron transport calculations have been theoretically investigated for multiple energy groups using Fourier analysis. Expressions for the multi-group error transition matrix and spectral radius have been found to be block-analogous to existing one-group results. odCMFD has been found to be unconditionally stable w.r.t. CM optical thickness in any energy group and offers superior convergence performance than both pCMFD and CMFD methods even with multiple energy groups. It has also been shown that the rate of convergence is primarily governed by the energy group having the largest CM total cross-section. In summary, this work has led to the development of code DIAMOND, a high-fidelity neutron transport modeling tool using MOC and Delaunay triangulation. The transport calculations are sped up using highly efficient acceleration techniques whose convergence properties have been analyzed both numerically and theoretically, and lead to improved understanding of these systems in the multi- group framework.

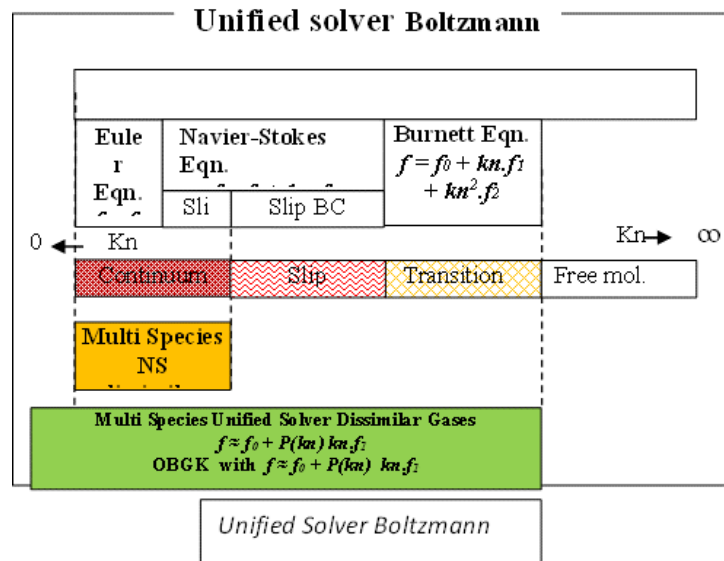


Thermal neutron flux in 17×17 PWR assembly

2.1.6 Modelling of multi-component compressible flows for wide range of Knudsen numbers

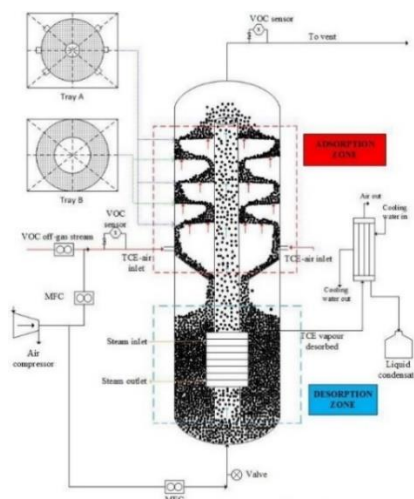
Multi-component compressible flow simulation has numerous applications in fields of micromechanical, vacuum and aerospace engineering. Such applications require solvers that can handle (i) continuum flows, (ii) non-continuum flow, (iii) shock related physical instabilities and (iv) multi-component system related numerical instabilities. Solvers reported in literature demonstrate such capabilities using unphysical models in their formulations. In the present research, a unified solver for multi-species compressible flows has been developed and its simulation capability has been demonstrated with dissimilar gases and Knudsen numbers ranging from continuum to transition flow regime. The Onsager's maximum entropy production principle (MEPP) based Bhatnagar Gross Krook (referred as OBGK) kinetic model has been used to derive the formulations, which ensure maximum entropy addition into the physical process, so that shock related physical instabilities are properly captured. This was performed for the first time and not reported in literature. In order to resolve the kinetic and hydrodynamic multi-scales in the flow a high-resolution algorithm based on WENO was developed. This developed algorithm along with a proposed predictor-corrector approach has minimized the multi-component system's numerical instabilities. This helps in accurately capturing the physics of any problem. The approach of linear irreversible thermodynamics (LIT) has been used to derive a new formulation for continuum flows and its capabilities has been demonstrated using Richtmyer Meshkov instability (RMI) problems. The extension of this approach to non-continuum flows has been modelled using a correction factor ($P(kn)$) over (LIT) instead of using a complicated second order perturbation. The governing equations were derived based on this hypothesis. The unified solver developed has been validated using various benchmark numerical (DSMC) test cases/ experimental data. Apart from wide Knudsen numbers, this solver can handle polyatomic gases with flexible Prandtl number, molecular weights and specific heat ratios. The developed scheme is (i) found to minimize unphysical oscillation, (ii) easily adaptable to existing FVM based NS solvers (iii) having

good resolution over wide range of Knudsen numbers, (iv) requires less computational time compared to DSMC solvers.



2.1.7 Experimental study and modelling of trichloroethylene vapour adsorption in fluidized bed

Trichloroethylene vapours are emitted during the sol-gel synthesis of solid breeder material, lithium titanate (Li_2TiO_3). These vapours are toxic, hazardous, and carcinogenic and can adversely affect the human health when exposed to for extended duration. Hence, the simultaneous adsorption and desorption of TCE vapours in a multistage circulating fluidized bed column was studied for its separation and recovery for reuse as a solvent. Activated carbon is a suitable adsorbent for the separation of organic pollutants because of its hydrophobic nature and non-polarity. The adsorption isotherms of TCE vapours in air (carrier gas) on activated carbon shows promising results with TCE adsorption of 624 mg/g. The hydrodynamic parameter evaluation of minimum fluidization velocity (um) and solids holdup on trays for activated carbon of particle sizes (212, 425, and 710 μm) helps control the extent of fluidization and calculate the adsorption efficiency. The continuous adsorption of TCE in carrier gas on activated carbon in packed, fluidized, and circulating fluidized bed shows that the packed bed adsorption shows highest breakthrough time for a given flowrate (90min), the fluidized bed shows the maximum adsorption capacity, and the multistage circulating fluidized bed showed higher adsorption efficiency of more than 85%. Effect of operating parameters of flowrate, inlet concentration of TCE, adsorption and desorption temperature help determine the optimum conditions for effective separation. Higher flowrates. ($u/um = 2$) and higher inlet concentration of TCE (65 mg/l) at the inlet results in faster breakthrough (6 min) and higher adsorbed amount (222-666 mg/g) due to the enhanced gas-solid mixing and uniform temperature distribution. Increasing adsorption temperature to 80 $^\circ\text{C}$ has a negative impact on the amount adsorbed with reduction of >45%. Higher desorption temperatures of 350 $^\circ\text{C}$ can facilitate complete removal of the TCE vapors from the carbon surface. The desorbed TCE vapors may be sent to a condenser for recovery of solvent. A linear driving force (LDF) model is developed to predict the transient and axial behavior of TCE concentration and the amount of TCE adsorbed per gram of activated carbon in the fluidized bed and the results were compared with the experimental breakthrough curves for validation.

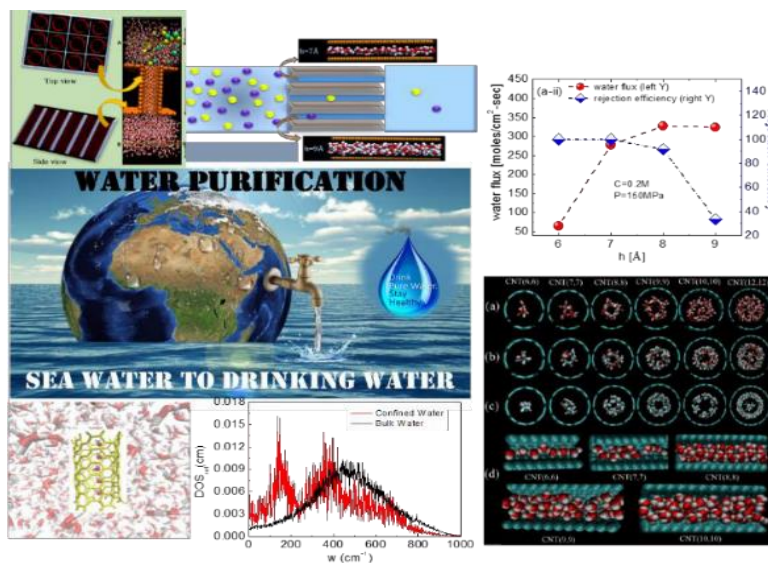


Schematic diagram of multistage circulating fluidized bed

The study will be helpful to treat the continuous emission of TCE vapours with simultaneous regeneration of adsorbent and recovery of TCE via condenser and keep the TCE emission under permissible value.

2.1.8 The dynamics and thermodynamics of fluid transport through hydrophobic channels of carbon nanotubes

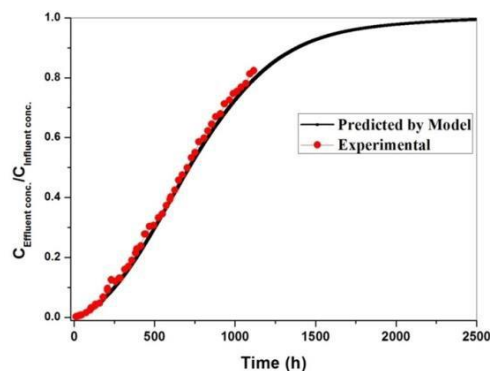
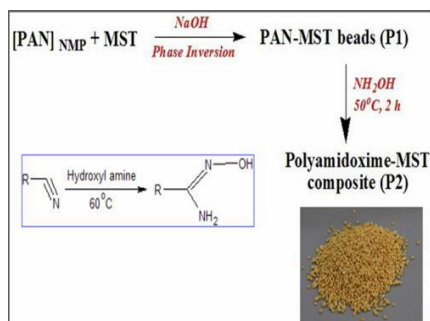
In order to search for an efficient membrane for water purification, the mechanistic pathway for fluid transport and desalination through Nano membrane have been performed using molecular dynamics simulations. The associated driving forces for transportation of water and methane in carbon nanotubes have been investigated in terms of absolute entropy, enthalpy, and free energy. The internal space wetting of hydrophobic nanotube was predicted to be free energy favored which is primarily dictated by increased rotational entropy. It was demonstrated that the gain in translation entropy is not unique to H bonding fluid like water but is also observed for non-hydrogen bonded fluids. Though H-bonding plays an important role in conduction, but it (H bond) is not the solitary driving factor for wetting of nanotubes. The transition of fluid behavior from sub-continuum to continuum regime has been captured with increasing nanotube diameter. A new quasi-universal relation between scaled diffusivity D^* and excess entropy S_{ex} has been developed for molecular fluids and fluid mixture in bulk and nanotube confinement. Furthermore, the water and ion flow are discussed with varied strength of pressure gradient and salt concentration for different scales of nanotube and graphene confinement. The results revealed that the membranes comprising nanotubes of 1.0–1.1 nm diameter can be optimized with average permeability 10^{-3} moles/cm²-sec-MPa and salt rejection efficiency more than 95% for efficient water desalination. The results predicted two orders of higher permeability with graphene membranes compared to conventional thin film membranes which seems to be associated with the breakdown of continuum hydrodynamic for nanoporous confinement. The results presented in the thesis are intended to provide a microscopic framework for understanding the structural, dynamical and thermodynamical integrity of fluids in nanoconfinement, and thus will be very useful for future experimental and computational nanofluidics system.



Water purification using nanotube and graphene nanomembranes

2.1.9 Development of nanosorbents and nanocomposites for radioactive waste cleanup

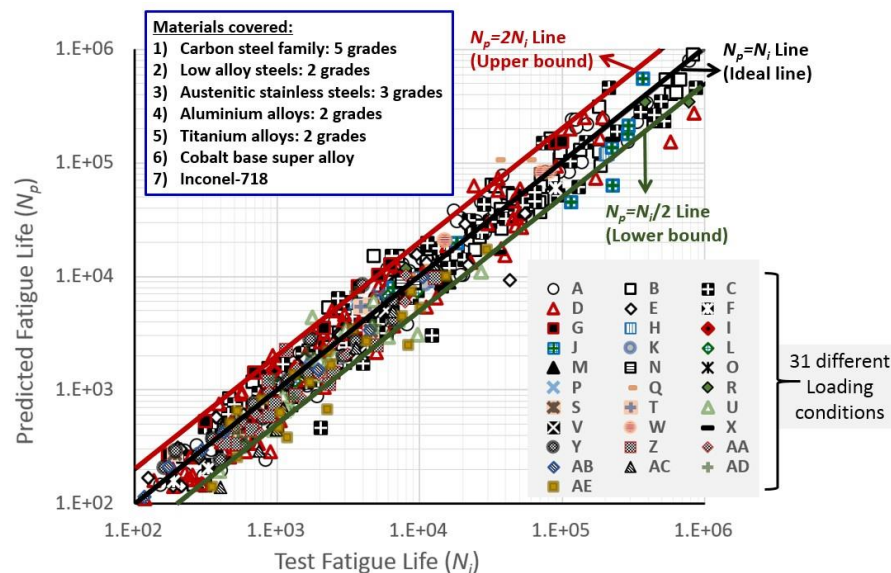
The work in the thesis addresses the separation of radionuclides from low-level waste utilizing synthesized nanocomposite. LLW is characterized by the large volume, low activity (mainly due to traces of ^{137}Cs & ^{90}Sr), relatively low dissolved solids (~ 5 g/L) and near-neutral pH. Three titanate-based sorbents, viz., MST, LHT-9 and CST and four composites have been synthesized using Cement, PAN and Chitosan binder. Results of detailed radio-elemental separation studies are highlighted as follows: Excellent Cs separation performance by CST-Cement composite column and Sr separation by MST-Chitosan was demonstrated by treating more than 5000 BV and 10,000 BV, respectively, of simulated LLW with separation efficiency of more than 99.9%. The synthesized, Monosodium-PAN-Amidoxime composite shows a very high affinity for Uranium. It is demonstrated that more than 12,000 BV of Uranium contaminated groundwater can be treated using a fixed bed column of the composite. It is inferred that the synthesized composite can find applications for the separation of U from groundwater.



Column performance of MPA for uranium uptake has been simulated using COMSOL. The experimental and model-predicted results were in good agreement, validating the model assumptions. The model prediction confirms that the residence time is a fundamental parameter to design the packed bed column in the present work.

2.1.10 A modified cyclic plasticity model for C-Mn steel and a new critical plane model to predict crack initiation under multiaxial cyclic loading

The piping/ vessel components of Indian Nuclear Power Plants (NPPs) are subjected to complex multiaxial cyclic conditions. These components are designed for envisaged cyclic conditions using standard codes. The current design procedures under complex multiaxial cyclic loading conditions do not adequately account for fatigue damage. Therefore, such design procedures result in inaccurate fatigue life assessments. In this regard, extensive fatigue tests have been conducted to determine the extent of fatigue damage under proportional and non-proportional axial-torsion conditions vis-à-vis simple uniaxial cycling on C-Mn steel. Various phenomenological critical plane models (in literature) have been explored for fatigue life assessment. The existing critical plane models are associated with subjectivity in calculation of resultant shear on oblique material plane under



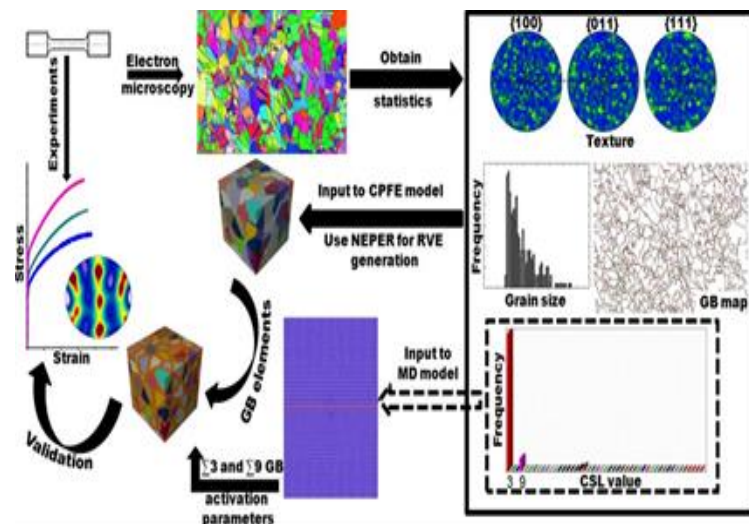
Comparison of predicted (using developed critical plane model) and experimental fatigue life for ferrous and non-ferrous materials/ alloys subjected to 31 loading paths

Further, as brought out from experimental studies, that C-Mn steel showed additional material hardening under non-proportional axial-torsion test cases than the corresponding proportional tests. This additional hardening is not simulated using conventional non-linear kinematic hardening rule of Chaboche model. The material subroutines have been programmed for popular cyclic plasticity models accounting for non-proportional hardening. A modified material model has been proposed which resulted in more accurate simulation of cyclic stress-strain response under uniaxial, proportional, and non-proportional axial-torsion conditions, as tested for C-Mn steel.

2.1.11 A multiscale model for simulation of plastic deformation behavior of Ni-based alloys with explicit consideration of the effect of grain boundaries

For polycrystalline materials, the plastic deformation behavior is governed by pre-existing defects like dislocations and grain boundaries (GBs). During deformation, GBs can act as obstacles, sources,

and sinks to dislocations. In reality, all these traits often co-occur in conjunction with bulk plasticity within the grains. All these processes are inherently multiscale in nature, and are, thus, modeled discretely using a single length scale or time scale tool. The modeling efforts are then linked through some empirical coupling across the scales which may not be representative of the actual phenomena. It is, therefore, essential to explore new avenues to model polycrystal plasticity incorporating physically-justified GB modeling schemes. This is the prime focus of the current work. The multiscale approach adopted is presented in schematic. Microstructural characterization provides the statistics on initial texture, grain size distribution and GB character distribution of the polycrystalline material. The statistical distribution of GBs determines the major CSL boundaries present in the alloy. Since thermally activated deformation mechanisms are prevalent under the investigated experimental conditions of uniaxial tension and compression at different temperatures, these GBs are modeled in the realm of atomistic simulations to quantify the activation parameters for partial dislocation nucleation from GBs. The extracted parameters are passed on to the flow rule of transition state theory based crystal plasticity model. At this level, interfaces are explicitly modeled by assigning discrete thickness to the elements representing GB affected region and the associated parameters are directly taken from lower scale atomistic simulations. For bulk grains, dislocation dynamics simulations are utilized to calibrate the hardening parameters for single phase polycrystalline materials and different starting initial textures are utilized to achieve an optimum hardening parameter set for multiphase polycrystalline materials for use in crystal plasticity simulations. The approach is validated by comparison with the experimental stress-strain curves and deformed textures.



Schematic of multiscale simulation methodology adopted in this work for appropriate inclusion of GB effects

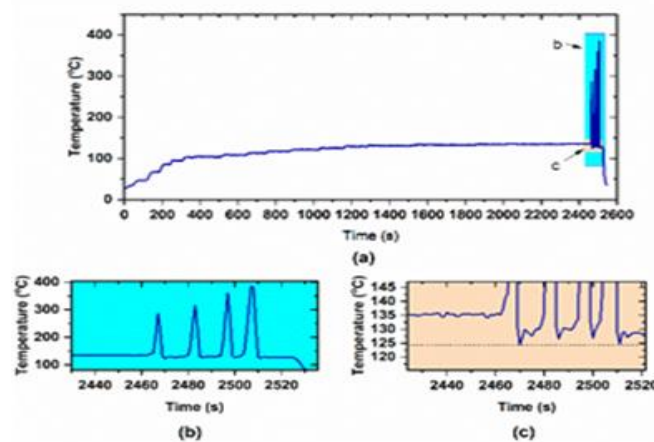
2.1.12 Study of departure from nucleate boiling in rod bundle of PWRs

Determining Departure from Nucleate Boiling (DNB) from the first principles has always been a great challenge to researchers. Conducting experiments at high pressure and high temperature (HPHT)

conditions, especially for PWR rod bundles, is technically challenging and highly expensive. An assessment carried out in the thesis has shown that the existing DNB correlations have a wide scatter and cannot be extrapolated to any geometry of choice. Moreover, apart from normal HPHT operating conditions, low pressure and low flow (LPLF) conditions can occur during accidental conditions of PWRs. An extensive literature review revealed that there is poor understanding of DNB under such LPLF conditions.

To determine DNB at HTHP conditions in rod bundles of PWRs, a generic computational fluid dynamics (CFD) model based on the two-fluid Eulerian approach coupled with heat flux partitioning has been developed. A robust CFD framework has been developed based on extensive assessment of existing boiling and momentum closures to predict subcooled flow boiling heat transfer. New empirical models have been developed for boiling closures to simulate the near-wall void fractions accurately in subcooled flow boiling. Using the CFD model, DNB has been predicted in tubes. Further, to reduce the empiricism involved in the modeling of boiling closures, semi-mechanistic models have been developed for bubble departure diameter and departure frequency based on force balance analysis. Using the developed semi-mechanistic models for bubble departure characteristics, DNB has been predicted in tubes at high pressure conditions. The developed CFD model has been extended to predict DNB in square and hexagonal lattices relevant to PWRs

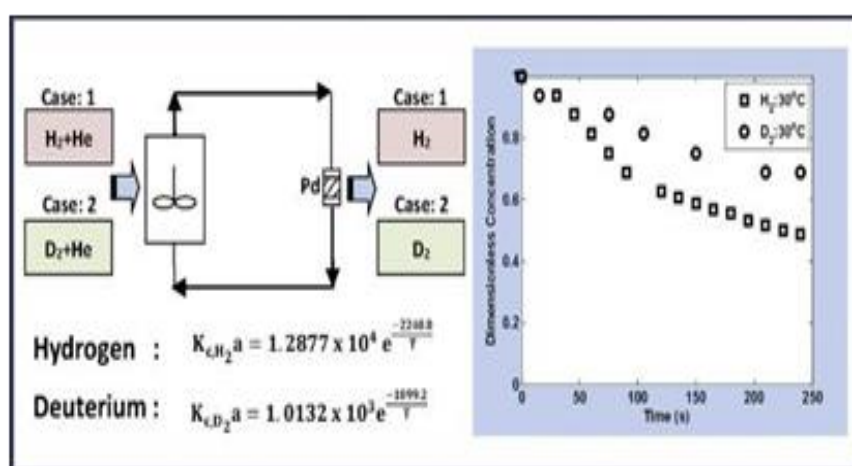
To understand the DNB phenomena at LPLF conditions, experiments have been carried out at low flow conditions. Experiments at low sub cooling conditions revealed that DNB occurred due to flow oscillations caused by flow pattern transition from slug to churn flow. This is different from the DNB phenomena at HPHT conditions that occur mainly due to bubble crowding. Interestingly, experiments revealed a new DNB mechanism different from previously believed theories at high sub cooling conditions. The observed phenomenon was coined as "Sonneting CHF". An interesting rhythmic flow pattern dance occurs at Sonneting CHF, during which the surface temperature rises and falls with amplitudes increasing and decreasing in every cycle until the heater trip-set point is reached. Contrary to the current beliefs, extremely unprecedented quenching scenarios occurred even though the heater surface temperatures were substantially high. This new understanding is likely to improve the models for safety analysis in the future.



(a) The DNB plot (Sonneting CHF); (b) The zoomed-in portion of the same plot in (a) indicating the surface temperature peaks; (c) zoomed portion of the plot (a) showing the lowest temperature recordings

2.1.13 Studies on the recovery and separation of hydrogen isotopes from inert gas

The objective of the present study is the evaluation of different processes for the recovery and separation of hydrogen isotopes from inert gas such as helium. The processes such as oxidation, adsorption, permeation, and electrochemical separation were studied in detail. In most of the cases, the experimental data on kinetics using heavier isotopes of hydrogen are very scarce. In catalytic oxidation, multi-step reaction mechanism in presence of platinum catalyst was analyzed and a simple rate expression is proposed and validated. A new mass transfer correlation was proposed to determine the gas film mass transfer coefficient in terms of Sherwood number, Schmidt number, and Reynolds number. The feasibility of recovery of hydrogen from helium by oxidation using metal oxides (viz, CuO) was established in a temperature range from 100°C to 200°C and the system was modeled using classical shrinking core model. Further, the recovery of hydrogen isotopes from helium using palladium-based adsorbent was studied and the rate limiting step is found out to be internal diffusion. A schematic of the process and the results are summarized in the schematic below.



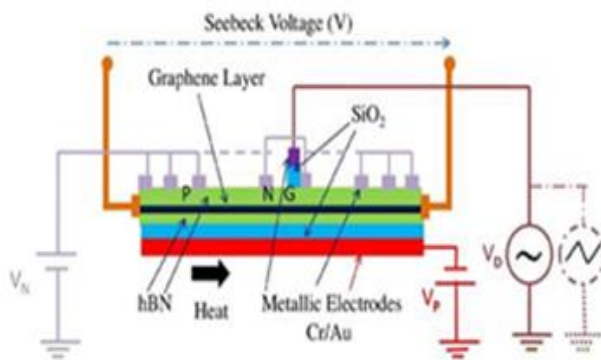
Process schematic & dimensionless concentration versus time for adsorption

A composite tantalum membrane was fabricated in-house using sputter coating technique. An optimum temperature range of operation is determined using tantalum membrane for hydrogen and deuterium. The separation of hydrogen from helium was studied further using an electrochemical reactor. In the electrochemical reactor, a current density of 2000 Am^{-2} could be achieved at a cell voltage of less than 100 mV and the electrochemical reactor was modeled as a plug flow reactor with side withdrawal. Finally, a comparison of different processes was made based on different criteria such as percentage gas recovery, mode of operation (batch/continuous), energy required, operating temperature and gas purity achieved in different processes. Based on all the above criteria, the electrochemical separation is proposed to be a promising option.

2.1.14 Studies and analysis of radioisotope thermoelectric generator

The work carried out is to investigate and develop an efficient thermoelectric generator (TEG) using the novel two-dimensional material graphene to replace the conventional semiconductor-based solid-state thermocouples used in the Radioisotope Thermoelectric Generator (RTG). Also, to design and develop a prototype RTG (PRTG) using Sr-90 radioactive liquid solution. The RTG is usually the

most desirable power source for unmaintained situations that need a few watts of electrical power for a longer duration, where batteries, fuel cells, and solar cells are impractical. An Important application of RTG is used as a power source in spacecraft, space probes, and satellites. An electronic resonant tunneling effect has been achieved in graphene superlattice heterostructure $[(AB)^N(T)(CD)^M]$ based TEG, which generates a large Seebeck voltage. The thermoelectric efficiency has further been increased by adopting the electron filtering technique in graphene superlattice-based TEG. Furthermore, an efficient tunable thermoelectric device has been designed based on n and p doped graphene superlattice heterostructure. In addition to this, an alternating voltage-biased self-tuned technique has been implemented in graphene superlattice heterostructure $[(NP)^{20}(D)(NP)^{20}]$ based thermoelectric device to increase the conversion efficiency.



Schematic diagram of the graphene heterostructure-based thermoelectric device



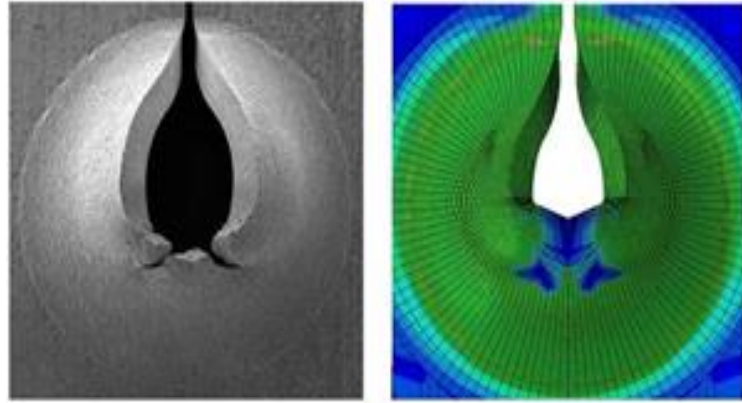
Schematic diagram demonstrating the PRTG using Sr-90 radionuclide to glow an LED

In addition, a Sr-90 radionuclide-based PRTG is designed and demonstrated using Bismuth telluride-based thermoelectric material for glowing an LED continuously. The experiment found that 1000 ml of a radioactive liquid solution containing 9800 Bq/ml of Sr-90 radionuclide is sufficient to glow a 150 μ W LED continuously (schematic shown on the right). The electrical output power and efficiency match with the COMSOL simulation result.

2.1.15 New methodology and correlations to assess fracture parameters by pre-cracked small punch tests - Theory and experimental verification

In the present thesis, a simplified methodology is developed to assess J-R data of structural steels 20MnMoNi55 and T91 using experimental and computed load-displacement data of p-SPT specimens. It was a hybrid approach. During the testing of p-SPT specimens, there is a possibility of having some extent of crack growth before the onset of peak load. This is reflected in the computation of a higher value of peak load by FE elastoplastic analysis without crack growth in comparison to the experimental value. A methodology is suggested in the present work to predict CTOD as a function of crack growth by using experimental peak loads and elastoplastic FE analysis. The CTOD can then be converted to J-integral using conventional correlation. The suggested method could reasonably estimate the J-initiation and J-R curves in comparison to literature values for two widely used structural materials.

To check the accuracy of the simplified method, one of the options is to make use of an advanced FE analysis with damage mechanics model, such as Gurson-Tvergaard-Needleman (GTN) model. A methodology is shown to predict the J-R curve by using FE analysis of the p-SPT specimen with the GTN parameters calculated using an artificial neural network (ANN). The J-integral can be calculated from CTOD using conventional correlation.



Crack branching observed in experiment and numerically simulated p-SPT specimen having crack length of 5.0 mm for T91 material

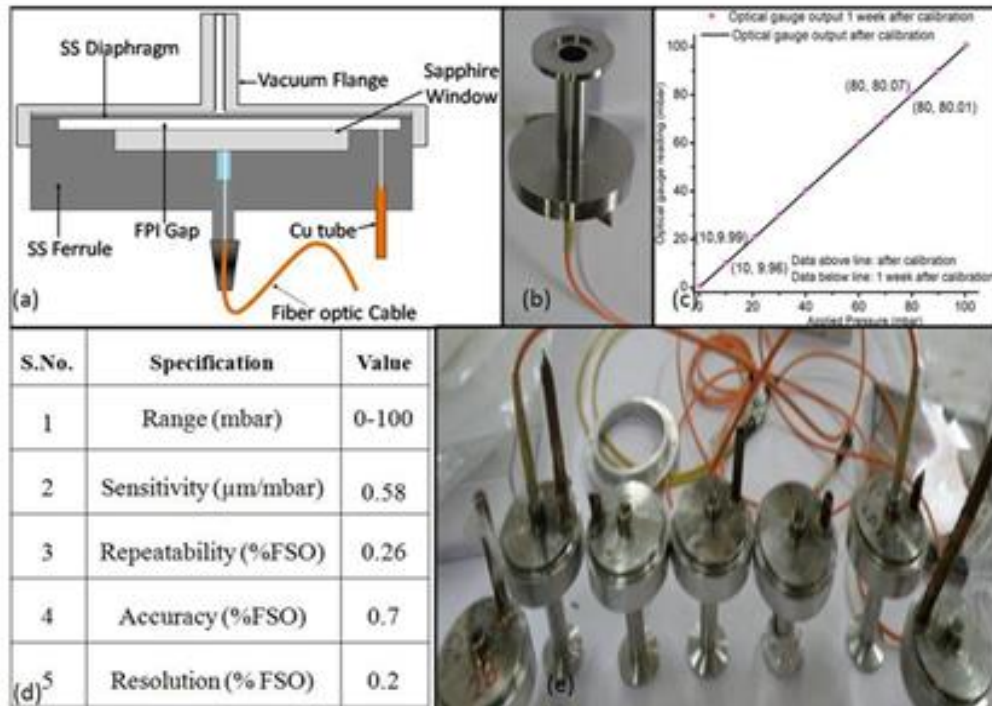
There is some degree of crack growth before the onset of peak loads during p-SPT specimens testing. This could be verified numerically by FE analysis along with the GTN damage model. It may also be observed that crack branching occurred after some amount of crack growth in experimental p-SPT specimens. This phenomenon also could be reproduced in numerical simulations by GTN analysis. The schematic shows the crack branching observed in an experiment and numerical simulation for T91 material.

In addition, parametric studies of three-dimensional FE analyses of p-SPT specimens with large deformation formulation are performed to evaluate the plastic constraint factor, which correlates CTOD with J-integral. Two correlations are developed based on the results of the parametric studies to calculate the plastic constraint factor analytically. The FE results of these parametric studies of p-SPT specimens are used to evaluate the eta plastic factor ($\eta_{plastic}$), which is used to calculate the plastic component of CTOD by directly using experimental load versus load line displacement data without conducting any rigorous numerical analysis. The form of the correlation shows that the plastic η factor depends on the geometrical parameter, namely, normalized effective crack length (a'/W').

2.1.16 Modelling and analysis of Fabry Perot Interferometer for pressure sensors with metallic diaphragms

Metals and metal alloys are commonly used for in electromechanical pressure sensors especially for harsh environments. But to the best of our knowledge, there is no precedence in literature for absolute type fiber optic fabry perot interferometer (FO-FPI) based pressure sensor with metallic diaphragm. Large flatness deviation and poor surface roughness of metallic diaphragms are found to be main obstacles in it. A generic model, for the multiple beam interference in a FPI, shows that parallelism and flatness should be less than 100 nm over an effective FPI surface and gap should be less than 100 μm to achieve finesse better than 3. It is shown that reflectivity of DTM machined metal mirrors (over a broad spectral range) is close to intrinsic one. An FPI based gauge type pressure sensor of range 0 – 7 bar is developed. It is manufactured by DTM process and has material of construction as Cu-Be alloy. The developed sensor has full-scale deflection, repeatability and resolution of 7.30 μm , 2.6%, 4% and 0.20% respectively. Another design is explored for absolute

type pressure sensor. A sensor of range 0– 100 mbar is developed with material of construction as SS316L. The pressure sensitive diaphragm of SS316L also acts as one of the reflective surfaces of FPI. Maximum finesse of 4.65 is achieved with such FPI. Accuracy and resolution of sensor are 0.7% and 0.2% respectively. Stretching improves the repeatability from 4% to 0.26%. The schematic, actual device and its comparison with reference gauge are shown in the schematic below.



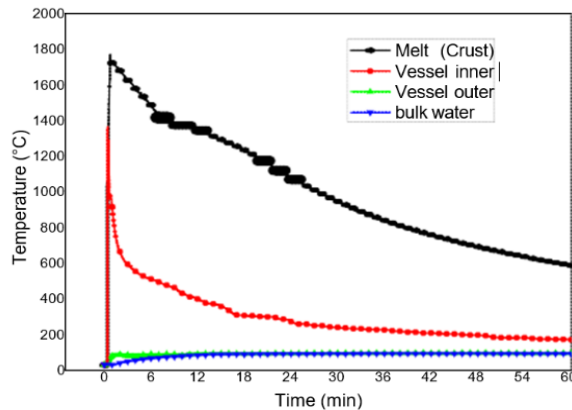
FPI based Pressure Sensor (a) Schematic, (b) Developed Sensor, (c) Comparison with reference gauge, (d) Specifications from test results & (e) Sensors of different ranges (varying with thickness of sensitive diaphragm)

2.1.17 Heat removal capability of calandria vault water from molten corium inside the calandria vessel during severe accident conditions

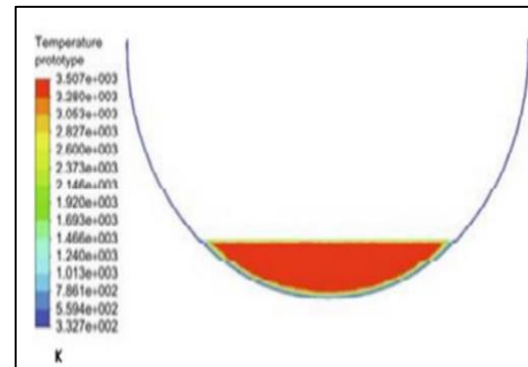
In PHWRs, during the case of severe accident, leading to melting of core and subsequent relocation of molten core debris at the bottom of CV, there is a concern on coolability of the molten core debris by vault water. This is because, if the molten corium breaches the CV and enters the calandria vault, large amount of hydrogen and other gases will be generated due to molten core concrete interaction, which will pressurise the containment and may lead to early containment failure. Hence, In-vessel retention (IVR) of corium by the CV is the only option in PHWRs for mitigation of core melt down accident. There are several scientific and

technological issues which need to be investigated for the success of IVR in PHWRs. The heat transfer phenomena inside the CV which contains molten corium is very complex as it involves multiple modes of heat transfer associated with phase change (melting and solidification). The crust formation and its growth, during the cooling of molten corium, needs to be understood. The influence of decay heat inside the corium on heat transfer and crust formation rate is never established. The natural convection heat transfer behaviors from single-phase to bulk boiling on the curved outer CV are not known. The phenomenology of Critical Heat Flux on outer surface of CV is

very complex due to downward facing heating, boiling natural convection and geometry of very large diameter and length.



Temperature distribution of melt, CV surface and vault water

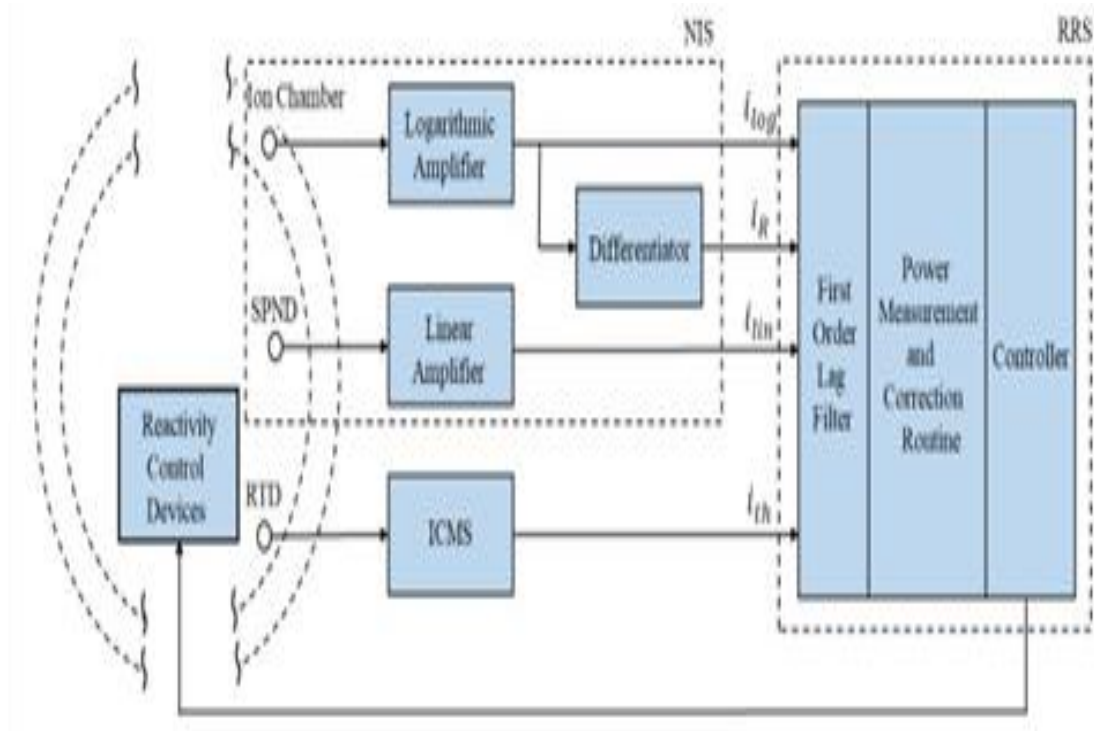


CFD Temperature distribution of corium for rototypic condition

To address the above issues, several experiments have been conducted in this research work. Scaling philosophy for heat transfer from molten corium to the vault water was developed for both stored heat and decay heat dominated regimes. The molten corium cooling behaviour by the vault water, the crust formation and growth rate, melt pool temperatures in radial and axial directions, CV inner and outer vessel surface temperature at different angular positions were experimentally measured up to melt temperatures of 2500 °C. The imposed heat flux on the vessel wall by the molten corium and the local heat transfer coefficient on the outer side of the CV wall were estimated from the measurements. Empirical models for convective heat transfer in single phase and boiling condition in the outer curved vessel of CV were developed. Critical heat flux which limits the maximum heat flux that can be removed from molten corium to vault water was experimentally measured. CFD models were developed for the heat transfer from corium debris to vault water and were benchmarked against the present experimental data. The models were applied to 700 MWe PHWR and capability of vault water to cool and retain the molten corium inside the CV of PHWR was evaluated.

2.1.18 Design of integral sliding mode control strategies for nuclear reactors

In the thesis, different Integral Sliding Mode Control (ISMC) strategies are proposed for both linear and non-linear model of Pressurized Heavy Water Reactor (PHWR) system affected by matched and mismatched type of uncertainties. The research began with designing the linear Optimal Integral Sliding Mode Controller (OISMC) to PHWR system affected by matched uncertainties. The optimal controller, which guarantees minimum control effort, is combined with the robust ISMC to ensure the robustness of the closed-loop system in the presence of uncertainties and external disturbances. To avoid the chattering, the boundary layer approach is used. In another work, linear Optimal Second Order Integral Sliding Mode Controller (OSOISMC) is proposed for PHWR system. In this work, to avoid the chattering, the discontinuous input of controller is designed using the super-twisting algorithm (STA) which is a second order Sliding Mode Controller (SMC). This controller needs states information and hence, a Second Order Sliding Mode Observer (SOSMO) is also designed.



Total power control loop of PHWR

The effect of mismatched uncertainties on system performance is also studied in the present work. To compensate the influence of mismatched uncertainties, a Generalized Extended State Observer Based-Integral Sliding Mode Controller (GESOB-ISMC) is proposed for linear PHWR system affected by mismatched uncertainties. The proposed control scheme is designed in two steps: in the first step a Generalized Extended State Observer (GESO) is designed to estimate the unmeasured states and the unknown mismatched uncertainty, and in the second step an ISMC is designed based on estimated state variables and mismatched uncertainty given by GESO. The thesis further proposes a Disturbance Observer Based-Adaptive Second Order Integral Sliding Mode Controller (DOB-ASOISMC) for linear PHWR system affected by both matched and mismatched uncertainties. A disturbance observer is introduced to estimate the mismatched uncertainties and its first order time derivative, which is then integrated with SMC. The control law is designed in such a way that the discontinuous signum function acts on the first-time derivative of the control input. So, the actual control input obtained after integration is continuous and hence, chattering free. An adaptive gain tuning algorithm is used to find the discontinuous control gain, thus the prior knowledge about the system uncertainties is not required.

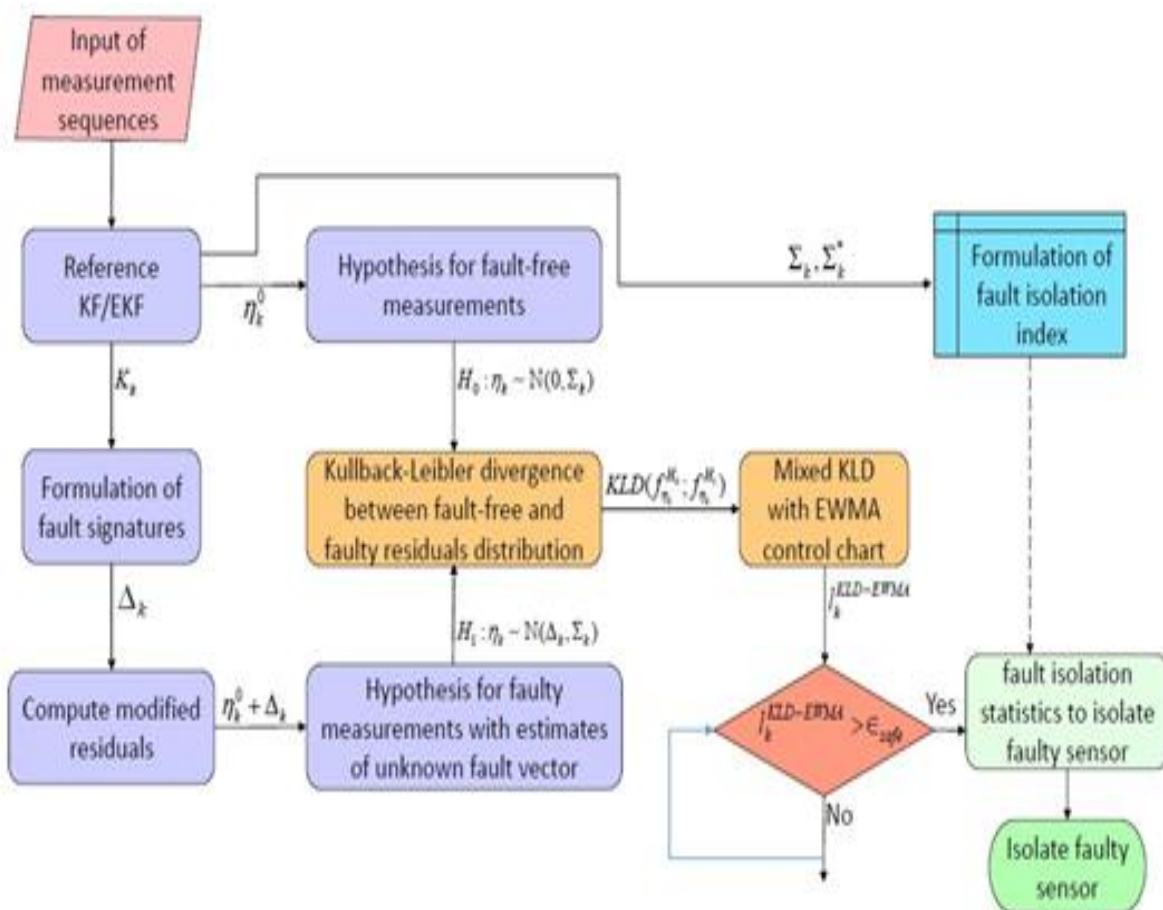
In another aspect of the thesis, a non-singular Adaptive Integral Terminal Sliding Mode Controller (AITSMC) is proposed for controlling nonlinear PHWR system. Compared to the linear sliding surface-based SMC, the nonlinear sliding surface-based Terminal Sliding Mode Control (TSMC) provides finite time convergence and high precision control.

2.1.19 Sensor fault detection and isolation using Bayesian Estimation & Kullback-Leibler Divergence

The research work carried out in the thesis proposes a model-based technique for sensors abrupt & incipient fault detection and isolation using Bayesian estimation and statistical distance measure. Highlights of the findings are mentioned below as:

Probabilistic filters based on Bayesian approach such as Kalman filter/extended Kalman filter have been utilized to formulate the fault signature and generation of fault detection index. Thereafter, fault decision function has been formulated by combining Kullback-Leibler divergence and exponential weighted moving average on generated fault detection index for incipient and abrupt fault detection. To achieve fault isolation, inconsistency in the covariance of the residual sequences have been analyzed.

Statistical characterization has been carried out for incipient fault detection methodology by considering fault-to-noise ratio as a criterion to analyze the sensitivity and reliability.



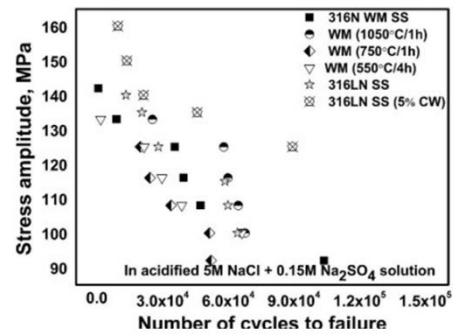
Flow-diagram for proposed sensor fault detection and isolation

Numerical illustration for process sensor’s fault detection and isolation of pressurizer instrumentation and primary loop of the reactor in Pressurized Water Reactor (PWR) type of Nuclear Power Plant (NPP) have been demonstrated for the effectiveness of proposed methodology.

2.2 Indira Gandhi Centre for Atomic Research, Kalpakkam

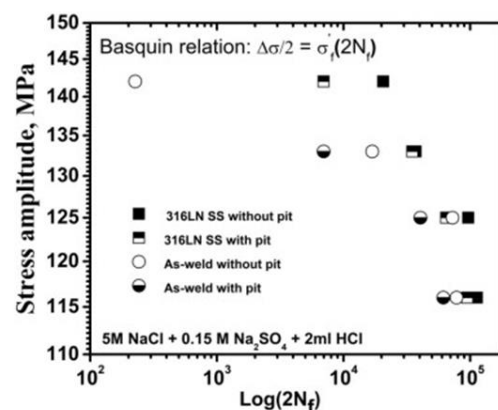
2.2.1 Environmentally assisted cracking behavior of type 316LN SS and its weldments

Environmentally assisted cracking, known as corrosion fatigue (CF), occurs due to the synergistic effect of applied cyclic stress, material properties and aggressive environment. Welding is an essential step in the fabrication of various essential components. Hence, it is important that the integrity of the weld joints is studied for their resistance towards electro-mechanical properties. The synergistic role of microstructural changes in the mechanism between electrochemical and mechanical properties is highlighted. Pitting corrosion and corrosion fatigue (CF) resistance of type 316LN SS with 0.07 wt.% nitrogen in mill-annealed and sensitized condition is compared with weldmetal in as-weld and thermally aged condition (solution annealing at 1050 °C/1h, stress-relieving at 750 °C/1h and dimensional stabilization at 550 °C/4h) in acidified 5M NaCl + 0.15M Na₂SO₄ environment.



S- N curve of type 316LN SS and its weldments in as-weld and thermally aged conditions.

The critical pitting potential and the passivity range showed poor corrosion resistance and accelerated corrosion current density for sensitized and thermally aged weld specimen. The ratio of I_r/I_a showed a value of 15% indicated degree of sensitization for 316LN SS specimen aged at 700 °C/24h whereas, thermally aged weld specimen showed a value of 0.01% due to deficiency of chromium depletion. Base and weld aged specimen showed degradation in tensile properties in chloride medium due to dissolution of depleted regions. The degradation in the mechanical strength exposed to a corrosive environment drives further studies towards electrochemical assisted cracking, especially under cyclic stress. CF analysis using Basquin relation has been presented at open circuit and at applied passive potential. A two-slope behaviour is reported. 316N WM thermally aged at 750°C/1h shows a decrease in fatigue life due to the formation of intermetallics. Crack initiation (CI) be controlled by altering the potential and temperature of the electrolyte. CI be identified by electrochemical techniques. The failure of weld metal occurred by a combination of TG cracking and stress-assisted dissolution (SAD) of δ -Fe. The role of transition of an electro discharged machined single pit into a small crack and its growth is studied to investigate the combined effect of stress concentration factor and local solution chemistry of the pit. Pre-pitted specimen showed a reduction in fatigue resistance as seen

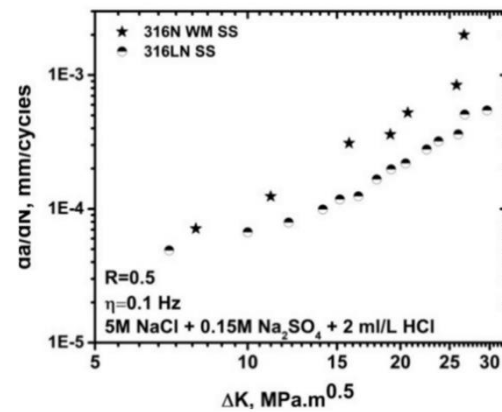


Semi log plot of type 316LN SS and its weldment on smooth and pre-pitted condition in acidified chloride environment.

as seen

in the schematic. The threshold stress intensity factor range for type 316 LN SS is derived to be between 3.8 to 4.3 MPa. $m_{0.5}$ in acidified chloride environment.

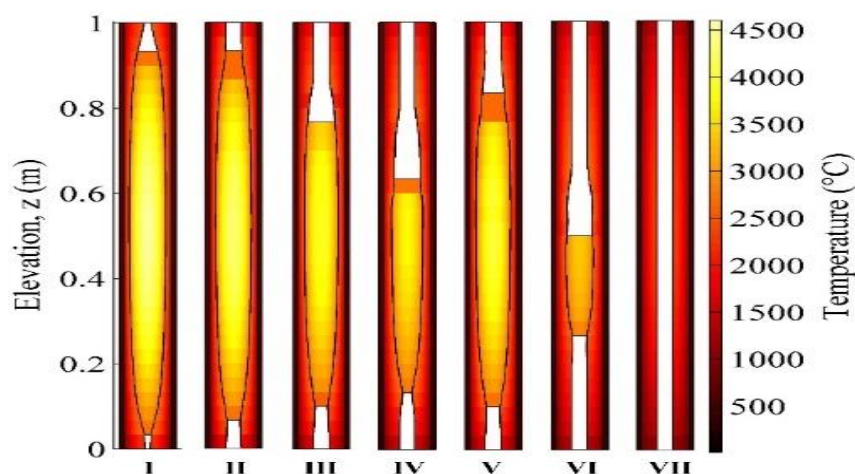
The relationship between strength and its sensitivity on FCG and CFCG rate is established. FCG thresholds for the welds are much higher than the base metal and FCG rates are lower for WM at RT. Temperature enhances the crack growth kinetics at low ΔK . In NaCl environment, CFCG threshold for the welds decreased, and CFCG rate increased compared to base metal as seen in the schematics. A Lower frequency of 0.1 Hz cause sufficient time for interaction resulting in a higher CFCG rate.



da/dN vs. ΔK curve of type 316LN SS and its weldment in 5M NaCl + 0.15M Na₂SO₄ + 2 ml/L HCl solution

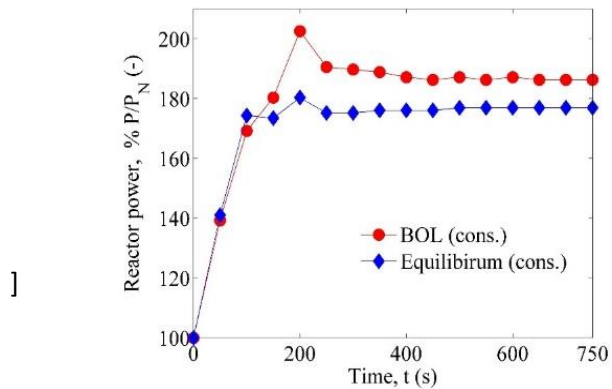
2.2.2 Development of multi-phase core thermal hydraulic models for fuel melting during severe accidents

Melting of nuclear fuel inside sodium-cooled fast reactor (SFR) fuel pins is followed by a hydrodynamic movement of molten fuel (known as *in-pin fuel motion*) amid the presence of fission gases. This movement, which is dynamically coupled with the core reactivity, is particularly important for the unprotected transient overpower (UTOP) accident, since a substantial amount of fuel melting occurs prior to pin failure. The main aim of the thesis is to simulate the melting and relocation of annular, mixed oxide ((U-Pu)-O₂) nuclear fuel during UTOP in SFR. Towards this aim, a Multi-phase In-pin Thermal hydraulic Relocation Algorithm (MITRA) is developed and benchmarked against the data of the CABRI reactor (Cadarache, France). The validated algorithm is subsequently utilized towards whole-core, dynamically coupled, neutronics/thermo-hydraulics simulations of UTOP using the specifications of a typical Indian SFR (500 MWe).

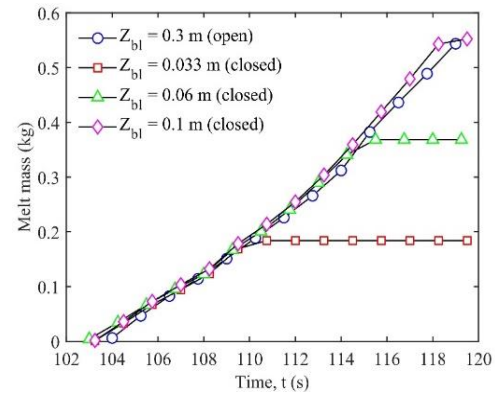


Conservative estimate of whole core melting and in-pin fuel motion for BOL core ($t = 750$ s).

Schematic shown above presents a thermal map of the fuel columns of the seven representative fuel pins from each zone (I-VII) of the SFR core at the end of UTOP transient. A conservative simulation of the beginning-of-life (BOL) core is shown (External reactivity insertion = 1.48 \$, Control rod withdrawal time = 250 s). The stabilized zone-wise temperature distribution, quantum of melting, locations of solidification, and locations occupied by molten fuel in each fuel zone are visible. The length of each melt column is proportional to the whole-core radial power profile. Therefore, the length of the melt column is greatest in Zone-I, followed by Zones II, V, III, IV, and VI.



Reactor power vs. time for FBR-500 reactor. (Conservative estimate).



Fuel relocation in top blanket column as a function of top blanket geometrical design.

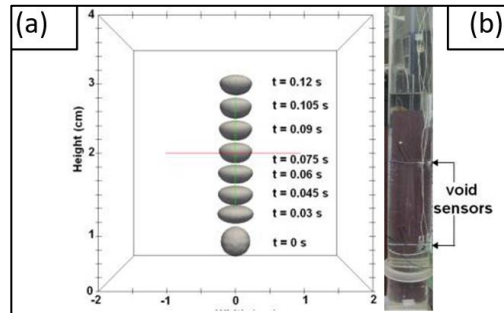
Schematic (left) presents the reactor power history responsible for the melting and in-pin fuel motion shown in (BOL conservative). It also presents the UTOP power history for the equilibrium core (conservative, 0.98 \$, external reactivity insertion). In both the cases, the reactivity insertion is initially countered by the fuel Doppler and fuel axial expansion feedbacks. Once melting initiates in Zone-II, the in-pin fuel motion feedback reduces the net positive reactivity and stabilizes the reactor power. In-pin fuel motion effectively mitigates UTOP in the equilibrium core; however, there is a significant power excursion in case of BOL core (204 % P_n). The thesis additionally investigates the possibility of enhancing the existing safety margin by employing annular axial blanket designs. Schematic (left) shown above presents the relocation of molten fuel from the fissile to fertile regions for different lengths of the annular top blanket cavity (Z_{bl}). Once melting exceeds a threshold of 34 % melt mass, the melt relocates out of the fissile region if vacant space is provided in the blanket column.

2.2.3 Mass transfer from rising mixed gas bubble in quiescent liquid pool of SFR

Pool scrubbing requires information on bubble dynamics and mass transfer. Since bubble dynamics controls the phenomenon, it is of interest to study the same using a judicious mix of numerical models and in-house experiments. This necessitates proper choices of system parameters such as bubble diameter and pool height. In addition, mass transfer from bubble requires inclusion of aerosol and vapor transport parameters. The thesis addresses key interesting issues in the field of bubble scrubbing related safety studies in SFRs.

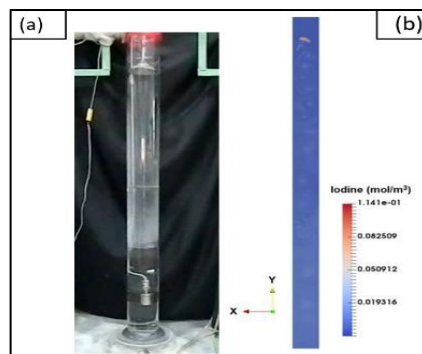
A semi-empirical model is developed to first understand the concept of pool scrubbing. The main phenomena governing the removal of aerosol and vapors from rising bubbles are identified. This is followed by reliable numerical simulation of bubble dynamics using OpenFOAM software to verify the empirical correlations used in the pool scrubbing model. The simulated terminal velocity and

shapes of the rising bubble as shown in Schematic on the right-hand side were found to agree well with the experimental results. In the experimental investigations, an innovative data processing technique was used to measure average bubble rise velocity in large pools of fluids based on in-house developed void sensors as shown in schematic (b) above. Finally, similarity between water and sodium systems on bubble dynamics is brought out to simplify SFR safety studies.



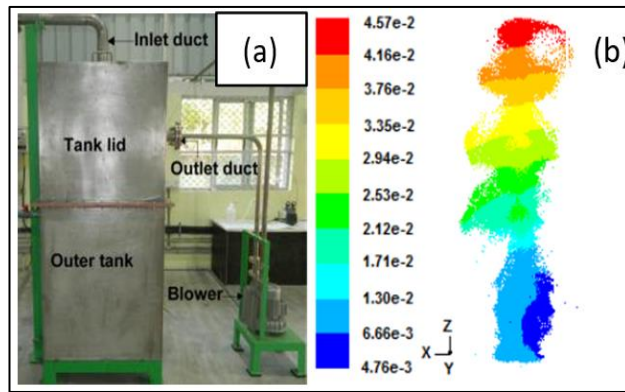
(a) Experimental setup (b) numerical model for air bubble dynamics in water.

The understanding of bubble dynamics gained from CFD and experimental studies have been extended to analyze mass transfer/scrubbing of vapors and aerosols encountered in liquid pool of SFR systems. An experimental water setup has been installed to study iodine vapor retention in water pool (schematic shown below). The setup consists of iodine bubble injection system, bubbler tank and bubble collection systems. The work uses iodimetric titration method for the measurement of iodine concentration in water samples. A numerical study on iodine retention in water pool is also carried out as shown in schematic (b) and is in good agreement with experimental results.



(a) Experimental setup (b) numerical model for iodine scrubbing in water pool.

Engineering scale model of a wet scrubber (SGBS) is setup (schematic below) to study the scrubbing efficiency of sodium fire aerosols during mixed gas bubble rising through water submerged gravel bed. Numerical simulations are also performed to evaluate aerosol penetration in a submerged gravel bed scrubber. At low gas flow rates, semiempirical model underpredicts the removal efficiency for aerosols; however, present CFD study predicts efficiencies as observed during in-house experiments for the typical size range of sodium combustion aerosols, hence, proving the suitability of SGBS as a passive device for sodium combustion aerosol removal.



(a) Experimental setup of submerged gravel bed scrubber and (b) numerical model results for aerosol penetration.

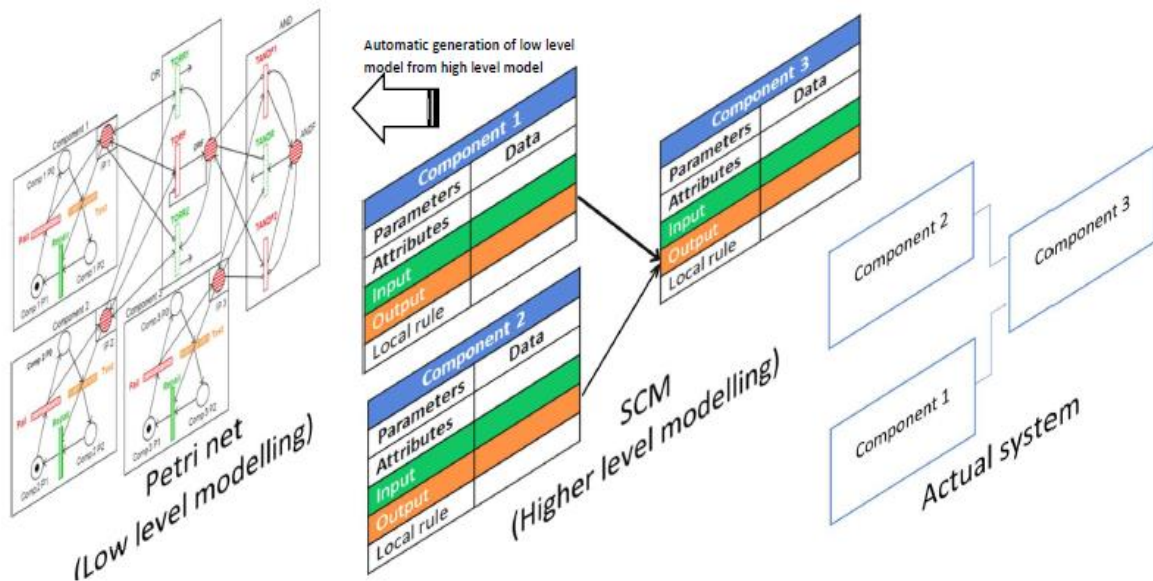
2.2.4 Study of advanced methods for reliability analysis of digital I & C systems

The development of Smart component method (SCM) for dynamic reliability analysis method. SCM is defined as a combination of object-oriented system representation and Monte Carlo simulation. It is developed for addressing existing challenges of existing dynamic reliability analysis methods such as the general modeling capability, scalability, and interface with other static or dynamic method, user-friendliness, and burden of proof-of-correctness. The object-oriented system representation includes the representation of the components and the interconnections of the components as objects. The objects are defined with their attributes and local rules. The system simulation is achieved by executing the local rules of the components sequentially and transferring the values of attributes using the interconnections. This type of system representation is called smart component system representation. A smart component simulator operates on the smart component representation of the system for probabilistic analysis, and estimates reliability attributes of the system.

The general modeling capability is ensured by the use of Monte Carlo simulation based simulator tool, where Monte Carlo methods are known as having the general modeling capability. Scalability attribute is addressed by sequential local rule execution carried out for system simulation. This yields system simulation time changes linearly with increase in number of components in the model. Additionally, the computational advancements through parallelism has made the Monte Carlo simulation based methods computationallyscalable. The method of automatic generation of Petri net model from smart component reliability model of the system provides interface with the existing methods. This method has the algorithms for identifying the hierarchy in the smart component system representation (by use of smart connector object as graph), and then, subsequently generating Petri net model. (Schematic shown below)

The object-oriented representation is considered as most user-friendly method of representation. The smart component representation of the system is built by a reliability analyst, and simulator acts as a black box to the analyst. This shifts the burden of proof-of-correctness from a reliability analyst to the dynamic reliability method, in the current case, to the smart component method's simulator.

The validation of the method is carried out by comparison of the reliability results with approximate method, Markov methomic tested system, decay heat removal system and fast reactor shutdown system.



Schematic illustrating the smart component method as higher level modelling in comparison with low level modelling of system

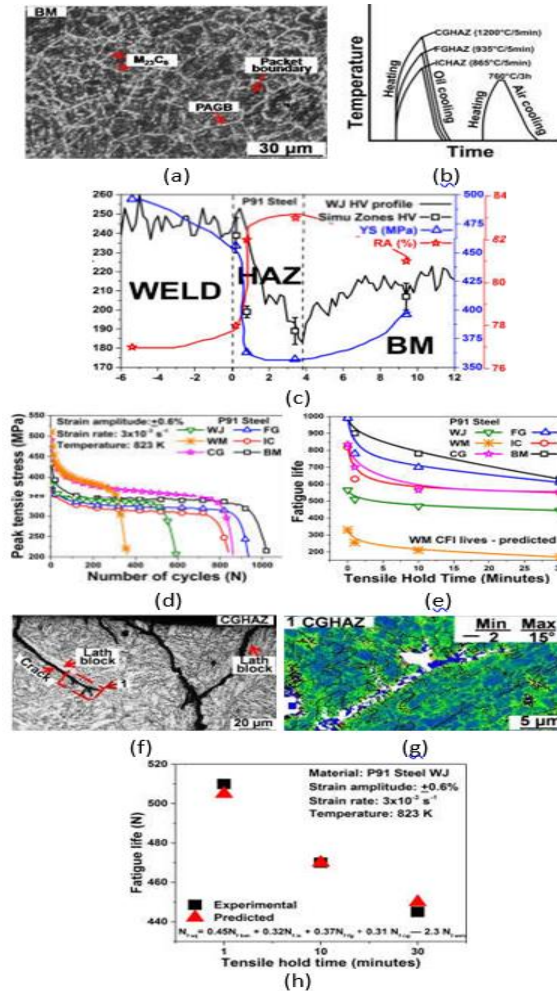
2.2.5 Study on tensile, low cycle fatigue and creep-fatigue interaction behavior of simulated micro-structures and actual weld joint of P91 steel

The study is the first of its kind and was carried out to understand tensile, low cycle fatigue (LCF) and creep-fatigue interaction (CFI) behavior and estimate the overall mechanical behavior of the P91 steel weld joint (WJ) through deformation/damage weighted factors of the constituent regions of the WJ. In-depth microstructural characterizations were carried out by employing SEM, fractography and EBSD techniques to explain the operative deformation/damage mechanism under the loading conditions.

The analysis using prior austenite grain (PAG) size, microhardness, and precipitate size (M23C6) as reference concluded that heat treatment temperatures of 1473 K, 1208 K and 1138 K are adequate to simulate the respective microstructures of coarse grain heat-affected zone (CGHAZ), fine grain (FG) HAZ and inter-critical (IC) HAZ of P91 steel WJ.

The CGHAZ and weld metal (WM) are the strongest and ICHAZ is the softest, whereas base metal (BM), FGHAZ and the actual WJ showed intermediate strength or cyclic stress response. The fatigue lives of all constituent regions and the actual WJ are in the order of $(BM=FG) > (IC \approx CG) > WJ > WM$. The fatigue life of the actual WJ depends upon various factors such as grain size, mechanical strength mismatch in two-phase region, i.e., ICHAZ (fine tempered martensite and over-tempered ferrite) and difference in the volume of each of the constituent regions in the actual WJ. The continuous decrease of dwell sensitivity of BM and FGHAZ is of concern even though their fatigue lives are higher than the other constituent microstructures and the actual WJ under CFI condition. The longer cracks and greater number of cracks decrease the

load-bearing capacity and lead to low fatigue lives of CGHAZ and ICHAZ under both LCF and CFI conditions. The difference in plastic strain accommodation/accumulating capacity of individual microstructures and their evolution during fatigue deformation are the governing factors for affecting cracking behavior and the resultant fatigue life.



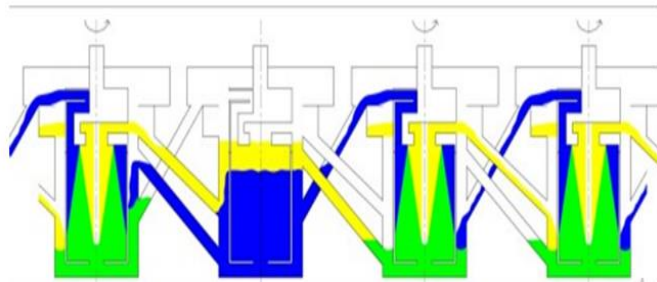
(a) Initial microstructure (BM), (b) schematic of HAZs simulation, (c) regional variations of yield strength and hardness, (d) cyclic stress responses (LCF) & (e) fatigue life vs hold times (CFI), (f) crack propagation and (g) local strain (KAM) measur measurement in CGHAZ (LCF) and (h) weld joint fatigue lives; predicated vs experimental (CFI) of P91 steel at 823 K.

A common empirical relationship (eq. 1) was established to estimate the fatigue life of P91 WJ using the weighted factor of each constituent region under both LCF and CFI loadings. The constituent regions with low weighted factors substantially contributed to the decrease of fatigue life of P91 WJ.

$$N_{f,wj} = 0.45N_{f,bm} + 0.29N_{f,ic} + 0.37N_{f,fg} + 0.31N_{f,cg} - 2.3N_{f,wm} \dots \dots \dots (1)$$

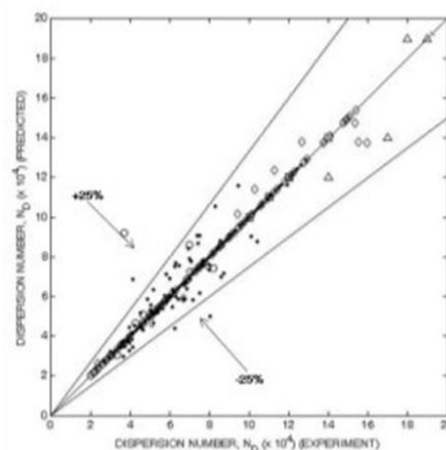
2.2.6 Hydrodynamic characteristics of annular centrifugal extractor and helical coil based fluidic diode pump

Annular Centrifugal Extractor (ACE) is a robust solvent extraction equipment and candid candidate for fast breeder nuclear reprocessing applications. ACE design is based on various thumb rules. However, the reliable design and scale-up of ACE are yet to be developed. Flow inside the ACE is highly turbulent, unsteady due to liquid level fluctuation in the annular region, air ingress and three-phase (air, heavy and light phase) operation during solvent extraction operation. The dispersion number (ND) is a primary design input and decides the size and operating speed of annular centrifugal extractor (ACE) for any given process throughput. ND value depends upon the system's physical properties, such as density, viscosity and interfacial tension. The measurement of ND is impossible for hazards (radioactive, corrosive, etc.) systems. In this work, the ND is measured by gravity/centrifugal separation for different aqueous and organic systems to cover wide range of physical properties. Based on the experimental and literature results, a novel data driven correlation containing physical properties and separation forces has been developed using the Random Forest technique for dispersion number.



Schematic view of aqueous and organic flow with inclined overflow (3rd stage motor failure condition) (blue colour - heavy phase, green colour - mixture, yellow colour - light phase)

During multistage operation, failure of motor/bearing in any single stage leads to the stoppage of an entire ACE cascade. In nuclear reprocessing applications, the stoppage of cascade leads to solvent degradation and defeats the advantage of ACE. A simple and innovative modification of inclined overflow line has been developed, demonstrated, and validated by flooding and mass transfer experiments in motor/bearing failed condition. The understanding of flow inside the rotating bowl is one of the grey areas in the ACE design. Computational fluid dynamics (CFD) may be a key tool to address or solve the above problem and it can be used to evaluate the existing ACE to optimize the operating parameters. The 2D CFD simulations have been performed for the prediction of zero-point flow rate with different turbulent models. The predictions of the SST k-omega model are closer to the experimental measurements



Parity plot for the comparison of ND measured experimentally against Random Forest based correlation.

Table 1. Zero-point flow w.r.t different turbulent models

Sr. No.	Details	Zero point flow (kg/hr)
1	Experimental	1.5
2	k-epsilon STD model	2.3
3	K-epsilon RNG model	2.3
4	SSt k-omega model	1.9

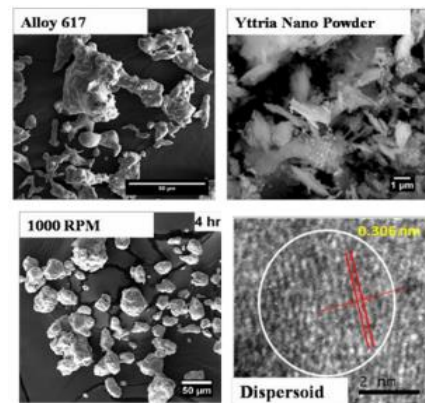
Airlift pumps are widely used for metering applications in reprocessing plants. However, airlift and fluidic pumps are not suitable for low throughput metering operations. A suitable alternate pumping system of a helical coil-based pulsating pump has been developed and demonstrated by pumping experiments with different operating conditions. The CFD simulations have been performed for the prediction of the pressure drop across the given helical coil. The simulation is extended to understand the pressure drop across the helical coil for various design parameters.

2.2.7 Synthesis and characterization of Ni-based oxide dispersion strengthened superalloys

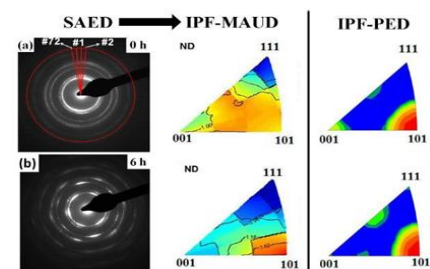
Optimum ball milling conditions - 1000 RPM, 6 h, imparted collision energy of, $E_c \sim 409.2$ J/g.hit. At higher rpm like 1500 ($E_c \sim 665.36$ J/g.hit) and 2000 rpm ($E_c \sim 939.68$ J/g.hit) - severe cold welding of powders and fracturing of milling balls.

Rietveld refinement of SAED pattern using MAUD - $\langle 110 \rangle$ texture parallel to the normal direction (electron beam direction)- evaluated by PED Shear Texture in milled powder - inhomogeneous rolling and compression of the trapped powder particle in between the balls and between the balls and walls of the jar is shown in second schematic. Both As-SPS and annealed specimen exhibited bimodal grain structure which is advantageous with fine grains providing strength by Hall-Petch relationship, and coarse grains provide ductility. Alloy 617 ODS derives its Strength from microstructural features such as grain boundaries of fine grains due to Hall-Petch relationship, solid solution strengthening, and dispersion strengthening Weak or randomized texture of the consolidated and annealed sample is advantageous since directionality affects the

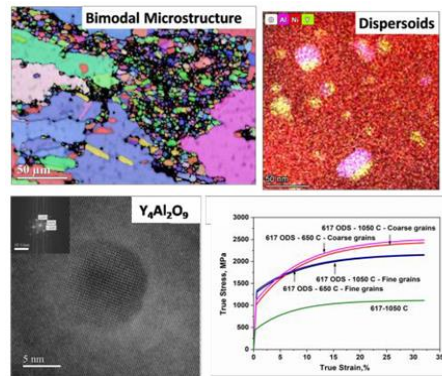
mechanical property. M23C6, M6C, Al₂O₃ precipitates are present in the matrix of both As-sintered and annealed samples in addition to the presence of fine uniform Y₃Al₅O₁₂, Y₄Al₂O₉, and new complex oxide rich in Ni, Y, Al and O. Alloy 617 ODS derives its strength from both precipitates and dispersoid in addition to solid solution strengthening element. γ' is not observed due to Al₂O₃ and Y-Al-O complex oxide formation. Alloy 617 ODS annealed at 1050 C displayed higher yield strength in comparison with conventional Alloy 617 under similar condition due to microstructure and micro texture contributions.



Optimisation of Mechanical milling



Texture analysis of single powder particle



Structure and Texture analysis of Alloy 617

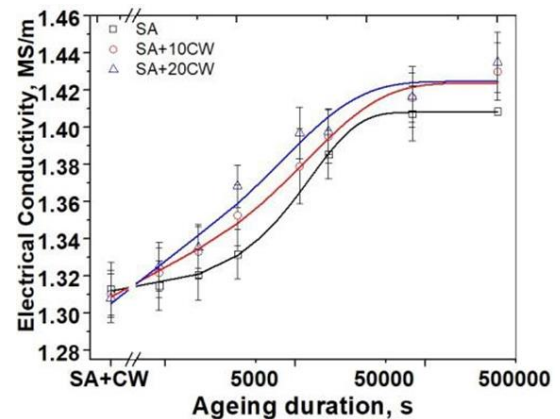
2.2.8 XRD line profile analysis for understanding the influence of cold work on ageing behaviour in 304HCu steel

The 304HCu steel is a Cu modified austenitic heat resistant stainless steel used for high temperature boiler tube applications. It has high strength and creep resistance due to formation of fine Cu-rich phases; M23C6 and MX type carbonitrides during ageing. To study the influence of cold work on precipitation behavior, 304HCu steel is solution annealed (SA) followed by cold worked (CW) for 10% and 20% reduction in thickness and isothermally aged at 650 °C. The CW 304HCu steel during isothermally ageing are characterized by using XRD technique, hardness, and electrical conductivity measurements. The changes in hardness and electrical conductivity (σ) with ageing are fitted with Johnson-Mehl-Avrami equation. The hardness increases due to both CW and ageing. However, the σ shows no change due to cold working but it increases with ageing as shown in schematic. The early peaking of σ in CW samples is attributed to accelerated precipitation kinetics. The change in kinetics of σ due to 10% and 20% deformation is equated to an apparent change in activation energy of 0.73 and 4.225 kJ/mol and as an equivalent increase in ageing temperature of 654 and 672 °C respectively. The microstrain estimated from various XRD line profile analyses (XRDLPA) viz. modified Williamson Hall (mWH) method, Warren- Averbach (WA) method and Stephens phenomenological model are compare for isothermally aged 17-4 precipitation hardenable steel. To separate the effects due to precipitation and dislocations on microstrain, the column length dependency of microstrain from WA analysis is proposed with the equation:

$$\langle \epsilon^2(L) \rangle = P_0 + P_1/L + P_2/L^2 \quad (1)$$

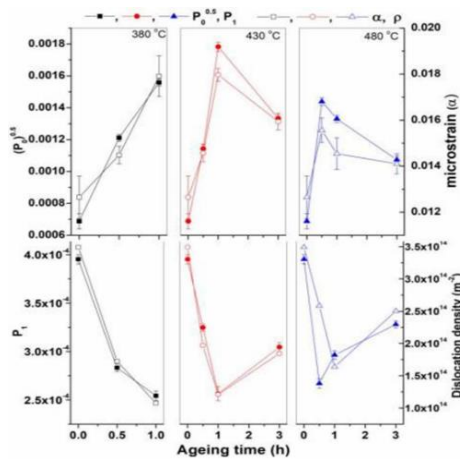
where P_0 is the long-range strain parameter and P_1 & P_2 are the short-range strain parameters.

The parameters P_0 and P_1 are correlated with microstrain (α) determined from mWH method and dislocation density (ρ) determined from Williamson-Smallman method respectively as shown in the

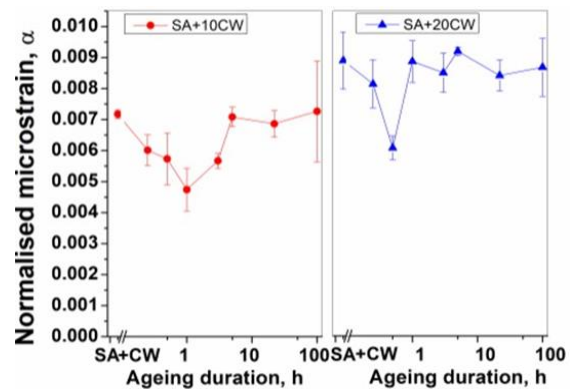


Variation of conductivity with ageing for SA, 10% and 20% CW.

schematic below (left). This indicates the simultaneous effects due to precipitates and dislocations are separated by determining P_0 and P_1 terms. Further, the XRD profiles obtained from synchrotron source for prior CW 304HCu steel has revealed variation in lattice parameter and microstrain with ageing. A reduction in lattice parameter with ageing is observed due to migration of precipitate forming elements from the matrix and it is higher for cold worked samples due to enhanced precipitation on dislocations. The variation in α determined from mWH method with ageing of prior cold worked 304HCu steel showed dominant dislocation annihilation effects on initial ageing and dominant precipitation effects on further ageing as shown in schematic on right below. Further, the microstrain obtained from WA analysis fitted with proposed Eqn. (1) has revealed linear behavior between P_1 and ρ .



Linear behavior of (P_0) with α

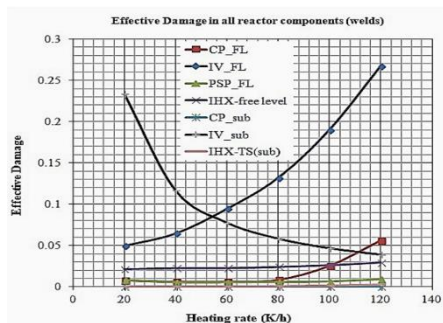


Variation of normalized microstrain (α) with ageing for 10% and 20% CW 304HCu steel.

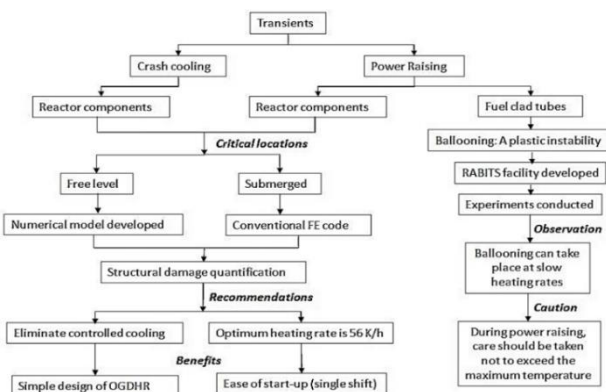
2.2.9 Investigation of structural damage in pool-type fast reactor components during thermal transients

The effect of heating and cooling rates during thermal transients namely power raising (during reactor start-up) and crash cooling (during reactor shutdown) have been identified as the gap areas in pool-type fast reactors, and studied in detail in the thesis. Literature survey suggests that the reactor components are the critical components during crash cooling and power raising. Fuel clad tubes can also be the critical locations during power raising. The critical locations in reactor are broadly categorized as submerged locations and free level locations. Conventional finite element codes are sufficient for the thermo-mechanical analysis at submerged locations but not for free level locations. Hence a numerical code has been developed for the free level locations. Creep-fatigue damage estimation has been done for both the locations for all the hot pool components. As the structural damage is low during crash cooling, a simplified scheme has been recommended for shutdown operation. optimization studies carried out at various heating rates for all the components suggests that inner vessel free level location and inner vessel submerged location are the critical locations. The effective creep-fatigue damage is the highest in inner vessel. When the presence of welds is considered, an optimum heating rate of 56 K/h is recommended during power raising as shown in schematic on the LHS below. The corresponding damage is 0.085, which is less than the allowable limit, 1. The study forms a benchmark for other fast reactors for deciding upon the heating rate during start-up of the reactor. The effect of heating rate in fuel clad tubes has been studied and it is found

that clad tubes can balloon at slower heating rates, if allowed to reach high temperatures in the range of 1273 K. As power raising operation involves slow heating, care should be taken not to exceed the envisaged maximum temperature. Microstructural investigation reveals that ballooning is a ductile failure, and it is a plastic instability caused due to grain coarsening and reduction in hardness and thickness. The summary of the thesis is pictographically represented in schematic on the RHS below



Effective damage in all reactor components



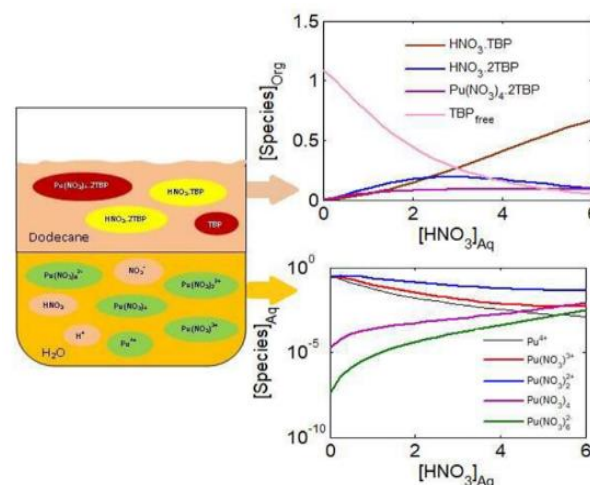
Summary and highlight of the thesis

2.2.10 Thermodynamic model for the prediction of distribution coefficient of major solutes in Tri alkyl phosphate for the flow sheet development in spent nuclear fuel reprocessing

Solvent extraction is one of the major unit operations carried out in the aqueous based nuclear fuel reprocessing process such as PUREX process. Solvent extraction process is often controlled by thermodynamic equilibrium hence solvent extraction process are carried out in multiple counter current extraction stages to achieve quantitative recovery of products. The distribution coefficient of solutes decides the number of stages required for the given solvent extraction duty. So, in order to minimize the experimental studies required for the determination of the distribution coefficient and for the design & optimization of solvent extraction flow sheet, distribution coefficient model is required in the entire concentration range. The thesis presents a thermodynamic model developed for the prediction of distribution coefficient. The distribution coefficient of major solutes such as HNO_3 , U (VI) and Pu (IV) in tri alkyl phosphate such as 1.1 M Tri-n-Butyl Phosphate (TBP) and Tri isoamyl phosphate (TiAP) was modeled. Thermodynamic model for the distribution coefficient of HNO_3 from HNO_3 - H_2O binary system was developed first. Then it was extended for the simultaneous extraction of HNO_3 & U (VI) and HNO_3 & Pu (IV) from their respective ternary system of HNO_3 -U (VI)- H_2O and HNO_3 -Pu (IV)- H_2O . Distribution coefficient was modeled using the law of mass action principle. The aqueous phase activity coefficients were estimated using electrolyte activity coefficient model. The equilibrium constant of the complex formation reaction and the interaction parameters in the activity coefficient model were estimated from the experimental extraction data. One of the highlights of the thesis is the application of local composition-based electrolyte activity coefficient model for the estimation of activity coefficient.

Also, the partial dissociation of HNO_3 in the aqueous phase and the speciation of Pu (IV) in the aqueous HNO_3 solution was accounted during the estimation of activity coefficient of aqueous species. The concentration of various species in equilibrium during the extraction of HNO_3 and

Pu (IV) as a function of aqueous HNO₃ concentration is shown in the schematic. The interaction parameters of eNRTL and eUNIQUAC activity coefficient model for the HNO₃-U (VI)-H₂O ternary system is the new information added to the literature. The accuracy of estimating the distribution coefficient while using the local composition and extended Debye Huckel based activity coefficient model was presented. The eUNIQUAC activity coefficient model gave the lowest Root Mean Square Deviation (%) for the estimation of distribution coefficient over the other activity coefficient model such as Pitzer, SIT and eNRTL. Also eUNIQUAC model has good extrapolation capability compared to all other models. The developed model will be useful for the flow sheet design and optimization in the reprocessing of typical Pu rich fast reactor spent nuclear fuel.



The equilibrium concentration of various species in aqueous and organic phase during the extraction of HNO₃ and Pu (IV)

2.2.11 New and improved methodology for high temperature design of bellows

Bellows are expansion joints which find wide number of applications in critical high temperature systems such as in sodium cooled fast reactor (SFR) systems. Typical operating temperatures of the SFR systems are around 823K - 843K at which failure modes such as creep and creep-fatigue interaction are significant. The available design practices for bellows operating at room temperature such as standards of EJMA do not comply with the nuclear design codes with respect to factor of safety (FOS) and the high temperature design practices such as ASME section-III, code case N290 are not properly addressing all the high temperature failure modes.

In the present work, based on the literature survey, SS36Ti and Inconel-625 are recommended for construction of high temperature bellows. The data required for high temperature design of the bellows viz. tensile, design fatigue curve, cyclic stress-strain curve, Norton creep law constants and parameters defining the visco-plastic constitutive model was arrived by a set of tensile, low cycle fatigue, creep, and creep-fatigue interaction tests on smooth cylindrical specimens of the materials at the design temperatures. In the present investigation, a new method for room temperature (RT) design of the bellows was recommended by modifying EJMA, in which the FOS complies with the standard design codes. A code in MATLAB was written for RT design of the bellows.

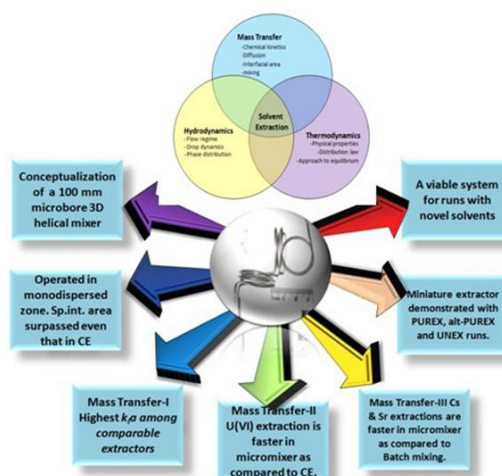
The design arrived based on the new method for room temperature service was analyzed subsequently by finite element (FE) analysis. When the operating stress range of the bellows was close to twice of the yield stress of the material, the design based on the linear elastic analysis (as per the method given in RCC-MR) was recommended. When the operating stress range was more and the bellows were operating in low cycle fatigue region, the design based on inelastic analysis was found to be more accurate. The proposed methodology was validated by testing the bellows at high temperature. Creep-fatigue testing of the bellows was done in a novel way by testing bellows in INSTRON machine which is generally used for testing of LCF and CFI tests of materials on cylindrical specimens. The present work concludes with qualifying the new methodology proposed for high temperature design of the bellows for any critical applications not limiting to nuclear systems.



Testing of bellows on INSTRON machine

2.2.12 Design, development, and demonstration of a miniature extractor for process Intensification in nuclear solvent extraction

The idea of the design of miniature extractor, envisaged in this research, included development of a miniature settler, much smaller than the ones reported in literature, and to demonstrate its functionality with different aqueous-organic pairs used in nuclear extraction. In addition, the prime motive was to develop a miniature extractor for flowsheet evaluations with novel solvents used in the entire nuclear fuel cycle operation with advantages of ultra small holdup and robust operation requiring few milliliters of radioactive feeds as well as solvents. After conducting an exclusive literature review, the microfluidic based miniature extractor was envisaged as a feasible design. A unique 3D helical mixer was constructed out of 100 μm microbore SS-316 tubing with mixer volume was 3.14 μL . This helical mixer was coupled to a unique miniature vertical glass settler of 1.2 mL working volume.



Objectives realized from research and development on microfluidic channel based miniature extractor for nuclear solvent extraction

In almost all the hydrodynamic experiments, estimated specific interfacial area was much higher than the 50 mm dia centrifugal extractor for the same aqueous organic pair indicating a higher degree of intensification. With 72 g/L U (VI) aqueous solution containing simulated fission products and PUREX solvent (30% TBP/dodecane), mass transfer runs were taken in several steps of extraction and stripping operations. Although, as per the literature, for centrifugal extractors, minimum 3s residence time is required for mixing to affect the U(VI) mass transfer, with the proposed miniature extractor with around 0.3 s residence time, mass transfer operations were conducted. The Cs and Sr extraction and stripping kinetics was investigated under batch

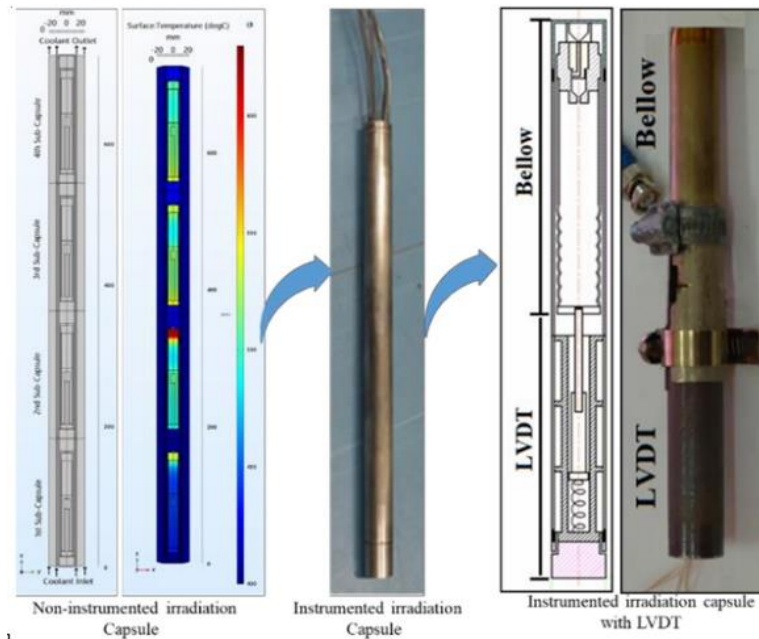
conditions in the nitric acid/CCD-PEG-FS-13 biphasic system. For Cs as well as Sr, the apparent extraction and stripping kinetics under micromixing conditions were much faster than that observed in the batch conditions. Miniature extractor operation was validated with nitric acid/30%TBP, nitric acid/36%TiAP and nitric acid/CCD-PEG-FS-13 aqueous-organic pairs for extraction as well as back-extraction operations. High specific extraction rates as well as high volumetric mass transfer coefficients were observed. For developed extractor, specific interfacial area and energy dissipation during mixing exceeded for centrifugal extractor for PUREX aqueous organic pair. The miniature extractor also meets the requirements of four generic principles of process intensification and it may be used in the future flowsheet studies with novel solvents in nuclear solvent extraction.

2.2.13 Design, analysis and development of irradiation capsules and sensors for material irradiation in fast reactor with out-of-pile validation

Material related studies are performed with the sample materials being subjected to irradiation to determine the changes in properties due to radiation and high temperature such as hardening, embrittlement, crack growth, void swelling, and creep deformation. For such studies, experiments are carried out in reactor using irradiation capsule and sensors. Temperature plays an important role in irradiation experiment. Therefore, it becomes necessary to measure and maintain the temperature in the specimens during the irradiation experiment.

In the present work the design, analysis, and development of non-instrumented and instrumented irradiation capsule with LVDT sensors has been presented for material irradiation, specifically in fast breeder reactor. The design analysis of non-instrumented irradiation capsule (NIIC) was performed in COMSOL-Multiphysics software. The design was based on inert gas-gap width variation to maintain constant temperature of the specimens throughout the irradiation experiment. The specialty of this capsule is that; up to four different samples can be irradiated at different constant temperatures in a single experiment. To measure the peak temperature of the NIIC during irradiation experiment a passive temperature monitoring method was studied based on Curie point of permanent magnet. This method provides the peak irradiation temperature after the irradiation experiment. To maintain the temperature of specimens during reactor operating condition (shutdown to full power), NIIC was found to be insufficient. Therefore, the temperature controlled instrumented irradiation capsule (TCIIC) was studied. The design of TCIIC was based on the gas-gap and heater coil concept. In this approach, external heater coils were used to maintain the specimen temperature when reactor is operated for low power generation. Or gas-gap to maintain the reactor temperature and vice versa. A prototype of TCIIC was developed, and out-of-pile experiment was carried out to maintain the temperature of specimens. In addition, LVDT sensor was studied and formulated to develop a LVDT based on structural parameter. To monitor the deformation and pressure during the experiment, high temperature and compact prototype LVDT was designed and attached with the irradiation capsule.

A temperature associated below pressure was measured by the prototype LVDT. It demonstrated the working temperature > 350 °C successfully. The thesis provides fresh perception on design of a non-instrumented and instrumented irradiation capsule for material irradiation in fast reactor at constant temperature and monitor the temperature by indirect method. It also provides novel idea for designing a compact high temperature LVDT sensor for various applications in fast reactor.



NIIC, TCIIC and instrumented irradiation capsule with LVDT sensor

2.3 Raja Ramanna Centre for Advanced Technology, Indore

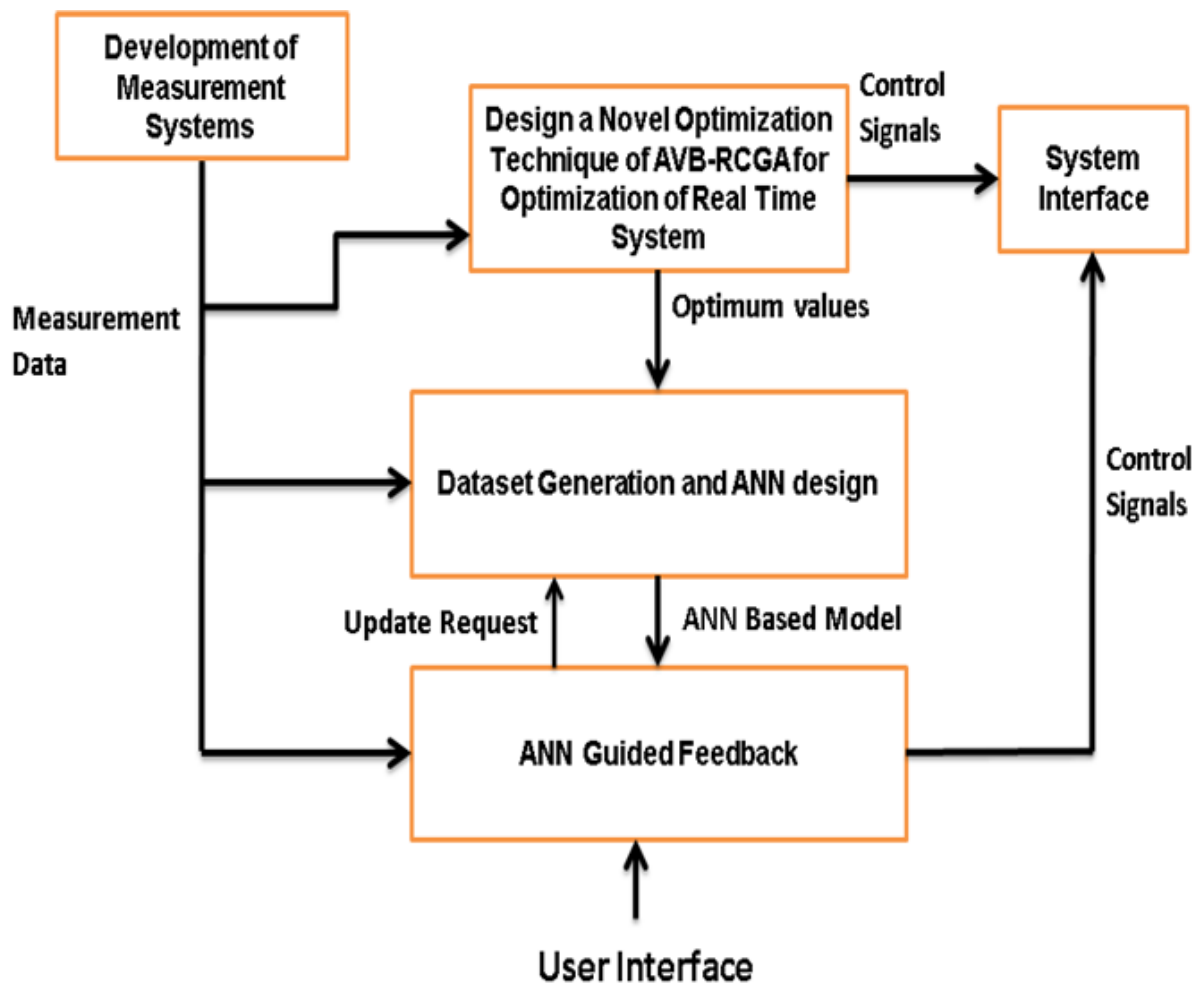
2.3.1 Intelligent approach to study transverse coupled bunch instabilities and their effects on performance of electron synchrotron

The application of artificial intelligence (AI) based approach for modelling unknown and nonlinear systems and creating adaptive feedback controller for the real-time system are the key features of the thesis. In this work, an Artificial Neural Network (ANN) based system has been developed towards identifying the system model. The real-time data obtained from the particle accelerator, Indus-2 synchrotron radiation source in this case, employing the measurement systems, forms part of this modelling. A novel approach involving the adaptive variable boundary based real coded genetic algorithm (AVB-RCGA) has also been developed to identify the near-optimal value of the operating parameters of the accelerator.

The Indus-2 accelerator is a complex machine posing operational challenges when it comes to improving the performance of machine which critically depends on manual process for fine tuning of machine parameters. Transverse coupled bunch instabilities (TCBI) is one of the major challenges that limit the high beam current operation and degrades the machine performance. The mitigation of TCBI using AI approach has been taken

up for research. The application of this R&D work has been validated on Indus-2. The schematic shows a flow chart of the thesis work. The schematic below shows that ANN based system modelling requires a dataset from a real-time system. Hence, systems for measurement of transverse coupled bunch mode (TCBM) level and betatron tune have been developed. TCBM levels denote the margin from the threshold beam current for the TCBI to be excited. These measurement systems have been

used by AVB-RCGA based algorithm to find the optimal values of the input parameters (betatron tune and sextupole magnet power supply currents). The optimal value derived from this module has been used to provide a range of input variables during dataset generation. These datasets have been used to create an ANN-based accelerator model that was used to provide a reference for the feedback controller. The feedback controller uses the system interface to set the current settings of the accelerator's magnet power supplies. The system was implemented on the Indus-2 and tested by beam experiments. From this, it was verified that the developed system improves the performance of the Indus-2 in term of maximum accumulated beam current without the use of active feedback (Transverse multi-bunch feedback) system for mitigation of TCBI. Without ANN guided feedback controller, the maximum achievable beam current is ~ 170 mA at beam injection energy, which is more than 210 mA with the feedback controller. This feedback system also reduces the need for manual tuning of system parameters during beam operation of the Indus-2. This enables system operation with higher performance in terms of higher current and maximization of beam utilization.

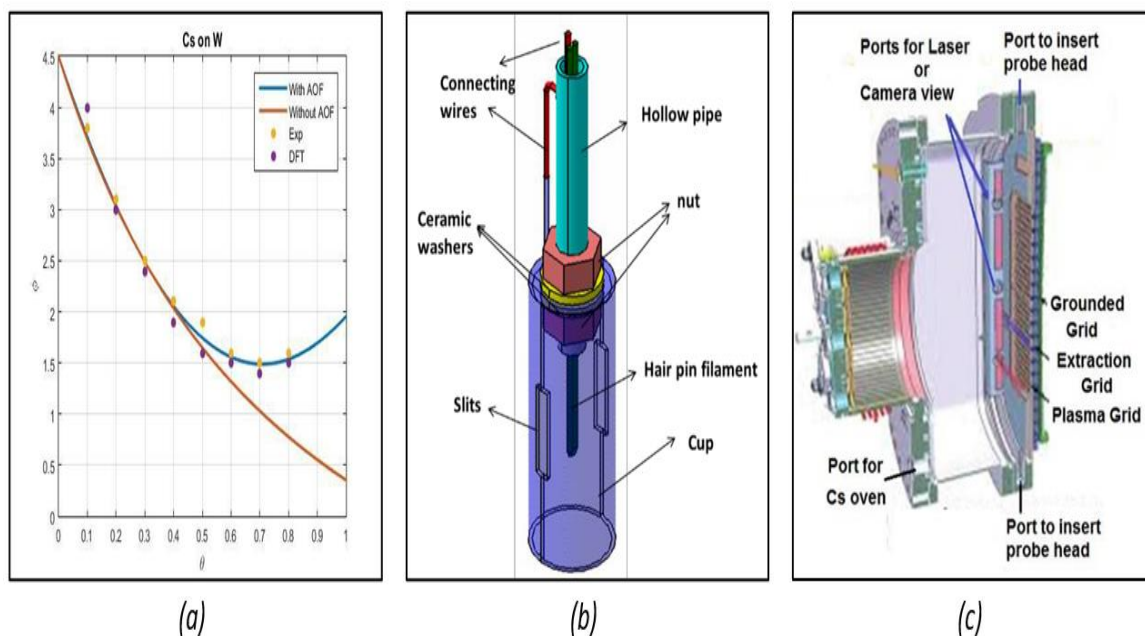


System flow diagram for ANN guided feedback controller including AVB-RCGA based system optimization

2.4 Institute for Plasma Research, Gandhinagar

2.4.1 Study of in situ measurement of work function and cesium dynamics

A phenomenological model is developed to explain previously observed experimental work-function curve as a function of cesium (Cs) monolayer coverage. The phenomenological model is developed on the framework of Langmuir's classical electrostatic dipole model in the of cesium-tungsten (Cs-W) system by including an angular orientation factor resulting from the self-interaction of the dipoles at higher coverage of alkali metals. The present model fits well for the full coverage range (0 – 1 monolayer) as show in schematic (a). A temperature-controlled vacuum compatible Cs delivery system is used for Cs injection. The nozzle geometry of the Cs delivery tube is optimized by Monte-Carlo technique to ensure good Cs distribution uniformity and desired Cs consumption rate of 2 mg/hr. A vacuum compatible, compact, easy to handle probe "PRISM" as shown in schematic below (b) is designed, fabricated, and used in the experiment, which can measure three different parameters related to Cs dynamics and its deposition effect on a surface. It can measure local Cs flux, Cs coverage and corresponding work function on the surface and help to find a correlation of these three parameters at a same location. The investigation shows that the work function of the caesiated polycrystalline tungsten surface reached below 3.06 eV under negative ion source relevant vacuum condition, where impurities like hydrogen gas, nitrogen gas, moisture, hydrocarbons, etc. are present. Through PRISM work function in correlation with Cs dynamics in negative ion sources (NIS) as shown in schematic (c) is foreseen to improve the yield of negative ion current to produce high power neutral beam injection system (NBI) required for present and future fusion devices like ITER and DEMO.



(a) The work function change vs. Caesium coverage on Tungsten surface as fitted by phenomenological model. (b) Schematic of vacuum compatible probe for in situ measurement (PRISM) of work function, Cs flux and Cs coverage. (c) Illustrates ports for laser and camera view for in situ measurement of work function, Cs flux and Cs coverage in negative ion sources.

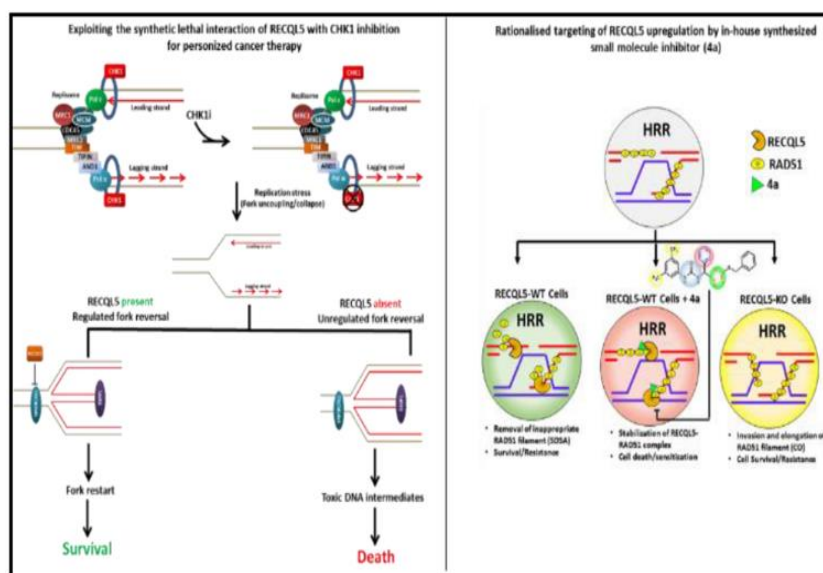
3. Life Sciences

During the period of the report, HBNI awarded 39 Ph.D. degrees in Life Sciences. Some of the theses are summarized below.

3.1 Bhabha Atomic Research Centre, Mumbai

3.1.1 Role of RECQL5 helicase in DNA repair and its implications in cancer therapy

RECQL5 is a multifunctional helicase involved in multiple DNA metabolic pathways responsible for providing stability to replication forks under normal conditions and more so under stress. Besides, RECQL5 expression is downregulated in multiple cancers including breast and gastric cancers. A synthetic lethal interaction between RECQL5 deficiency and silencing/functional inhibition of checkpoint kinase 1 (CHK1) was discovered in cancer cells. Mechanistically, it was found that overactivation of a DNA remodeling enzyme, SMARCAL1 is the primary cause for synthetic lethality. It is thus proposed that RECQL5 is involved in the controlled activation of SMARCAL1 required for regulated processing of stalled replication forks, leading to sustainable repair by both Break Induced Replication (slow) and 53BP1 mediated repair (fast) pathways. Unregulated fork reversal under RECQL5 deficiency leads to generation of copious amounts of single-ended DSBs that are bound by 53BP1 making them difficult to be processed and repaired. This results in the formation of toxic DNA intermediates responsible for synthetic lethality in RECQL5-deficient cancer cells under CHK1 inhibition. This study revealed a novel role of RECQL5 for mitigation of replication stress under CHK1 inhibition. Conversely, RECQL5 protein overexpression in breast cancers is also strongly correlated with poor prognosis, survival and therapeutic resistance.

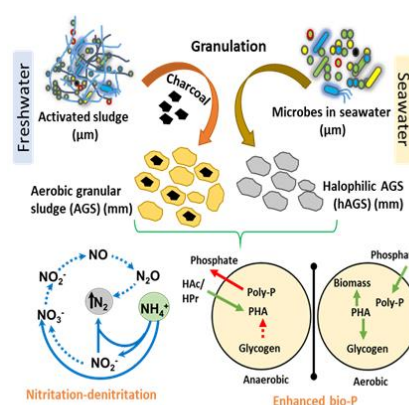


Targeting the differential expression of RECQL5 for better therapeutic outcome. RECQL5 deficiency can be harnessed by synthetic lethality with CHK1 inhibitor and RECQL5 overexpression by using a pharmacological inhibitor

The thesis investigated the mechanism of action of a small oxadiazole urea molecular hybrid (MH) molecule inhibitor of RECQL5 that preferentially target and eliminate RECQL5-expressing breast cancers. The activity of MH is specific to RECQL5 and does not have any effect on other members of RECQL family. Functional activity of RECQL5 was potently inhibited by MH by stabilizing the RECQL5-RAD51 physical interaction; leading to impaired and incomplete HR with preferential killing of RECQL5-expressing breast cancer cells. Treatment with MH also led to efficient sensitization of cisplatin-resistant breast cancers with no effect on transformed mammary epithelial cells. Pharmacologically, oral route of administration of MH was effective in reducing the burden of RECQL5-expressing breast tumors (human xenograft) in NUDE-mice. Also, MH presented no appreciable toxicity to the vital organs, making it a prospective candidate for further pharmacological investigations.

3.1.2 Nitrogen and phosphorus removal mechanisms in aerobic granular sludge sequencing batch reactors

For sustainable biological wastewater treatment, use of Aerobic Granular Sludge (AGS) is gradually taking centre stage. The thesis focuses the study of this system for deciphering mechanisms of N and P removal. Exposure of AGS gradually to increasing concentrations of ammonium ions during its generation in over a years period rendered them capable of near complete removal of ammonium within 24 h subsequently. During this generation period, a reduction in microbial diversity in the granules due to selection of certain bacterial groups was observed. This resulted in occurrence of energy efficient nitrification-denitrification and anammox pathways. Since, the Phosphorus removal was found to be limited at 40% and only for meeting cellular requirements, improvisation of AGS was carried out. To improve granulation and P removal, granulation of activated sludge was studied in the presence of charcoal particles in SBRs using different carbon sources. Bio-P removal via enhanced bio-P removal (EBPR) was rapidly established with differential enrichment of polyphosphate accumulating organism (PAO) clades. Interestingly, the biofilms contained higher abundance of PAO clades and performed EBPR, but not the co-existing granules, suggesting segregation of functional microorganisms. Further improvement was carried out to cater to saline environments, by introducing halophilic microbes present in the seawater. This new approach enabled rapid granulation of halophilic microorganisms of seawater (34 ppt) resulting in halophilic AGS (hAGS) which showed efficient ammonium, total nitrogen and phosphorus removal at 34 ppt. Cultivation of hAGS from autochthonous halophilic microorganisms proves to be a promising approach for achieving biological N and P removals from hypersaline seawater-based wastewaters.



Schematics for effective N and P removal.

3.1.3 Anticancer activities of organic diselenides and their mechanisms of action

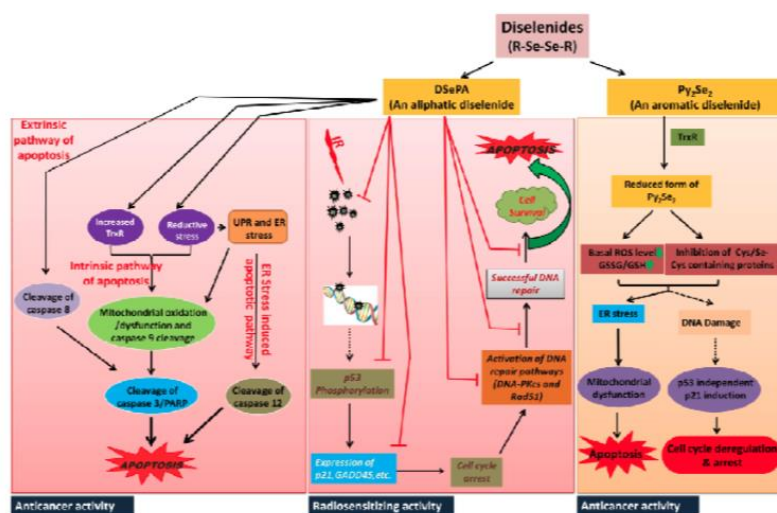
Lung cancer is one of the leading causes of death associated with the cancer worldwide. Due to non-selectivity and side-effects associated with chemotherapeutic agents, development of safe and efficacious agents is the primary focus for researchers. In this context, selenium-based compounds

being redox active have been explored for their chemotherapeutic activity. Preliminary screening of selenium-based redox active organic compounds revealed that DSePA and Py_2Se_2 exhibited better cytotoxicity in vitro. Hence, their in vivo anti-cancer activity and mechanism of action in non-small cell lung carcinoma (NSCLC) were investigated. Both DSePA and Py_2Se_2 elicited a dose and time-dependent cytotoxicity with $\text{IC}_{50} \sim 10 \mu\text{M}$. With regard to the mechanisms of action, DSePA treated cells exhibited biphasic response with reductive stress preceding oxidative stress followed by apoptosis involving effectors of intrinsic, extrinsic and endoplasmic reticulum (ER) pathways. On the other hand, Py_2Se_2 treatment caused reductive stress, DNA damage, cell cycle deregulation and ER dependent apoptosis. DSePA induced the expressions as well as activities of GPx and thioredoxin reductase (TrxR). On the contrary, Py_2Se_2 treatment inhibited their activities. DSePA being an aliphatic diselenide is a much safer derivative with a significantly higher LD_{50} dosage as compared to that of well-studied Cys-Se-Se-Cys in murine models. DSePA exhibited potential radio-sensitizing activity by preventing phosphorylation of p53 and DNAPKs and thereby inhibited the cell cycle arrest and DNA repair. The anticancer and radio-sensitizing potential of DSePA was also confirmed by in vivo studies using A549 xenograft in NOD-SCID mice. The in vivo studies confirmed that administration of DSePA orally in the dose range of 1-5 mg/kg b.w. daily for four weeks was well tolerated and significantly suppressed the growth of A549 derived xenografts. In conclusion, DSePA exhibited potential antitumor activity against human lung cancer models and its mechanism of action is attributed to the induction of apoptosis through reductive stress.

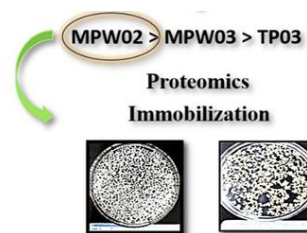
3.1.4 Characterization of uranium tolerant bacterial diversity from Tummalapalle uranium mining region and their prospective application in bioremediation

The thesis is aimed at identifying and characterising bacteria from alkaline uranium mining region that can tolerate and remediate heavy elements like uranium. These microbes adapt well to the heavy metal rich environment and also contribute to biogeochemical cycling. During this study microbial sequestration of uranium from carbonate-rich

alkaline Tummalapalle uranium mine water was carried out using high-throughput next-generation sequencing (NGS) based meta-genomics analysis. The study revealed that the alpha and beta diversity in the mine tailing samples were significantly different when compared to other sampling sites. Uranium sequestration studies indicated that the tail pond isolate TP03 (*Bacillus* sp.) has a maximum loading



Mechanism of actions of anticancer and radio-sensitizing activity of organic diselenides investigated in this thesis



The workflow for microbial sequestration of uranium by Tummalapalle isolates.

capacity of 4.3 mg U/g dry biomass. Whereas, two isolates from the mine pond water namely; MPW02 (*Aeromonas* sp.) and MPW03 (*Bacillus* sp.), had the maximum loading capacity of 105 and 30 mg U/g dry biomass, respectively. Furthermore, the high uranium sequestering isolate MPW02 was chosen for proteomics studies to understand the underlying mechanism involved in uranium sequestration as well as in the context of uranium induced differential expression and alternations in the cellular process. Most of the up-regulated proteins were related to central metabolism, energy conversion, DNA replication, repair proteins. Presence of proteins involved in the inorganic ion transport and metabolism suggest uranium accumulation at the expense of ATP. The protein studies did not help delineate any U-sequestration specific pathways, which could be due to the low abundance of these proteins. In order to assess the individual microbial species from the mine water responsible for sequestering uranium, studies were carried out using aerobic granules from pure culture of *Aeromonas* which showed a maximum loading capacity of 6.5 mg U/g dry biomass. Likewise, when *Aeromonas* cells were immobilized in chitosan-alginate beads a maximum loading capacity of 9.5 mg U/g dry biomass was obtained. The study envisages the application of various alkaliphilic bacteria in mono or multispecies biofilms or in granular biomass for a tailored bioremediation scheme.

3.2 Institute of Mathematical Sciences, Chennai

3.2.1 Exposome and health: Characterization and network-based exploration of diverse environmental chemical spaces

Humans are exposed to environmental chemicals in their everyday life and such exposure can contribute to the incidence of several chronic diseases. Characterization, monitoring and regulation of the ever-increasing space of environmental chemicals for their potential adverse health effects is both necessary and challenging. To this end, there has been growing interest in characterizing the human exposome along with the genome to better understand the environmental factors crucial for human health and disease. The thesis focuses on environmental chemicals that have gained significant attention from



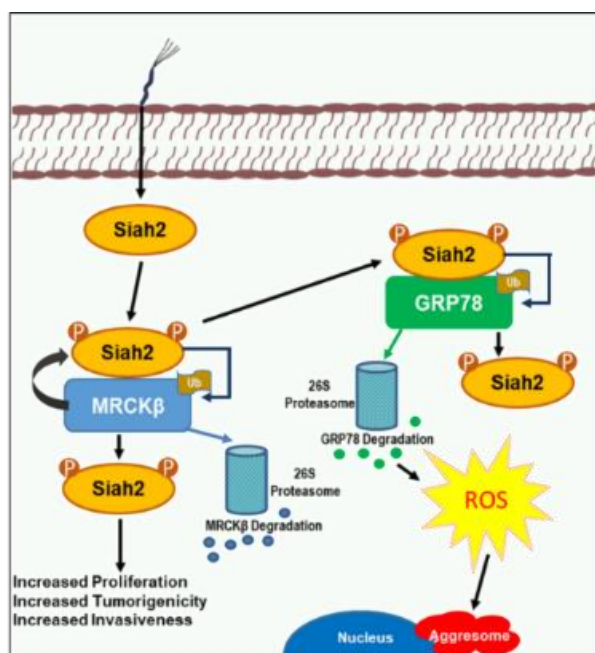
scientists, regulatory authorities, and the public, due to their potential health concerns. To link chemical exposomes to health effects, a systematic compilation, curation, and exploration of the existing information contained in published toxicological studies on diverse groups of environmental chemicals was undertaken. Specifically, the thesis focuses on five groups of chemicals with toxicological relevance, namely, endocrine disrupting chemicals (EDCs), environmental neurotoxicants, human milk contaminants, fragrance chemicals in children's products, and exogenous chemicals detected in human tissues. Extensive computational analysis of the compiled toxicological information for the five groups of environmental chemicals was performed. Similarity networks of these environmental chemicals based on similarity in chemical structures or target genes were investigated. Bipartite networks of environmental chemicals and their target genes, and tripartite networks of environmental chemicals, their target genes, and associated diseases, were constructed to reveal perturbed pathways and potential disease comorbidities related to chemical exposure. A comprehensive adverse outcome pathway (AOP) network for endocrine-mediated perturbations was constructed, and thereafter, graph-theoretic measures were employed to identify the critical biological events associated with endocrine disruption upon chemical exposure. To show the utility of this research for chemical risk assessment, a comparative study using several chemical lists that are a part of inventories, guidelines, or regulations was performed to assess the regulatory status and source of the diverse groups of environmental chemicals considered in the thesis. These analyses reveal that several environmental chemicals of concern are part of everyday exposures, and moreover, many of these chemicals are found to be produced in high volume. In sum, the curated resources and multi-pronged analyses of diverse environmental chemical spaces described in the thesis will facilitate ongoing research to link environmental exposures to human health.

3.3 National Institute of Science Education and Research, Bhubaneswar

3.3.1 Understanding phosphorylation-mediated changes in the subcellular localization and functioning of Siah2 protein in the context of *Helicobacter pylori*-mediated gastric cancer

Helicobacter pylori infection induces various pathological conditions in human stomach including gastric cancer. Many oncogenic factors that contribute to gastric cancer progression are induced by *H. pylori* infection. The E3 ubiquitin ligase Siah2 protein is one such factor. Post-translational modifications (PTMs) determine stability, activity, and subcellular localization of Siah2. Various PTMs of Siah2 have been reported. However, the role of phosphorylation on Siah2 stability and function in *H. pylori*-mediated gastric cancer remained unexplored. The thesis aimed to understand the role of phosphorylation of Siah2 on its functioning and subcellular localization. A novel mechanism involving Siah2 phosphorylation by a serine (Ser)/threonine (Thr) kinase MRCK β was elucidated. MRCK β -mediated phosphorylation of Siah2 at Ser⁶ and Thr²⁷⁹ residues were found to modulate the stability of Siah2. Phosphorylated-Siah2 promoted the proteasomal degradation of MRCK β . Siah2 and its phosphorylation regulated reactive oxygen species (ROS) generation by controlling the cellular abundance of an antioxidant protein GRP78. Increased mitochondrial localization of Siah2 and phosphorylated Siah2 along with decreased level of mitochondrial GRP78 were observed in *H.*

pylori-infected cells. Enhanced ROS generation promoted the formation of cytoprotective aggresomes. Abrogation of phosphorylation of Siah2 at Ser⁶ and Thr²⁷⁹ residues decreased the invasive and proliferative potential of *H. pylori*-infected gastric epithelial cells. Phosphorylation at Siah2 Ser⁶ and Thr²⁷⁹ residues were also validated in human gastric cancer biopsy tissues and murine model of gastric cancer. In conclusion, this study identified the importance of phospho-Siah2 as a diagnostic and therapeutic marker of *H. pylori*-mediated gastric cancer.

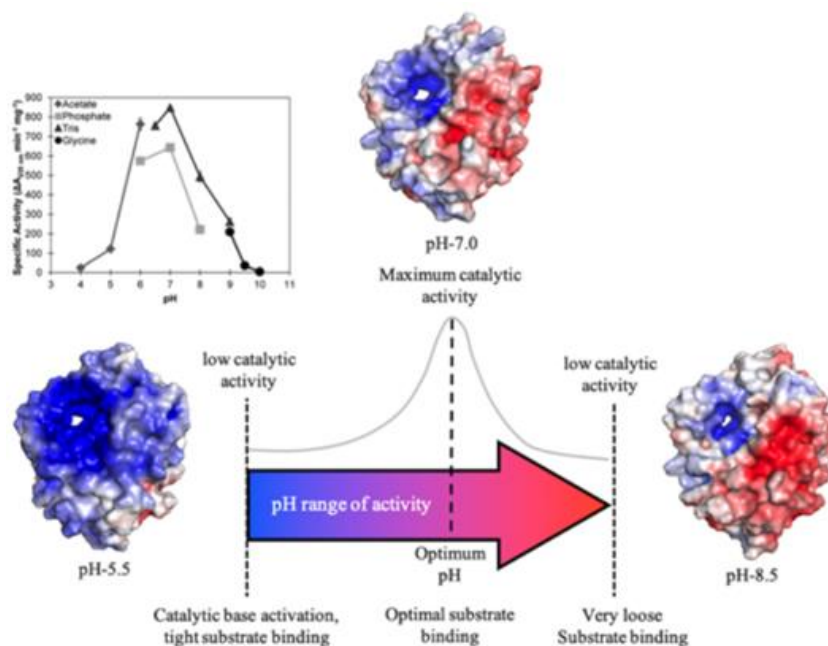


Phosphorylation of Siah2 at Ser⁶ and Thr²⁷⁹ enhances ROS generation, aggresome formation, proliferation, and invasiveness of *H. pylori*-infected gastric epithelial cells

3.3.2 Mechanistic insights into the functioning of a novel pH directed multi-substrate specific Polysaccharide Lyase (PL) SMLT1473, and analyses of conserved 'substrate-pH of activity' pairing among diverse PL folds

Biofilm formation is one of the mechanisms by which bacteria gain resistance to antibiotics and chemical disinfectants. Polysaccharide lyases (PLs) are important class of proteins that are excreted by bacteria to degrade sugars in the extracellular matrix of the host. The PLs enzymes are therefore can be used to degrade or remove biofilm. A pH-dependent PL (SMLT1473) from pathogenic strain 'K279a' of *Stenotrophomonas maltophilia* tends to cleave different substrates under different acid concentrations. The present work is focused on such a Carbohydrate Active enzyme (CAZymes) responsible for ubiquitous and diverse anionic polysaccharides turnover. To understand the mechanism of novel pH-directed multi-substrate specificity, the crystal structures of SMLT1473 in the apo- and substrate-bound form are solved at various pH range (pH-5.0 to 9.0) using X-ray crystallography. Solved crystal structure revealed that Smlt1473's active site architecture is a tunnel in both 'apo' and 'substrate-bound' states. The tunnel is formed due to interactions involving a significantly longer N-terminal lid loop. PyMol *in-silico* analysis generated electrostatic models

highlighting that the substrate-binding surface of pH-tuned Smlt1473 is responsible for the catalytic turnover of sugar substrates with varying negative charge densities. This is the first report of creating a wild-type enzyme-substrate complexes by non-specific pH trapping. Further, the structural superimposition of Smlt1473-Mannuronate and Smlt1473-Hyaluronate reveals Smlt1473's flexibility to accommodate stereo-chemically different substrates. To elaborate further on the 'Substrate-pH of activity pairing' among different classes of PLs, both sequence and structural alignments were performed. Interestingly, they found structural convergence among PLs, which fundamentally vary as these proteins fold. The present work provides several important structural insights into mechanisms utilized by novel (SMLT1473) and related PLs for effective substrate turnover. The biology uncovered here can be extended to overcome biofilm production of algal blooms although a cocktail of PL's would be required for efficient clearance.

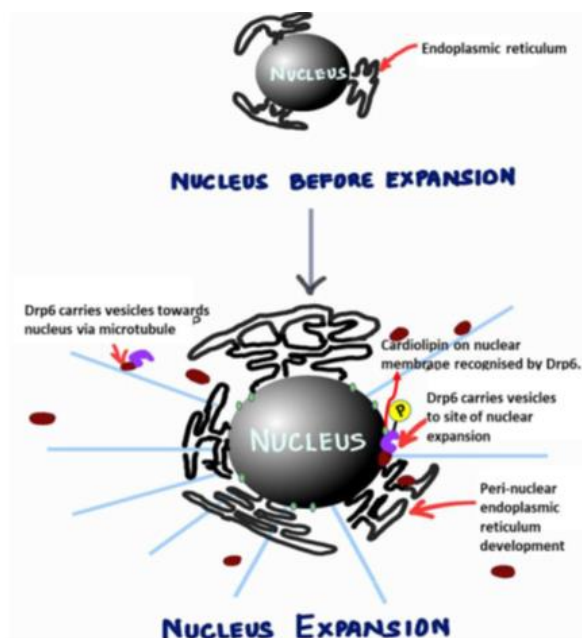


The pH-directed changes on Smlt1473's poly-Glucuronidase activity

3.3.3 Mechanism and regulation of Dynamin Related Protein 6 (Drp6) nuclear recruitment in *Tetrahymena thermophila*

Dynamins are a group of large GTPases involved in various cellular functions such as endocytosis, mitochondrial fission and fusion, endoplasmic reticulum membrane fusion, cytokinesis. They perform these functions by remodelling the target membrane either by fission, fusion or tubulation. All the known dynamins rely on specific lipid for membrane binding and undergo cycles of self-assembly/disassembly. These properties like membrane binding and self-assembly/disassembly are known to be regulated by post-translational modifications in some of the members. Dynamin related protein 6 (Drp6) is a nuclear remodelling dynamin found in *Tetrahymena thermophila*. It plays an essential role during transition of micronucleus to macronucleus, a stage during sexual reproduction where the nucleus expands profusely in its volume. Earlier it is shown that a single isoleucine residue at 553 position (I553) of Drp6 is required for nuclear membrane association by interaction with cardiolipin. Through various biochemical and biophysical approaches, the work in the thesis

demonstrates the mechanism of nuclear recruitment specificity. It is shown that the loss of cardiolipin binding with mutation at I553 is not due to change in the protein structure or conformation, and the amino acid residues in the vicinity are not important for providing cardiolipin binding specificity. Using an *in vitro* fusion assay, it is observed that Drp6 carries out membrane fusion function suggesting it as a fusion dynamin. It is further observed that Drp6 brings about membrane fusion by facilitating tethering and tubulation of the underlying membrane. This study also delineates the mechanism of nuclear expansion and shows that Drp6 regulates nuclear expansion by modulating perinuclear endoplasmic reticulum (ER) network formation. The nuclear expansion by Drp6 is found to be dependent on microtubule structure. The mass-spectrometric analyses identified presence of phosphorylation in four serine residues, and the results show that phosphorylation of serine at 248 position (S248) regulates nuclear localization and membrane fusion function of Drp6 by enhancing cardiolipin binding affinity and reducing GTPase activity (schematic below). The overall study provides the mechanism and regulation of Drp6 recruitment to nuclear envelope and nuclear expansion.



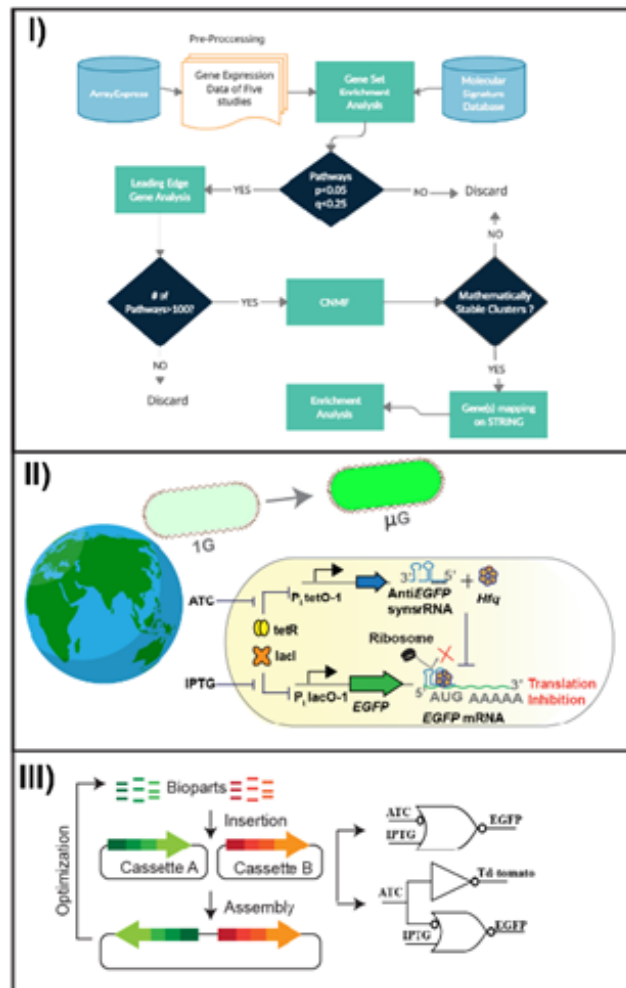
Proposed model for mechanism of nuclear expansion by Drp6

3.4 Saha Institute of Nuclear Physics, Kolkata

3.4.1 Synthetic and systems biology methods for application in gene circuits and microgravity related space biology

How microgravity works at the cellular and genetic level is a long-standing question for the space biology community. Answering this question is difficult for two reasons. i) because microgravity is a weak perturbation, the change in gene expression in microgravity is small for most genes; ii) conventional data analysis ignores the small change in gene expression, preventing the identification of altered molecular pathways in microgravity. The thesis developed a new systems biology analysis

pipeline that identifies altered molecular pathways in microgravity by utilising advanced statistical and machine learning tools. Various whole genome human gene expression data from space experiments and simulated microgravity experiments were analyzed, and the results identified the involvement of several unidentified molecular pathways related to immunity, cancer, and other diseases. It seems microgravity may cause more diseases than known, including various types of cancer. The study further suggests various new insights explaining how anti-cancer drugs might work better in microgravity, the plausible molecular genetic reason for the change in smelling behaviour of astronauts in space, and how lower shear stress around the cells in microgravity brings about immune deregulation through secondary messenger molecular pathways. In the present work, the first microgravity biosensor has been developed using synthetic genetic systems inside the bacteria *E. coli*, where in microgravity the expression of fluorescent proteins changes and can be read by any fluorescence reader. The present work is the first to integrate microgravity as a physical signal within cellular processes in a human designed way and it is demonstrated by controlling the cell division process of *E. coli* with applied microgravity. The thesis further developed a synthetic biology pipeline, named Network Bricks, to assemble and optimise various genetic parts. Inspired by the physical hierarchy of electronics, a Network Brick was used for the assembly and optimization of a synthetic genetic IMPLY gate, and a 2-input-2-output integrated logic circuit in a single *E. coli* cell. Taken together, the thesis has significance in solving real challenges in long duration human space travel.

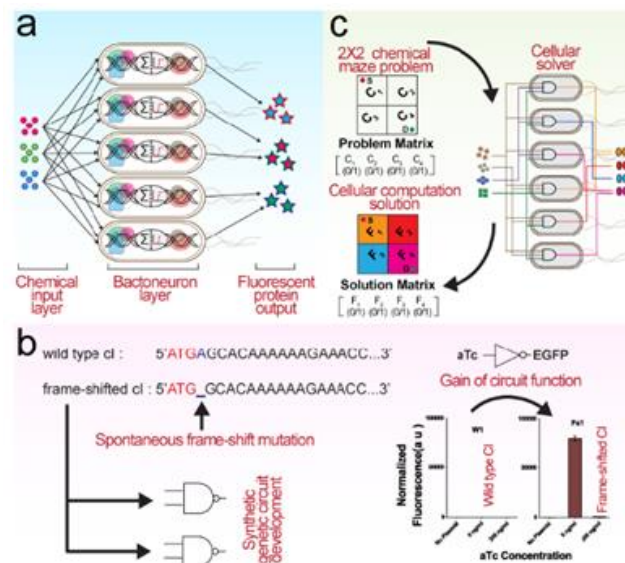


I) Established Systems Biology Pipeline II) Microgravity responsive Circuit III) Network-Brick Pipeline

3.4.2 Synthetic genetic devices for higher order information processing in living cells

Forward engineering of synthetic genetic circuits-based artificial information processing devices has been carried out by applying hierarchical computer and electronic design principles to biology in order to accomplish cellular biocomputing. Half adders, half subtractor, full adder, multiplexers, and channel selector are some of the notable examples of such devices with high computing power that process higher level information in microbes and mammalian cells. Expansion of the computing power of such devices with increasing complexity might lead to the solving of complex computing problems in certain areas where living cell-based biocomputing might outperform traditional computers. The thesis

focuses on distributed computing in engineered bacteria. The single layer artificial neural network (ANN) as a computing system has been adapted to develop a design framework for building complex computing functions in living *E. coli* cells. Such a design approach has been successfully employed in building synthetic genetic higher order information processing devices including a biological 2-to-4 decoder and a biological 4-to-2 priority encoder. A set of molecular engineering rules that could directly translate functional truth tables into bactoneural forms have been established. The generation of spontaneous mutations within the synthetic genetic circuits often leads to loss of the circuit function. It has been shown that a nonfunctional genetic circuit becomes functional by spontaneous frame-shift mutation of a transcription factor λ CI in *E. coli*. This study emerged during the cloning of the λ CI gene, one important bio-part used in the ANN-based work. This mutated gene has further been applied to create synthetic genetic NOR and NAND gates. Maze generation and solving are challenging problems in mathematics and computation. It has been designed and demonstrated that distributed computing with engineered *E. coli* can solve abstract computational problems such as 2X2 maze problems in defined chemical space. Six engineered *E. coli* cell populations, sharing the total computational load, got organized in a single layer within a mixed culture condition and worked as a computational solver, capable of solving the chemically generated maze problems as well as determining the number of solvable and unsolvable problems for a given maze size.

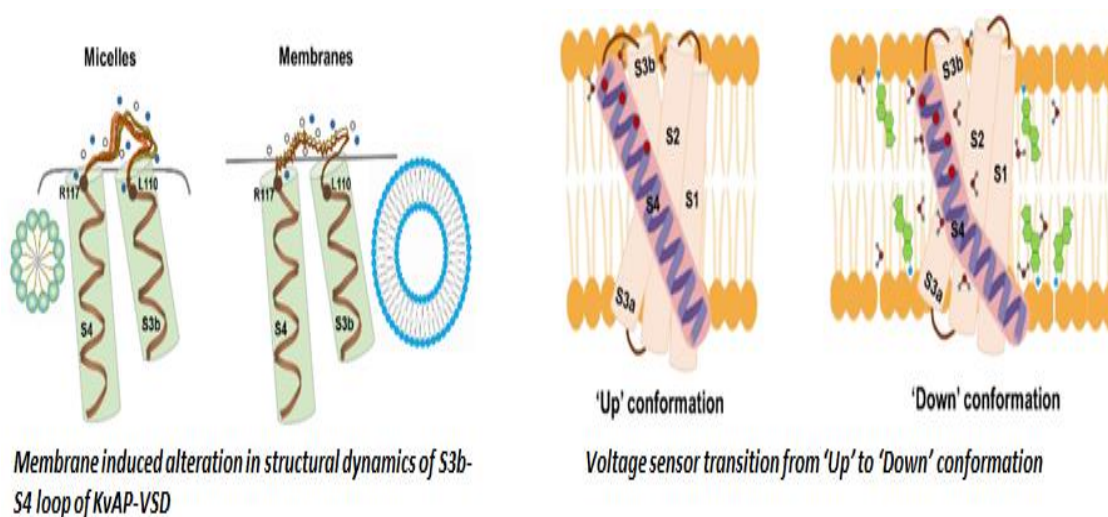


(a) Single layer ANN type architecture in engineered *E. coli*.
 (b) Frame-shifted CI causing gain of circuit function, and its application. (c) *E. coli*-based distributed computing device solving chemically generated 2X2 maze problems.

3.4.3 Structural dynamics of the KvAP voltage sensor during lipid-dependent gating

Cell membrane not only provides a boundary to the cells and the organelles but also serves as place for sending and receiving signals, ionic exchange, neurotransmitter uptake and release, and vesicular trafficking. For acting on the cells, while a few signalling agents easily pass through the membrane, a range of substances and drugs interact with the proteins present in the membrane. The ion channels are integral membrane proteins closely associated with the surrounding membrane lipids. The lipid-

protein interaction not only stabilize the structures of the ion channels but also influence its gating. Voltage-dependent potassium (K_v) channels are crucial for electrical and cellular signalling. The voltage-sensing domain (VSD) in response to changes in membrane potential causes pore opening for ion conduction. In addition, pharmacological agents or toxins bind to VSD and modulate the gating of K_v channels. The structural dynamics associated with the voltage sensor during its conformational change, however, is not well understood. The thesis explored the changes in structural dynamics of the voltage-sensor of the voltage-gated K^+ channel, KvAP in membrane-mimetic systems using isolated KvAP-VSD. The structural dynamics of the S3b-S4 loop, a toxin target has been studied, and compared its organization and dynamics in micelles and membranes using site-directed fluorescence approaches. The results demonstrated the correlation of the conformational heterogeneity of the sensor loop with its environment heterogeneity in membranes. It has been found that the structural dynamics is independent of membrane surface charge and curvature. The lipid-dependent gating of VSD 'Down' and 'Up' conformation was studied in reconstituted liposomes composed of phospholipids



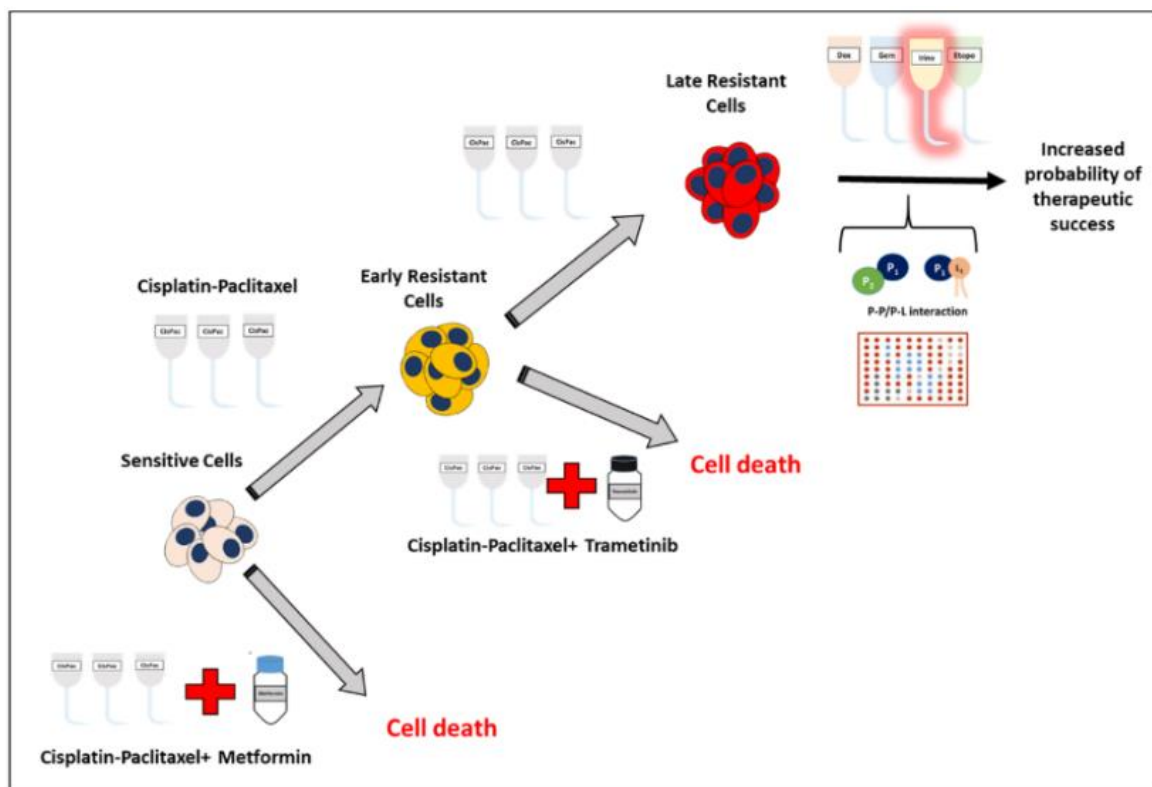
and non-phospholipids. The results highlight the impact of an altered lipid-protein interface that has a strong influence on stabilizing the functional conformations of the KvAP sensor. In addition, the effectiveness of the 'dual-detergent strategy' to purify the KvAP sensor has been studied. This strategy will result in reduced cost of extraction by ~ 2000 fold. Some of the findings from the thesis have been featured in 'New and Notable' section of *Biochemical Journal*. It states that this research 'goes a step further delineating conformational dynamics for the functionally important voltage-sensing paddle loop', highlighting the importance of this work in our understanding of the toxin-sensor interaction and voltage-dependent gating of K_v channels in the membrane.

3.5 Tata Memorial Centre, Mumbai

3.5.1 A study on understanding the modulation in MAPK/ERK and PI3KCA/Akt signaling during acquirement of drug resistance

The thesis pertains to study the effect of repurposing of the commonly prescribed drug against Type 2 and gestational diabetes, metformin as therapeutics in treating epithelial ovarian cancer (EOC). This

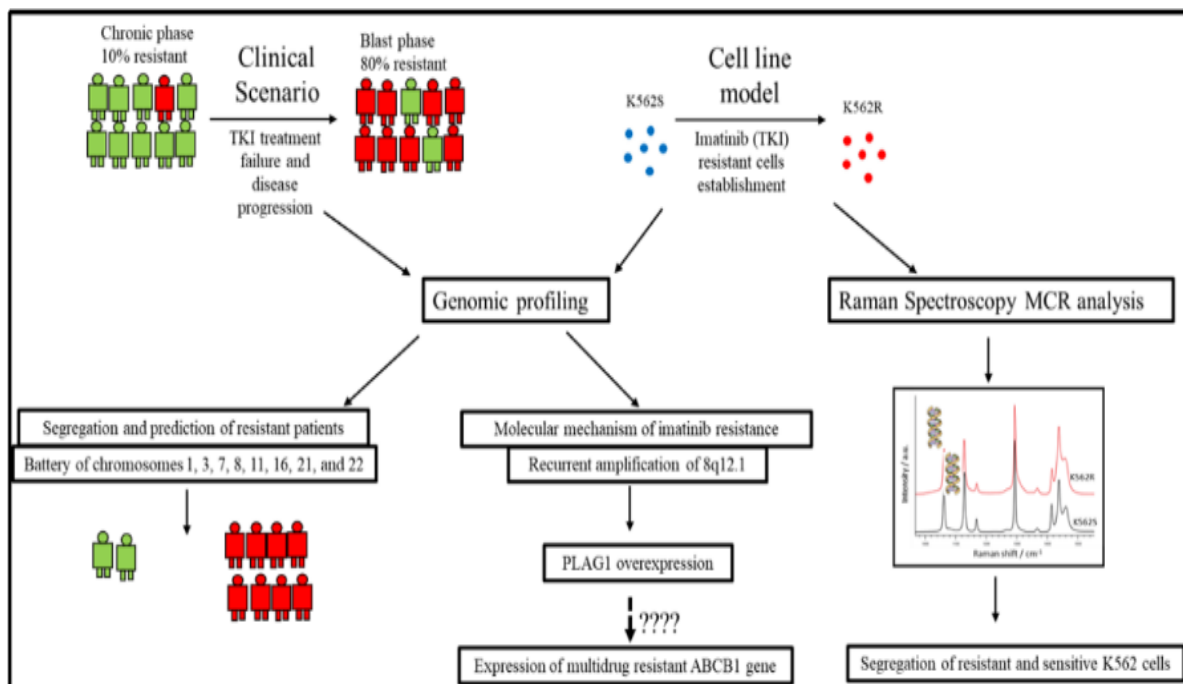
study highlights how metformin can play a role in sensitizing platinum-resistant tumour cells to targeted chemotherapy and/or delaying the acquirement of platinum-resistance in previously sensitive tumour cells. While non-platinum agents like doxorubicin, gemcitabine, irino/topotecan and etoposide are regularly used in treating highly platinum resistant phenotype as the second line of therapy, these are often times associated with severe cytotoxicity. It is known that upregulation of the insulin-like growth factor 1 (IGF-1) receptor, IGF1R expression promotes development of chemoresistance at an early stage in EOCs, while increased AKT activation in presence of low IGF1R levels maintains a highly resistant phenotype in cellular models. However, the literature is still sparse on how these signalling pathways are altered as ovarian cancer cells become more and more resistant to platinum-taxol treatment. Bioluminescence Resonance Energy Transfer (BRET) studies has been used to pinpoint how MAPK/ERK and PI3K/AKT signalling pathways are modulated during acquisition of chemoresistance in ovarian cancer cells and tried to predict the response of highly chemoresistant cells to metformin, along with other non-platinum agents for identifying the optimal choice of therapy. This study proposes that activation of the ERK1/2 signalling cascade negatively affects the sensitivity of platinum-taxol resistance cells to non-platinum drugs. It is further shown that inhibiting ERK to combat chemoresistance at an early stage could be facilitated by inhibition of drug induced autophagic flux. For this, a new luciferase based autophagy sensor, mtFL-p62 has also been developed to monitor real-time autophagic flux *in-vivo*.



A stage specific therapeutic intervention approach to deter platinum-taxol resistance in cancer cells

3.5.2 Genomic profiling of blast cells from different clinical stages of CML

Chronic Myeloid Leukemia (CML) epitomises successful targeted therapy with 86% patients in chronic phase (CP) treated with imatinib attaining remission. However, this treatment is a maintenance therapy and not curative, which leads to administration of imatinib for very long durations. Some patients acquire resistance to imatinib during treatment and if the alternate therapeutic strategies fail, disease progresses to blast crisis (BC). Around 80% patients in BC are resistant to tyrosine kinase inhibitors and have poor survival. Prediction of predisposition to developing secondary resistance before start of treatment in CP, also delineating the molecular basis of imatinib resistance in BC may improve the treatment outcome. Based on the reported recurrence of chromosomal aberrations (CA) across leukemias and demonstration of their role in pathogenesis the thesis aimed at profiling of CAs in CML patients to predict secondary resistance and to delineate the underlying molecular mechanism. CA profile generated with Cytoscan HD array identified that chromosomes 1, 3, 7, 8, 11, 16 and 22 harboured frequent aberrations in imatinib-unresponsive CML patients. By using this battery of chromosomes, unsupervised hierarchical clustering could segregate imatinib sensitive and resistant patients as well as was able to predict resistance. The altered genomic content due to chromosomal gains and losses was captured in MCR assisted Raman spectroscopy analysis and could segregate imatinib sensitive and resistant K562 cells. Genomic analysis of CML samples as well as K562 cell line identified recurrent chromosomal amplification at 8q11.2-12.1. On functional evaluation of genes residing at this locale were PLAG1 was found to be playing a role in imatinib resistance. PLAG1 being a transcription factor, increased the expression of multidrug resistance ABCB1 gene which is associated with chemo resistance. PLAG1 knockdown resulted into reduced expression of ABCB1 which may be responsible for decrease in IC₅₀ for imatinib in resistant K562 cells with knocked-down PLAG1. Thus, the present study provides insights on to the molecular mechanism of imatinib resistance.

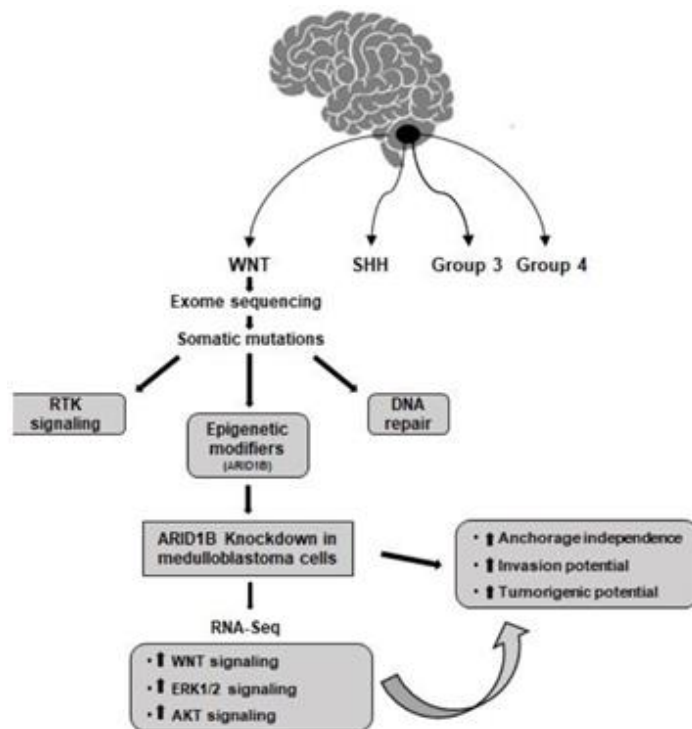


3.5.3 Role of epigenetic modifiers in pathogenesis of medulloblastoma

Medulloblastoma is the most common paediatric embryonal brain tumor accounting for about 20% of all childhood brain tumor cases. It is highly malignant, and the current treatment includes maximal surgical removal of the tumor followed by radiation and chemotherapy. Although this treatment has improved survival, about 30% of the patients still succumb to the disease, and the survivors often suffer from long-term neurological deficits. This warrants the need for a better treatment mechanism. Cancer is a genomic disease, and understanding the genetic landscape can open up new avenues. Gene expression profiling studies of medulloblastomas have identified four distinct subgroups- WNT, SHH, Group 3, and Group 4. The WNT subgroup has the best long-term survival of > 90%, and Group 3 with the worst five-year survival of 65%. Whole-genome/exome sequencing studies have identified the alterations in epigenetic modifier genes, thus highlighting the need to understand the role of epigenetic modifiers in medulloblastoma pathogenesis.

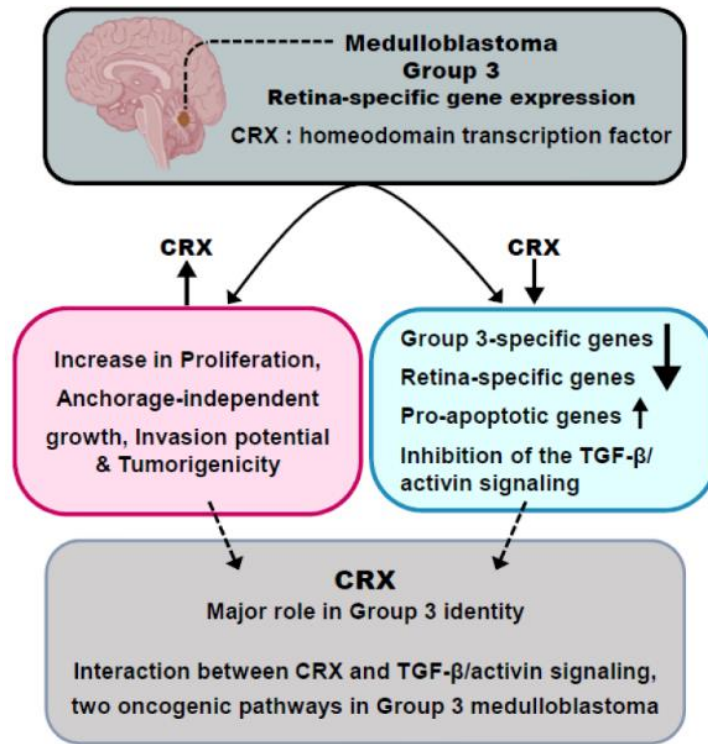
The thesis focuses on understanding the role of two such epigenetic modifiers in the medulloblastoma pathogenesis.

ARID1B is a highly conserved DNA-binding component of the mammalian SWI/SNF chromatin-remodeling complex, and the SMARCA4 gene encodes a protein with a helicase domain and acts as a catalytic subunit of the SWI/SNF complex. This study reports ARID1B gene is most likely haploinsufficient in WNT subgroup medulloblastomas due to monosomy 6. The shRNA-mediated ARID1B knockdown increased medulloblastoma cells' growth and malignant potential. ARID1B downregulation led to the activation of multiple oncogenic signaling pathways like canonical WNT signaling, MAPK signaling, and PI3K/AKT signaling pathway by downregulating the expression of several negative regulators of these pathways. Thus, ARID1B keeps a check on multiple signaling pathways by affecting the transcription of the genes involved in the negative and positive regulation of these pathways. In the WNT subgroup medulloblastoma, reduced expression of this gene is observed, most likely due to monosomy 6, and therefore the signaling pathways remain aberrantly active, leading to oncogenesis. Thus, ARID1B appears to act as a tumor suppressor gene in the WNT subgroup medulloblastoma. On the other hand, SMARCA4 knockdown decreased proliferation, induced myogenic differentiation of medulloblastoma cells, and did not affect the canonical WNT signaling pathway. Thus, a distinct role of the two components of the SWI-SNF complex is unravelled by these studies in the pathogenesis of medulloblastoma.



3.5.4. Deciphering functional role of the genetic alterations in medulloblastoma, a common malignant brain tumour in children

Medulloblastoma is a highly malignant primary brain tumour that accounts for ~20% of all central nervous system (CNS) tumours in children. Among all the medulloblastoma subgroups, Group 3 is the most aggressive subtype and has the worst prognosis. Medulloblastoma is divided into four major molecular subgroups, namely WNT, SHH, Group 3, and Group 4, primarily based on the gene expression profiles. The present thesis aims at understanding the differential expression profile and its functional significance in different types of medulloblastoma. Group 3 medulloblastoma have shown overexpression of Cone Rod Homeobox (CRX), one of the



master regulators of photoreceptor differentiation. The photoreceptor program is specific to the retina and is not present in the normal cerebellum. In the present study, it was observed that CRX expression increased the proliferation, anchorage-independent growth, invasion potential, and tumorigenicity of medulloblastoma cells indicating the oncogenic role of CRX. CRX knockdown resulted in the upregulation of several pro-apoptotic genes, indicating the important role of CRX in cell survival. Transcriptome analysis revealed that TGF- β /activin and the BMP signaling were inhibited upon CRX knockdown indicating TGF- β /activin signaling pathway and CRX may regulate each other's expression. Therefore, simultaneous targeting of the two oncogenic pathways that is CRX and TGF- β /activin could be an effective therapeutic strategy for the Group 3 α subtype of medulloblastoma. The thesis also examines on DDX3X which is the second most frequently mutated (52% of cases) gene in medulloblastoma after β -catenin. DDX3X has been reported to have contrasting roles in different types of cancers acting either as an oncogene or a tumour suppressor. This dual role of DDX3X is mainly because it is a multifunctional protein and is involved in multiple cellular processes. shRNA-mediated downregulation of DDX3X resulted in a reduction in the proliferation and clonogenic potential of the medulloblastoma cells. DDX3X knockdown resulted in downregulation of cell cycle regulatory genes and steroid pathway genes which could be the mechanism behind the growth inhibitory effect of DDX3X knockdown in the medulloblastoma cells. DDX3X knockdown resulted in the upregulation of NOD-like and Toll-like receptor and death receptor signaling pathway genes which could mediate cell death upon the loss of DDX3X expression in medulloblastoma cells. Interestingly, medulloblastoma-associated DDX3X mutants retained their ability to form stress granules that would enable the survival of the cells under stress.

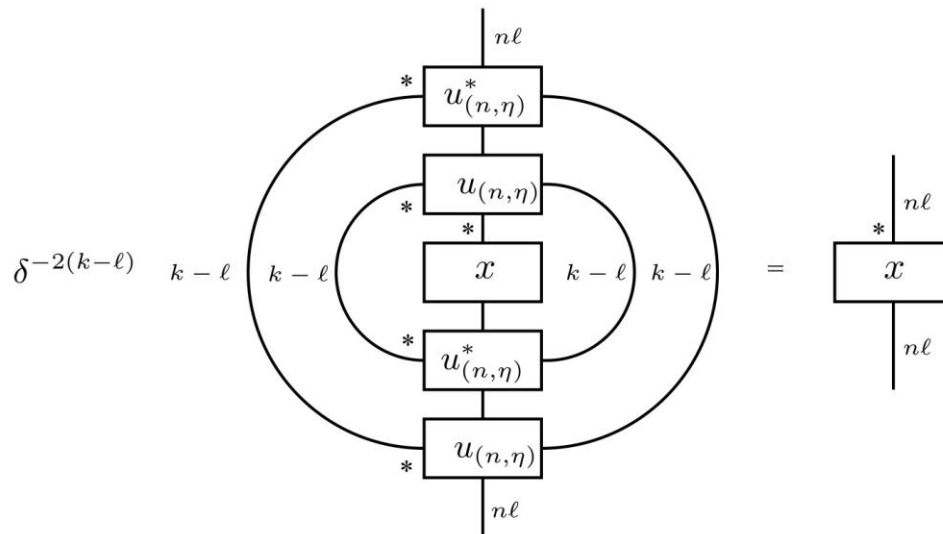
4. Mathematical Sciences

During the period of report, HBNI awarded 21 Ph.D. degree in Mathematical Sciences in a variety of research areas such as Quantum information theory, Hyperbolic systems of conservation laws, Graph theory, Finite Geometry, Cryptography and Algebraic Geometry. Some of the theses are summarized below.

4.1 Institute of Mathematical Sciences, Chennai

4.1.1 Planar algebras, quantum information theory and subfactors

The thesis mainly deals with the mathematical objects known as planar algebra and their connection to quantum information theory. The content of the thesis can be divided into three parts. In the first part, the generalized notion of a biunitary element in a planar algebra is defined and the author identifies certain objects arising quantum information theory as some particular biunitary elements in the spin planar algebra. In the second part the construction of subfactor planar algebras from biunitary elements is described which in turn associates subfactors to the objects of interest in quantum information theory. Finally, the subfactor planar algebras associated to the classic objects *Latin squares* is examined. It is proved that the subfactor planar algebra associated to any Latin square is the subgroup-group planar algebra of a subgroup-group pair constructed from Latin squares.



Double circle relation

The main results from the thesis are given below:

1. Let P be the spin planar algebra. Then there is natural 1-1 correspondences between the following sets:
 - 1) {0,1}-biunitary elements in P and Hadamard matrices of size $n \times n$,
 - 2) {0,1}-biunitary elements in P and quantum Latin squares of size $n \times n$,
 - 3) {0,2}-biunitary elements in P and biunitary matrices of size $n^2 \times n^2$ and
 - 4) (A, R) biunitary elements in P and unitary error bases in $M_n(C)$.

2. (i) Let P be a C-star planar algebra and u be a $\{0, 1\}$ biunitary element in P . Associated to u , a C-star planar subalgebra Q of (I, ϵ) cabling of P can be constructed.

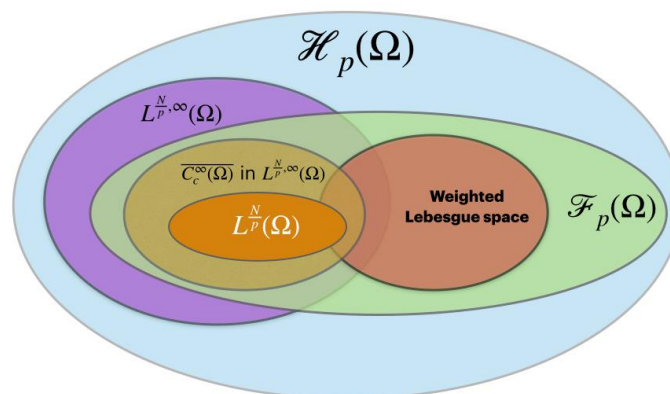
(ii) If P is the spin planar algebra and u is a $\{0, 1\}$ biunitary element in P , then the C-star planar subalgebra Q obtained from the above-mentioned construction is a subfactor planar algebra. If $l=1$, then Q is an irreducible subfactor planar algebra.

3. Let L be a Latin square of size $n \times n$. Then the subfactor planar algebra Q associated to the biunitary element u obtained from the Latin square is the subgroup-group planar algebra.

4.1.2 On the Hardy type potentials

In the present work, the generalisations of the following three fundamental inequalities: the Hardy inequality, the Hardy-Rellich inequality, and the logarithmic Sobolev inequality have been studied. Mainly, the weighted Hardy, the weighted Hardy-Rellich, and the weighted logarithmic Sobolev inequalities have been studied. More precisely, the locally integrable weight functions for which one of the above inequalities hold have been explored. Each of these inequalities has been studied separately.

1. The weighted Hardy inequality. A locally integrable function which satisfies the weighted Hardy inequality is called a Hardy potential. Using Mazya's characterization, the optimal Banach function space for Hardy potentials has been identified. Further, sufficient conditions on the Hardy potentials have been provided that ensure the best constant in the weighted Hardy inequality is attained in the Beppo-Levi space. Some embedding theorems of the Beppo-Levi space have also been discussed.



Venn diagram of the space of Hardy Potentials

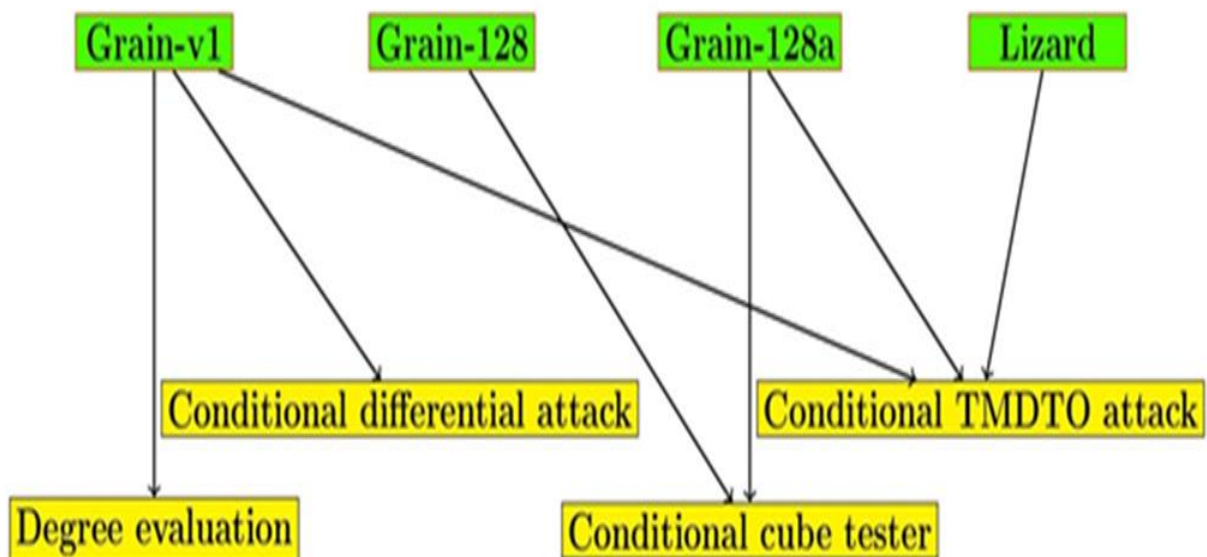
2. The weighted Hardy-Rellich inequality. Depending on the dimension, various Lorentz and Lorentz-Zygmund spaces that give admissible weight functions for the weighted Hardy-Rellich inequality have been identified. Certain weighted Lebesgue spaces that give another class of admissible weights have been provided.

3. The weighted logarithmic Sobolev inequality. In the similar spirit, an admissible space for the weight functions for which the weighted logarithmic Sobolev inequality holds has been identified. Also, the conditions under which the best constant in this inequality is achieved have been obtained.

4.2 National Institute of Science Education and Research, Bhubaneswar

4.2.1 Cryptanalysis of stream ciphers

In the present work, some popular cryptanalysis of well-known stream ciphers has been explored. The differential attack is a well-known cryptanalysis method for a stream cipher. A conditional differential attack on Grain-v1 using a two-bit difference vector in IV (Initialization Vector) has been proposed. Grain-v1 for 112, 114 and 116 rounds can be distinguished from random sources in single, weak, and related key setups with a 99%, 73%, and 62% success rate. In recent days several types of attacks, including cube tester, have been used to analyze Grain-128a. But searching for a good cube is a challenging task in cube tester. A heuristic approach has been proposed using three strategies, maximum initial zero, maximum last zero, and maximum last α (introduced in the present work), to find good and smaller dimensional cubes for Grain-128 and Grain-128a. The conditional cube testers have been designed using the heuristic to distinguish Grain-128a for 191 round (Single key setup), 201 round (Weak key setup), and Grain-128 for 207 round (Single key setup), 235 round (Weak key setup), respectively. After that, the focus was on the TMDTO (Time Memory Data Trade-off)



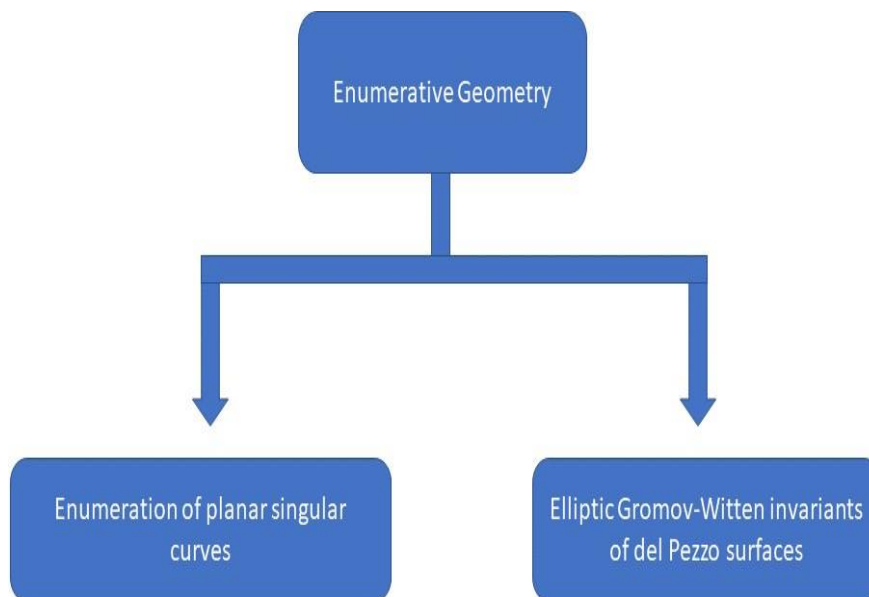
Different types of attacks on popular ciphers

attack by using a state bit recovery attack to analyze Grain-v1, Grain-128a, and the lightweight stream cipher Lizard. A general algorithm to recover the maximum number of state bits by fixing fewer state bits of any cipher has been proposed. Maximum 33, 48, and 24 state bits are recovered by fixing 45, 54, and 50 state bits for Grain-v1, Grain-128a, and Lizard. A conditional TMDTO curve for three different conditions has also been proposed. Using this, some excellent results were obtained for Grain-v1, Grain-128a, and Lizard. In the last contribution chapter of the thesis, an algorithm has been proposed to find the algebraic degree of NFSR update functions of Grain-v1, which helps us calculating the degrees of LFSR update and output functions. Using the above algorithm, the degrees of output and state update functions up to 54 rounds for Grain-v1 have been calculated.

4.2.2 Enumerative geometry of curves in a moving family of surfaces

Curve counting theory of complex projective plane $\mathbb{C}P^2$ is very classical. In the present work, two different curve counting problems are discussed which are generalizations of enumerative geometry of plane curves.

First, curves in $\mathbb{C}P^3$ which lie inside a hyperplane of $\mathbb{C}P^3$ are considered; such curves are called as the planar curves. Enumerative geometry of planar curve is the same as curve counting theory in a moving family of $\mathbb{C}P^2$, instead of fixing one $\mathbb{C}P^2$. An explicit formula has been obtained to count the number of degree d planar curves in $\mathbb{C}P^3$ having δ nodes and another singularity \mathfrak{X} of codimension $c_{\mathfrak{X}}$ that intersect r lines and pass through s points such that $r + 2s = \frac{d(d+3)}{2} - (\delta + c_{\mathfrak{X}})$ and $\delta + c_{\mathfrak{X}} \leq 4$. To find the formulas, smooth deformation theory has been used, and using this the situation when singularities collide has been analyzed. For example, it has been shown that if two nodes collide, it produces a tacnode, and in the collision of three nodes, it either a triple point or a singularity of type A_5 results. Enumerative geometry made a substantial progress through the so-called Gromov-Witten theory over the last three decades. The main object of study in this theory is the moduli space of stable maps.



Flow Diagram of various enumerative geometric problems

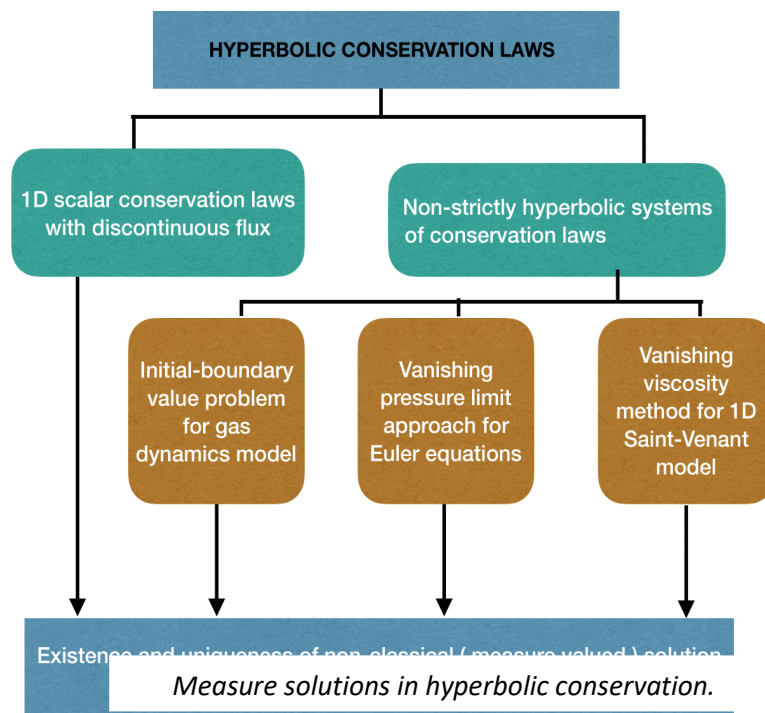
Using the intersection theory of the moduli space of stable maps, certain numerical invariants are defined which are known as the so-called Gromov-Witten invariants. In the present work, a recursive formula to count the elliptic ($g = 1$) Gromov-Witten invariants of del Pezzo surfaces has been obtained. A result of Ravi Vakil, which states that genus g Gromov-Witten invariants of del Pezzo surfaces are enumerative, links Gromov-Witten invariants and enumerative geometry in this set up. It is worthwhile to note that $\mathbb{C}P^2$ is itself a del Pezzo surface. Thus, it gives a generalization of enumerative geometry of $\mathbb{C}P^2$.

4.2.3 Solutions in the class of measures for some hyperbolic systems of conservation laws and scalar conservation laws with discontinuous flux

The thesis is concerned about the existence and uniqueness of the non-classical (measure-valued) solutions for the following conservation laws arising from various physical models: (i) Euler equations of compressible fluid flow and its generalisation, (ii) system of non-strictly balance laws arising from 1D Saint-Venant model, (iii) initial-boundary value problems for 1D pressureless gas dynamics model and (iv) scalar conservation laws with discontinuous flux function as shown in schematic.

The focus of the thesis was to obtain the explicit formulae for the above systems. For the system mentioned in (i), the shadow-wave method was used and a vanishing pressure limit approach which can be viewed as a variant of the vanishing viscosity method. In the presence of small pressure, the system is strictly hyperbolic thus by using Lax theory, a solution was constructed and found its distributional limit as the pressure term approaches zero. The obtained distributional limit satisfies as the solution in a weak sense.

For the system mentioned in (ii), the vanishing viscosity method was used. A transformation like Hopf-Cole transformation was used to linearise the parabolic approximation (viscous approximation) of the system, and then by passing to the limit an explicit formula was obtained. Using Volpert’s product it was shown that the obtained explicit formula is a solution. The initial value problem for the system mentioned in (iii) in one and higher space dimension has been extensively pursued in the literature in the past decades but to the best of our knowledge, no attempts have been made so far to solve the initial-boundary value problem. The work of Huang is extended by introducing a second type of potential-boundary potential. Furthermore, the boundary condition is designed in a physically meaningful way. For the scalar conservation laws with discontinuous flux (for over compressive flux pair) mentioned in (iv), first, the vanishing viscosity method was used to obtain an explicit formula for a special type of flux function. For general over compressive flux pair, a weak formulation is proposed which allows concentration along t-axis and an explicit formula is constructed satisfying the weak formulation. A numerical scheme is proposed which effectively captures the solution and its convergence analysis is carried out.



4.2.4 Centrality in connected graphs and some related indices

The thesis is a study about different central parts of connected graphs and some graphical indices related to them. The center, centroid, characteristic set and the subtree core are four distinct central parts of a tree whereas the center, median and the security center are three distinct central parts of a graph. Related to these central parts, there are some topological indices associated with a graph. The Wiener index and the total eccentricity index are two such topological indices related to the median and the center, respectively. The *subgraph core* and the *characteristic center* as two new central parts of a graph have been defined and studied their centrality behaviour. It is shown that the subgraph core and the characteristic center are different from the center, median and the security center.

Among all trees on n vertices, the tree which maximizes the distance between the characteristic center and the subtree core was obtained. The asymptotic nature of the distances between different central parts are also studied. The study was continued to obtain the trees which maximize the distances between different central parts over trees with fixed diameter and over binary trees on n vertices. Over binary trees on n vertices, a conjecture posed by Smith et al. in "H. Smith, L. Szekely, H. Wang, and S. Yuan, on different middle parts of a tree, *Electronic Journal of Combinatorics*, 25 (2018), no. 3, paper 3.17, 32 pp" was proved which tells about the class of trees which maximizes the distances between any two of center, centroid and subtree core. The members of the class which maximize these distances were also characterized. The subgraph index associated with the subgraph core of a graph is introduced. The *subgraph index* of a graph G is defined as the total number of connected subgraphs of G . The graphs which extremize the subgraph index over unicyclic graphs were obtained, unicyclic graphs with fixed girth and over graphs with fixed number of pendant vertices. For each of these classes of graphs, a sharp upper and lower bound have been given for the subgraph index. The study has been continued for the Wiener index and the total eccentricity index.

The *Wiener index* of a graph is defined as the sum of distances between all its unordered pairs of vertices. The graphs which extremize the Wiener index were characterized over graphs with fixed number of pendant vertices. Further, the graph which minimizes the Wiener index over graphs with fixed number of cut vertices was also obtained.

The *total eccentricity index* of G is defined as the sum of eccentricities of all its vertices. The graphs which maximize the total eccentricity index over graphs with fixed number of pendant vertices were obtained and the graphs which minimize the total eccentricity index over graphs with fixed number of cut vertices. Further, over graphs with s cut vertices, the graphs maximizing the total eccentricity index for $s=0,1, n-3, n-2$ were obtained and proposed a conjecture for $1 < s < n-3$.

4.2.5 Combinatorial characterizations of point and line sets in $PG(3, q)$ with respect to a quadric

Let $PG(d, q)$ be the d -dimensional projective space defined over a finite field of order q . For a nonempty set \mathcal{L} of lines of $PG(d, q)$, a set B of points of $PG(d, q)$ is called an \mathcal{L} -blocking set if each line of \mathcal{L} meets B in at least one point. An \mathcal{L} -blocking set B in $PG(d, q)$ is said to be minimal if B has no proper subset which is also an \mathcal{L} -blocking set in $PG(d, q)$. Blocking sets are combinatorial objects in finite geometry with several applications and have been the subject of investigation by many

researchers with respect to varying sets of lines. The first step in this regard has been to determine the minimum size of a blocking set and then to characterize, if possible, all blocking sets of that cardinality. When \mathcal{L} is the set of all lines of $PG(d, q)$, a classical result by Bose and Burton says that if B is a blocking set in $PG(d, q)$ with respect to all its lines, then $|B| \geq (q^d - 1)/(q - 1)$ and equality holds if and only if B is the point set of a hyperplane of $PG(d, q)$.

In $PG(3, q)$, consider an elliptic quadric $Q^-(3, q)$, a hyperbolic quadric $Q^+(3, q)$ and a quadratic cone \mathcal{K} with base an irreducible conic in some plane of $PG(3, q)$. Let $\mathcal{Q} \in \{Q^-(3, q), Q^+(3, q), \mathcal{K}\}$. Every line of $PG(3, q)$ meets \mathcal{Q} in either 0, 1, 2 or $q + 1$ points. A line L of $PG(3, q)$ is called external if $|L \cap \mathcal{Q}| = 0$, secant if $|L \cap \mathcal{Q}| = 2$, and tangent if $|L \cap \mathcal{Q}| = 1$ or $q + 1$. The set of all lines of $PG(3, q)$ that are external were denoted by \mathcal{E} , \mathcal{S} and \mathcal{T} , secant and tangent, respectively, with respect to \mathcal{Q} .

In the present study, for $\mathcal{Q} \in \{Q^-(3, q), \mathcal{K}\}$, the minimum size \mathcal{L} -blocking sets in $PG(3, q)$ was considered, where the line set \mathcal{L} is one of \mathcal{E} , \mathcal{T} , \mathcal{S} , $\mathcal{E} \cup \mathcal{T}$, $\mathcal{E} \cup \mathcal{S}$ and $\mathcal{T} \cup \mathcal{S}$.

When $q = 2$ and $\mathcal{Q} \in \{Q^-(3, 2), Q^+(3, 2)\}$, all minimal \mathcal{E} -blocking sets in $PG(3, 2)$ were classified, up to isomorphisms. When $q = 3$ and $\mathcal{Q} \in \{Q^-(3, 3), Q^+(3, 3)\}$, all next-to-minimum size \mathcal{E} -blocking sets in $PG(3, 3)$ were classified, up to isomorphisms. A characterization of the secant lines with respect to a hyperbolic quadric in $PG(3, q)$ for odd $q \geq 7$ was also given based on certain combinatorial properties.

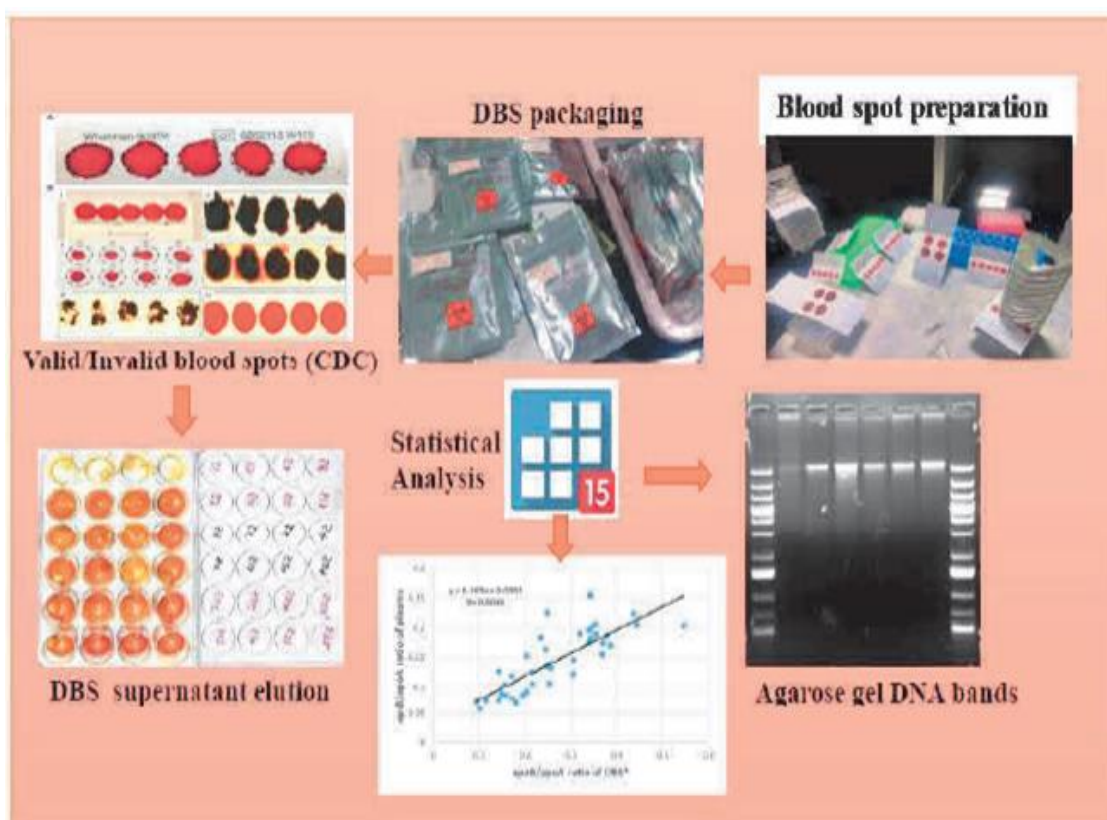
5. Medical & Health Sciences

During the period of report, HBNI has awarded Ph.D. degree to 1 student in Medical & Health Sciences on successful completion of academic programme. The summary of the doctoral theses is given below.

5.1 Tata Memorial Centre, Mumbai

5.1.1 Efficacy of dried blood spots for assessing biomarkers in field epidemiological studies

The aim of the thesis was to use dried blood spots for assessing biomarkers in field epidemiological studies. Dried blood spots (DBS) prepared from EDTA blood samples collected from healthy population, transported over different time duration (24/48/72 h) and stored at different temperatures (4 °C and -20 °C). The samples were studied to see the storage and transportation impact on the stability of various biomarkers. Commercial ELISA kits were used for testing IgG antibody against *H. pylori* and apolipoproteins but column-based method for gDNA extraction. DBS samples were processed as per kit manufactured protocol and the data were analyzed using commercially available statistical software STATA. Research finding reflect DBS could be a remarkable tool to measure the analytes/ biomarkers even if it is stored at different temperatures and varying transport duration. All these supports the feasibility of DBS to be utilized for conducting field epidemiological studies.



Schematic showing an observational study to investigate the biomarkers assessment through Dried Blood Spots

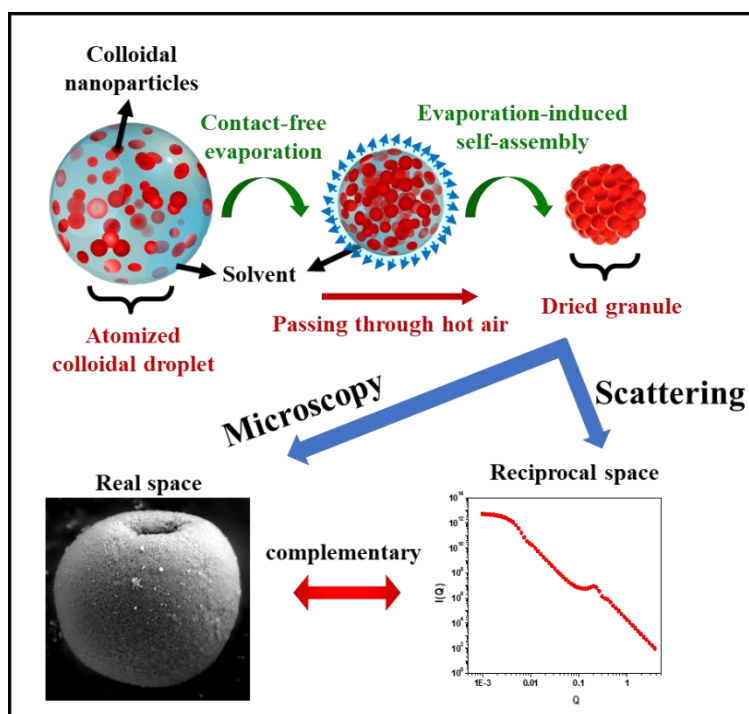
6. Physical Sciences

During the period of report, HBNI awarded 113 Ph.D. degree in Physical Sciences in a variety of research areas such as Condensed matter physics, Nanoscience, Surface physics, Material science, Spintronics, X-ray Multilayer, Radiological Physics, Computational Spectroscopy, Density Functional Theory, Quantum information and computation, Nuclear physics, Neutrino Physics, Plasma Physics and Astroparticle Physics and Cosmology. Some of the theses are summarized below.

6.1 Bhabha Atomic Research Centre, Mumbai

6.1.1 Formation of hierarchical nanostructured micro-granule by self-assembly and its characterization by small-angle scattering

The broad objective of the thesis was to understand certain novel phenomena in correlated nanostructured micro-granules, synthesized by rapid evaporation of contact-free colloidal droplets through spray-drying. Small-angle scattering was employed for quantitative structural information of these novel nanostructured systems. The thesis aimed to establish a correlation between physicochemical attributes with the formation mechanism of the novel granular structure obtained by evaporation-induced self-assembly. The thesis focused primarily on three aspects; i) The effect of **nanoscale confinement** in the composite micro-granules, ii) The role of **competitive interfacial interactions** during evaporation induced self-assembly and its influence on resulting structural correlation, and iii) The effect of **shape anisotropy of the colloidal particles** in tuning the structural correlation. Moreover, the thesis demonstrated a few plausible applications of the synthesized micro-granules, particularly towards water purification and electro-responsive applications.



Schematic illustrating the formation of nanostructured micro-granules by evaporation induced self-assembly and their characterization using complementary methods of small-angle scattering and scanning electron microscopy.

demonstrated a few plausible applications of the synthesized micro-granules, particularly towards water purification and electro-responsive applications.

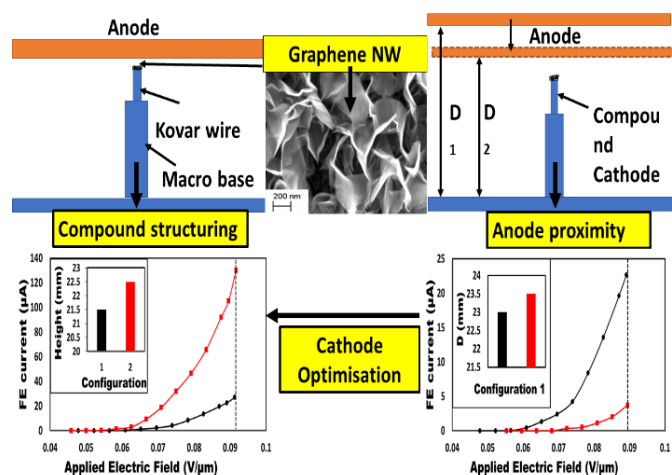
Owing to the self-assembly, micro-granules possess a multi-level structure spanning over a few nanometers to several microns. Thus, extensive structural characterization of these granules, over a wide length scale, has been indispensable to establish a structure-function correlation. Complementary techniques of scattering and imaging, involving **Small-Angle X-ray Scattering (SAXS)**,

Small-Angle Neutron Scattering (SANS), and **Field-Emission Scanning Electron Microscopy (FESEM)** were used to understand the mesoscopic structural details of the synthesized micro-granules through rigorous mathematical modelling and analysis. In addition to the revealing novel phenomena in these micro-granules, the thesis also demonstrated the **salient features and performance of a newly developed and commissioned SAXS beamline** at Indus-2 synchrotron that was used for obtaining most of the scattering data. A schematic representation illustrating the formation mechanism of correlated nanostructured micro-granules and their structural characterization using both scattering and imaging methods has been depicted in Fig. 1.

6.1.2 Studies on nano-structured field emission cathode for beam generation in electron gun

Nano-structured based field emission electron source device has garnered a lot of attention worldwide due to its potential use in many applications where a conventional thermionic emission-based electron source is deemed unsuitable. This new technology has also emerged as an alternative to prevailing thermal emitters, which, if replaced by nano structured cathode can improve the performance of electron source device. Over the years, many experimental groups have focused their attention on developing good quality nano material for application in field emission. However, the field emission performance of such a device not only depends on the quality of cathode material but also on the different geometric parameters associated with the device. Nano structured field emission device is a multidimensional system where the actual emitter dimension is found in the range of few nano meters to microns but the overall dimensions of the diode lie in the range of mm. Determining the role of the device geometry on overall field emission characteristics of the electron source is crucial for the device design. Optimization of device geometry has the potential to improve the field emission performance of a cathode sample manifold without introducing any change in the nano emitter geometry.

The aim of the thesis is to develop an all-encompassing framework for field emission performance evaluation of an electron source which will incorporate the effect of various device geometry parameters starting from nano scale up to macro length scale. In this work, the results of numerical as well as experimental investigation pertaining to a novel diode geometry have been discussed. The new diode geometry adopted in this work utilizes the twin benefit of multi-stage cathode construction following the Corrected Schottky conjecture (CSC) and the anode proximity effect for enhancement of field emission current from a nano-structured sample. The results provide the first ever experimental verification of CSC. Further numerical and experimental studies of the novel gated diode are carried out for electron beam generation. Finally, a novel hybrid approach for multi-dimensional treatment of device geometry for electron trajectory calculation has been

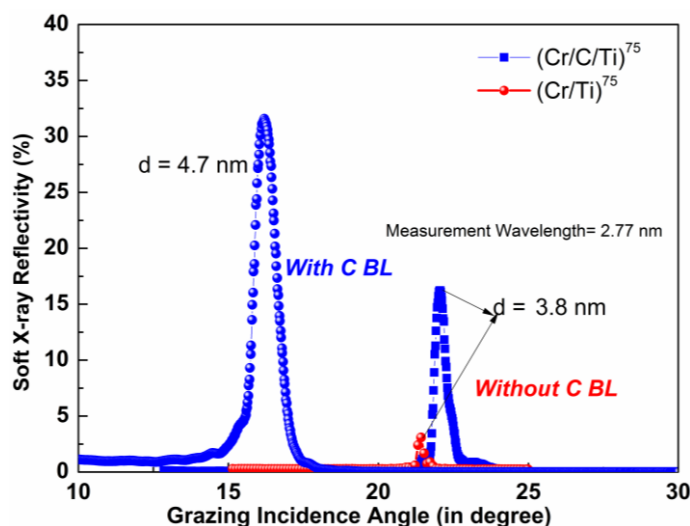


Increase in field emission current of Graphene nanowall sample due to twin advantage of compound structured cathode following Corrected Schottky conjecture and anode proximity effect.

developed in the present work. The work in the thesis points towards developing a new technique for manipulation of field emission current from a nano structured cathode.

6.1.3 Preparation and characterization of thin film multilayer devices for application in water window regime of soft X-Ray

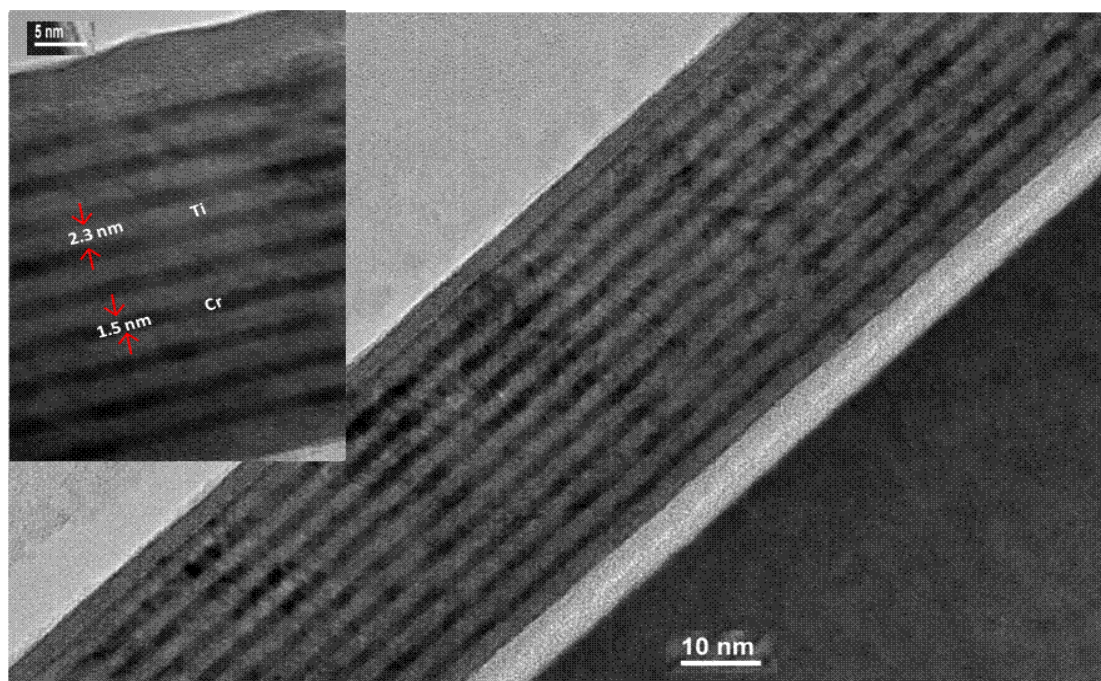
Soft X-ray microscopy in the water window regime of 2.3-4.4 nm (wavelength above O K-edge but below C K-edge) has the potential of producing high resolution as well as high contrast images of biological samples, as water does not absorb in this wavelength regime, however, organic materials, which are dominantly carbon-based, show strong absorption. The most important components of water window soft x-ray microscopes are the Schwarzschild objectives coated with thin film multilayer (ML) soft X-ray mirrors, which are basically artificial Bragg reflectors fabricated by sequentially deposited alternate absorber and spacer layers, having high contrast in their Fresnel reflection coefficients. Three important material combinations, viz., Co/Ti, Cr/Ti and Cr/Sc, which theoretically possess quiet high reflectivity in water window regime, are chosen for investigations in the present work. These ML's have been prepared by magnetron and ion beam sputtering techniques and have been characterized mostly by specular X-ray reflectivity, diffused X-ray scattering and cross-sectional TEM. Since it is well known that interface imperfections i.e., roughness and diffusion at the interfaces and their propagation across a ML is very critical for its performance as a device, the focus of the present work has been to characterize the buried interfaces of the ML's thoroughly using various techniques and to reduce the interface imperfections by application of barrier layers.



Soft X-ray Reflectivity of 75 bi-layer Cr/Ti and Cr/C/Ti ML measured at 2.77 nm soft X-ray wavelength with synchrotron radiation

In case of Co/Ti ML's of moderately low bi-layer thickness (d) of 4.2 nm, it has been found that the interfaces are primarily dominated by interface roughness and a cumulative accumulation of interface roughness takes place with increase in number of bi-layers and $\sim 2.5\%$ peak reflectivity has been obtained at a 3.07 nm wavelength for a 21.5° grazing angle of incidence. With ultra-short $d = 1.8$ nm, however, interface diffusion is found to play the key role in determining the performance of the ML's

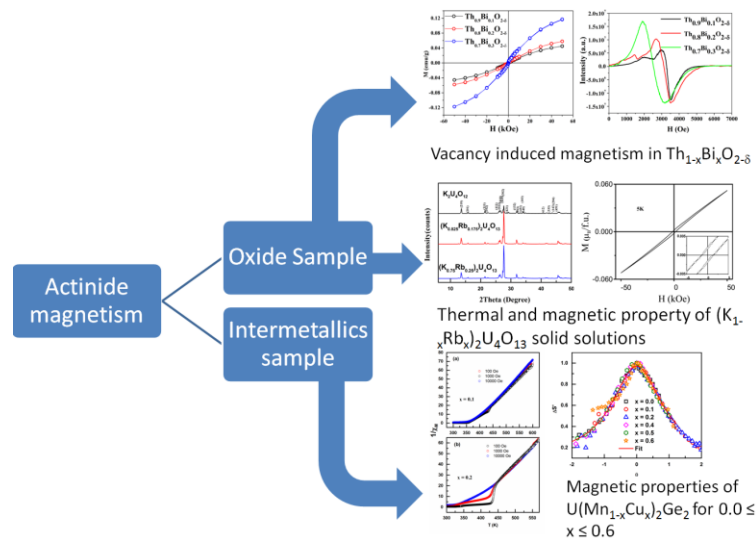
and Co diffuses into Ti layers significantly. For Cr/Ti ML's when d is varied from 2.1nm to 3.8 nm, Cr films undergo discontinuous to continuous transition, interface imperfection of Ti-on-Cr interfaces is dominated by interface diffusion at low Cr thickness (discontinuous) regime and by interface roughness at high Cr thickness (continuous) regime, while in case of Cr-on-Ti interface, interface roughness dominates throughout the whole thickness regime. Using interface engineered Cr/C/Ti ML, remarkably high soft X-ray reflectivity of $\sim 31\%$ is achieved, which is the highest reflectivity reported so far in the literature in this wavelength regime [Figs 1,2]. Unlike Co/Ti & Cr/Ti ML's, accumulation of interface imperfections has not been observed in case of Cr/Sc ML's. Rather, interface width is found to decrease as number of bi-layers increases and no saturation or decline in Bragg peak reflectivity is found until 100 nos. of bi-layers. When C or B_4C barrier layer is introduced at the interfaces, it is found that enhancement in reflectivity is more with B_4C barrier layer compared to that with C. It is seen that C forms an intermixed layer with Sc and leads to carbide formation at the interface, which then acts as shielding and prevents further interdiffusion, while, B_4C hardly penetrates Sc and stops the overlapping between Sc and Cr directly by wetting the corresponding interface.



Cross-sectional TEM micrograph of 10-bilayer (Cr/Ti) multilayer

6.1.4 Structural and magnetic properties of actinide oxides and alloys

When magnetic atoms/ions are embedded into solid, the moments start to communicate via various direct and indirect interactions and produce different long range ordered states. Depending on the interaction the orderings are categorized as ferromagnetic, antiferromagnetic, ferrimagnetic, spinglass etc. Magnetism for any elements is dictated by the unpaired electron in the outer orbital. For actinides 5f electrons are responsible for the observed magnetic property. Two types of magnetism like itinerant and localized can be observed in actinide compounds depending on the inter actinide distance. The studied magnetic properties in actinide compound in the thesis is divided into two types compounds e.g. oxide and intermetallics. The highlights of the work discussed in the thesis are as follows:



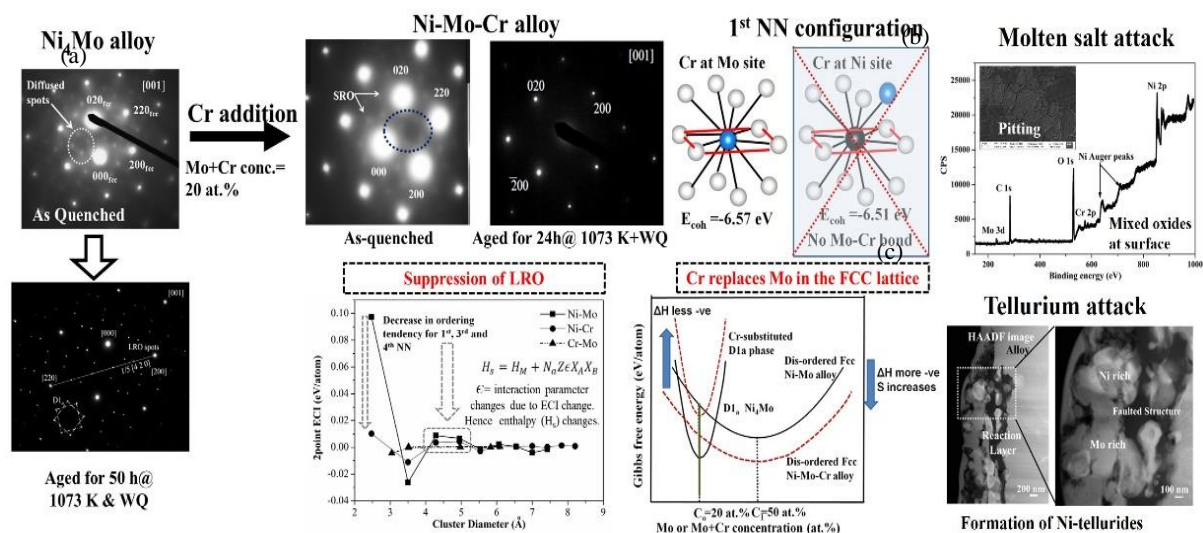
1. Vacancy induced magnetism can be observed due to aliovalent doping of Bi into ThO_2 matrix up to a doping level of 30 at% of Bi. The compounds were characterized by XRD and EXAFS. Magnetic study suggested a ferromagnetic ordering at 70K. EPR study suggested that the magnetism was originating due to the oxygen vacancy present in the doped compounds.
2. $\text{K}_2\text{U}_4\text{O}_{12}$ and $\text{Rb}_2\text{U}_4\text{O}_{12}$ are the two non-isostructural compounds that forms solid solutions in the limited range. Uranium in these compounds is present as U(V) and U(VI). As U(V) is magnetic in nature hence magnetism in mixed-valent orthorhombic compound $(\text{K}_{1-x}\text{Rb}_x)_2\text{U}_4\text{O}_{12}$ with $x = 0$ and 0.15 was studied. Both the samples exhibit two transitions, one around 25K and the other close to 10K. While the transition near 25 K is similar in both the samples.
3. Magnetic study on Cu doped UMn_2Ge_2 intermetallics indicated antiferromagnetic to ferromagnetic phase transition at around 200 K with the transition temperature T_c decreasing with increasing Cu doping.
4. Another striking feature is the appearance of Griffith's phase above magnetic ordering temperature due to short range magnetic spin correlations arising on account of Cu incorporation in the parent UMn_2Ge_2 lattice above ferromagnetic ordering temperature T_c .
5. A study on magnetic entropy change (ΔS_M) was carried out on this series of intermetallics around the second order phase transition. A reasonably good magnetic entropy changes with peak value ($\Delta S_M^P = 2.87 \text{ JK}^{-1}\text{K}^{-1}$ for 0-90 kOe field change) could be observed in the UMn_2Ge_2 around T_c .

6.1.5 Phase transformations and structure property correlations in Ni-Cr-Mo alloys

India has adopted a sustainable development goal of Thorium utilization in Molten Salt Reactor (MSR) as a part of the third stage of Indian nuclear power program. The challenging task in this technology development is related to the selection of suitable structural materials exhibiting high temperature microstructural stability and resistance to molten salt attack combined with radiation damage and fission product attack. Ni-Cr-Mo based alloys (Hastelloy N) have recently regained interest due to their rising importance in molten salt reactors. From fundamental point of view, the presence of several competing stable and metastable superlattice structures in the Ni-Mo based alloys make this system very attractive in understanding the evolutionary stages of chemical ordering that are governed by the nearest neighbour (NN) configuration and their interaction energies. The addition of Cr in Ni-Mo alloys changes the relative stabilities of the competing superlattice structures – a factor that

determines the constituent phases in commercial Hastelloy N and still remains a topic for investigation.

The pair and multisite interaction parameters (related to pair interaction energies) for Ni-Mo system evaluated using Cluster Expansion based approach indicates a clear preference for unlike atoms at first coordination shell and stabilization of the ordering tendency. Addition of Cr destabilizes not only the long-range ordered $D1_a$ phase but also the short-range order represented by $\langle 1 \ 1/2 \ 0 \rangle$ ordering wave vectors by preferentially bonding with Ni as the first NN in the face centered cubic (fcc) lattice replacing Mo. The SRO and the site preference of the Mo and Cr atoms were accurately determined for the first time using the EXAFS study. The addition of a ternary element reduces the thermodynamic driving force for ordering (both SRO and LRO) by suitably altering the enthalpies of formation and the entropy. In the enthalpy part, the addition of a ternary element leads to a change in the pair and multisite interaction energies resulting in a more negative value of the formation energy (higher stability) for the disordered phase. Complimentary diffraction, EXAFS and simulation studies unequivocally establish the stability of the disordered fcc structure which is crucial for the long-term use of the selected Ni-Mo-Cr alloy at elevated temperatures.



(a) Suppression of SRO to LRO transition in Ni-Mo alloy after addition of Cr. Microstructural evolution in Ni-Cr-Mo alloy after (b) molten salt (in presence of oxygen) and (c) tellurium attack, respectively.

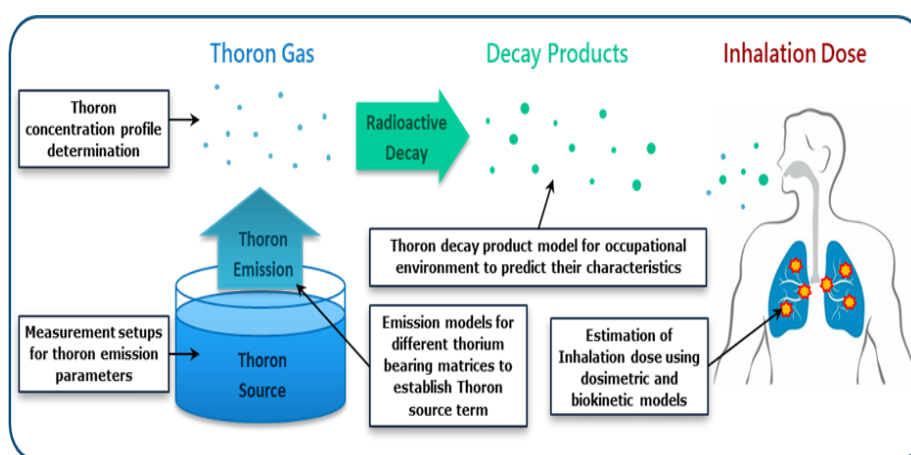
Furthermore, the in-service degradation mechanisms in Ni-Mo-Cr alloys when subjected to simulated service conditions of fluoride melt (FLiNaK salt containing) and fission product tellurium (10 mg/cm^2) at elevated temperatures were also established. Oxygen enhanced the corrosive attack by forming oxides with partial coverage, thereby forming galvanic cells with the surrounding exposed alloy. The formation mechanism of Ni-Te type precipitates was established and could be explained based on low solubility of Ni in tellurium as well as high magnitudes of NN interaction energies.

This study has provided insights to understanding the phase transformation mechanisms as well as the microstructural stabilities of the alloy in reactor environment indicating that the alloy possesses favourable properties for use at operating conditions.

6.1.6 Estimation of inhalation risk due to thoron and decay products in thorium fuel handling facilities

In context of the imminent plan of India to take up thorium-based nuclear reactors for generation of electrical power and the large number of facilities that will be required to cater to thorium fuel cycle, the study of thoron risk in these facilities achieves considerable significance. Exposure to thoron and its decay products will be an issue of concern for radiological protection of personnel due to the high thoron emission potential of the materials to be handled. In order to address it, a conceptual framework was developed which divided the issue into three components:

- 1) Source term estimation,
- 2) Thoron and decay product behaviour in occupational environment
- 3) Dose calculation.



Tools and methods to estimate the thoron source term, the properties of thoron and its decay products and to estimate the radiological dose and risk for the environments of thorium handling facilities

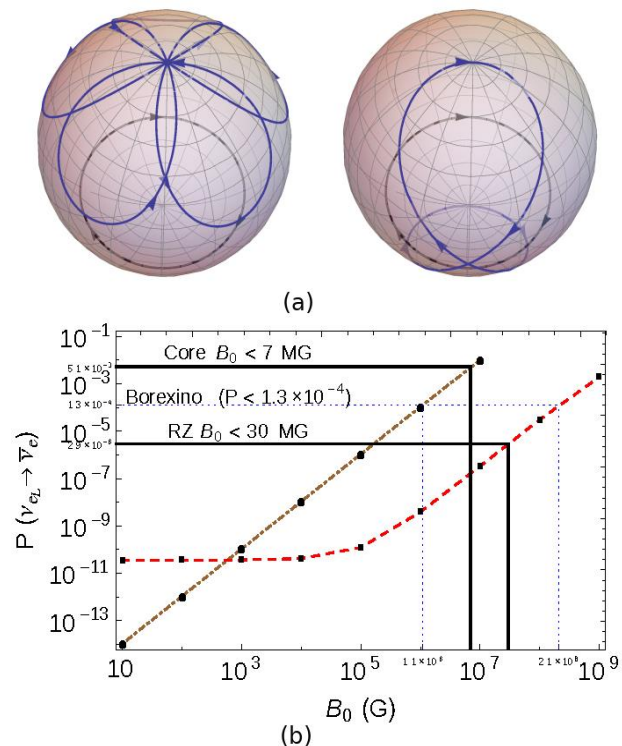
The thoron emission model for porous source matrix was developed and validated for thorium powders and monazite rich sand. Experimental study for thoron emission from thorium bearing liquid during bubbling was carried out and compared with theoretical model. The thoron concentration profile around a source was modelled and validated for two different environments. A model was developed to predict properties of thoron decay products in occupational environment and their parametric dependencies by sensitivity analysis. It was validated through multi-parametric measurements in a thorium processing facility and through measurements in houses. The radiation dose to Indian radiation occupational worker was studied using a program written for implementation of latest ICRP bio-kinetic and dosimetric model.

The work presented in the thesis provides necessary tools for estimation of risk in facilities catering to thorium-based reactors. These will be very useful to make predictions for thoron right from its source term to its concentration in workplaces and finally the radiation dose and risk. This information will be of immense help in planning for the radiation protection measures and systems at the stage of designing of the facilities.

6.1.7 Electromagnetic properties of neutrinos and phenomenology of neutrino oscillations

Neutrinos are fundamental particles in the Standard Model. The experimental observation of oscillation among different neutrino flavors implies that the neutrinos have non-zero mass. This also suggests the existence of an extended Standard Model, in which neutrinos acquire electromagnetic properties through quantum loop effects. The electromagnetic interactions of neutrinos can generate new effects such as spin-flavor oscillations in presence of background electromagnetic fields which might play an important role in determining Dirac or Majorana nature of neutrinos.

In the present work, the phenomenology of neutrino flavor and spin-flavor oscillations in solar and astrophysical environments has been studied. In solar interiors the magnetic fields may be sufficiently large to cause appreciable neutrino transitions. Thus, the neutrinos detected at Earth may act as a messenger of information about the solar magnetic fields. The combination of matter, magnetic field and vacuum mixing will result in transitions $\nu_{eL} \rightarrow \nu_{\mu R} \rightarrow \bar{\nu}_e$ of the ^8B solar neutrinos produced in the solar interiors. These transition probabilities were numerically evaluated and the results were compared with the Borexino experiment. It was found that whereas Borexino bounds were too weak to place any upper limit on the magnetic field in the radiative zone of the Sun, for the solar core magnetic field it was possible to place an upper bound $B_0 < 1.1 \times 10^6$ gauss, which is an improvement by a factor of almost one-seventh of the current largest helioseismological bound.



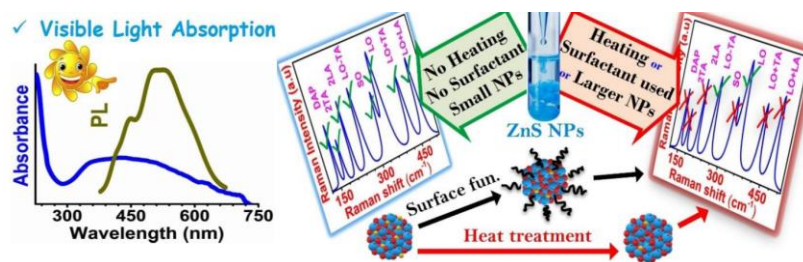
(a) Bloch Sphere representation of neutrino spin rotation, (b) Transition probability $\nu_{eL} \rightarrow \bar{\nu}_e$ of solar neutrinos detected at Earth.

The geometric picture of neutrino flavor and spin-flavor oscillations gives us important new insights about the nature of this phenomenon. In this picture the evolution of neutrino states can be visualized by studying the trajectory of neutrino spin-polarization vector in projective Hilbert space of the system. An analytical expression of adiabatic, non-adiabatic and noncyclic geometric phases which arise during such an evolution for both pure and mixed neutrino states has been derived. For two flavor neutrino oscillations, the geometric phase was shown to be independent of the Majorana phase. In addition, it was shown that the mixed state geometric phase can be used as a measure of coherence of the neutrino beam. The results obtained of the mixed state geometric phase generalize several of the previously obtained expressions of the pure state geometric phase for both two and three flavor neutrino oscillations.

6.2 Indira Gandhi Centre for Atomic Research, Chennai

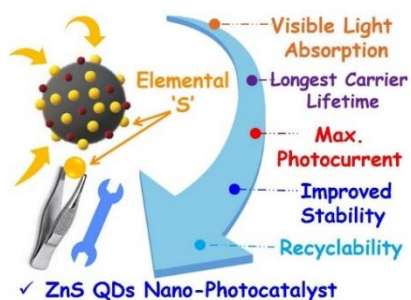
6.2.1 ZnS nanoparticles for photocatalysis, optical detector and environmental remediation

Surfactant-free wet chemical synthesis of different cubic ZnS NPs with tunable optical and electronic properties is achieved by the control of precursor concentrations and synthesis parameters. Purity of the cubic phase, spherical shape, narrow size distribution, presence of Zn and S elements, tuning a wide range of bandgap values, quantum confinement effect, and presence of unique and useful defect states are discussed and evaluated by XRD, TEM, EELS, UV-vis absorption, PL, and Raman spectroscopy. Unfurling of the obscured phonon modes like surface optical (SO), disorder activated phonon (DAP), and anharmonic modes are realized for the first time. Studies with surface functionalization, heat treatment of ZnS NPs along with temperature dependent Raman and PL measurements provide significant insights into the critical influences of synthesis conditions and evidence further for the nanoscale surface modulations as a necessary condition for the evolution of the observed surface phonon modes in the cubic ZnS NPs. The experimentally observed SO mode is also verified theoretically for different ZnS NPs along with the effect of the dielectric medium.



Optical and electronic Properties of ZnS Nanoparticles

Unique use of the unusual visible absorption of ZnS NPs for the detection of a wide range of (nM to μ M) Ag^+ concentrations in an aqueous medium by the UV-vis spectroscopy is demonstrated for the first time. The contactless optical method is cost-effective, portable, and environmentally friendly. The specificity of Ag^+ detection is compared against commonly present ions (Na^+ , K^+ , Ca^{2+} , Mg^{2+} , Mn^{2+} , and Ba^{2+}) and other heavy metal ions such as Pb, Hg, Cd. For investigation of photocatalytic efficacy of ZnS NPs, a custom-made and calibrated photo-reactor is built successfully to carry out photocatalytic performances for different pollutants. The complete degradations of methylene blue (MB), methyl orange (MO), trinitrophenol (TNP), paracetamol (PCM), and tetracycline (TC) are achieved in a record minimum time under irradiations of UV to visible lights by using ZnS nano-photocatalysts. The smallest particle ZnS NPs with the highest surface defects, especially enriched with the elemental type sulfur defects (ES) show the best photocatalytic performances.



Photocatalytic properties of ZnS nanoparticles

6.2.2 Hyperthermia in magnetic fluids: effects of *in situ* orientational ordering, magnetic susceptibility, physio-chemical properties of dispersant medium and clustering on heating efficiency

The major objectives of the thesis were: i) to probe the effect of initial susceptibility on radio frequency alternating magnetic field (RFAMF) induced heating efficiency in a system of superparamagnetic magnetic nanoparticles (MNPs) with nearly similar saturation magnetization, where the contributions from relaxation dynamics are decoupled, ii) enhancing hyperthermia efficiency by an external static magnetic field induced *in situ* orientational ordering of superparamagnetic MNPs in aqueous dispersions, iii) probing the variations in RFAMF induced heating efficiency of superparamagnetic MNPs as a function of medium viscosity using complex AC magnetic susceptibility approach, iv) probing the role of pH dependent conformational changes in surface stabilizing agents on interfacial heat transfer during RFAMF induced heating of magnetic nanoemulsions and v) investigating the role of primary crystallite size and cluster size on RFAMF.

Initial magnetic susceptibility along with relaxation dynamics plays a crucial role in RFAMF induced heating of superparamagnetic MNPs. For lower RFAMF amplitude, the variation of specific absorption rate (SAR) is dominated by the initial susceptibility irrespective of the saturation magnetization values. The concentration-dependent reduction in SAR is the result of the decrease in initial susceptibility with superparamagnetic MNP concentration.

A decrease in SAR in biological media due to increased medium viscosity is detrimental for practical applications of magnetic fluid hyperthermia (MFH). A novel experimental protocol is proposed, which is based on DC magnetic field induced *in situ* orientational ordering of superparamagnetic MNPs to enhance the SAR. In the presence of a DC magnetic field, the superparamagnetic MNPs in liquid form linear chain-like structures, which leads to enhancement in effective magnetic anisotropy, thus resulting in higher SAR. ~ 62% increase in SAR is observed when a DC field of ~100 Oe is applied *in situ*.

A non-monotonic variation of SAR with viscosity is observed for superparamagnetic MNPs dispersed in a liquid and agar-based hydrogels. The underlying phenomenon was analyzed using the AC susceptibility approach and simulations further suggested a possibility of ~ 3 fold enhancement in SAR within the biological safe field-frequency limit. This shows the possibility of optimizing SAR in a viscous medium. Approximately 50 % enhancement in SAR was observed with reducing medium pH for oil-in-water magnetic nanoemulsions, stabilized with polyacrylic acid (PAA) due to the globule-to-coil conformational transition of PAA. The pH-dependent variation of local concentration of PAA resulted in a change in interfacial thermal resistance at the oil water interface, which is responsible for the SAR variation. The obtained findings are beneficial for designing optimal superparamagnetic MNPs for efficient MFH applications.

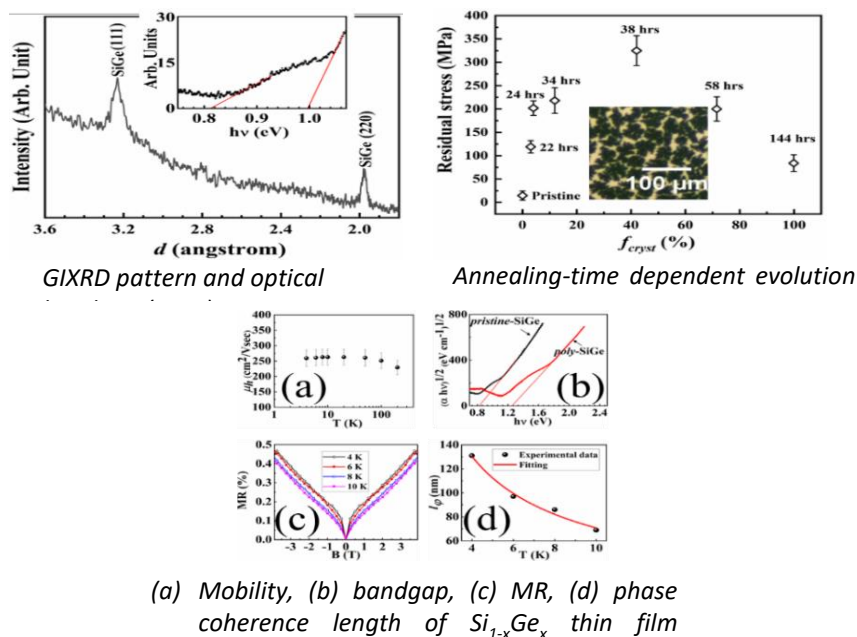
6.2.3 Low temperature synthesis of large grain polycrystalline $\text{Si}_{1-x}\text{Ge}_x$ thin films and their properties

The superior fundamental properties of $\text{Si}_{1-x}\text{Ge}_x$ thin film compared to Si, its crystalline quality and the processing temperature are the key factors for its application in semiconductor and flexible electronics.

industry. In the thesis, methods of achieving $\text{Si}_{1-x}\text{Ge}_x$ thin films with high crystalline quality at low temperature and with improved electrical and optical properties are addressed.

Using optimized layer thickness, deposition temperature, polycrystalline- $\text{Si}_{1-x}\text{Ge}_x$ thin film is achieved at 400 °C through solid phase crystallization (SPC). Obtained film results in dual optical bandgap when subjected to post-deposition annealing and can be a potential absorber of NIR spectrum in solar cells. Al Induced crystallization (AIC) of SiGe/Al system leads to polycrystalline- $\text{Si}_{1-x}\text{Ge}_x$ thin film formation on corning glass substrates at 350 °C after 144 hrs of annealing. The grown polycrystalline film has a large grain size of $\sim 50 \mu\text{m}$. The evolution of stress in the film, that finally leads to layer exchange and formation of polycrystalline- $\text{Si}_{1-x}\text{Ge}_x$ on the substrate is shown in the schematic.

The high crystalline quality polycrystalline- $\text{Si}_{1-x}\text{Ge}_x$ thin film achieved through AIC has high hole mobility ranging from 260 - 225 cm^2/Vsec . The film is degenerate and has a blue-shifted bandgap in NIR region (Fig. 3(b)). It can be a potential candidate in rear layer of p/n/p⁺ solar cells. The AIC grown film shows weak-antilocalization behaviour in magnetoresistance (MR) response, under weak magnetic field and low temperature (4-10K). The high phase coherence length ($l_\phi \sim 131 \text{ nm}$), spin relaxation time 0.2 ps makes a possibility of using such films in spintronics application with further optimizations.

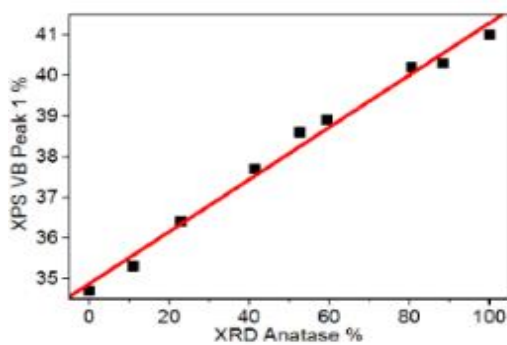


6.2.4 Surface phase composition analysis using x-ray photoelectron spectroscopy valence band analysis: Role of oxide film thickness and phase composition on corrosion resistance and antibacterial property of titania

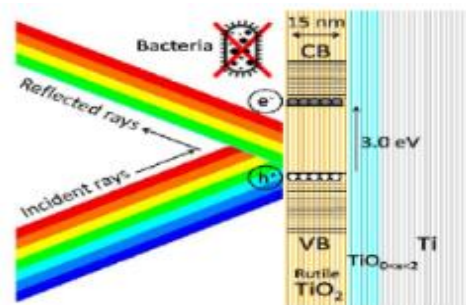
A new method for determining the phase composition of a binary phase powder by analyzing the XPS valence band has been developed and validated in two different nanomaterials of Fe_2O_3 and TiO_2 polymorphs. The phase fractions determined were found to be in good agreement with the XRD analysis. The XPS valence band data were deconvoluted and their relative peak area is analyzed to obtain the phase information. A linear correlation of the XPS valence band peak area with the phase concentration is observed as shown in the schematic below. This methodology has been extended to

successfully determine the surface phase compositions of TiO₂ films grown on CP-Ti by thermal air oxidation and their role on the corrosion resistance and antibacterial property of CP-Ti is also explored for the first time. The TiO₂ films at oxidizing temperature up to 200 °C were amorphous, with thickness ~ 7 nm, which was transformed directly to rutile phase at ≥ 300 °C (thickness > 10nm), without the formation of an intermediate anatase phase. The oxide film grown at 400 °C for 1 h was relatively smooth and defect-free with optimum thickness (~ 15 nm) where the blue light (3.0 eV at 410 nm), which matches with the band gap of the rutile phase, is preferentially absorbed generating increased e⁻-h pairs. Thus, the 15 nm thick rutile phase TiO₂ film showed the highest corrosion resistance while the phenomenon of thin film interference enhanced the photo catalytic activity and thus antibacterial property of the TiO₂ film as shown in the schematic. The contribution of sub-stoichiometric oxides at the TiO₂-Ti interface is well accounted in the electrochemical impedance spectroscopy analysis for the first time and was in excellent agreement with the experimentally observed structure of the oxide films formed.

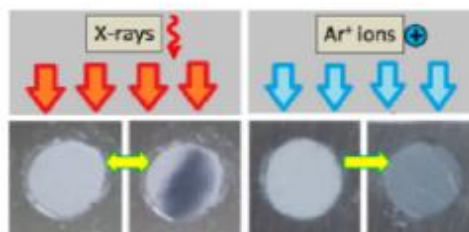
V_Os and Ti³⁺/Ti²⁺ defect states in TiO₂ are found to be responsible for the darkening of TiO₂ on x-ray irradiation and sputtering, respectively (schematic below). X-ray induced blackening of TiO₂ in UHV is caused by the lower V_O formation energy and the insulating nature of amorphous TiO₂. The V_Os are highly unstable on air exposure and the ultra thin surface layer (~ 1 nm) of TiO_{2-x} due to V_O creation on x-ray irradiation was responsible for the 'reversible switching' of color in the TiO₂ powder. Generation of V_Os need not result in the creation of relatively stable Ti³⁺ states, if their defect concentration is < 5 at.% in the TiO₂. Both the Ti-O bonds in the amorphous TiO₂ and the C-O bonds in an organic material are sensitive to the soft x-ray irradiation.



Schematic showing the relationship between the XPS valence band peak area and XRD determined wt.% of the anatase phase of TiO₂ nanopowders.



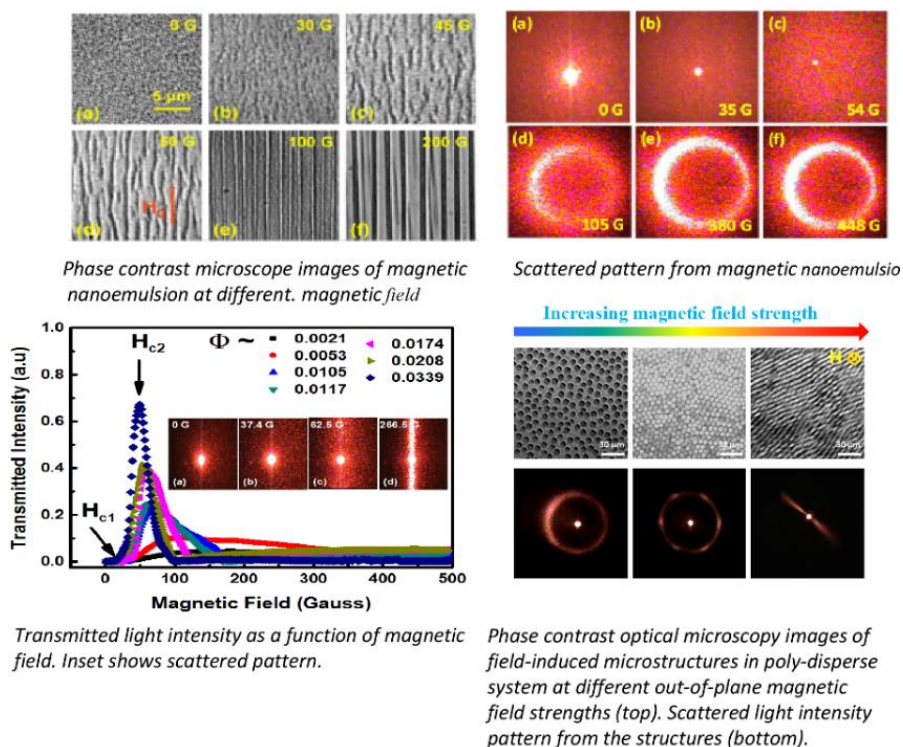
Schematic of thin film interference phenomenon for the ~ 15 nm thick rutile TiO₂ film grown over CP-Ti at 400 °C for 1 h.



Photographs of the amorphous TiO₂ powders before and after x-ray exposure and Ar⁺ ion sputtering in UHV.

6.2.5 Studies on parameters influencing field induced microstructures in magnetic fluids and its influence on optical properties

Magnetic fluids are a class of smart materials which alter their physical properties such as optical, rheological, and thermal properties in the presence of an external magnetic field. The magnetic field induced aggregation and de-aggregation process in magnetic fluids can alter the propagating light pathways that can give rise to interesting optical phenomena. Though field induced aggregation is rich with theoretical and simulation data, systematic experimental studies on equilibrium and non-equilibrium structures in real magnetic fluids are scarce. The main objectives of the thesis were to understand the parameters influencing the field driven structures in magnetic fluids (both material and magnetic field), its temporal evolution and dynamics. The role of surface charge on the critical magnetic field for various structural transitions in magnetic nanoemulsion of different volume fractions is studied for the first time. Three distinct critical magnetic fields are identified from the changes in the field dependent transmitted light intensity, corresponding to the commencement of small aggregate formation, complete formation of linear aggregates and the formation of densely packed columnar solid like structures through zippering of individual chains which are shown in schematic. The field induced anisotropic structure formation in the emulsion is also demonstrated from the ring like pattern.

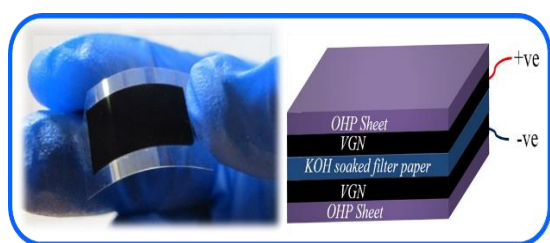


The dependence of transmitted light intensity in ferrofluid emulsion on critical field and volume fraction is established. The field induced optical transparency and its origin in magnetic nanoemulsion is demonstrated for the first time. Correlation between the field induced transparency, magnetic fields and Φ is established. New insights into the size polydispersity on field-induced equilibrium and non-equilibrium structures in ferrofluids are obtained. The structural transitions from isotropic columnar, through hexagonal close packed, to striped patterns on increasing the magnetic field in the sample with high polydispersity are shown in the schematic. The results from the study will be useful for the

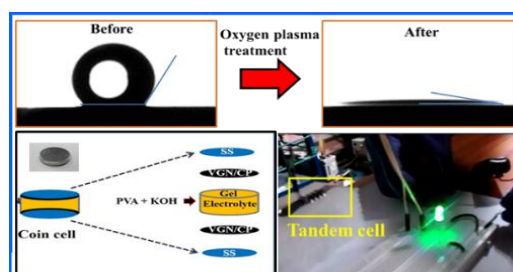
design of light-controllable magnetic-fluid-based devices such as light modulators, light switches, ferrofluid-based robots and lab-on-chip devices.

6.2.6 Surface modification and polymer-free transfer of vertical graphene nanosheets for electrochemical capacitor applications

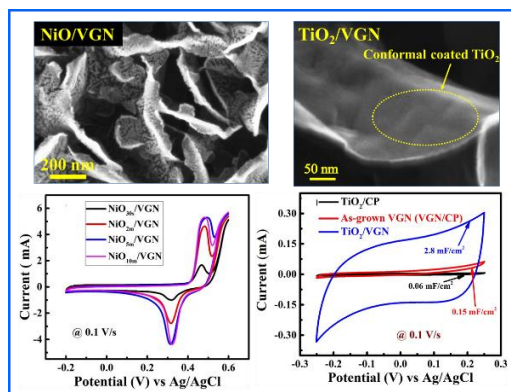
The thesis primarily focused on improvement of the charge storage capacity of vertical graphene nanosheets (VGN). Herein, the capacitance enhancement is achieved by surface modification (plasma activation and metal/metal oxide decoration) of the VGN, while retaining its unique geometry. An effort is made to understand the role of surface functionalization and charge-transfer on capacitance performance. Also, a simple and easily scalable polymer-free transfer process is established to fabricate VGN based flexible supercapacitor device. Furthermore, the combination of hybrid electrolyte (Tetra ethylammonium tetrafluoroborate + sulfuric acid) with chemical activation is attempted to enhance the charge storage performance of VGN electrodes.



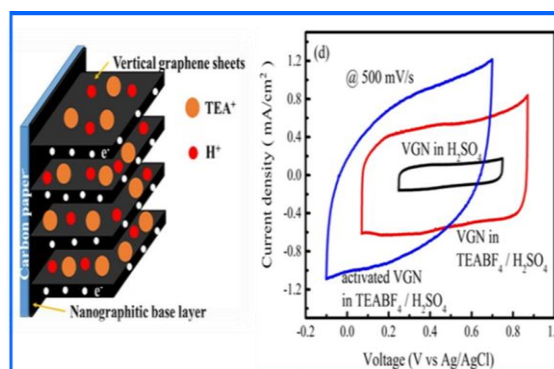
Transferred VGN and schematic of the SC device



Super-hydrophilic VGN after plasma treatment and schematic of the device with practical application



Metal oxide/VGN hybrid electrodes and their electrochemical capacitor performance.



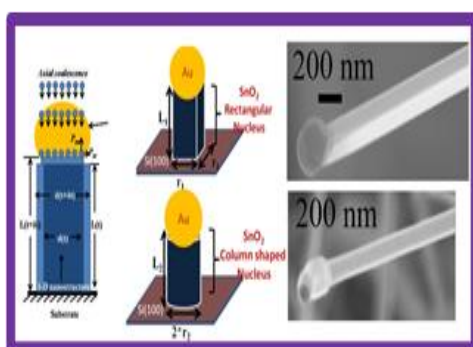
SC performance of VGN in hybrid electrolyte.

6.2.7 Growth and applications of low dimensional SnO₂

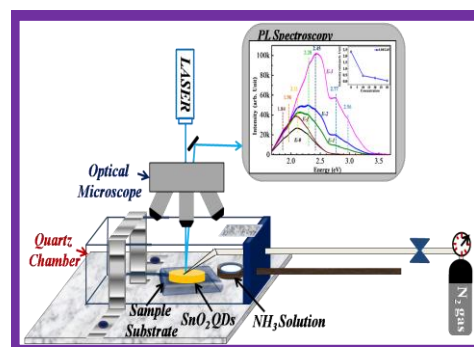
The present thesis focuses synthesis of SnO₂ nanostructures (NSs) and understanding the defects in lower dimensions of SnO₂ nanostructures, such as nanoparticles (0-D) and nanowires and μ B (1-D). Its beneficial properties are clubbed together with graphene oxide (GO) in the form of GO-SnO₂ nanocomposites. Apart from detailed characterization and elucidation of prevalent defects in NSs, utilizations of these NSs for various applications like PL based selective ammonia sensing, electrochemical capacitor for energy harvest, photocatalysis for environmental remediation, resistive sensor at low temperature, waveguide utility of 1-D NSs, and unusually high dielectric value are explored. A simple chemical route is followed to synthesis SnO₂ quantum dots (QDs), which are further

used to obtain different sizes of nanoparticles (NPs) and defects distributions by annealing process in air atmospheres at various temperatures. 1-D SnO_2 nanostructures (NSs) are grown by vapor liquid solid (VLS) and vapor solid (VS) processes using a chemical vapor deposition (CVD) technique. The correlation of the growth temperature of the VLS technique and the evolved shape of 1-D NSs is established through Gibb's free energy minimization.

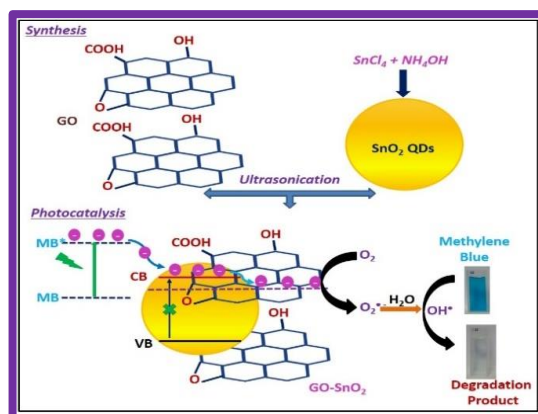
Strongest plasmonic field with the optimized Ag nanonets is made to elucidate for first time the observation of any Raman allowed mode in the SnO_2 QDs. The related high-pressure study supports it well. The revelation of a Raman forbidden but IR active mode in the 25 nm SnO_2 NPs is demonstrated. Selective detection for trace NH_3 at room temperature is achieved exclusively by deciphering the hugely enhanced obscured blue emission PL from the SnO_2 QDs. By exploitation the functional group of GO with superior conductivity of SnO_2 QDs improved electrochemical hybrid capacitors are demonstrated for energy harvest. Fastest MB degradation (3 min) by SnO_2 QDs as nanophotocatalyst is achieved under the UV light exposure using a laboratory made photocatalysis set up. Significant progress in environmental manner for the dye degradation is achieved with a visible light in a record 30 min by the GO- SnO_2 composite. The critical role of band alignment, delay in recombination of $e-h$ and presence of functional groups in GO are further discussed for the relevant mechanism. Two SnO_2 NPs of similar size with different oxygen vacancy (O_v) distributions are made. The underlying physics and typical role of O_v on the enhanced dielectric values are detailed. Critical role of O_v defects in the resistive detection of trace amount (<200) ppm green house CH_4 is explained for low temperature (50 °C) sensor.



Presentation of VLC growth with SEM Images of NWS



PL based NH_3 detection at RT

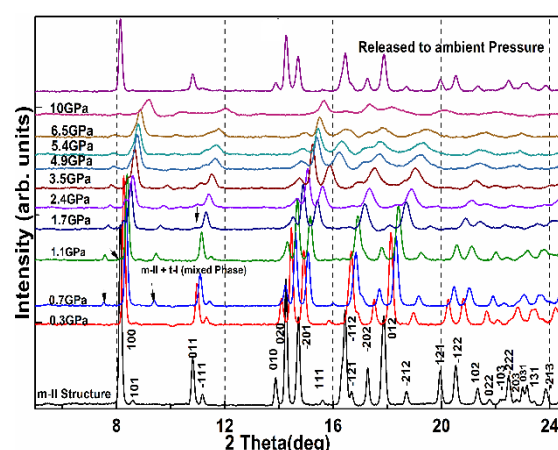


Visible light driven MB degradation by the ex-situ GO- SnO_2 composite.

6.2.8 Synthesis and pressure induced phase transformation studies of some organic ferroelectrics

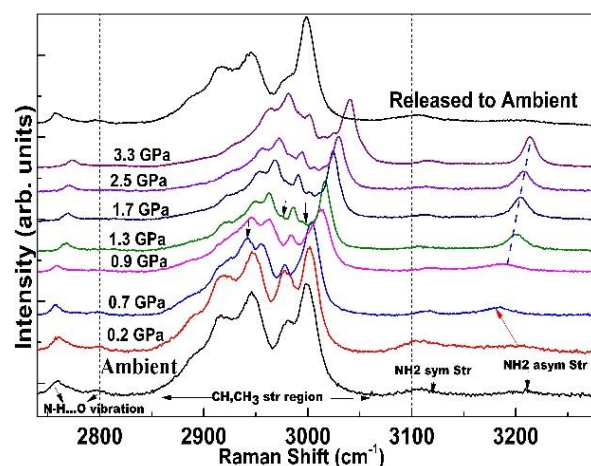
Molecular organic materials are of current interest due to their multi-functionality, ease of processing, and low cost. They exhibit pressure and temperature-induced polymorphism and conformation changes, which affect their physical and chemical properties. There are efforts to synthesize small molecular ferroelectrics, but few have Curie temperature (T_c) above room temperature. A major aim of the present work was to understand high-pressure polymorphic phase transitions and to explain the role of intermolecular interactions in phase stability.

Density functional theory calculations were performed to assign the phonon modes in Diisopropylammonium bromide (DIPAB), Diisopropylammonium perchlorate (DIPAP) and in Benzyl ammonium lead tetrachloride (BALC). In DIPAB, new peaks appeared in the lattice mode region and CH_3 stretching region giving indication of conformational change. XRD investigations reveal that the m-II phase (space group $P2_1$) is partially transformed into a centrosymmetric, nonpolar triclinic (P-1) structure at 0.7 GPa. Ferroelectricity is expected to weaken under compression above 0.7 GPa and ferroelectricity may disappear at a higher pressure when the m-II phase is fully converted into triclinic P-1 phase. On releasing the pressure, the ambient structure is fully recovered.



Pressure-dependent X-ray diffraction plot of DIPAB m-II phase. Arrows in the plot indicate new peaks at that pressure

High-pressure Raman spectra of DIPAP show discontinuity in the NH_2 bending and stretching mode frequencies and the appearance of new bands at 0.7 GPa suggest a phase transition by a rearrangement in the hydrogen network. Broadening of lattice modes at 1.3-1.7 GPa indicates a loss of crystalline nature above 1.7 GPa. High-pressure synchrotron X-ray diffraction of DIPAP shows an isostructural phase transition at 0.6 GPa and confirms amorphization at 1.5 GPa that may lead to a loss of ferroelectricity above this pressure.



Pressure dependent Raman spectra of DIPAP in the region $2750\text{-}3300\text{ cm}^{-1}$.

A structural phase transformation of BALC from the ambient $Cmc2_1$ structure is evident at 1.8 GPa from the Raman spectra, and this is confirmed by our high-pressure X-ray diffraction studies that point to a centrosymmetric structure $Cmcm$ at 1.7 GPa. The ambient phase is recoverable on decompression. The high-pressure transition is identified to be due to a distortion in the $PbCl_6$ octahedra and a conformation change in the molecule. There are several discontinuities, broadening, and splitting of the Raman bands, corresponding to NH_3 units above 1.8 GPa that point to rearrangements in the hydrogen bond network in the new phase. As the new phase is a centrosymmetric structure, BALC is expected to lose its ferroelectricity above ~ 1.8 GPa.

6.3 Institute of Physics, Bhubaneswar

6.3.1 Zero-energy modes and strong correlation effects in topological system

The advent of topological insulators (TIs), around a decade ago has immensely revolutionised the field of modern quantum condensed matter physics. The theoretical and experimental search for exotic zero-modes (e.g., Jackiw-Rebbi and Majorana fermions etc.) has boosted up after the discovery of them. Typically, the physics of topological phases in condensed matter systems are well described by the non-interacting electronic band theory. However, to explain many new emerging phases (e.g., Mott insulator, Superconductivity, Kondo effect, etc) one needs to consider the effect of strong electron-electron interaction. The main highlight of the thesis is to search for exotic zero modes and study of the interplay of topology and correlation in topological systems.

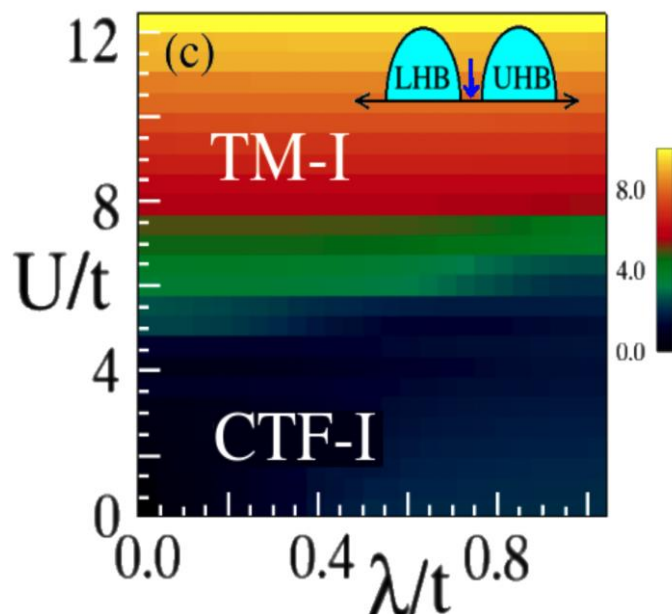


Illustration of the U - λ phase diagram.

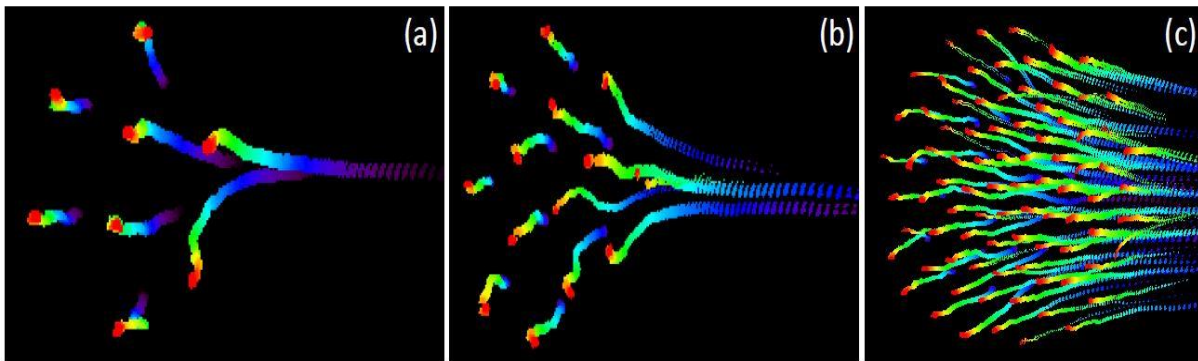
The main outputs of the thesis are the followings: (a) an advantageous route is proposed to realise Jackiw-Rebbi zero modes in a non-uniform three-dimensional TI nanowire and their possible transport signature as a zero-bias peak in differential conductance has also been discussed. (b) The impact of strong correlation (Hubbard U) in Lieb lattice consisting of a singular flat band and topological dispersive bands in the presence of spin-orbit coupling (λ) is discussed. By employing the slave rotor mean-field theory, the U - λ phase diagram is obtained. At half-filling, this consists of two correlated phases, (i) correlated topological flat band insulator (CTF-I) and (ii) topological Mott insulator (TM-I). The blue (red) region corresponds to CTF-I (TM-I) phases. It is also shown that all the correlation-driven insulating phases host helical edge modes exhibiting linearly dispersing spinon bands. (c) In recent years, controlling quantum phases of matter through the application of light has gained extensive research interest. Given this background, the work is focused on the interplay of strong correlation (U) and external drive in a triangular lattice, under the off-resonant ($\hbar\Omega \gg U$) condition, where Ω is

the frequency of the external drive. In the presence of the drive, and small U , the system exhibits a repeated metal-insulator transition as a function of the drive amplitude A for the emerging spinon bands. In the large U limit, it is established that the freezing of the charge fluctuations on the interacting sub-lattice stabilises an emergent, low energy “half-filled non-interacting Kane-Mele model” whose band gaps can be tuned by the external drive amplitude A .

6.4 Institute for Plasma Research, Gandhinagar

6.4.1 Experimental investigation of complex plasma crystals in a DC glow discharge plasma

A complex plasma system consists of highly charged dust grains embedded in a pool of electrons, ions, and neutral atoms. The strong coupling in complex plasma leads to the freezing of the system to a crystalline phase, and in the weakly coupled regime, the system acts as a fluid. Most of the laboratory investigations on plasma crystals are carried out in RF plasmas, and there are very few reported studies of complex plasma crystals in DC glow discharge plasmas.



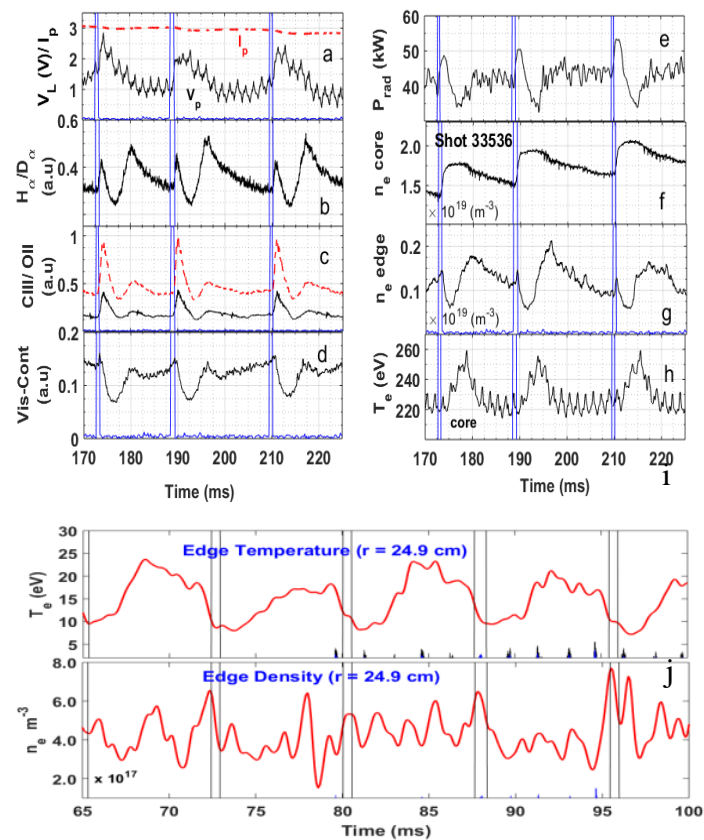
Trajectories of dust particles while they enter the dust cluster. Colors represent the progress of time with blue representing the initial time and red the final time. (a) Addition of two particles to a cluster with $N \sim 6$. (b) Addition of five particles to a cluster with $N \sim 9$. (c) Addition of ~ 40 particles to a cluster with $N \sim 30$.

In the present thesis, a stable complex plasma crystal is produced in DC glow discharge plasma for the first time using an asymmetric electrode configuration. This crystalline structure is thoroughly characterized through a host of structural analysis tools along with the estimation of dust temperature and Coulomb coupling parameter using Langevin dynamics. Response and stability of complex plasma crystal towards a perturbation is investigated in another set of an experiment. Crystal is found to be exhibiting micro-cracks in the region where a test particle exists and retaining the initial state while the perturbation is removed, which shows the viscoelastic nature of a strongly coupled two-dimensional crystal. Further, small complex plasma clusters with different numbers of particles are produced and the results emphasizes the dependency of the thermodynamics of the plasma cluster with its hexagonal configuration. Also, the self-organization of a complex plasma cluster from an excited state to the ground state is studied by estimating the dynamic entropy of individual dust particles. Finally, the nature of the phase transition of a complex plasma crystal has been studied and shown to be of the first order kind with nearly instantaneous melting to a liquid state with an infinitesimal change in the neutral gas pressure. When the size of the crystal is increased a novel mixed phase, state is observed and its transitions as a function of the neutral pressure has been studied.

6.4.2 Effect of short gas-puff pulses and biased-electrode on transport, MHD instabilities, plasma-wall interaction, and runaway electrons in ADITYA-U tokamak

Suitable tailoring of the edge plasma region of a tokamak is essential to safeguard both the core-plasma and the material boundary surfaces as it isolates the hot core plasma from the metal boundary of the machine. The edge parameters such as the radial profiles of temperature and density, the plasma rotation and the radial electric field control the macro- and micro-instabilities, which enhances the transport of particle and energy across the magnetic field lines. In the present work, the edge region of the medium-sized ADITYA-U tokamak is altered systematically by applying shot bursts of gas-puffs and by introducing a biased electrode to study the influence of edge parameters on particle and heat transport, MHD instabilities, particle exhaust and runaway electron confinement.

One of the important results of the thesis is the improved understanding of the cold-pulse phenomena (CPP), in which the local edge cooling heats the core plasma, in terms of linear-Ohmic-confinement regime (LOC) to saturated-Ohmic-confinement (SOC) transition. As shown in schematic (a-j), the CPP is triggered by fuel gas injection in the edge region and it is explained by local transport models. The observed sharp density rise in the core plasma during CPP is found to be due to the increased inward pinch and a reduction in the ion-orbit loss. The injection of fuel gas also induces transient plasma detachment, as seen by the simultaneous drop in edge density and temperature. (Schematic i-j). If the plasma remains in LOC, the global confinement is increased in the detached state, whereas, if the same detached state is obtained in plasma in SOC regime, the global confinement degrades. There exists an upper limit to the duration of detached plasma state, which is dependent on the overall plasma parameters as well as the modified edge plasma in the detached state.



(a) Loop voltage, line emission of H/D signal (b) and CIII/OII (c), visible-continuum (d), radiated power (e), chord-averaged density (f) and edge density (g) and chord-averaged temperature (h), simultaneous reduction in edge temperature (i) and density (j).

The edge parameters are also effective in controlling the macro-instability like Drift-Tearing (DT) mode and runaway electrons, which can cause severe damage to the vessel walls and peripheral components. By suitable modification of the edge plasma poloidal rotation with a biased electrode, it is shown that the DT mode rotation and its growth rate can be effectively controlled. Hence, it is proven experimentally that the plasma poloidal rotation does impact the DT mode rotation. The radial

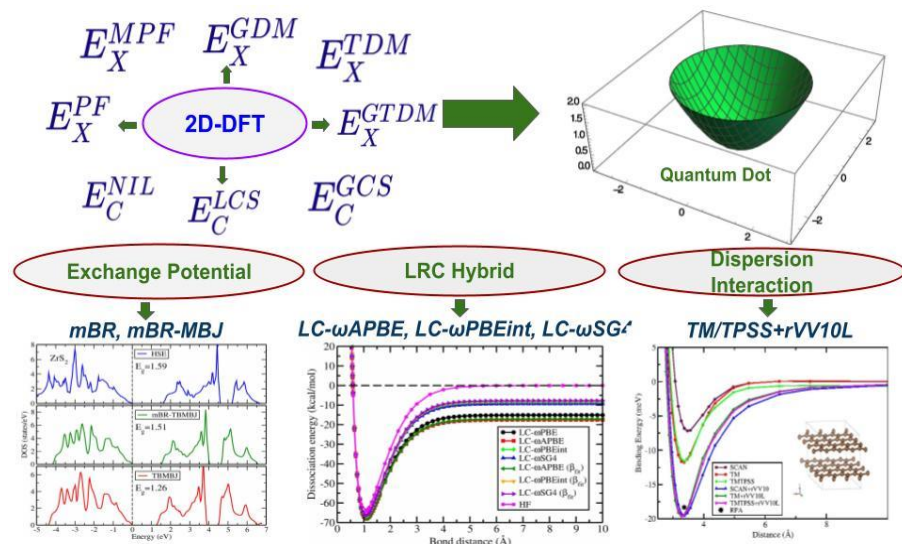
electric field modification with biased electrode is also shown to influence the runaway electron dynamics. The runaway electrons can by force be confined after the complete termination of the plasma current by biasing an electrode appropriately during the disruption phase of the discharge.

6.5 National Institute of Science Education and Research, Bhubaneswar

6.5.1 Advance density functionals based on model exchange holes for a wide range of molecular and solid-state systems

The density functional theory (DFT) is one of the best methods for describing various physical and chemical properties of solid-state systems and molecular complexes. The accuracy of DFT depends on the approximated form of the exchange-correlation (XC) energy functional. In the present work, the work on the recent advancement in the approximation of XC functionals and their convenient applications is presented. The XC energy may be thought as the Coulomb interaction energy between the electron density and the XC hole charge density. So, by modeling the XC hole, it is possible to get the energy and potential. Using the exchange hole and the coordinate transformed exchange hole, a parameter free and

very simple analytic form of the exchange energy functional is constructed. Also, a parameterized form exchange energy functional is modelled from the exchange hole and using different choices of scaled Fermi momentum. For the correlation energy functional, the Colle-Salvetti correlated wave



Different density functional methods constructed in the thesis and their applications.

function is adopted, and with help of 2D Becke88 exchange functional form, a simple gradient dependent correlation energy functional is modeled. These 2D functionals are very promising when applied to parabolic and Gaussian quantum dots and can be used to artificial graphene like quantum dot systems. Next, with help of transformed 3D exchange hole, an asymptotically correct potential known as modified Becke-Roussel (mBR) is modelled. Applying mBR potential in the framework of MBJ method, our proposed mBR-MBJ potential is seen to predict better band gaps of bulk materials. Next, three type of long-range corrected hybrid (LRC) methods are constructed from APBE, PBEint, and SG4 GGA functionals by constructing their respective exchange holes through reverse engineered exchange holes. These LRC functionals follow reference values of different properties of molecular complexes accurately after making the XC functional to follow the linear response local spin density constraint. In the final part of the thesis, the focus is on the dispersion dominated systems and use of density functionals in predicting properties a large set of van der Waals systems. The methods

proposed TM+rVV10L and TMT PSS+rVV10L are concluded to give better binding energies and bonding distances of dispersion dominated systems.

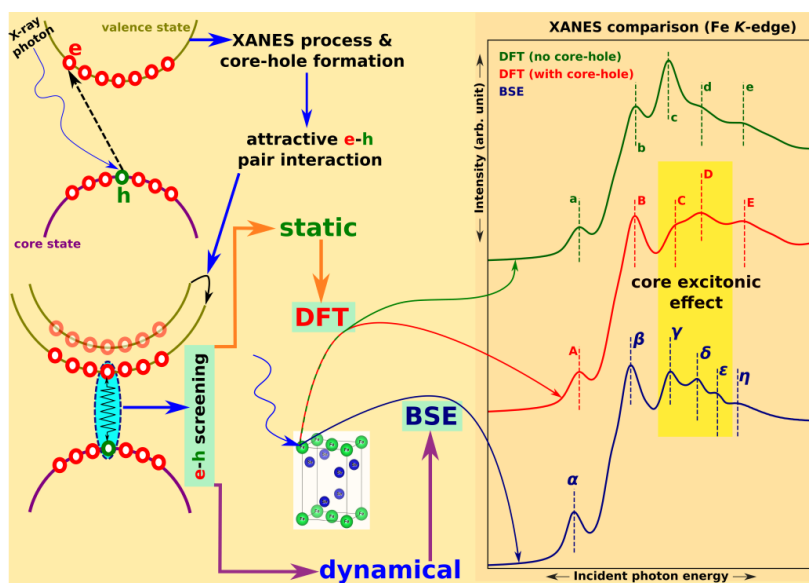
6.6 Raja Ramanna Centre for Advanced Technology, Indore

6.6.1 Theoretical studies on core electron spectroscopy of some novel iron based and chalcogenide materials

The thesis deals with the detailed theoretical studies involving core electron spectroscopy and electronic structure of several novel superconducting compounds like, i) $\text{Ca}_{1-x}\text{RE}_x\text{FeAs}_2$ of 112-family (RE = Rare-Earth elements: La, Ce, Pr, Nd, Sm, Gd), ii) KFe_2As_2 and CaFe_2As_2 of 122-family, iii) CaFeAsF of 1111-family, iv) FeSe of 11-family, v) $\text{CaKFe}_4\text{As}_4$ of 1144-family, vi) $\text{KCa}_2\text{Fe}_4\text{As}_4\text{F}_2$ of 12442-family, vii) LiFeAs and NaFeAs of 111-family, and viii) layered transition metal dichalcogenide NbSe_2 .

Associated challenges for accurate modeling of core electron spectroscopic processes has been overcome by using Density Functional Theory (DFT) and Bethe-Salpeter equation (BSE) based first principles

techniques. In many cases, the theoretical predictions agree well with experimental data or multiple scattering based existing theoretically calculated results (wherever available). Each chapter of the thesis is dedicated to one or more significant utilities of core electron spectroscopy for the aforementioned materials like-the effect of electron doping, coordination environment sensitivity, hydrostatic pressure, magnetic impurity intercalation and point defects, electron-hole pair excitonic interaction.



Schematic of the core electron spectroscopic study of iron-based superconductor FeSe revealing different levels of electron-hole excitation. (inset).

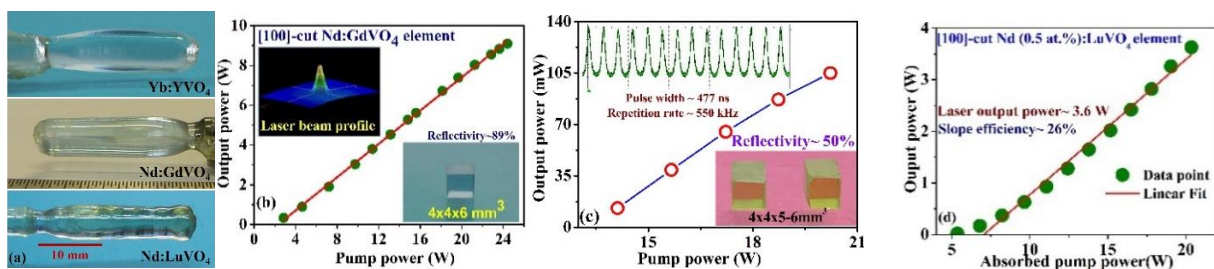
6.6.2 Growth and investigations of rare earth doped orthovanadate laser host single crystals

Rare-earth doped orthovanadate, due to their long fluorescence lifetime, low threshold, large emission cross-section and high absorption coefficient, are the material of choice for the development of compact diode pumped solid-state laser. These lasers are in high demand for various applications, including range finding, material processing, medical treatment, in basic research and defense etc.

The present work focuses on the growth of rare earth doped orthovanadate namely, YVO_4 , GdVO_4 and LuVO_4 single crystals by optical floating zone (OFZ) technique and detailed investigation of optical (absorption, emission, refractive index, and fluorescence life characteristics) and structural properties

of the grown crystals for efficient laser, optical devices, and multifunctional laser host crystals over a long range of doping concentration. Further, the thesis also reports the fabrication of laser elements and demonstration of lasing. The high quality single crystals of Yb:YVO₄, Nd:GdVO₄ and Nd:LuVO₄ were grown by OFZ technique as shown in the schematic. Multiple doping (Yb/Er; Nd/Yb; Cr/Nd) in the gain medium was also explored to augment multi-functionality and better efficiency of the gain medium. The absorption cross-section of Yb:YVO₄ crystals at 972 and 985 nm was found to be maximum for 2.94 at.% Yb doping. The photo luminescence (PL) study revealed that 972 nm diode laser would be more efficient for pumping Yb:YVO₄ laser gain medium. In Yb co-doped Er:YVO₄ crystals, the value of spectroscopic quality factor is invariant with respect to the Yb concentration. The emission at 1550 nm due to Er ion enhances significantly with the excitation of Yb ion at 952, 972 and 985 nm, indicating efficient pumping of Er through Yb ions thus confirming Yb acting as a sensitizer in Er:YVO₄ to generate eye safe laser.

Nd co-doped Yb:YVO₄ single crystals were grown for the first time by OFZ technique. PL spectra revealed that Nd ions act as sensitizer for Yb:YVO₄ for efficient pumping of the gain medium. The spectroscopic quality factor, PL intensity and fluorescence life-time of Nd:GdVO₄ suggest that the optimum concentration of Nd for best lasing is 0.8 at.%. Continuous wave (CW) lasing was demonstrated at 1064 nm (with 808 nm pumping) with [100]-oriented Nd:GdVO₄ laser elements. The laser output power of ~ 9.1 W was achieved with slope efficiency in the range of ~42 - 49.7%, which is comparable to that of commercial Nd:GdVO₄ crystal. Cr co-doped Nd:GdVO₄ crystals were also grown by OFZ technique for the first time for self Q-switching application in ambience containing different oxygen partial pressure to control Cr valency. The fabricated laser element was used to obtain self Q-switched pulsed laser operation with avg. output power ~105 mW, pulse width ~477 ns and repetition rate ~550 kHz. Further, the growth of Nd:LuVO₄ crystals and the demonstration of lasing was carried out for the First time in India. The CW laser emission at 1066 nm with output power of 3.6 W has been obtained in [100]-oriented elements by end pumping with 808 nm diode laser. The output of the research work provides valuable input towards development of indigenous import substitutes for laser host materials, a step towards self-reliance in the development of laser systems for various technological applications.

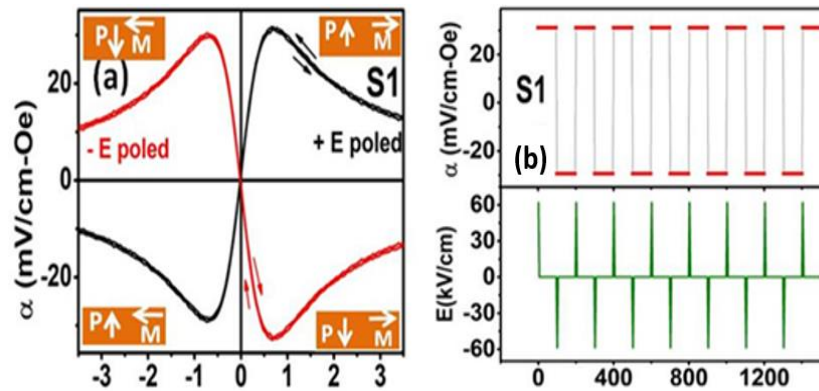


(a) As grown crystals of rare earth doped orthovanadates (b) CW laser output of Nd:GdVO₄ crystal (c) Self Q-switching in Cr co-doped Nd:GdVO₄ crystal (d) CW laser output of Nd:LuVO₄ crystal.

6.6.3 Studies on REFeO₃ (RE: Sm, Tm & Dy) and their composites in P(VDF+TrFE) for magnetoelectric memory application

The unprecedented use of functional magnetic materials is revolutionizing modern technology. The use of magnetic materials is quite vast. Some examples are; analogue and digital data storage, power

generation and transmission, electronic devices, magnetic therapy medical devices and drug delivery, sensors, and scientific equipment are the names to few. Functional magnetic materials exhibit unique magnetic properties, which can



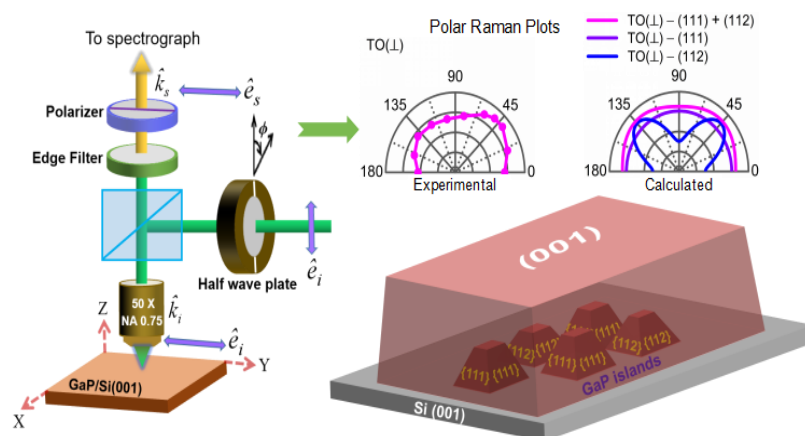
The ME coefficient (α) as a function of dc-bias magnetic field for SFO/P(VDF-TrFE) composite films. (b) Switching of ME coefficient (α) for memory application.

be altered when subjected to an applied excitement such as; magnetic field, electric field, and ultra-fast lasers. In this context, REFeO₃ (RE stands for rare earth) family of the compounds is the best candidate that shows exotic magnetic properties which are very useful in spintronic applications. SmFeO₃ (SFO), a family member of REFeO₃ has $T_N^{Fe} \sim 680$ K and highest spin-reorientation transition (SRT) temperature $T_{SR}^{Fe} \sim 450$ K– 480 K among all family members. The synthesis of SFO in both bulk & nano form and their structural, dielectric, and magnetic characterizations are described in the thesis. The mechanism behind the high dielectric constant of SFO is explained, which has been missed in the literature. The particle size effect on the magnetic properties of SFO is studied extensively. The modification in structural and magnetic properties of SFO due to the doping of RE³⁺ (Tm³⁺ & Dy³⁺) has been explored extensively. The observation of spin-phonon coupling in SRT transition of Sm_{0.5}Tm_{0.5}FeO₃ and Sm_{0.6}Dy_{0.4}FeO₃ solid-solution and their possible explanation is emphasized. An eccentric contraction in lattice parameters of SFO, Sm_{0.5}Tm_{0.5}FeO₃, and TmFeO₃ due to the spontaneous magnetostriction mechanism at low temperature owing to the Exchange striction mechanism is highlighted in the thesis. A correlation between the structural and magnetic properties is established, which would help in the ongoing studies on Orthoferrite. The T_{SR}^{Fe} of SFO at room temperature (RT) for use in the spintronic application is also achieved. The magnetostrictive property of SFO and Sm_{0.7}Tm_{0.3}FeO₃ has been utilized to make flexible magnetoelectric composite films using P(VDF-TrFE) ferroelectric polymer. The magnetoelectric coupling coefficient observed in these composites is found relatively larger than the single-phase multiferroics. The novel use of SFO/P(VDF-TrFE) composite has been demonstrated in non-volatile memory applications for the first time. The novel use of SFO/P(VDF-TrFE) composite has been demonstrated in non-volatile memory applications for the first time.

6.6.4 Raman spectroscopy study of epitaxially integrated polar GaP on non-polar Si and Ge substrates

The best of both the GaP and group IV (Si, Ge) semiconductors for technological and economical interests can be combined through their epitaxial integration, and tremendous efforts are being made for many years to realize this. However, the high-quality epitaxial integration of III-V compound semiconductors (e.g., GaP) on Si and Ge substrates unavoidably poses challenges due to polar/non-polar interface, lattice mismatch and diffusion at the hetero-interface. In this work, a novel approach towards Raman spectroscopy technique in conjunction with AFM has been employed to investigate

bulk, crystallographic morphed surfaces, and interfaces of epitaxially grown GaP/Si and GaP/Ge hetero-structures. Through uniquely employed co-localized Raman-AFM and spatially resolved polarized Raman measurements from cross-sectional surface, it is discovered that the wurtzite/zinc-blende crystal phase co-existence at GaP-Ge interface results in additional phonon modes in Raman spectra of GaP/Ge(111) epilayer. Also, the atomic inter-diffusion across the GaP-Ge hetero-interface has been elucidated via wavelength dependent Raman spectroscopy. Further, the one-of-a-kind application of spatially resolved Raman spectroscopy from cross-sectional surface of GaP/Si(111), has enabled the detection of nanometer scale (~ 100 nm) variations along the depth of hetero-structure. This novel methodology has successfully resolved the structural allotropes and strain distributed zinc-blende GaP phases along the depth of GaP/Si(111) hetero-structure. A complex azimuthal-angle dependent polarized Raman spectroscopy is applied creatively to determine orientation of energetically favorable and defect-exposed higher-index $\{111\}$ and $\{112\}$ crystal facets in GaP/Si(001), and thereby the origin of symmetry forbidden and additional phonons of GaP epilayer. To the best of our knowledge, this is first of its kind study on hetero-structures. The inferences made from this study are extrapolated to actualize the integration of new GaP/Si and GaP/Ge hetero-structures having far superior surface and crystalline quality. This study establishes a purely optical technique, *i.e.*, Raman spectroscopy as a standard and expeditious methodology to obtain important information on III-V/group-IV and other advanced hetero-structures as well as in their evaluation for device fabrication.



Azimuthal angle-resolved polarized Raman spectroscopy facilitates the understanding of interfacial nucleation during initial stages of epitaxial growth, and the structural intricacies of overgrowth layer.

6.7 Saha Institute of Nuclear Physics, Kolkata

6.7.1 Phenomenology of some particle dark matter models and their implications in gravitational wave emissions from early universe

The Standard Model (SM) of particle physics is very much successful in explaining the basic properties of all known elementary particles as well as three of the known fundamental interactions (the electromagnetic, weak, strong interactions). However, it fails to address some important physics issues such as dark matter (DM), the origin of neutrino mass, dark energy, *baryogenesis* etc. Also, in the SM the electroweak phase transition (EWPT) is not of first-order but it is a smooth crossover with the observed value of Higgs mass of 125.09 GeV, hence within the SM framework, gravitational waves

(GW) production from the strong first-order phase transition (SFOPT) is not possible. An extension of the SM is essential to describe such problems. With these motivations, some SM extended particle physics models are proposed to explore two important aspects of physics, one is the phenomenology of particle dark matter and the other one is the production of GWs from the early Universe. The proposed particle physics models are constructed by minimal extension of SM such as by a scalar or pseudoscalar or a fermion. The thesis also discusses some possible mechanisms within which DM can be indirectly detected. A fermionic DM model is proposed in the thesis by extending the SM sector with a Dirac fermion and a real pseudoscalar to explore the indirect detection of DM via the production of synchrotron radiation from the annihilation of DM at the galactic centre (GC) region under the influence of the GC magnetic field. The detection possibilities of such signals are investigated at the ongoing and future radio telescopes such as SKA, GMRT, Jodrell Bank and MeerKAT. In the thesis, two-particle dark matter models namely (i) singlet scalar extended inert doublet model (IDM) and (ii) singlet-doublet vector-like leptonic DM in the framework of the two Higgs doublet model (2HDM) are set up to explain the production of GWs from SFOPT in the early Universe. The first-order phase transition properties were explored and the consequent production of GWs was induced by considered particle physics models. The intensities and frequencies of the GWs produced from the SFOPT were also calculated and their detection possibilities were discussed at the future space-based and ground-based detectors such as eLISA, BBO, ALIA, DECIGO, U-DECIGO and aLIGO. It was found that the proposed model is compatible with dark matter searches and able to produce GW signals. In the present work, another particle physics model is proposed to address two production mechanisms of GWs, one is from the annihilation of domain walls (Dws) and the other is from the strong first-order phase transition in the early Universe. The particle physics model is built by extending the SM sector with two complex scalar singlets. The GW intensity and frequency from both the production mechanisms namely annihilation of DWs and SFOPT has been calculated. It is found that the GW intensity from DWs attain a peak around \sim nanohertz (nHz) whereas GWs from SFOPT attains a peak around \sim centihertz (cHz). It is also shown in the thesis that the calculated GW signal can be detected by pulsar timing array (PTA) experiments for the low-frequency signal, on the other hand, a high-frequency signal can be detected by GW interferometers. Thus, the detection of such GW spectrum will open up a new direction to know about the early Universe cosmology and the physics beyond the SM. Finally, the thesis deals with the cooling of neutron stars (NSs) by the axion emission. In the thesis, it is shown that if the particle axion emitted from the NS with the gammas and neutrinos, it better addresses the NS cooling data. To this end, an upper bound on axion mass and the lower bound on axion decay constant has also been derived.

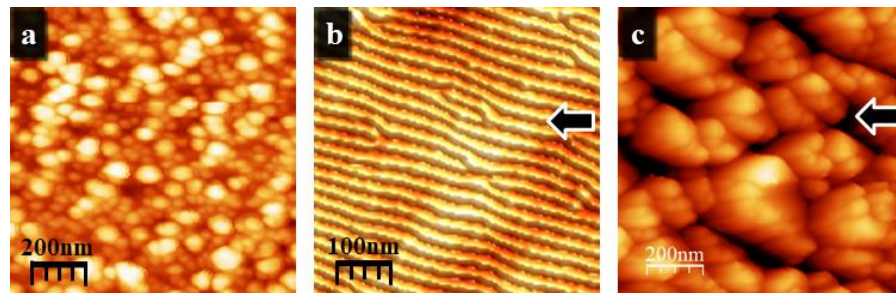
6.7.2 Ion-induced nano-patterning of solid surfaces at low energy bombardment regime

The thesis focuses on a comprehensive study on the mechanism behind the pattern formation in a multi-component system. The creation of nano-dimension patterns on solid surfaces of different amorphous and crystalline materials employing low energy ion beam sputtering (IBS) has drawn a considerable research interest from the past several years. The co-deposition of metal contaminants or impurity using co-sputtering of a surfactant or seeding material concurrently with IBS is another viable method for surface-structuring. However, understanding of the patterning mechanism in presence of foreign impurities is quite vague. In spite of the long-term prevalence of the existing theoretical models, it is impossible to predict the formation of patterned surfaces when IBS is carried out concurrently with co-deposition of foreign impurity or seeding material. In this context,

understanding and interpreting the empirical foundation of ion induced pattern formation in presence of contaminants is an emerging study. From application standpoint, the generated nano-patterned surfaces with ripples, dots, cones etc. structures have always been in huge demand owing to their numerous potentials uses in various fields including microelectronics, optoelectronics, magnetic storage devices and so on.

In this work, the multicomponent system is realized in two processes. Firstly, by in-situ deposition process i.e., by incorporation of impurity or foreign material during ion bombardment of an elemental surface. The later one is an ex-situ method where deposition of foreign material is performed on the ion bombarded pre-

patterned sample. A variety of newly observed patterns like ripples with obliquely lying wave vector, nano-mounds, nano-hillocks etc. as depicted in fig.1 are generated in this



Atomic force microscopic images of (a) nano-mound, (b) nano-ripple and (c) nano-hillocks generated on a Si surface by bombardment of Ar⁺ ion beam at 0°, 30° and 67° respectively.

work. To investigate the unique behavior of such structured surfaces, the underlying theoretical approaches behind the patterning mechanism has been carried out and a new theoretical model is established. The generalized model formed is found to be in fair agreement with the observed experimental findings and provides a deeper understanding of the role played by the impurities.

6.7.3 Astroparticle physics with particle dark matter models, neutrinos and gravitational waves from first order electroweak phase transition

The thesis pursues three major topics of astroparticle physics namely particle dark matter (DM) phenomenology, neutrino oscillations and primordial Gravitational Waves (GWs) in the early Universe. Although the properties of the fundamental building blocks of the elementary particles as well as their fundamental interactions (not including gravity) can be immensely described by the Standard Model (SM) of particle physics but it fails to address sine phenomena like explaining the neutrino mass, the particle nature of DM and other issues such as triviality, naturalness problem etc. It is unknown to us whether the DM is constituted by single particle component or multi type of particles. In addition, the sources of the ultrahigh energy (UHE) neutrinos observed by Km² IceCube detector still remains a mystery. Apart from these above-mentioned phenomena, it is believed that even though the electroweak phase transition is a smooth crossover within the SM framework, but it can be of first order phase transition if simple extensions of SM is considered by adding some scalars which could be well a candidate of DM. The highlights of thesis dealing with these issues are following. The thesis explores two component Weakly Interacting Massive Particle (WIMP) – Feebly Interacting Massive Particle (FIMP) DM model by extending the SM with a fermion and a scalar. The observed gamma-ray (γ -ray) excess from the Galactic Centre (GC), DM self interaction from 72 colliding galaxy clusters as well as the 3.55 keV X-ray line etc. can be simultaneously explained in the present model. Also, in order to explain DM self interaction a two component FIMP (both are scalars) DM model is proposed in the thesis. A detailed analysis of the γ -ray fluxes from 45 dwarf galaxies produced from possible DM

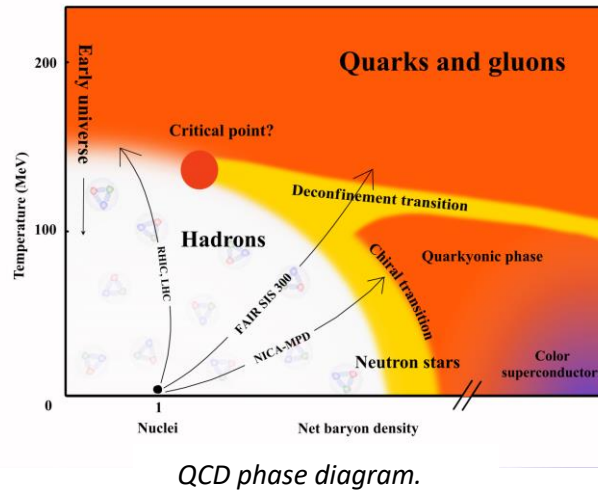
annihilation have been done in the thesis with two different particle DM models, one is WIMP-FimP model and the other one is Kaluza-Klein (KK) DM in theories of extra dimensions. The possible cascading decay of superheavy dark matter (SHDM) into UHE neutrinos (PeV energy range) in the context of UHE neutrino spectrum at IceCube is also addressed in the thesis, where some constraints on SHDM mass and its decay lifetime have been given. The possible existence of the sterile neutrino as well as the effect of the neutrinos decaying unparticles on the detection yield at IceCube in 4-flavour (3 active + 1 sterile) neutrino framework are also investigated in the thesis. In addition, a proton blazar model is proposed in the thesis which can consistently explain the observed electromagnetic spectrum in combination with the neutrino events observed by the IceCube detector from the three blazars namely TXS 0506+056, PKS 0502+049 and GB6 J1040+0617. The thesis also probes the effects of violation of equivalence principle (VEP), if it has existence in nature, for the case of long baseline (LBL) neutrinos in 4-flavour scenario. Lastly the thesis deals with the GW emissions from a strong first order electroweak phase transition by simple extensions of SM with scalars, which are produced via freeze-in mechanism. This transition may happen from a metastable minimum to the true minimum through electroweak bubble nucleation. The detectabilities of such GWs at the future space-based detectors have also been investigated in the thesis.

6.7.4 Thermodynamics of hot and dense QCD matter in non-trivial background

Our universe is believed to be in the quark-gluon plasma (QGP) phase after big bang when the temperature of the universe was very high. To mimic this condition and study the QGP matter, a lot of efforts have been put by the experimentalists and theorists of the heavy ion collision research community for last few decades. In recent years a novel research has emerged as some studies have argued about the production of substantially high magnetic field of the order of $\sim 10^{14}$ T or even stronger at non-central heavy-ion collisions. Therefore, it is interesting to ask how QGP behaves in presence of a background magnetic field. In the present work, the thermodynamics of the magnetized QGP at finite density has been studied within one-loop hard thermal loop perturbation theory.

The magnetic field strength decreases rapidly after the collision. There are several arguments regarding the time dependence of the field strength which is supposed to vary with the electrical conductivity of the medium. However, in the present work, strong field approximation (Lowest Landau Level approximation) was considered for the initial times. For later time, the weak magnetic field approximation was used. The quarks get directly affected by the magnetic field and its energy becomes quantized. The Schwinger propagator was used for fermions to compute the gluon self-energy in a magnetized medium. Some interesting findings were obtained, e.g., three non-degenerate dispersive modes of gluon, the change of the Debye screening mass. Additionally, two dispersive modes of quark in strong field approximation were found as quark dynamics becomes 1+1 dimensional in lowest Landau level. Using the quark and gluon effective propagator, the pressure of QGP within one-loop HTL perturbation theory was found. High temperature expansion has been used for this computation. Also the results of high temperature expansion and full results in weak field limit were compared where it was seen that the difference of the two results is insignificant. In strong field limit, a fascinating trend of the transverse pressure of the system with magnetic field strength was found, which decreases with the field strength indicating the shrink of the system along transverse direction at very high field strength. The QCD matter shows paramagnetic nature. Analytic expressions for the

second order quark number susceptibility (QNS) of the magnetized QGP were also found. Similar to the pressure of the system, QNS also shows anisotropic nature in strong field limit.

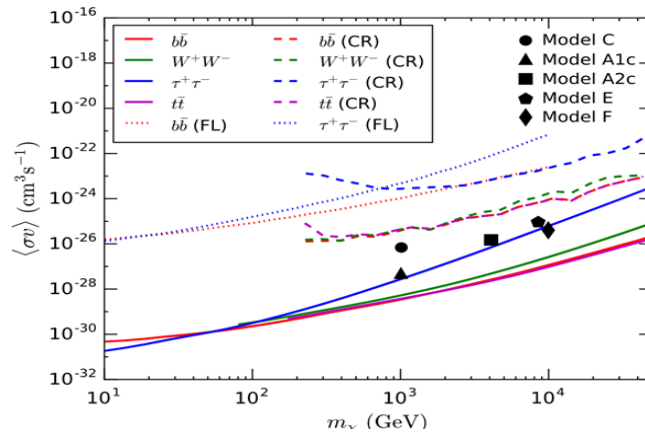


6.8 Harish-Chandra Research Institute, Prayagraj

6.8.1 Dark matter and new fundamental physics

While existing direct search and collider experiments have not yet found any signature of a dark matter (DM) candidate and thus impose constraints on its microscopic properties, I show in my thesis that the indirect search of DM based on the observation of radio signals which are induced by e^\pm generated from DM initiated processes inside galaxies or galaxy clusters may become an alternative avenue for unveiling the nature of DM. I find that the Square Kilometre Array (SKA), mostly with 100 hours of observation, should be able to detect radio synchrotron signals of minimal supersymmetric standard model (MSSM) DM annihilation, for cases where the superparticle masses are well above the reach of the LHC. This observation holds even for conservative values of astrophysical parameters, and thus underscores a new potential of the SKA. I show that the enhancement of trans-TeV DM induced radio signals is possible mainly due to: (a) abundance of energetic e^\pm in the annihilation spectra of heavier DM particles, (b) dominant annihilation to a pair of bottom quarks and (c) a sizable annihilation rate. Simultaneously, effects of various astrophysical parameters (e.g., magnetic field (B), diffusion (D0)) on radio synchrotron signals produced from the annihilation of trans-TeV DM particles have been studied in detail. In addition to these, I use the Murchison Widefield Array (MWA) radio telescope data to constrain DM annihilation in 14 dwarf spheroidal (dSph) galaxies. It is found that, for μG level B-fields in dSphs, MWA-I data provide constraints that are comparable to existing limits from gamma-ray and cosmic-ray observations; however, MWA-II can give better constraints for a large region of the DM parameter space extended from a few GeV DM mass to a DM mass which is at the TeV scale. The MWA-I data is also used on the globular cluster ω Cen as well as its γ -ray observation by Fermi-LAT to constrain the astrophysical parameter space (i.e., B-D0 plane) in ω Cen. Through this analysis, it is shown that the current MWA data can already provide significant limits on model parameters and thus improves the prospects for understanding various astrophysical parameters in galactic objects such as ω Cen. The prospects of constraining the MeV DM particles and primordial black holes (PBHs) at the upcoming SKA telescope has also been explored. By comparing the SKA limits with existing indirect detection bounds (e.g., Planck's CMB constraints) on MeV DM and

PBH DM abundance, it is found that, even for conservative choices of D_0 in dSphs, the SKA can provide better probe for MeV DM particle with masses up to few tens of MeV and for PBHs with masses that are above a factor times 10^{15} to 10^{17} g. In parallel, it is shown that these SKA limits, even independently of D_0 , can be stronger than those predicted by future MeV γ -ray experiments. Additionally, regions in the diffusion parameter space of MeV e^\pm (produced from MeV DM or PBHs) inside a dSph, that give rise to observable signals at the SKA are also marked out.

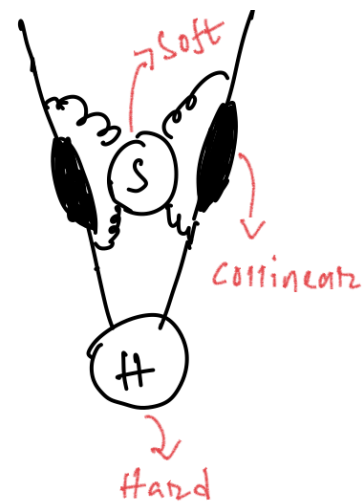


Sensitivities (solid lines) of observability of radio flux from Draco dSph in the $\langle \sigma v \rangle$ - m_χ ($m_\chi^{0.1}$ in MSSM) plane at SKA1 with 100 hours, for various DM annihilation channels. Dashed and dotted lines denote the upper limits from cosmic-ray (CR) and Fermi-LAT (FL) data, respectively. The black points represent various MSSM

6.9 The Institute of Mathematical Sciences, Chennai

6.9.1 Infrared structure of gauge theory: A comparison between N = 4 SYM and QCD

The Core part of the thesis deals with the universal Infrared structure and transcendental properties of scattering amplitudes and Infrared (IR) safe cross sections in N =4 SYM. Computations of scattering amplitudes and IR Safe Cross sections in N =4 SYM serves as theoretical laboratory to unravel the rich IR structure of not only QCD but also a wide class of non-abelian gauge theories. Factorisation of IR sensitive contributions and their universal structure in Gauge theory amplitudes and in scattering cross sections provide unique opportunity to understand the IR structure of the theory. In addition to that understanding the scattering amplitudes and cross sections wrt different transcendental Weight will help to devise new techniques to compute enormously complicated multiloop and multileg Observables. Here, by appropriately defining the IR safe observables, collinear Altareli-Parisi splitting functions up to second order in the perturbation theory have been obtained. The splitting functions and the IR finite cross-sections demonstrate several interesting connections with those in the perturbative QCD. The process independent soft distribution function up to third order in the perturbation theory



has been determined and shown that it is universal i.e., independent of the operators as well as the external states. Interestingly, the soft distribution function in $N=4$ SYM theory matches exactly with the leading transcendental part of the corresponding one in the QCD. This enables one to predict the third order soft plus virtual cross section for the production of the on-shell singlet states. In addition to that, the first calculations of two-point two-loop form factors (FFs) have been presented with two identical operator insertions in $N=4$ SYM theory. The supersymmetry protected half-BPS primary and unprotected Konishi operators have been considered. Unlike the Sudakov FFs of half-BPS primary, the FFs involving two half-BPS operators are found to contain lower transcendental weight terms in addition to the highest ones. Moreover, in contrast to Sudakov FFs, the highest weight terms of the FFs of double half-BPS no longer match with that of double Konishi. It was also found that the principle of maximal transcendentality which dictates the presence of identical highest weight terms in the scalar FFs of half-BPS and quark/gluon FFs in QCD does not hold true anymore for insertions of two identical operators. The absence of any additional ultraviolet counterterm that could arise from the contact interaction between two composite operators has been discovered.

6.9.2 QCD Corrections and Resummation Beyond Threshold in Hadronic Collisions

The discovery of the Standard-model-like-Higgs boson in 2012, at the Large Hadron Collider (LHC), has marked an epoch in the history of High energy particle physics. Ever since this crowning achievement, one of the main objectives of the present colliders has been to understand and measure the fundamental scattering reactions with unprecedented experimental precision. In order to interpret these observed phenomena with the underlying theoretical models, one needs a precise understanding of the involved processes at the quantum level. Hence my thesis works primarily concentrates on deepening our understanding of Infrared (IR) structure of the gauge theories. The works presented in the thesis mainly focuses on the perturbative calculations of hadronic cross sections in Quantum Chromodynamics (QCD). There are two main fronts following which any higher order radiative corrections are computed. Firstly, the determination of the complete behaviour of a given observable at a fixed order as an expansion in powers of the strong coupling constant. Secondly, the resummation of the whole perturbative series, which is indispensable for accurate phenomenological predictions.

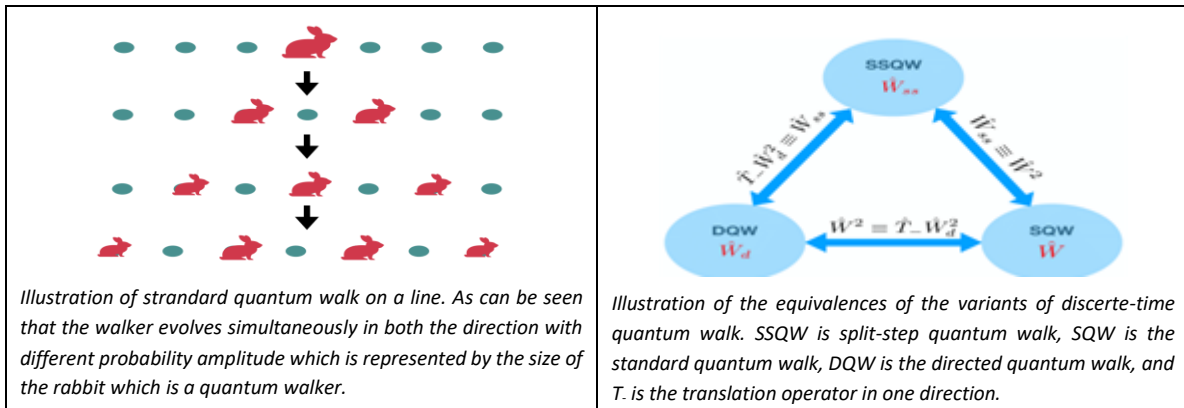


Tree level diagram for Higgs production in association with a massive vector boson.

In the context of Fixed Order Computations, the calculations of the three loop virtual corrections to Higgs productions through bottom quark annihilations and lepton pairproduction through Drell-Yan process have been presented. The two-loop virtual correction to Higgs production in association to vector boson is also presented. In the context of Resummation Computations, the resummed corrections to Higgs production through bottom quark annihilation have been presented. A new formalism for resumming next to threshold logarithms for Higgs production as well as for Drell Yan is introduced in the thesis.

6.9.3 Quantum simulation and computation using discrete-time quantum walk

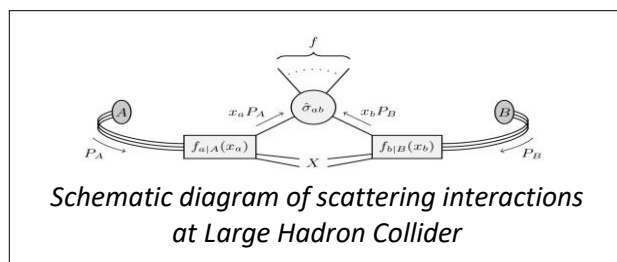
Quantum walk is a quantum analogue of classical random walk and has been extensively used for developing quantum algorithms for quantum simulations and quantum computation. In the present work, the unique features of the variants of discrete-time quantum walk namely, directed quantum walk, standard quantum walk, and split-step quantum walk has been used.



These variants of the discrete-time quantum walk have been used for developing new protocols and efficient quantum circuits for quantum simulation. A new way of realizing universal quantum computation using a single particle quantum walk has also been presented. Due to the important role of the evolution parameter in the dynamics of discrete-time quantum walk, an optimal probe for the estimation of evolution parameter has also been given. The objective of the research work carried out in the thesis is to show the versatility of discrete-time quantum walk and its application in different area of quantum information and computation.

6.9.4 Radiative corrections and resummation effects to Higgs physics in QCD

The core part of the thesis deals with computing higher order QCD and QED corrections for the production cross sections of various scattering processes at Large Hadron Collider involving Higgs boson or Drell-Yan di-lepton pairs in the final states. The computations are performed within the



Standard Model (SM) and perturbative techniques were employed for the calculations. In the first part, the fixed order approach is discussed to compute higher order corrections concerning two kinds of observables: (1) QCD corrections for the di-Higgs production to second order, and (2) mixed QCD-QED corrections to Higgs production at second order. For both these processes, the dominant gluon contributions are known to unprecedented accuracy, and hence our motive is to capture the corrections arising from the sub-dominant bottom-quark annihilation channel. Computing di-Higgs production provides valuable information on the trilinear self-coupling of Higgs boson and thereby on the shape of Higgs potential. The computation of QCD-QED corrections involves dealing with the interference effects of QCD and QED interactions. Numerical analysis on both these results at the LHC energy manifests the reduction in unphysical scales, hence confirming the reliability of our results.

Section III
List of students who have completed
Ph.D. during the period August 1, 2021-July 31, 2022

Discipline: Applied Systems Analysis

Sr No	Student Name	CI Name	Enrollment No	Thesis Title
1	Sreekanth Bathula	BARC	STRA01201404001	Modelling the Dispersion Dynamics of Radiological Dispersal Device
2	Medha Nayak	NISER	APSA11201604001	From Fear to Festivity: Multi-Stakeholder Perspectives on Human-Elephant Interactions in Balasore, Odisha

Discipline: Chemical Sciences

Sr No	Student Name	CI Name	Enrollment No	Thesis Title
1	Aditi Arun Dalvi	BARC	CHEM01201304026	Studies on the Recovery of Protactinium-231 from Natural Source
2	Amar Dutt Pant	BARC	CHEM01201404001	Rapid Radiochemical Separation Methods for Analysis of Actinides and Long Lived Fission Products in Environmental Samples
3	Amitabha Nandi	BARC	CHEM01201504012	Ultrafast Dynamics of Excitons and Charge Carriers in Thin Films and Nanoaggregates of Polyaromatic Molecules
4	Amrita Dhara Prakash	BARC	CHEM01201404020	Effect of Additives on Structural and Physico - chemical Properties of Alkali Borosilicate Glass and Alternative Glass Forming Systems Intended for Immobilization of Radioactive Waste
5	Arvind Suresh Rao Ambolikar	BARC	CHEM01201704001	Electrochemistry of Uranium (VI) and Plutonium (IV) on Carbon- and Platinum- Nanostructures
6	Ashish Pandey	BARC	CHEM01201504002	Wavelength-Dispersive X-Ray Fluorescence Spectrometric Characterization of Mixed Oxide Fuel during Fabrication
7	Kamaldeep	BARC	CHEM01201404023	Dosimetric Studies of Cancer Patients Undergoing Therapy with [Lutetium-177]-DOTATATE, EDTMP and PSMA-617

8	Kousiki Ghosh	BARC	CHEM01201604003	Radiochemical Separation Studies on Light and Heavy Ion Induced Reactions on Different Halide Targets
9	Laboni Das	BARC	CHEM01201504015	Radiation Chemical Studies of Ionic Liquids and Deep Eutectic Solvents for their Application in the Synthesis of IV-VI Semiconductor Nanomaterials
10	Mohsin Jafar	BARC	CHEM01201404019	Preparation and Structural Investigations on Zirconolite and Pyrochlore based Ceramics: Potential Materials for Nuclear Back End Application
11	Papu Samanta	BARC	CHEM01201604001	Photoinduced Electron Transfer Processes in Homogeneous and Microheterogeneous Media Involving Organic & Inorganic Donor-Acceptor Systems
12	Praveena N.	BARC	CHEM01201304022	Studies on Synthesis, Characterization, Uranium Solubility and Speciation in Alkali Borosilicate, Calcium Phosphate, Zinc and Lead Iron Phosphate Glasses for High Level Waste Vitrification
13	Ratanesh Kumar	BARC	CHEM01201504014	Studies on Electrolytic Method for Mineralization of Nitroaromatic and Nitramine Compounds
14	Sasi Bhushan Kodukula	BARC	CHEM01201404010	Molecular Ions for the Isotope Ratio Measurement of Lithium and Boron by Thermal Ionization Mass Spectrometry
15	Shah Raju Vasanji	BARC	CHEM01201504004	One-Step Preconcentration and Determination of Uranium and Plutonium Using Thermal Ionization Mass Spectrometry
16	Sitangshu Chatterjee	BARC	CHEM01201504010	Integrated Isotope-geochemical Investigation in the Selected Geothermal Areas of India
17	Subhadip Roy	BARC	CHEM01201604006	Studies of Metabolites and Ions at Aqueous Interfaces by Surface-Sensitive Spectroscopic Technique
18	Sumanta Mukherjee	BARC	CHEM01201504008	Thermodynamic Studies of Fuel Salts for Molten Salt Reactor

19	Amit Manivannan	IGCAR	CHEM02201504001	Some Studies on Suitable Materials for Immobilization of Contaminated Sodium and Removal of Radionuclides from Liquid Sodium
20	Chebrolu Venkateswara Rao	IGCAR	CHEM02201604006	Investigations on the Extraction Behavior of Actinides in Ionic Liquid Medium and the Physicochemical and Aggregation Properties of the Ionic Liquid Phase
21	Geetisubhra Jena	IGCAR	CHEM02201504007	Development of Graphene Oxide Based Composite Coating With Improved Corrosion Resistance and Antibacterial Properties
22	J. Deepitha	IGCAR	CHEM02201604003	Solubility Studies on Ligands in Supercritical Carbon Dioxide Medium and its Application to Extraction of some Heavy Metal Ions
23	Pamarthi Amesh	IGCAR	CHEM02201604005	Development of Organo-Functionalized High Capacity Adsorbents for the Recovery of Uranium from Aqueous Solution and Seawater
24	Patchapureddy Vinod Kumar	IGCAR	CHEM02201604017	Lanthanide and Uranium Doped Strontium Borophosphate Phosphors for Dosimetry and Lighting Applications
25	Sruthi P. K.	IGCAR	CHEM02201604009	Pentavalent Phosphorus Bonding Interaction of POCl ₃ with Oxygen, Halogen, Nitrogen, and π -electron Donors: Matrix Isolation Infrared and Computational Studies
26	Subramee Sarkar	IGCAR	CHEM02201604008	Evaluation of tris(2-methylbutyl) Phosphate as an Extractant for Nuclear Materials Processing Applications: A Comparison with tri-n-alkyl Phosphates
27	Venkata Trinadh Vinjavarapu	IGCAR	CHEM02201604016	Knudsen Effusion Mass Spectrometric Studies on Systems of Interest in Nuclear Technology
28	Ankita Bal	NISER	CHEM11201504010	Synthesis of Nitrogen Based N-Heterocycles via Metal Free

29	Bibhuti Bhusana Palai	NISER	CHEM11201604002	Syntheses and Biochemical Evaluation of Tropolonylated Peptide and Nucleic Acid Analogues
30	Debashruti Bandyopadhyay	NISER	CHEM11201504012	Design and Development of Benzo Fused Heterocycles via C-H/C-Br Bond Functionalization
31	Jiban Krushna Das	NISER	CHEM11201604004	Metal Chalcogenides and Phosphides Based Electrode Materials: An Efficient Catalyst for Energy Conversion and Storage Applications
32	Kiran Bharadwaj	NISER	CHEM11201604033	Studies of Photophysical Processes of Semiconductor Nanomaterials and Molecular Fluorophores in Supramolecular Assemblies
33	Milan Pramanik	NISER	CHEM11201604021	Reactivity Control of Alkenes, Alkynes and Alcohols for C-S Bond Formation Reactions
34	Nishant Sharma	NISER	CHEM11201504004	Computational Studies of Aromatic Substitution and Gas-surface Reactions
35	Pragati Biswal	NISER	CHEM11201604007	Syntheses and Functionalization of N-Heterocycles via Rhodium Catalysed C-H Activation
36	Sajal Kumar Patra	NISER	CHEM11201604008	N-substituted and N-unsubstituted Porphyrinoids: Synthesis, Structure, Spectroscopic Characterization and Applications
37	Shaikh Samser	NISER	CHEM11201604010	Pyrazole and BINOL Phosphoric Acid Based Palladium Catalysts and their Application in Organic Transformations
38	Shreenibasa Sa	NISER	CHEM11201604011	Thiophene and Pyrazole based Fluorescent Boron Compounds: Synthesis and Study of Bidentate Mercury and Tin Compounds
39	Subhayan Chakraborty	NISER	CHEM11201504015	Enhancement of Diamagnetic CEST MRI Contrast Efficiency: An Electronic and NMR Experimental Parameter Optimization Approach

Discipline: Engineering Sciences

Sr No	Student Name	CI Name	Enrollment No	Thesis Title
1	Amitava Roy	BARC	ENGG01201904016	Hydrodynamics of Drop Formation in Liquid - Liquid Systems: Experimental and Simulations
2	Aruna Devi	BARC	ENGG01201304006	Microstructural Characterization of Irradiation Induced Defects In Nuclear Structural Materials
3	Arya Das	BARC	ENGG01201604003	Structure & Dynamics of Radionuclide - Ligand-solvent Systems in the Fuel Reprocessing: Molecular Dynamics Simulations Studies
4	Kamal Sharma	BARC	ENGG01201204003	Continuous and Intuitive Control of a Robot Manipulator using Brain-Computer Interface
5	Karimulla Shaik	BARC	ENGG01201304017	Analytical and Experimental Studies of Flexible Rotor-bearing-damper System to Identify Instability Mechanism
6	Lakshay Jain	BARC	ENGG01201504035	Study of Neutron Transport in Heterogeneous Assemblies using Method of Characteristics Coupled with Delaunay Triangulation
7	Nagendra Sashikumar Gadiyakari	BARC	ENGG01201404006	Modelling of Multi-Component Compressible Flows for Wide Range of Knudsen Numbers
8	Nikam Shradha Vilas	BARC	ENGG01201604023	Experimental Study and Modelling of Trichloroethylene Vapour Adsorption in Fluidized Bed
9	Pooja Sahu	BARC	ENGG01201604002	The Dynamics and Thermodynamics of Fluid Transport through Hydrophobic Channels of Carbon Nanotubes
10	Priyanka Kamble	BARC	ENGG01201604021	Development of Nanosorbents and Nanocomposites for Radioactive Waste Cleanup

11	Punit Arora	BARC	ENGG01201604012	A Modified Cyclic Plasticity Model for C-Mn Steel and a New Critical Plane Model to Predict Crack Initiation under Multiaxial Cyclic Loading
12	Sagar Chandra	BARC	ENGG01201704002	A Multiscale Model for Simulation of Plastic Deformation Behavior of Ni-based Alloys with Explicit Consideration of the Effect of Grain Boundaries
13	Sai Raja Gopal Vadlamudi	BARC	ENGG01201604022	Study on Departure from Nucleate Boiling in Rod Bundle of PWRs
14	Sandeep K. C.	BARC	ENGG01201504021	Studies on the Recovery and Separation of Hydrogen Isotopes from Inert Gas
15	Shakti Kumar Mishra	BARC	ENGG01201504030	Studies and Analysis of Radioisotope Thermoelectric Generator
16	Shikalgar Taslim Dastagir	BARC	ENGG01201504006	New Methodology and Correlations to Assess Fracture Parameters by Pre-cracked Small Punch Tests - Theory and Experimental Verification
17	Shrinkhla Ghildiyal	BARC	ENGG01201404005	Modeling and Analysis of Fabry Perot Interferometer for Pressure Sensors with Metallic Diaphragms
18	Sumit Vishnu Prasad	BARC	ENGG01201504001	Heat Removal Capability of Calandria Vault Water from Molten Corium inside the Calandria Vessel during Severe Accident Conditions
19	Surjagade Piyush Vinayakrao	BARC	ENGG01201504011	Design of Integral Sliding Mode Control Strategies for Nuclear Reactors
20	Suryakant Gautam	BARC	ENGG01201404027	Sensor Fault Detection and Isolation using Bayesian Estimation & Kullback-Leibler Divergence
21	Vivekananda Sinha	BARC	ENGG01201404018	Hydrodynamic and Mass Transfer Studies in a Pulsed Disc and Doughnut Extraction Column
22	A. Poonguzhali	IGCAR	ENGG02201505016	Environmentally Assisted Cracking behavior of Type 316LN SS and its Weldments

23	Anuj Dubey	IGCAR	ENGG02201405005	Development of Multi-Phase Core Thermal Hydraulic Models for Fuel Melting during Severe Accidents
24	Arjun Pradeep	IGCAR	ENGG02201504006	Mass Transfer from Rising Mixed Gas Bubble in Quiescent Liquid Pool of SFR
25	Darpan Krishnakumar Shukla	IGCAR	ENGG02201604002	Study of Advanced Methods for Reliability Analysis of Digital I & C Systems
26	K. Mariappan	IGCAR	ENGG02201404008	Study on Tensile, Low Cycle Fatigue and Creep-Fatigue Interaction Behavior of Simulated Microstructures and Actual Weld Joint of P91 Steel
27	M. Balamurugan	IGCAR	ENGG02201204014	Hydrodynamic Characteristics of Annular Centrifugal Extractor and Helical Coil based Fluidic Diode Pump
28	M. Sivakumar	IGCAR	ENGG02201405007	Synthesis and Characterization of Ni-based Oxide Dispersion Strengthened Superalloys
29	Manoj Kumar Raja	IGCAR	ENGG02201104029	XRD Line Profile Analysis for Understanding the Influence of Cold Work on Ageing Behaviour in 304HCu Steel
30	Rosy Sarkar	IGCAR	ENGG02201604006	Investigation of Structural Damage in Pool-Type Fast Reactor Components during Thermal Transients
31	S. Balasubramonian S.	IGCAR	ENGG02201404003	Thermodynamic Model for the Prediction of Distribution Coefficient of Major Solutes in Tri Alkyl Phosphates for Flow Sheet Development in Spent Nuclear Fuel Reprocessing
32	Scsp Kumar Krovvidi	IGCAR	ENGG02201505001	New and Improved Methodology for High Temperature Design of Bellows
33	Shekhar Kumar	IGCAR	ENGG02201404004	Design, Development and Demonstration of a Miniature Extractor for Process Intensification in Nuclear Solvent Extraction

34	Suman Saurav	IGCAR	ENGG02201504019	Design, Analysis and Development of Irradiation Capsules and Sensors for Material Irradiation in Fast Reactor with Out-of-Pile Validation
35	Vidhyasagar Jhade	IGCAR	ENGG02201804002	Heat Transfer Analysis to Study the Cooling Capability of Core Catcher Assembly under Fuel Meltdown Scenario in a Fast Reactor
36	Pranjal Singh	IPR	ENGG06201604003	Study of In Situ Measurement of Work Function and Cesium Dynamics
37	Surendra Yadav	RRCAT	ENGG03201304001	Intelligent Approach to Study Transverse Coupled Bunch Instabilities and their Effects on Performance of Electron Synchrotron

Discipline: Life Sciences

Sr No	Student Name	CI Name	Enrollment No	Thesis Title
1	Pooja Gupta	BARC	LIFE01201504007	Understanding DNA Repair Pathways to Sensitize Werner (WRN) RECQL Helicase Deficient Cancers
2	Rajitha K.	BARC	LIFE01201604007	Bacterial Biofilms and Their Role in Barnacle Larval Settlement Inhibition
3	Reema Chaudhary	BARC	LIFE01201504013	Molecular Studies on Cell Division Regulation in Deinococcus Radiodurans R1
4	Saikat Chakraborty	BARC	LIFE01201404003	Role of RECQL5 Helicase in DNA Repair and its Implications in Cancer Therapy
5	Saitya Raju Amula	BARC	LIFE01201604009	Chromosomal Translocations in Human Lymphocytes: Influence of γ -radiation and the Role of DNA Repair Factors
6	Sarvajith M.	BARC	LIFE01201604006	Nitrogen and Phosphorus Removal Mechanisms in Aerobic Granular Sludge Sequencing Batch Reactor

7	Uday Kumar Banala	BARC	LIFE01201604010	Characterization of Uranium Tolerant Bacterial Diversity from Tummalapalle Uranium Mining Region and Their Prospective Application in Bioremediation
8	Usha Yadav	BARC	LIFE01201504009	Premature Chromosome Condensation Based Rapid Biodosimetry Strategies for High Doses and Non-Uniform Exposures
9	Vishwa Vipulkumar Gandhi	BARC	LIFE01201604001	Anticancer Studies of Organic Diselenides and Their Mechanism of Actions
10	Chandrashekar K. A.	IMSc	LIFE10201504003	Contact-mediated Signaling in Developmental Pattern Formation
11	Janani R.	IMSc	LIFE10201604004	Exposome and Health: Characterization and Network-based Exploration of Diverse Environmental Chemical Spaces
12	Dipika Mishra	NISER	LIFE11201504005	Role of a C-terminal Amphipathic Helix in the F Plasmid Segregating Protein SopA in Membrane Binding, Polymerisation, DNA Binding and Plasmid Maintenance
13	Himani Dey	NISER	LIFE11201404005	Mechanism and Regulation of Dynamin Related Protein 6 (Drp6) Nuclear Recruitment in Tetrahymena Thermophila
14	Pragyesh Dixit	NISER	LIFE11201404007	Understanding Phosphorylation-Mediated Changes in the Subcellular Localization and Functioning of Siah2 Protein in the Context of Helicobacter pylori-Mediated Gastric Cancer
15	Raktim Mukherjee	NISER	LIFE11201704004	The Impact of Starch- and Fat-Rich Diets on Intestinal Microbiota, Metabolism, and Immunity in Differentially Immune-Biased C57BL/6 and BALB/c Mice
16	Rashmita Das	NISER	LIFE11201504004	Characterization of TRPV4-mediated Channelopathies and Effect of TRPV4 in Mitochondrial Function and Regulation

17	Shubhant Pandey	NISER	LIFE11201404010	Mechanistic Insights into the Functioning of a Novel pH Directed Multi-substrate Specific Polysaccharide Lyase (PL) SMLT1473, and Analyses of Conserved 'Substrate-pH of activity' Pairing Among Diverse PL Folds
18	Anindita Das	SINP	LIFE05201604002	Structural Dynamics of the KvAP Voltage Sensor During Lipid-Dependent Gating
19	Gargi Biswas	SINP	LIFE05201604006	Experimental and Computational Approaches to Study Protein Stability, Unfolding and Design of PPlases from Leishmania spp
20	Kathakali Sarkar	SINP	LIFE05201504002	Synthetic Genetic Devices for Higher Order Information Processing in Living Cells
21	Payel Mondal	SINP	LIFE05201504003	Transcription Regulation by Transcription Factor 19 (TCF19) in Association with Tumour Suppressor Proteins during Glucose Metabolism
22	Satyaki Chatterjee	SINP	LIFE05201604001	Gating-induced Structural and Functional Dynamics of Magnesium Channels in Membranes
23	Sayak Mukhopadhyay	SINP	LIFE05201504008	Synthetic and Systems Biology Methods for Application in Gene Circuits and Microgravity Related Space Biology
24	Suparna Saha	SINP	LIFE05201504010	Understanding Neuromyelitis, Demyelination and the Role of Aquaporin 4
25	Tulika Chakraborty	SINP	LIFE05201504001	Structure of the Transcription Regulator VpsR Implicated in Biofilm Formation and its Regulation by the Second Messenger c-di-GMP in Vibrio Cholerae
26	Akash Ramchandra Deogharkar	TMC	LIFE09201404012	Role of Epigenetic Modifiers in Pathogenesis of Medulloblastoma
27	Aniketh Bishnu	TMC	LIFE09201504006	A Study on Understanding the Modulation in MAPK/ERK and PI3KCA/Akt Signaling During Acquirement of Drug Resistance

28	Arijit Mal	TMC	LIFE09201404006	Studies on Role of EpCAM Modulation during Acquirement of Radiation Resistance in Breast Cancer Cells
29	Chaudhary Nazia Mohammed Saeed	TMC	LIFE09201504013	Characterization of Pathways that Promotes Tumorigenesis, Radio and Chemo Resistance upon Plakophilin3 Loss
30	Das Lipi Ashok	TMC	LIFE09201504012	Proteomics Studies of a Set of Predictive and Prognostic Protein Biomarkers in Head and Neck Squamous Cell Carcinoma
31	Masurkar Shalaka Arun	TMC	LIFE09201304004	Deciphering functional Role of the Genetic Alterations in Medulloblastoma, a Common Malignant Brain Tumour in Children
32	Mojidra Rahul Mahendra	TMC	LIFE09201404014	Genomic Profiling of Blast Cells from Different Clinical Stages of CML
33	Mudasir Rashid	TMC	LIFE09201504014	Delineating the Molecular Mechanism(s) Involved in Regulating the Expression of H3 Genes in Human Cancer
34	Sanketkumar Girishkumar Shah	TMC	LIFE09201504021	Deciphering the Transcriptional Regulation of Differentially Expressing H2A isoform
35	Sarika Kishan Tilwani	TMC	LIFE09201504016	The Role of 14-3-3e in Regulating Development of the Epidermis
36	Shalini K. S.	TMC	LIFE09201404004	Understanding the Crosstalk of Mesenchymal Stem Cells and Gamma Delta T Cells in the Tumor Microenvironment
37	Sudeshna Roy Chowdhury	TMC	LIFE09201504010	Biogenesis Dynamics and Functions of Cargo Vesicles in Early Secretory Pathway and in Extracellular Milieu
38	Sumit Kumar Mishra	TMC	LIFE09201604016	Evaluation of Gold-Nanosphere Based Photothermal Therapy Potential in Mouse Model of Cancer

39	Usha Amrutlal Patel	TMC	LIFE09201404005	Analysis of HPV, EGFR and Hypoxia Markers and Their Association with Clinical Outcome in Subjects with Locally Advanced Squamous Cell Carcinoma of Head and Neck
----	---------------------	-----	-----------------	--

Discipline: Medical & Health Sciences

Sr No	Student Name	CI Name	Enrollment No	Thesis Title
1	Abhinendra Kumar	TMC	HLTH09201304001	Design of an Efficient Venturi-Scrubber for Retention of Radionuclides during Severe Accident of a Nuclear Reactor

Discipline: Mathematical Sciences

Sr No	Student Name	CI Name	Enrollment No	Thesis Title
1	Lalit Vaishya	HRI	MATH08201504004	Some Problems on Sign Change and Shifted Convolution Sums of Fourier Coefficients of Certain Automorphic Forms
2	Mohit Mishra	HRI	MATH08201704002	Structure of the Class Groups of Totally Real Number Fields
3	Rahul Kaushik	HRI	MATH08201604003	Commutators and Commutator Subgroups in Finite P-Groups
4	Rishabh Agnihotri	HRI	MATH08201704001	Arithmetical Properties of Fourier Coefficients of Hilbert Modular Forms
5	Souvik Pal	HRI	MATH08201704005	On Level Zero Integrable Modules over Extensions of Lie Tori
6	Abhranil Chatterjee	IMSc	MATH10201604004	Algorithmic Results using Noncommutative Algebraic Complexity
7	Arindam Biswas	IMSc	MATH10201604002	Algorithms for NP-hard Problems in the Sublinear-space Regime
8	C G Karthick Babu	IMSc	MATH10201504010	A Study on Some Arithmetic Properties of the Beatty Sequences
9	Jayakrishnan M.	IMSc	MATH10201405003	Cross and Part: Beyond the Known Boundaries
10	Mrigendra Singh Kushwaha	IMSc	MATH10201504006	A Study of Kostant - Kumar modules via Littelmann paths

11	Niranka Banerjee	IMSc	MATH10201504007	Dynamizing Graph Classes and Output Sensitive Fault Tolerant Graph Problems
12	Rupam Karmakar	IMSc	MATH10201404005	Positive Cones of Cycles and Seshadri Constants on Certain Projective Varieties
13	Sridhar Poojyam Narayanan	IMSc	MATH10201504002	Two Restriction Problems in the Representation Theory of Symmetric Groups
14	Sruthymurali Murali	IMSc	MATH10201504001	Planar Algebra, Quantum Information Theory and Subfactors
15	Ujjal Gunodhar Das	IMSc	MATH10201504004	on the Hardy Type Potentials
16	Abhrojyoti Sen	NISER	MATH11201604001	Solutions in the Class of Measures for Some Hyperbolic Systems of Conservation Laws and Scalar Conservation Laws with Discontinuous Flux
17	Anantadulal Paul	NISER	MATH11201604003	Enumeration of Singular Curves with Prescribed Tangencies
18	Dinesh Pandey	NISER	MATH11201704001	Centrality in Connected Graphs and Some Related Indices
19	Nilkantha Das	NISER	MATH11201604004	Enumerative Geometry of Curves in a Moving Family of Surfaces
20	Puspendu Pradhan	NISER	MATH11201704002	Combinatorial Characterizations of Point and Line Sets in $PG(3,q)$ with Respect to a Quadric
21	Santu Pal	NISER	MATH11201604005	Cryptanalysis of Stream Ciphers

Discipline: Physical Sciences

Sr No	Student Name	CI Name	Enrollment No	Thesis Title
1	Arundhati Bute	BARC	PHYS01201504007	Investigation of Effect of Deposition Parameters on Composition, Structure, and Properties of Plasma Deposited Boron Carbide Thin Films
2	Avik Das	BARC	PHYS01201604001	Formation of Hierarchical Nanostructured Micro-granule by Self-assembly and its Characterization by Small-Angle Scattering

3	Biswaranjan Nayak	BARC	PHYS01201304043	Beam Dynamics Studies of High Current Electron Beam in DC and RF Linac
4	Buddhadev Kanrar	BARC	PHYS01201504004	Structural and Magnetic Properties of Actinide Oxides and Alloys
5	Devendra Kumar Dwivedi	BARC	PHYS01201404013	Development of 3D Multi-Physics Simulation Tool for Coupled Neutronics - Thermal Hydraulics Studies of Safety Transients in High Temperature Reactors
6	Indrajeet Singh	BARC	PHYS01201504003	Development of Deterministic and Stochastic Methods for Physics Analysis of High-Temperature Reactors
7	Jaydeep Datta	BARC	PHYS01201504022	A Study of Alternative Gas Mixtures of RPC & Different Aspects of Neutrino Oscillation for ICAL at INO
8	Jigyasa Batra	BARC	PHYS01201304001	Characterization of Wire-Based Z-Pinches for Efficient Energy Coupling
9	Kanchan Kushwaha	BARC	PHYS01201504001	Production of Medically Important Radioisotopes in the Medical Cyclotron Facility (PETtrace-800) using Indigenously Developed Solid-Target Irradiation Assembly
10	Kanse Sandeep Dattatraya	BARC	PHYS01201304016	Estimation of Inhalation Risk due to Thoron and Decay Products in Thorium Fuel Handling Facilities
11	Lakshminarayana Yenumula	BARC	PHYS01201504005	Studies of X-Ray and Gamma Ray Imaging Techniques for Nuclear Fuel Cycle Components and Industrial Applications
12	Madhu Ghanathe	BARC	PHYS01201604024	Structural, Magnetic, Electronic, and Magnetotransport Properties of Magnetization Compensation Materials
13	Mazumdar Aparajita Soumitra	BARC	PHYS01201504024	Study of Cryogenic Properties of Tin Alloys for the Development of a Superconducting Bolometer
14	Nitin Mehrotra	BARC	PHYS01201304031	Design Optimization of Heavy Ion RFQ and External Buncher

15	Nitin Ramesh Kakade	BARC	PHYS01201604025	Study of Dose Enhancement in Nanoparticle Aided Radiotherapy
16	Piyali Sarkar Roy	BARC	PHYS01201604005	Preparation & Characterization of Thin Film Multilayer Devices for Application in Water Window Regime of Soft X-Ray
17	Pratip Mitra	BARC	PHYS01201604022	Simulation Based Optimization of Indigenously Developed Inorganic Scintillators and Various Light Sensors to Develop Gamma Spectrometer Systems
18	Rajeswari Pradhan Rout	BARC	PHYS01201504002	Development of Passive Bronchial Dosimeter for Measurement of Inhalation Dose Due To Radon/Thoron Decay Products
19	Rakhee Menon K.	BARC	PHYS01201304002	Studies on Flash X-ray (FXR) Generation from Intense Relativistic Electron Beams (IREB)
20	Rumu Halder Banerjee	BARC	PHYS01201504015	Phase Transformations and Structure Property Correlations in Ni-Cr-Mo Alloys
21	Sandeep Joshi	BARC	PHYS01201604004	Electromagnetic Properties of Neutrinos and Phenomenology of Neutrino Oscillations
22	Sanjay Chandra Andola	BARC	PHYS01201404014	Investigations on Z-pinch Devices for Pulsed Radiography and Material Characterization
23	Shreya Ghatak Sarkar	BARC	PHYS01201304012	Studies on Nano-Structured Field Emission Cathode for Beam Generation in Electron Gun
24	Suryanarayan Mondal	BARC	PHYS01201404020	Multiplicity of Muon in 2m x 2m Detector and Charge Ratio of Cosmic Muon at Madurai
25	Arpan Kar	HRI	PHYS08201504001	Dark Matter and New Fundamental Physics
26	Arpita Sen	HRI	PHYS08201404001	First Principles Studies of Electronic and Magnetic Properties of Atomic Clusters and Surfaces of Polar Oxides
27	Avirup Ghosh	HRI	PHYS08201405003	Aspects of Some New Physics Scenarios Containing Dark Matter

28	Ratul Mahanta	HRI	PHYS08201405001	Topics in Conformal Field Theory and String Theory
29	Saptarshi Roy	HRI	PHYS08201405005	Implementation of Quantum Information Protocols in Physical Systems
30	Akshaya Devi E.	IGCAR	PHYS02201504019	First Principles Study of Energetics of Atomic Defects and Stability of B1-type oxides in BCC Ferromagnetic Iron
31	Chitra N.	IGCAR	PHYS02201604001	Modeling and Experimental Validation of Emanation and Transport Mechanisms of Radon/Thoron in Soil Matrices of Southern Coastal Area, India
32	Dillip Kumar Mohapatra	IGCAR	PHYS02201504025	Studies on Parameters Influencing Field Induced Microstructures in Magnetic Fluids and Its Influence on Optical Properties
33	G. M. S. Krishna Chaitanya	IGCAR	PHYS02201204014	Development of Glancing Angle Imaging Methodology (GAIM) for Detection of Protrusion and Bowing of PFBR Fuel Sub-Assemblies
34	Jakathamani S.	IGCAR	PHYS02201504026	Unconventional Dosimeters based TL, OSL and EPR Techniques for Retrospective Dose Assessment
35	M. Raghu Ramaih	IGCAR	PHYS02201504028	Photoinduced Deflection Studies in Si Microcantilevers: Role of Incident Laser Parameters and Microcantilever Dimensions
36	Nanda Gopal Krishna D.	IGCAR	PHYS02201304013	Surface Phase Composition Analysis using X-Ray Photoelectron Spectroscopy Valence Band Analysis: Role of Oxide Film Thickness and Phase Composition on Corrosion Resistance and Antibacterial Property of Titania
37	Pragyna Parimita Swain	IGCAR	PHYS02201504021	Measurement and Analysis of Magnetocardiograms for Shielded and Unshielded Setups
38	Rabindra Nath Juine	IGCAR	PHYS02201604004	ZnS Nanoparticles for Photocatalysis, Optical Detector and Environmental Remediation
39	Radhakrishna B.	IGCAR	PHYS02201304010	Compound Wave-retarders Towards Structuring the Light Beam

40	Rajeswari J. R.	IGCAR	PHYS02201604015	Numerical Modeling Studies on the Impact of Land Surface Processes on the Boundary Layer Structure, Mesoscale Circulations, Air Pollution Dispersion and Precipitation
41	Sharadhanjali Sahoo	IGCAR	PHYS02201504011	Synthesis and Pressure Induced Phase Transformation Studies of Some Organic Ferroelectrics
42	Sinduja M.	IGCAR	PHYS02201604006	Investigations on the Role of Defects in the Thermoelectric Properties of the Nanostructured Bismuth Telluride
43	Sruthi Mohan	IGCAR	PHYS02201504001	AB Initio Simulations and Experimental Studies of Irradiation-Induced Defects in Zr and Al Containing ODS Steels and Constituent Y4Zr3O12 Precipitates
44	Surojit Ranoo	IGCAR	PHYS02201504007	Hyperthermia in Magnetic Fluids: Effects of In Situ Orientational Ordering, Magnetic Susceptibility, Physio-Chemical Properties of Dispersant Medium and Clustering on Heating Efficiency
45	Twisha Sain	IGCAR	PHYS02201504010	Low Temperature Synthesis of Large Grain Polycrystalline Si _{1-x} Gex Thin Films and their Properties
46	Ajjath A. H.	IMSc	PHYS10201604004	Radiative Corrections and Resummation Effects to Higgs Physics in QCD
47	Amlan Chakraborty	IMSc	PHYS10201305001	Infrared Structure of Gauge Theory: A Comparison Between N = 4 SYM and QCD
48	Anupam A H	IMSc	PHYS10201405002	Generalized BMS Symmetry and Double Soft Theorems
49	Dhruv Pathak	IMSc	PHYS10201305009	Probing Structural and Orbital Properties of Binary Pulsars
50	Kamal Tripathi	IMSc	PHYS10201404006	Confined Polymers in Biophysical Contexts
51	Pooja Mukherjee	IMSc	PHYS10201604002	QCD Corrections and Resummation Beyond Threshold in Hadronic Collisions
52	Pritam Sen	IMSc	PHYS10201305003	A Study of Infra-red behaviour of Gauge Theories Involving Dark Matter

53	Ria Sain	IMSc	PHYS10201305005	Model Independent Study of the Rare Decay of b-Baryon
54	Shibasis Roy	IMSc	PHYS10201305004	SU(3)-flavor Analysis of Hadronic Bottom Baryon Decays
55	Shivani Singh	IMSc	PHYS10201604009	Quantum Simulation and Computation using Discrete-Time Quantum Walk
56	Subhankar Khatua	IMSc	PHYS10201405003	Low Energy Theories of Quantum Magnets: Emergent Descriptions and Order by Singularity
57	Sujoy Mahato	IMSc	PHYS10201604003	Surface Defects from Fractional Branes
58	Varun Jitendra Kumar Gupta	IMSc	PHYS10201504001	Surface Operators, Holography and BPS Equations
59	Amir Shee	IoP	PHYS07201504008	Studies an Active Systems
60	Atanu Maity	IoP	PHYS07201504007	Classical Orders, VBS, QSL in Fisher Lattice & Spin Wave Analysis in Hollandite lattice
61	Sayan Jana	IoP	PHYS07201604005	Zero-Energy Modes and Strong Correlation Effects in Topological Systems
62	Sujay Shil	IoP	PHYS07201404017	Signatures of Seesaw Models at Colliders
63	Avnish Kumar Pandey	IPR	PHYS06201404002	Non-neutral Sheath Region around Surfaces in Low Temperature Plasma containing Negative Ions
64	Chandan Danani	IPR	PHYS06201204011	Computational Modeling of Tritium Release from Porous Ceramic Pebbles
65	Hariprasad M. G.	IPR	PHYS06201604001	Experimental Investigation of Complex Plasma Crystals in a DC Glow Discharge Plasma
66	Macwan Tanmay Martin	IPR	PHYS06201604006	Effect of Short Gas-Puff Pulses and Biased-Electrode on Transport, MHD Instabilities, Plasma-Wall Interaction and Runaway Electrons in ADITYA-U Tokamak

67	Abhilash Patra	NISER	PHYS11201504001	Advance Density Functionals Based On Model Exchange Holes For A Wide Range Of Molecular And Solid State Systems
68	Bikash Patra	NISER	PHYS11201504012	Design and Application of the Meta-GGA and Range-separated Hybrid Exchange-Correlation Functionals
69	Gour Jana	NISER	PHYS11201504014	Finite Temperature Study of Strongly Correlated Systems
70	Iyer Vijay Janardhan	NISER	PHYS11201304009	Development and Calibration of Semiconductor Detectors for Dark Matter Searches
71	Manoar Hossain	NISER	PHYS11201404006	Self-Energy Corrected Tight-Binding Framework in Directed Hybrid Orbital Basis from First Principles
72	Moumita Patra	NISER	PHYS11201404007	Aspects of $N = 3$ Chern-Simons Quiver Gauge Theories with ADE Classification
73	Parthajit Biswas	NISER	PHYS11201704029	Membrane Paradigm for Large-D Black Holes in AdS/dS Background
74	Purbasha Sharangi	NISER	PHYS11201604004	Spinterface in Metal/Organic Semiconductor Thin Films
75	Saili Dutta	NISER	PHYS11201404009	The Distribution of Neutral Hydrogen in the Local Universe
76	Samir Banik	NISER	PHYS11201504016	Search for Lightly Ionizing Particles in SuperCDMS and Simulations of Neutron Backgrounds
77	Subhajit Pal	NISER	PHYS11201504018	A Spin-Flipper in the Vicinity of a Superconductor
78	Subir Sen	NISER	PHYS11201604009	Magnetic Antiskyrmions in Heusler Shape Memory Alloys
79	Azam Ali Khan	RRCAT	PHYS03201504004	Studies on REFeO_3 (RE: Sm, Tm & Dy) and their Composites in P(VDF+TrFE) for Magnetoelectric Memory Application
80	Megha	RRCAT	PHYS03201604008	Theoretical Investigations on Reactivity of Pure and Mixed Nanoclusters towards Some Environmentally Important Gases

81	Mohammad Soharab	RRCAT	PHYS03201604006	Growth and Investigations of Rare Earth doped Orthovanadate Laser Host Single Crystals
82	Preeti Pokhriyal	RRCAT	PHYS03201504001	Study of Structural and Physical Properties of Transition Metal and Rare Earth Based Multiferroic Oxides
83	Priyabrata Mudi	RRCAT	PHYS03201604003	Contribution of Inter-Valley Scattering in Optical Spin Orientation in GaAs/AlGaAs based Spin Hall Devices
84	Rahul Aggarwal	RRCAT	PHYS03201404005	Raman Spectroscopy Study of Epitaxially Integrated Polar GaP on Non-polar Si and Ge Substrates
85	Rijul Roychowdhury	RRCAT	PHYS03201404010	Spectroscopic Investigations on MOVPE Grown Gallium Phosphide Epi-layers Integrated on Polar and Non-Polar Substrates
86	Sahadeb Ghosh	RRCAT	PHYS03201504008	Studies on the thin Films and Heterostructures of β -Ga ₂ O ₃ and Fe Substituted β -Ga ₂ O ₃
87	Sonal Saxena	RRCAT	PHYS03201204011	Studies on Broadband Terahertz Radiation from Ultra-short Two-color Laser Induced Plasma
88	Soumyadeep Ghosh	RRCAT	PHYS03201604009	Theoretical Studies on Core Electron Spectroscopy of Some Novel Iron based and Chalcogenide Materials
89	Anindita Deka	SINP	PHYS05201704016	Ion-induced Nano-patterning of Solid Surfaces at Low Energy Bombardment Regime
90	Apurba Dutta	SINP	PHYS05201504014	Magnetic, Electrical and Magnetotransport Properties of Rare-Earth and Transition Metal Based ABO ₃ Type Compounds
91	Aritra Das	SINP	PHYS05201504023	Effects of Magnetic Field in Heavy-Ion Collision Phenomenology
92	Ashok Kumar Mondal	SINP	PHYS05201604012	Study of Astrophysical Reactions using Indirect Method
93	Avik Paul	SINP	PHYS05201604001	Phenomenology of some Particle Dark Matter Models and their Implications in Gravitational Wave Emissions from early Universe

94	Bibhuti Bhusan Jena	SINP	PHYS05201504007	Magnetic Coupling across the Antiferromagnetic-Antiferromagnetic Interface
95	Bithika Karmakar	SINP	PHYS05201604019	Thermodynamics of Hot and Dense QCD Matter in Non-Trivial Background
96	Dipak Mazumdar	SINP	PHYS05201604005	Physical Properties and Related Phenomena in Some Selected Rare-Earth Transition Metal-Based Perovskite Compounds
97	Madhurima Pandey	SINP	PHYS05201504019	Astroparticle Physics with Particle Dark Matter Models, Neutrinos and Gravitational Waves from First Order Electroweak Phase Transition
98	Pintu Barman	SINP	PHYS05201604020	Nanostructuring on Solid Surfaces using Low Energy Atomic and Cluster Ions
99	Piyasi Biswas	SINP	PHYS05201604021	Study of Quasi-elastic Scattering at Near Barrier Energies for Weakly Bound Systems
100	Prasant Kumar Rout	SINP	PHYS05201504015	Search for New Resonances in the Diphoton Final State in Proton - Proton Collisions Using the CMS Detector at LHC and Studies on the CMS Forward Muon Spectrometer in the HL-LHC Scenario
101	Prithwijita Ray	SINP	PHYS05201604022	Vibrational Structures of Nuclei near Z=50 Shell Closure
102	Ram Sewak	SINP	PHYS05201604006	Studies on Some Technologically Important Intermetallic Compound of Zr/Hf/Ti and Pd/Co/Ni by Nuclear Probing
103	Sayan Ghosh	SINP	PHYS05201604009	Investigations on Some Physics Issues and Experimental Aspects of Dark Matter Search
104	Snehal Mandal	SINP	PHYS05201504013	Magnetotransport and Magnetic Properties of some Doped Manganite Thin Films and Deterostructures
105	Sridhar Tripathy	SINP	PHYS05201504006	Imaging with Cosmic-ray muons using Gaseous Detectors

106	Sunita Sahoo	SINP	PHYS05201604017	Characterisation of Low Mass Target Superheated Liquid Detector and Its Application to Dark Matter Search
107	Tanmay Maiti	SINP	PHYS05201604013	Transport Properties of Quantum Hall Edge States
108	Ajit Kumar	VECC	PHYS04201404005	Development and Performance Studies of GEM based Tracking Detectors for the Compressed Baryonic Matter (CBM) Experiment at FAIR
109	Mahfuzur Rahaman	VECC	PHYS04201504010	Transport Phenomena of Strongly Interacting Matter: Extensive and Nonextensive Scenarios
110	Sanchari Thakur	VECC	PHYS04201504011	Near Side Jet Yield from Two Particle Identified Triggered Correlation in PbPb Collisions at 5.02 TeV ALICE
111	Santanu Pathak	VECC	PHYS04201504009	Effect of Pressure on Structure and Electronic Environment of Pristine, Ta-doped HfO ₂ and its Implications
112	Shreyasi Acharya	VECC	PHYS04201504012	Multiparticle Production in Proton-proton Collisions at the LHC Energies
113	Sumit Kumar Saha	VECC	PHYS04201504008	Jets in Proton-Proton, Proton-Lead and Lead-Lead Collisions at the CERN Large Hadron Collider

Section IV

**List of students who have completed M.Tech. and
M.Sc. (Engg.) during August 1, 2021-July 31, 2022**

M.Tech.

S. No	Student Name	CI Name	Discipline	Enrollment No	Thesis Title
1	Namrata Ravindra Birnale	BARC	Instrumentation Engineering	ENGG01201901011	Advanced Signal Processing Techniques and Algorithms for an Acoustic Signal Based Loose Part Monitoring System
2	Avichal Agarwal	BARCTS (AMD), Hyderabad	Exploration Geosciences	ENGG1G201801014	Alteration Characterisation of Fracture Zone and its Implication in Uranium Mineralisation in and around Gollavaripalle-Udumula-kur area, Kadapa and Anantapur districts. Andhra Pradesh.
3	Monu Kumar	BARCTS (AMD), Hyderabad	Exploration Geosciences	ENGG1G201801016	Characterization of Uranium Mineralisation in Geratiyon Ki Dhani Area, Sikar district, Rajasthan, India.
4	Manoj Kumar Routray	BARCTS (AMD), Hyderabad	Exploration Geosciences	ENGG1G201801010	Characterization of Uranium Mineralization and Development of Genetic Model for Sabraoli Occurrence, Alwar Group, Alwar district, Rajasthan, India.
5	Sanket Kalishankar Das	BARCTS (NFC), Hyderabad	Metallurgical Engineering	ENGG1A201801010	Comparative Corrosion Studies of Titan-24 with SS 304L and Zircaloy-4 In Nitric Acid Environment for Reprocessing Plants
6	Nalla Lakshmi Venkatesh	BARC	Electronics Engineering	ENGG01201901007	Deep Learning Based Surface Defect Detection

7	Dommati Jalander	BARCTS (AMD), Hyderabad	Exploration Geosciences	ENGG1G201801017	Delineation of Structural Features, Favourable for U-mineralization Within Basement and Derivation of Basement Configuration Below the Khairagarh Group of Rocks by using Gravity, Magnetic and Time Domain Electromagnetic (TEM) Surveys in between Bijepar - Ramatola tract, Gondia district, Maharastra.
8	Ayush Srivastava	BARCTS (AMD), Hyderabad	Exploration Geosciences	ENGG1G201801004	Delineation of the Subsurface Structural Features Favourable for Uranium Mineralisation using IP/Resistivity and Magnetic Techniques along Hulkal-Halbhavi tract, Bhima basin, Yadgir district, Karnataka.
9	Nishtha Shreya	BARC	Instrumentation Engineering	ENGG01201801007	Design and Performance Analysis of FPGA based Handheld Instrument for Large Volume Data Transfer with High Throughput
10	Bandaluppi Sreekar	BARC	Instrumentation Engineering	ENGG01201901017	Design of Fault Detection Scheme for U-tube Steam Generator Level Sensors
11	Vandeep Bharatbhai Godhani	IGCAR	Mechanical Engineering	ENGG02201801003	Design Optimization on the Performance of In-Vessel Handling Machine on Account of High Burnup and the Associated Irradiation Damages

12	Sachin Rathi	BARC	Electrical Engineering	ENGG01201801029	Design, Development and Characterization of Pulse Power Supply for Solid State RF Amplifiers
13	Hanumant Ramling Choudhari	IGCAR	Chemical Engineering	ENGG02201801005	Determination of Physical and Chemical Properties of Novel Solvents and Sizing of Equipment for Solvent Extraction for Separation of Radioactive and Non-radioactive Components.
14	Shubham Kumar	BARC	Metallurgical Engineering	ENGG01201901058	Development of Alumina/Aluminide Coating on P91 Steel by Pack Cementation and Thermal Oxidation
15	Soumya Sinha	BARC	Metallurgical Engineering	ENGG01201901059	Development of Hybrid Ni-Ti Shape Memory Alloy Composite for Damping Applications
16	Vinoy Arockiadas Dsouza	BARCTS(AM D), Hyderabad	Exploration Geosciences	ENGG1G201801006	Establishment of Deformation Pattern in Kanchankayi East-Hulkal-Halbhavi Sector of Kurlagere-Gogi-Gundanahali (KG) Fault and its Implications on Uranium Mineralisation, Yadgir district, Karnataka.
17	Abhijith V.	BARCTS(AM D), Hyderabad	Exploration Geosciences	ENGG1G201801011	Establishment of Litho-structural Characteristics of Siwaliks in Kangra Sub basin to Understand the Control of Uranium Mineralisation along Paniali - Loharkar - Galot tract, Hamirpur District, Himachal Pradesh.

18	Gagandeep Singh	BARC	Civil Engineering	ENGG01201801013	Fragility Assessment of RC Structure using Incremental Dynamic Analysis Considering Variability of Ground Motion, Damping and Soil Parameters
19	Rachana Phulera	BARCTS (AMD), Hyderabad	Exploration Geosciences	ENGG1G201801008	Geochemical Characterization and Tectonic Environment of Uraniferous Bangana-palle Quartzite of Kurnool Group, Sarangapalli Area in the Northern Margin of Paland subbasin, Guntur district, Andhra Pradesh.
20	Bibhu Prasad Das	BARCTS (AMD), Hyderabad	Exploration Geosciences	ENGG1G201801003	Global Optimisation Approach for Magnetic and IP/Resistivity Data to Decipher Subsurface Structural Features and Conductive Zones Favourable for Uranium mineralisation in Rajpura Area, NE of Prithivipura, Sikar district, Rajasthan.
21	Mohammad Osama	IGCAR	Mechanical Engineering	ENGG02201801012	Hydraulic Characterisation of Non-Return Valve for Sodium Service through CFD Analysis
22	Abhilash Bhardwaj	BARC	Computer Engineering	ENGG01201901029	Instantaneous Coarse Registration between Medical Imaging Data and Estimated Head Pose of Patient for Robot Assisted Neurosurgery
23	Jeevan Singh Dangi	IGCAR	Chemical Engineering	ENGG02201801006	Investigation of Fuel Melt and Grid Plate Interaction Moments after CDA

24	Rajat Saxena	BARC	Electrical Engineering	ENGG01201801028	Investigation of Magnetic Pulse Technique for Crimping and Joining Applications for Electrical cables.
25	Mantosh Mandal	BARC	Metallurgical Engineering	ENGG01201901061	Kinetics of Micro-structural Changes in P92 Steel due to Thermal and Mechanical Processes during Manufacturing
26	Sachin Aggarwal	BARCTS(AMD), Hyderabad	Exploration Geosciences	ENGG1G201801012	Litho-structural and Geochemical Characteristics of Uraniferous Basement Rocks and Gulcheru Quartzite in and around Veldurthi Area along Western Margin of the Cuddapah Basin, Kurnool district, A.P.
27	Chinnamilli Ramanjaneyulu	BARCTS (AMD), Hyderabad	Exploration Geosciences	ENGG1G201801005	Modeling and Inversion of Magnetic and IP/Resistivity data for Delineating Favourable Target area for Uranium Mineralization in Chhota Udaipur area, Ajmer district, Rajasthan.
28	Shwetha Narayani R.	BARC	Instrumentation Engineering	ENGG01201801010	Modelling and Simulation of Electro Hydraulic Governing System
29	Tenali Sudheer Reddy	IGCAR	Mechanical Engineering	ENGG02201801002	Multi-body Dynamic Simulation of Large Diameter Bearing to Study the Effects of Bearing Support Profile on Bearing Performance
30	Adarsh Mishra	BARC	Electronics Engineering	ENGG01201901004	Performance Evaluation of FPGA-based Hardware Accelerator for HPC application

31	Ankur Kumar	BARCTS (AMD), Hyderabad	Exploration Geosciences	ENGG1G201801009	Petrogenesis and Lithostructural Analyses of Singhbhum Group of Metasediments at Southern Extremity of Singhbhum Shear Zone and their Potential for U-Cu Mineralization in Kesharpur-Kusumbari-Tilogoria-Dumurdiha Tract, Mayurbhanj District, Odisha.
32	Rohit Kumar Saini	BARCTS (AMD), Hyderabad	Exploration Geosciences	ENGG1G201801001	Petromineralogical and Geochemical Characterization of Rehatikho Formation, Chhattisgarh Super-group in Singhora Protobasin to Decipher Controls of Uranium and Fluorite Mineralization in Parts of Mahasamund District, Chhattisgarh and Bargarh district, Odisha.
33	Sanjeeb Kumar Dehingia	BARCTS (AMD), Hyderabad	Exploration Geosciences	ENGG1G201801002	Petro-mineralogical and Geochemical Characterisation of Rhyolitic Tuff and Associated Rocks around Buriwara, Barmer District, Rajasthan and their Potentiality for REE Mineralisation.
34	Divyanshu Pawar	BARC	Electronics Engineering	ENGG01201801034	Seismic Data Compression in Multiscale Framework
35	Shubham Bharati	BARC	Civil Engineering	ENGG01201801014	Seismic Performance Evaluation of RC Structure using Simplified Nonlinear Model for Shear Walls

36	Ranjan Prakash	BARC	Radiological Safety Engineering	ENGG01201801065	Selective Removal of Uranium from U Bearing Wastes using Suitable Sorbents
37	Debjani Dutta	BARC	Electrical Engineering	ENGG01201801021	Simulation, Analysis and Comparison of Pulse Width Modulation Techniques in Inverters.
38	Prathamesh Manoj Berde	BARC	Electronics Engineering	ENGG01201901003	Spear Phishing Email Detection using the Stylometric and Psychometric Features of Email
39	Pranav Raj Tyagi	BARCTS (AMD), Hyderabad	Exploration Geosciences	ENGG1G201801007	Structural and Sedimentological Studies of Badami Sediments and its Implication on Uranium Mineralization along Deshnur-Gujanal Tract, Belgaum district, Karnataka.
40	Shilpa Raj	BARC	Metallurgical Engineering	ENGG01201901060	Study and Evaluation of Roll Bonding Characteristics in Plate Fuel Elements
41	Amit Arya	BARC	Mechanical Engineering	ENGG01201901031	Study of Effect of Stress Biaxiality on Plastic Flow Behavior and Ductility of Zr _{2.5} Nb Pressure Tube Material
42	Ashish Kumar Singh	BARC	Radiological Safety Engineering	ENGG01201801071	Study of Effectiveness of Sheltering in Case of Radioactive Releases
43	Amit Rawat	BARC	Mechanical Engineering	ENGG01201901042	Study of High Temperature Mechanical and Fracture Properties of Alloy 690 for Waste Vitrification Application

44	Sushil Kumar Sharma	BARC	Mechanical Engineering	ENGG01201801053	Study of Welding and Thermal Aspects of Newly Designed Dipole Chambers and Thermal Absorbers for INDUS-2 Storage Ring
45	Ajayveer Singh	BARC	Mechanical Engineering	ENGG01201801038	Study on Friction Stir Welding of AA6061-T6 to AISI-304L for Establishment of a Correlation Between Welding Parameters and Weld Quality.
46	Shubham	BARC	Instrumentation Engineering	ENGG01201801009	Study, Modelling, Simulation and Design of Non- Intrusive Type Eddy Current Flow Meter for Liquid Metal Loop
47	Santosh Balaji Panchal	BARC	Electrical Engineering	ENGG01201801030	System Study Modeling Simulation, Implementation and Testing of Soft-switching Based Induction heater
48	Ujjwal Yadav	BARC	Electrical Engineering	ENGG01201801031	Theoretical and Experimental Comparison of the Performance of Si and SiC Switching devices in switch mode power converters
49	Sujaan Khan	BARC	Mechanical Engineering	ENGG01201801052	Thermal Analysis of PET Target for Medical Cyclotron
50	Sagar Kumar	BARCTS (AMD), Hyderabad	Exploration Geosciences	ENGG1G201801013	To Establish Genesis of Polymetallic Uranium Mineralization in Paleoproterozoic Metasediments of Khetabari Formation in Laggi Gamlin-Siki areas, West

					Siang District, Arunachal Pradesh.
51	Ankit Badiwal	BARC	Chemical Engineering	ENGG01201801001	Early Detection of Agglomeration in Fluidized Bed during Thermal Denitration of Sodium Nitrate
52	Azim Uddin Siddiqui	BARC	Electronics Engineering	ENGG01201801033	Study and Performance Analysis of Machine Vision Based System for Three Dimensional Measurements of Industrial Components
53	Shubham Raghuwanshi	BARC	Mechanical Engineering	ENGG01201801050	Particulate Matter Dispersion Modelling for an Accidental Leak in a Ventilated Room
54	Subhajit Pandey	BARCTS (AMD), Hyderabad	Exploration Geosciences	ENGG1G201801015	Establishment of Facies Variation in Kaimur Group of Rocks and their Association with Uranium Mineralization in Dhoha-Dursendi Area, Gwalior, District, M.P.

M.Sc. (Engg.)

Sr. No.	Name of the student	CI	Programme	Enrolment No
1	Vaibhav Ranjan	IPR	M.Sc. (Engg)	ENGG06201603004
2	Partha Pratim Nandy	VECC	M.Sc. (Engg)	ENGG04201803001

Section V

**List of students who completed D.M., M.Ch.
and M.D. degrees during August 1, 2021-July 31, 2022**

D.M. Degree

S. No	Student Name	CI	Academic Programme	Enrollment No
1	Swapna Chitra V	TMC	D.M.- Critical Care Medicine	HLTH09201810044
2	Tarun Arun Sahu	TMC	D.M. - Critical Care Medicine	HLTH09201910035
3	Kushal Rajeev Kalvit	TMC	D.M. - Critical Care Medicine	HLTH09201910036
4	Unique Tyagi	TMC	D.M.-Gastroenterology	HLTH09201910037
5	Aadish Kumar Jain	TMC	D.M.-Gastroenterology	HLTH09201910038
6	Falguni Hota	TMC	D. M. Interventional Radiology	HLTH09201910061
7	Swaminathan K.	TMC	D.M.- Pediatric Oncology	HLTH09201910039
8	Anisha Panda	TMC	D.M.- Pediatric Oncology	HLTH09201910040
9	S. Vignesh	TMC	D.M.- Pediatric Oncology	HLTH09201910041
10	Jobanputra Kunal Naishadh	TMC	D.M.- Medical Oncology	HLTH09201910042
11	Shah Minit Jalan	TMC	D.M.- Medical Oncology	HLTH09201910043
12	Chinthala Sravan Kumar	TMC	D.M.- Medical Oncology	HLTH09201910044
13	Mannavi Suman	TMC	D.M.- Medical Oncology	HLTH09201910046
14	Darshit Kalpeshkumar Shah	TMC	D.M.- Medical Oncology	HLTH09201910047
15	Alok Shetty K.	TMC	D.M.- Medical Oncology	HLTH09201910048
16	Anbarasan S.	TMC	D.M.- Medical Oncology	HLTH09201910049
17	Madala Ravi Krishna	TMC	D.M.- Medical Oncology	HLTH09201910050
18	Abhishek Sharma	TMC	D.M.- Medical Oncology	HLTH09201910051
19	Muttuluri Hemanth	TMC	D.M.- Medical Oncology	HLTH09201910052
20	Munot Pritesh Naresh	TMC	D.M.- Medical Oncology	HLTH09201910053
21	Rahul Kumar Rai	TMC	D.M.- Medical Oncology	HLTH09201910055
22	Ashutosh Jain	TMC	D.M.- Medical Oncology	HLTH09201910056
23	Saswata Shah	TMC	D.M.- Medical Oncology	HLTH09201910057
24	Divakar Sharma	TMC	D.M.-Onco-Pathology	HLTH09201910058
25	Tushar Agarwal	TMC	D.M.-Onco-Pathology	HLTH09201910059
26	Subhashree Subhasmita Dash	TMC	D.M.-Onco-Pathology	HLTH09201910060

M.Ch Degree

S. No	Student Name	CI	Academic Programme	Enrollment No
1	Rupesh Kumar Singh	TMC	M.Ch-Surgical Oncology	HLTH09201810010
2	Dipanjana Biswas	TMC	M.Ch-Surgical Oncology	HLTH09201810016
3	Narayanan R.	TMC	M.Ch-Surgical Oncology	HLTH09201910012
4	Kaustubha S. Gour	TMC	M.Ch-Surgical Oncology	HLTH09201910013
5	P. Kaushik Rao	TMC	M.Ch-Surgical Oncology	HLTH09201910015

6	Devesh Sanjeev Ballal	TMC	M.Ch-Surgical Oncology	HLTH09201910016
7	Lovedeep Singh	TMC	M.Ch-Surgical Oncology	HLTH09201910017
8	Sheshank Mahajan	TMC	M.Ch-Surgical Oncology	HLTH09201910019
9	Rajyalakshmi Puvvada	TMC	M.Ch-Surgical Oncology	HLTH09201910021
10	Vidur Garg	TMC	M.Ch-Surgical Oncology	HLTH09201910023
11	Bansod Yogesh Kisan	TMC	M.Ch-Surgical Oncology	HLTH09201910025
12	Pujari Avinash	TMC	M.Ch-Surgical Oncology	HLTH09201910026
13	Gomathi Shankar V.	TMC	M.Ch.-Surgical Oncology	HLTH09201910027
14	Harshit Srivastava	TMC	M.Ch-Surgical Oncology	HLTH09201910029
15	Rajat Kamra	TMC	M.Ch-Surgical Oncology	HLTH09201910030
16	Shivpal Saini	TMC	M.Ch-Surgical Oncology	HLTH09201910031
17	Aman Rastogi	TMC	M.Ch-Surgical Oncology	HLTH09201910032
18	Chhatrala R. Mansukhlal	TMC	M.Ch-Surgical Oncology	HLTH09201910033
19	B Mahendra Varma	TMC	M.Ch-Surgical Oncology	HLTH09201910034
20	Sudhanshu Hedau	TMC	M.Ch-Plastic & Reconstructive Surgery	HLTH09201910001
21	Ruby Singh	TMC	M.Ch-Plastic & Reconstructive Surgery	HLTH09201910002
22	Abhishek Shitole	TMC	M.Ch-Plastic & Reconstructive Surgery	HLTH09201910003
23	Kantamani Bala Teja	TMC	M.Ch-Head & Neck Surgery	HLTH09201910007
24	Vidula Madhukar Mestry	TMC	M.Ch-Head & Neck Surgery	HLTH09201910008
25	Gurukeerthi B	TMC	M.Ch-Head & Neck Surgery	HLTH09201910009
26	Kinshuk Chatterjee	TMC	M.Ch-Head & Neck Surgery	HLTH09201910010

M.D. Degree

S. No	Student Name	CI	Academic Programme	Enrollment No
1	Vidya Arun Lawhale	TMC	M.D.-Anaesthesiology	HLTH09201709005
2	Harish Y. Krishna	TMC	M.D.-Anaesthesiology	HLTH09201909001
3	Amy Saira Elias	TMC	M.D.-Anaesthesiology	HLTH09201909002
4	Sakshi Sharma	TMC	M.D.-Anaesthesiology	HLTH09201909003
5	Keerthana K.	TMC	M.D.-Anaesthesiology	HLTH09201909004
6	Sanjoli Singhal	TMC	M.D.-Anaesthesiology	HLTH09201909005
7	Sukhpreet Singh	TMC	M.D.-Anesthesiology	HLTH09201909006
8	Satya Kumar Moharana	TMC	M.D.-Anaesthesiology	HLTH09201909007
9	Arti Dwivedi	TMC	M.D.-Anaesthesiology	HLTH09201909008
10	Isha Hajara Mohammad	TMC	M.D.-Anaesthesiology	HLTH09201909009
11	Samrudhi Bhanushali	TMC	M.D.-Anaesthesiology	HLTH09201909010

12	Niki Dineshkumar Patel	TMC	M.D.-Anaesthesiology	HLTH09201909011
13	Mrunmayai Hemant Jadhav	TMC	M.D.-Anaesthesiology	HLTH09201909014
14	Disha Chetan Rajput	TMC	M.D.-Anaesthesiology	HLTH09201909015
15	Urmila Phad	TMC	M.D.-Anaesthesiology	HLTH09201909016
16	Pallavi Adhik Desai	TMC	M.D.-Anaesthesiology	HLTH09201909018
17	Badalkumar Rameshprasad Dhurwe	TMC	M.D.-Anaesthesiology	HLTH09201909020
18	Aarti Mahesh Makhija	TMC	M.D.-Anaesthesiology	HLTH09202009014
19	Indira Radhakisan Kasar	TMC	M.D.-Anaesthesiology	HLTH09202009023
20	Minu Rose George	TMC	M.D.-Immuno-Haematology & Blood Transfusion	HLTH09201909068
21	Umakant H. Mokalikar	TMC	M.D.-Immuno-Haematology & Blood Transfusion	HLTH09201909069
22	Ashwini C.	TMC	M.D.-Nuclear Medicine	HLTH01201909001
23	Vaidya Bhakti Vyankatesh	TMC	M.D.-Nuclear Medicine	HLTH01201909002
24	Arya Nair S.	TMC	M.D.-Nuclear Medicine	HLTH09201909071
25	Sonali Thakur	TMC	M.D.-Nuclear Medicine	HLTH09201909072
26	Ramchandani Varun Ravi	TMC	M.D.-Nuclear Medicine	HLTH09201909073
27	Hemant Bhagwan Raundale	TMC	M.D.-Nuclear Medicine	HLTH09201909074
28	Yogesh Subhash Gawale	TMC	M.D.-Nuclear Medicine	HLTH09201909075
29	Vikrant Vilasrao Bhosale	TMC	M.D.-Nuclear Medicine	HLTH09201909076
30	Shreya Suresh Nair	TMC	M.D.-Palliative Medicine	HLTH09201909021
31	Sachin Ravji Gunde	TMC	M.D.-Palliative Medicine	HLTH09201909022
32	Prajakta Dilip Bhagat	TMC	M.D.-Palliative Medicine	HLTH09201909023
33	Abirami K	TMC	M.D.-Pathology	HLTH09201709029
34	Khushi Nehal Naik	TMC	M.D.-Pathology	HLTH09201909024
35	Vinayak Nalinkumar Dave	TMC	M.D.-Pathology	HLTH09201909026
36	Aditi Rathi	TMC	M.D.-Pathology	HLTH09201909027
37	Ashwini Satish Duggad	TMC	M.D.-Pathology	HLTH09201909028
38	Sheenal Anil Bhatia	TMC	M.D.-Pathology	HLTH09201909029
39	Manali Sanjay Ranade	TMC	M.D.-Pathology	HLTH09201909030
40	Suvarna Ravindra Pawar	TMC	M.D.-Pathology	HLTH09201909031

41	Saminabano Mohd Shamim Ansari	TMC	M.D.-Pathology	HLTH09201909032
42	Pooja Narayan Shinde	TMC	M.D.-Pathology	HLTH09201909034
43	Ashish Dilip Uke	TMC	M.D.-Radiation Oncology	HLTH09201809054
44	Amiya Agrawal	TMC	M.D.-Radiation Oncology	HLTH09201909053
45	Kanala Tejaswi Sreevatsava	TMC	M.D.-Radiation Oncology	HLTH09201909054
46	Debanjan Chakraborty	TMC	M.D.-Radiation Oncology	HLTH09201909055
47	Meenakshi Nivedha J.	TMC	M.D.-Radiation Oncology	HLTH09201909056
48	Shakhtivel Mani	TMC	M.D.-Radiation Oncology	HLTH09201909057
49	Suman Gopal Ghosh	TMC	M.D.-Radiation Oncology	HLTH09201909058
50	Jayshriben Vishnubhai Jansari	TMC	M.D.-Radiation Oncology	HLTH09201909059
51	Priyanka Subhash Pathare	TMC	M.D.-Radiation Oncology	HLTH09201909060
52	Gayatri Shantaram Patil	TMC	M.D.-Radiation Oncology	HLTH09201909062
53	Shraddha Vilas Kenekar	TMC	M.D.-Radiation Oncology	HLTH09201909063
54	Amruta Rajendra Shinde	TMC	M.D.-Radiation Oncology	HLTH09201909065
55	Rajat Gopal Agrawal	TMC	M.D.-Radiodiagnosis	HLTH09201909036
56	Deep Bimalbhai Mehta	TMC	M.D.-Radiodiagnosis	HLTH09201909037
57	Shubham Suryavanshi	TMC	M.D.-Radiodiagnosis	HLTH09201909038
58	Antariksh Vijay Vijan	TMC	M.D.-Radiodiagnosis	HLTH09201909039
59	Aditi Venkatesh	TMC	M.D.-Radiodiagnosis	HLTH09201909040
60	Sandesh Voosala	TMC	M.D.-Radiodiagnosis	HLTH09201909041
61	Sharadhini K.	TMC	M.D.-Radiodiagnosis	HLTH09201909042
62	Nandi V Prudveesh Kumar Reddy	TMC	M.D.-Radiodiagnosis	HLTH09201909043
63	Smeet Atul Gandhi	TMC	M.D.-Radiodiagnosis	HLTH09201909044
64	Kunal Nigam	TMC	M.D.-Radiodiagnosis	HLTH09201909045
65	Shradha Mohan Lad	TMC	M.D.-Radiodiagnosis	HLTH09201909046
66	Pashmina Prakash Kandalgaonkar	TMC	M.D.-Radiodiagnosis	HLTH09201909047
67	Shubham Hanumant Shinde	TMC	M.D.-Radiodiagnosis	HLTH09201909048
68	Rohan Ramesh Khadtare	TMC	M.D.-Radiodiagnosis	HLTH09201909049
69	Manoj Rajesh Ambhure	TMC	M.D.-Radiodiagnosis	HLTH09201909051
70	Yogesh Shivaji Bhagwat	TMC	M.D.-Radiodiagnosis	HLTH09201909052



HOMI BHABHA NATIONAL INSTITUTE

(A Deemed to be University u/s of UGC Act 1956 and a Grant-in-Aid
Institute of the Department of Atomic Energy, Govt. of India)

2nd Floor, Training School Complex,
Anushaktinagar, Mumbai 400 094
Ph: 022 25597554, 022 25597626

www.hbni.ac.in